Investigation of the function of δ-cadinene synthase with aza-analogues and site directed mutagenesis

A thesis submitted to Cardiff University

for the degree of Doctor of Philosophy by:

Marianna Loizzi

Supervisor: Rudolf K. Allemann

2017

DECLARATION

This work has not been submitted in substance for any other degree or award at this or any other university or place of learning, nor is being submitted concurrently in candidature for any degree or other award.

Signed …………….………………(candidate)   Date ………………….……………….……

STATEMENT 1

This thesis is being submitted in partial fulfillment of the requirements for the degree of ………(insert MCh, MD, MPhil, PhD etc, as appropriate)

Signed …………….…….………… (candidate)   Date …………………………….……………

STATEMENT 2

This thesis is the result of my own independent work/investigation, except where otherwise stated, and the thesis has not been edited by a third party beyond what is permitted by Cardiff University's Policy on the Use of Third Party Editors by Research Degree Students. Other sources are acknowledged by explicit references. The views expressed are my own.

Signed …………….…….…………..…(candidate)   Date …………………….…………………

STATEMENT 3

I hereby give consent for my thesis, if accepted, to be available online in the University's Open Access repository and for inter-library loan, and for the title and summary to be made available to outside organisations.

Signed …………….…….…………… (candidate)   Date …………………………………………

STATEMENT 4: PREVIOUSLY APPROVED BAR ON ACCESS

I hereby give consent for my thesis, if accepted, to be available online in the University's Open Access repository and for inter-library loans **after expiry of a bar on access previously approved by the Academic Standards & Quality Committee.**

Signed ……………….…….……………(candidate)   Date …………………………………….……

Abstract

Terpenes are one of the most structurally varied families of natural products with extraordinary chemical properties that have been exploited for numerous applications. Sesquiterpene synthases are a family of metal-dependent enzymes that catalyse the cyclisation of farnesyl diphosphate (FDP) into a myriad of complex C_{15}-isoprenoid hydrocarbons, the sesquiterpenes. δ-Cadinene synthase (DCS) from *Gossypium arboreum* (cotton tree) catalyses the formation of δ-cadinene (DCN), a bicyclic intermediate in the biosynthesis of important phytoalexins such us gossypol. Two mechanistic proposals have been made for the formation of δ-cadinene: a 1,10-ring closure mechanism leading to the key intermediate germacradienyl cation, or a 1,6-ring closure leading to the α-bisabolyl carbocation. Previous investigation with fluorinated FDP analogues were in partial agreement with both scenarios and hence it was not possible to distinguish unambiguously between the two possible cyclisation reactions.

To investigate the catalytic mechanism of DCS, enantiopure samples of the aza-analogues of α-bisabolyl cation and germacradienyl cation were needed. These compounds are designed as stable structural and electrostatic mimics of the putative short-lived carbocationic intermediates generated by terpene synthases, and hence often act as potent reversible competitive inhibitors (low K_i) of these enzymes.

Here, the enantioselective total synthesis of *R*- and *S*- aza-analogues of the α-bisabolyl cation are described as well as the partial racemic synthesis of aza-germacradienyl cation. Both enantiomers of aza-bisabolyl cation were good mimics of α-bisabolene. They were competitive inhibitors of DCS, providing evidence for a 1,6-cyclisation closure.

The second part of the project involved the investigation of the role of tryptophan 279 for the desolvation of the active site of DCS and therefore for the formation of DCN. Seven mutants of W279 were created. The data obtained showed that W279 is essential to prevent water from entering the active site and form the hydroxylate terpenoid germacradien-4-ol (GD4ol). Mutagenesis studies yielded a mutant, W279A, capable of making GD4ol as the sole product.

Acknowledgements

First, I would like to thank my supervisor, Professor Rudolf Allemann, for giving me the opportunity to undertake this exciting work, and for his continued support and advices throughout my Ph.D. He made me definitively a better scientist and a stronger person.

I also would like to thank Dr. David Miller for his patience in proof reading this thesis and his help during the years; and to Dr. Veronica Gonzalez for in teaching me the molecular biology techniques during my second year. I also would like to thank Dr. J. Faraldos for all the long talks about chemistry and biochemistry.

Special thanks goes to Dr. Xiaoping Tang, not only for her helpful advises on organic chemistry, but also for the therapeutic shopping sessions who made my days much better after a reaction did not work. Also, thank you to Dr Robert Jenkins and the technical support staff for their help.

I would like to thank all the members of the Allemann group, who made my days in the lab enjoyable: Mel, Chris, Victor, Raquel, Ed, Dan, and everyone else.

A big thank you goes to Antonio, my colleague, flatmate and friend. I could have not survived this journey without you.

I would like to thank the Cardiff Family: Clara, Virg, Lisa, Mike, Jakub, James, Becca, Matt, Amie and Charlie for the nights at Pen and Wig, the afternoon teas at Mackintosh Place, and the dancing at Live Lounge. A big thank you goes to Ewa, to be always there when I need it.

Special thanks go to the "Italian Community" in the Pharmacy department, with special mention to the gym girls: Elisa, Ale, Gilda, Lorena, Giulia, Birgidt and Silvia. Also thank you Cinzia: your continuous support and our coffees and chocolate have been essential for this project.

A special thank you to Mike, also a Dr. in chemistry, who guided me and put up with me even when I was tired and irritable. I could not have done it without your stubborn support and your scientific advices.

Finally, my sincere gratitude goes to my parents and family, especially Anna and Matteo, without whose support and love I would not be where I am today.

CHAPTER 1   Introduction

1.1 Terpenes

Terpenes are the largest and most diverse family of natural products with more than 60,000 different compounds isolated from various sources, primarily from plant extracts, but also from fungi, animals and microbes.[1] Historically, they were classified according to the number of isoprene units (Figure 1.1). Depending on the number of isoprene units they contain, terpenes are classified into subclasses (Table 1.1).[2] Furthermore, the hydrocarbon chain can be functionalised to include ether, aldehyde, alcohol, carboxylic acid, ester or ketone moieties, forming a theoretically endless class of compounds, known as terpenoids. Many terpenes and terpenoids have found applications as pharmaceuticals, fragrances, flavourings, cosmetics, colorants or agrochemicals. [3]
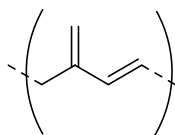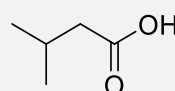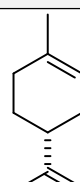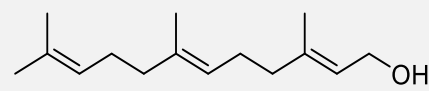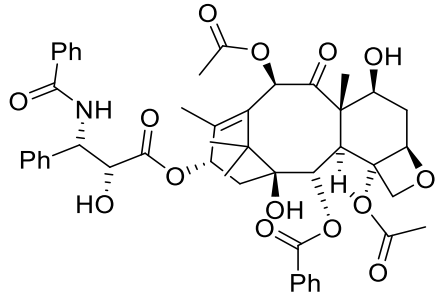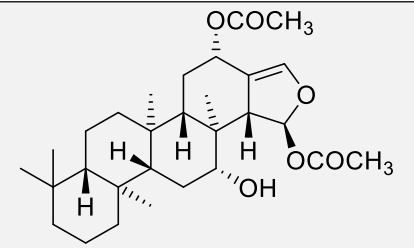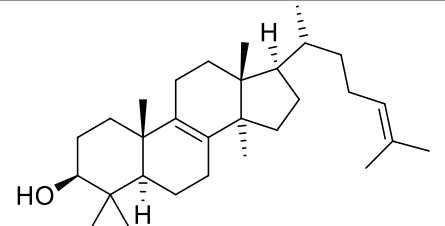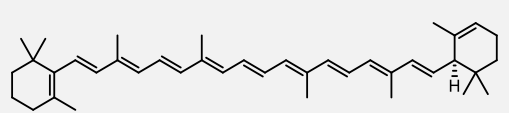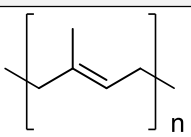
Figure 1.1 Isoprene unit

Table 1.1 Terpenes classification and examples

Terpene Subclass	Number of Isoprene Units	General Formula	Example	Chemical Structure
Hemiterpenes	1	C_5H_8	isovaleric acid	
Monoterpenes	2	$C_{10}H_{16}$	limonene	
Sesquiterpenes	3	$C_{15}H_{24}$	farnesol	

Diterpenes	4	$C_{20}H_{32}$	paclitaxel	
Sesterterpenes	5	$C_{25}H_{40}$	heteronemin	
Triterpenes	6	$C_{30}H_{48}$	lanosterol	
Tetraterpenes	8	$C_{40}H_{64}$	carotene	
Polyterpenes	n	$(C_5H_8)n$	natural rubbers	

As shown in Table 1.1, terpenes and terpenoids include many classes of different compounds, from simple molecules such as limonene, mostly used as fragrances, to the more structurally complex paclitaxel, a taxane drug with potent anti-neoplastic and anti-mitotic properties. In fact, it is the large diversity of terpenoids, and thus their numerous applications, that has been attracting the interest of scientists and industrialists for decades.

1.2 Biological functions of terpenoids and their applications

In nature, the majority of terpenes are found in plants, although they are present in very small concentrations in all forms of life. In the Plantae kingdom, terpenes and terpenoids are very often the plant's primary or secondary metabolites, and they play different roles.

Plants are autotropic organisms, hence they are able to synthesise all the so-called primary metabolites: chemicals that are essential for their growth, development and survival. On the other hand, plants depend on other organisms in order to reach their optimal growth and to complete their life cycle. In order to interact with the surrounding environment, plants produce the so-called secondary metabolites, compounds that are not essential for the plant, but are synthesised in response to an external stimulation or necessity. These chemicals can be toxic or harmful, when used as a defense against pathogens or herbivores, or they can act as attractants for potential pollinators. Sometimes this metabolism is defined as "specialised metabolism" because it acts as a specific response to a specific natural problem.

1.2.1 Terpenoids as primary metabolites

Primary metabolites are chemicals directly involved in the normal development and reproduction of an organism, and they usually play an intrinsic function. There are several examples of terpene-related primary metabolites, of which the most common are sterols,[4–8] carotenoids,[9–11] quinones,[12,13] and related compounds (Figure 1.2).
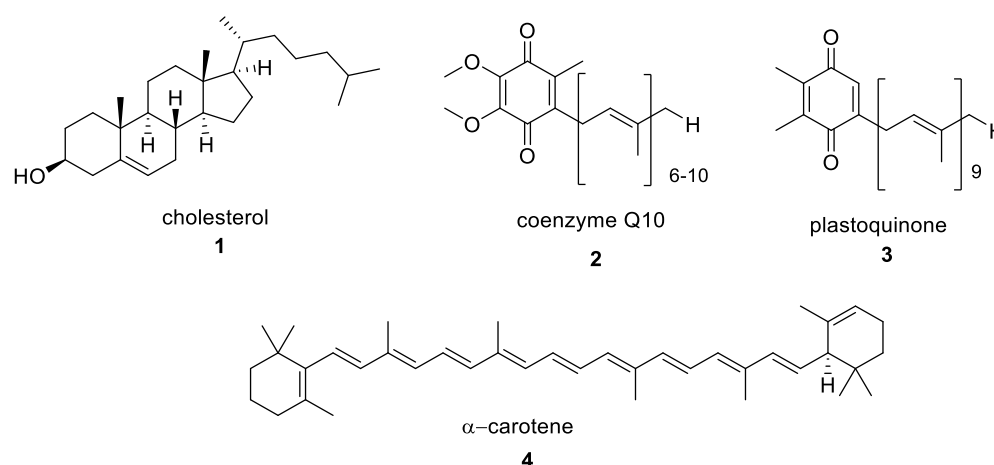
Figure 1.2 Chemical structures of some primary metabolites terpenoids.

1.2.2 Terpenoids as secondary metabolites

Plant secondary metabolites are not essential for the survival of the plant, but they regulate the plants balance and interaction with the environment. There are plenty of examples of terpenoid secondary metabolites (Figure 1.3), which have a significant importance in the medicinal chemistry and cosmetic field. [3,14-15]

gossypol
5

(R)- and (S)-camphor
6

artemisinin
7

paclitaxel
8
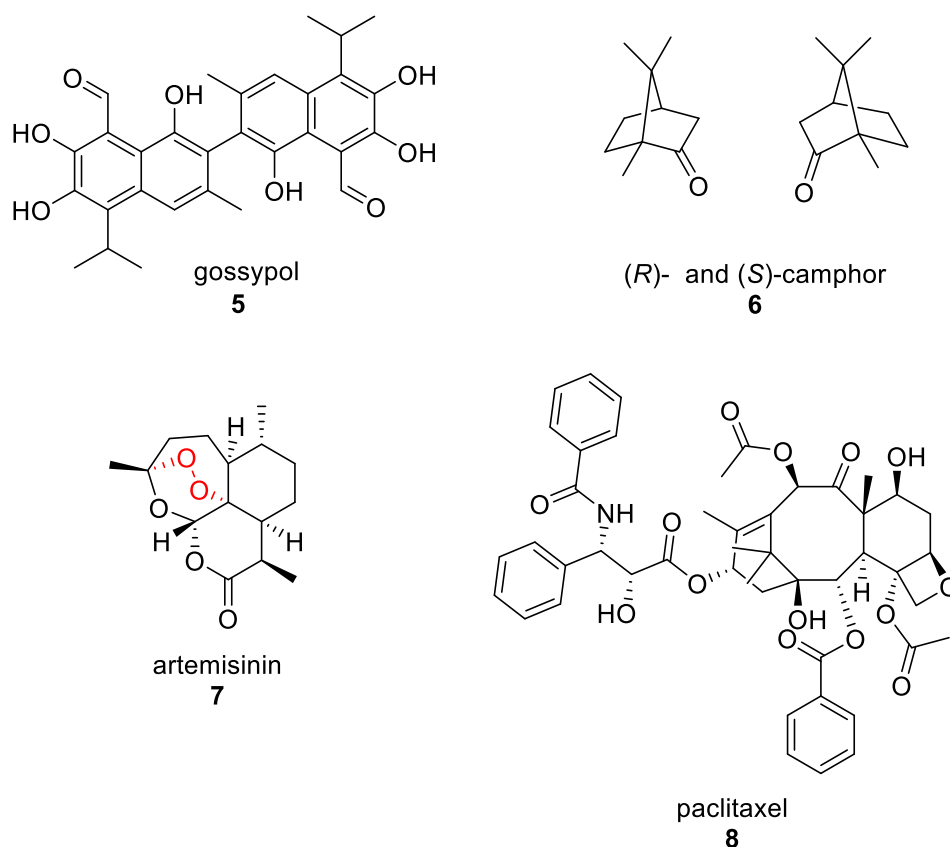
Figure 1.3 Chemical structure of some secondary metabolites terpenoids used for medical purposes.

There are many other secondary metabolites with a terpenoid structure, which are used for non-medical purposes, such as flavoring ((R)-limonene **10**, geraniol **9**) and as insect repellents (7-epizingiberene **11**), just to name a few of them (Figure 1.4).

geraniol
9

(R)-limonene
10

7-epizingiberene
11
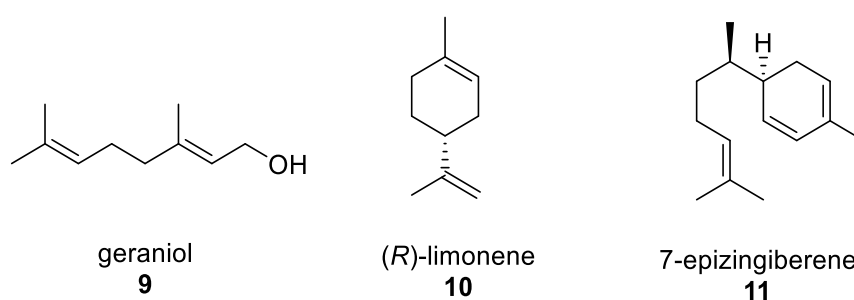
Figure 1.4 Chemical structure of geraniol, (R)-limonene and 7-epizingiberene.

Taking all the above into consideration, it can be seen how terpenes and terpenoids have important applications in everyday life. Therefore a detailed understanding of their biosynthesis is essential in order to broaden and improve their current uses as well as define new ones.

1.3 Terpene biosynthesis

Whilst terpenes are formally derived from isoprene, their actual biosynthesis does not involve free isoprene at all. Instead, the universal building blocks of their biosynthesis are isopentenyl diphosphate (IDP, **17**) and dimethylallyl diphosphate (DMADP, **18**). [15] These two compounds can be synthesised through two different routes, the mevalonate pathway and the 1-deoxy-D-xylulose-5-phosphate pathway (DXP) (also known as the non-mevalonate pathway). In the mevalonate pathway, (Scheme 1.1) three molecules of acetyl-CoA (**12**) are condensed by the enzymes acetoacetyl-CoA thiolase and hydroxymethylglutaryl CoA synthase to form the intermediate hydroxymethyl-3-glutaryl CoA (HMG-CoA, **14**), which undergoes NADPH- dependent reduction to form mevalonic acid (**15**). **15** is then phosphorylated twice by two molecules of ATP to yield 5-disphosphomevalonic acid (**27**). After decarboxylation and a loss of diphosphate, IDP (**17**) is formed. The isomerisation of IDP to DMADP (**18**) is catalysed by the enzyme IDP isomerase by allylic rearrangement.[16,17]
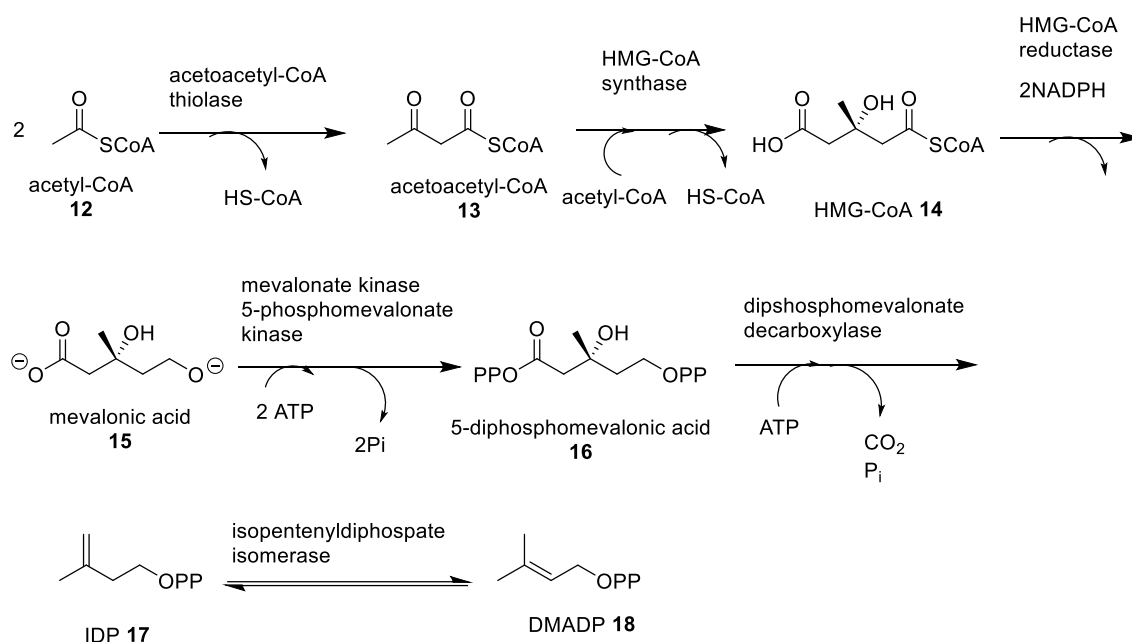
Scheme 1.1 The mevalonate biosynthetic pathway to IDP and DMADP.

In the non-mevalonate pathway (Scheme 1.2), which is absent in humans and occurs in some bacteria and inside plastids in plants, IDP and DMADP are formed separately starting from the same percursors.[18] Pyruvate (**19**) and glyceraldehyde-3-phosphate (**20**) undergo a thiamine diphosphate (TDP) dependent condensation to form the 1-deoxy-D-xylulose-5-phosphate (DOX, **21**) intermediate. During this reaction, the carboxylic group of the pyruvate is lost to form CO_2. The next steps

include a rearrangement and a NADPH-dependent reduction, catalysed by the enzyme IspC, and 2-C-methyl-D-erythritol-4-phosphate (MEP, **23**) is formed. The enzyme IspD transfers cytidyl monophosphate (CMP) to the terminal phosphate of MEP to form an intermediate **24**, which is then phosphorylated by IspE to yield **25**. The consequent elimination of the CMP catalysed by IspF yields the cyclic intermediate **26**. The final steps of the non-mevalonate pathway are catalysed by two oxygen sensitive iron-sulfur proteins: IspG and IspH. The mechanistic modes of these two enzymes are still not completely known. The formation of **27** and its ring opening is thought to involve a free radical intermediate, while the formation of final DMADP and IDP seems to involve the transfer of two electrons from the iron-sulfur cluster of the protein IspH.[19]
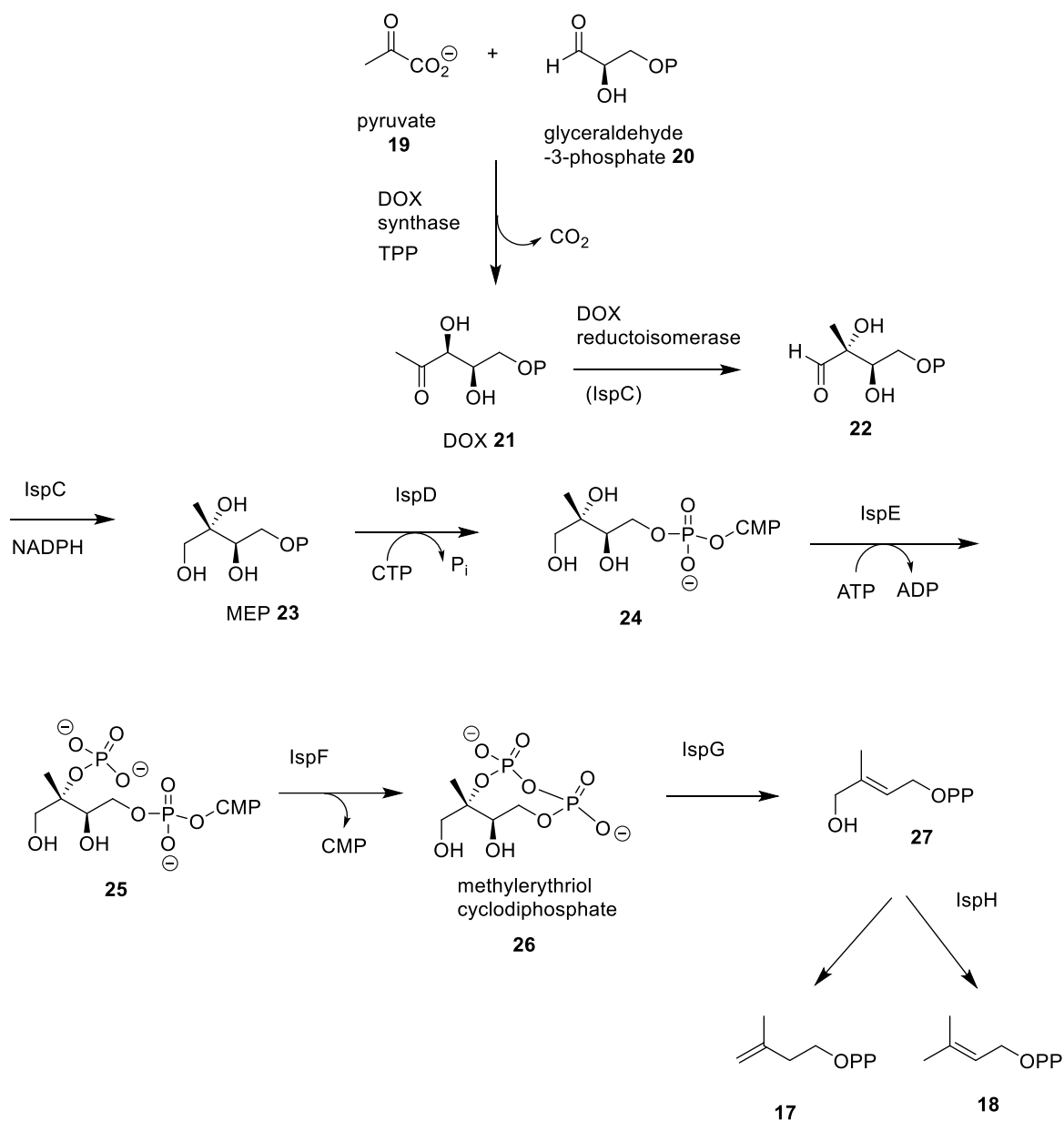
Scheme 1.2 Formation of DMAP and IDP through the non-mevalonate pathway.

1.4 Isoprenyl diphosphate head to tail elongation

The precursor geranyl diphosphate (GPP, **29**) and farnesyl diphosphate (FDP, **31**) are biosynthesised by a chain elongation of IDP (**17**) and DMADP (**18**), which occurs via 'head to tail' condensations (Scheme 1.3).

The reactions catalysed by GDP and FDP synthases proceed through an initial metal dependent ionisation of DMADP (**18**) to give a reactive carbocation-diphosphate ion pair. A nucleophilic attack from the π-system of the IDP (**17**) molecule to C-1 of DMADP follows, creating a ten carbon cationic intermediate (**28**). Elimination of a proton from C-2 generates geranyl diphosphate (GDP, **29**), the universal precursor to monoterpenes. A second condensation takes place with another IDP unit to make farnesyl diphosphate (FDP, **31**) following a similar reaction.
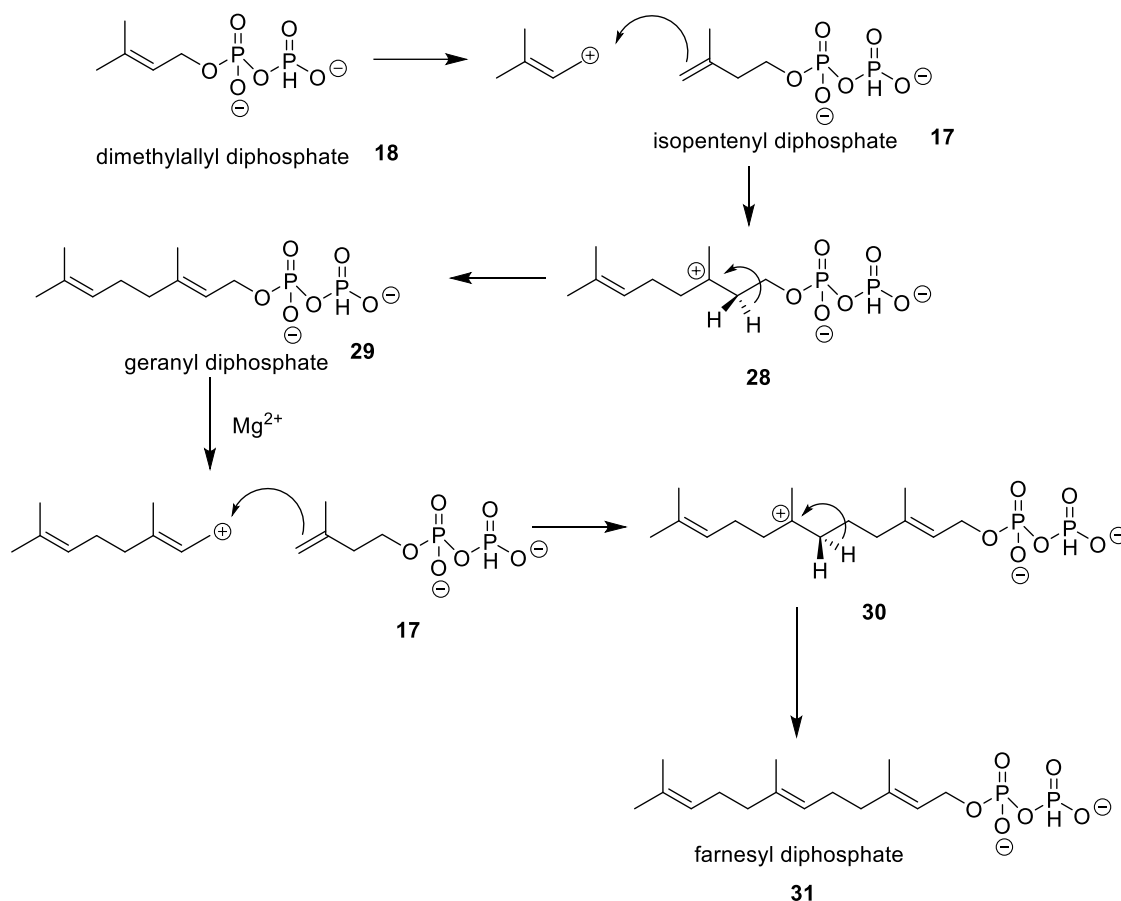
Scheme 1.3 The conversion of DMADP and IDP to GDP and FDP.

The linear farnesyl diphosphates (**31**) then can undergo a series of different rearrangements and cyclisations, catalysed by terpene synthases, to form a

multitude of cyclic hydrocarbon products, which are usually intermediates in the biosynthesis of more complex terpenoids with a wide range of bioactivities.

This study focuses on the enzyme δ-cadinene synthase (DCS), a sesquiterpene synthase that catalyses the cyclisation of FDP to δ-cadinene (DCN). The full catalytic mechanism of DCS is not fully known yet. To better understand the mechanistic mode of DCS, two additional sesquiterpene synthases were taken into consideration during this work, aristolochene synthase from *Penicillium roqueforti* (PR-AS or more simply AS in this study) and amorphadiene synthase from *Artemisia annua* (ADS), whose mechanisms of action are well documented in the literature. [20–23]

1.5 Sesquiterpene synthases

1.5.1 Structure function correlations

Terpene cyclisation and non-cyclisation mechanisms can be divided into three phases: 1: generation of a reactive carbocation; 2: deprotonation, cyclisation and/or hydride shifts within the intermediate; and 3: quenching of the final carbocation by a base. [24] Depending on how terpene synthases initiate the catalysis, they can be subdivided into two classes. Class I terpene synthases initiate catalysis by the metal-triggered departure of the diphosphate group (PP$_i$), whereas class II terpene synthases start catalysis by protonation of the distal double bond (or an epoxide derivative) of the linear isoprenyl diphosphate. Class I enzymes include mono-, sesqui- and some diterpene synthasee, class II includes some di- and all tri- and tetraterpene cyclase, including those involved in the biosynthesis of cholesterol. [25]

Sesquiterpene synthases are class I terpene synthases and catalyse the metal-dependent cyclisation of the linear precursor FDP into a multitude of C-15 linear, mono-cyclic, bi-cyclic and tri-cyclic compounds, with different bioactivity and precise stereochemistry. These enzymes have a conserved tertiary structure consisting of α-helices and short loops and turns, denominated as a class I terpene synthase fold. The active site is cone-shaped and situated in the C terminal domain surrounded by the main α-helices. [26] Most fungal and bacterial sesquiterpene synthases are active as ~40 kDa monomers, but some homodimeric exceptions exist, such as trichodiene synthase.[27] In addition, plant enzymes have a second N terminal domain, called the β-domain. When the enzyme is in the open conformation (*i.e.* not bound to the substrate), the β-domain often appears to be in a disordered state,

whereas it becomes ordered when the protein assumes a closed conformation due to ligand binding. Although no catalytic chemistry appears to happen in the amino-terminal domain, recent work has demonstrated that it plays an essential role in covering and protecting the active site from bulk water.[28] [29]
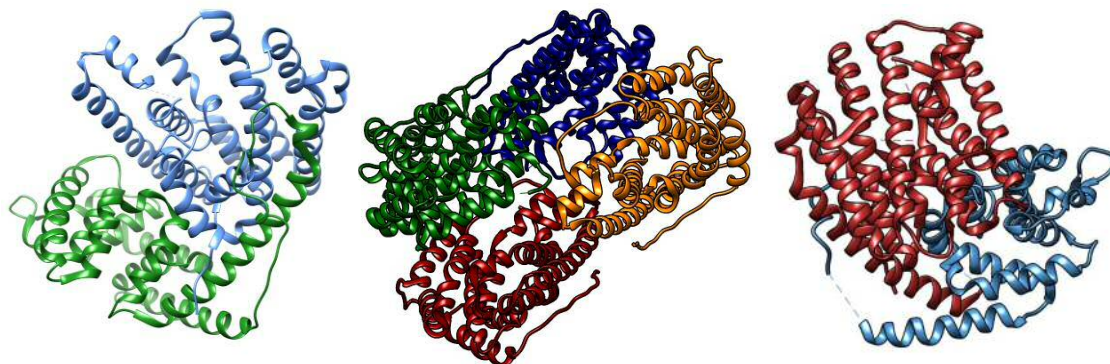
Figure 1.5 Ribbon representation of three terpene synthases. Left: Cartoon representation of Amorphadiene Synthase (ADS). The homology model is based on the crystal structure of α-bisabolol synthase from *A. annua* (4GAX.pdb) with 82% sequence identity to ADS. Light green denotes the N-terminal domain and light blue denotes the catalytic C-terminal domain. [24] Centre: tetramer of aristolochene synthase from *Aspergillus terreus* (AS) (3bnx.pdb);[30] Right: δ-cadinene synthase from *Gossypium arboretum* (DCS) (3g4f.pdb).[31] Red: C-catalytic domain; Cyan: N-terminal domain.

Although there is low sequence identity between the sesquiterpene synthases, they all contain a conserved region, which is responsible for the binding of three Mg^{2+} ions, highlighting the importance of these regions. The metal cluster is necessary for the full activation of the enzyme. Also, the binding of three Mg^{2+} cations is essential for triggering the departure of the PP_i and initiate catalysis.

The conserved region consists of two motifs. The first is an aspartate rich sequence **D**DXX(X)**D/E** located on helix D, which is responsible for binding two of the Mg^{2+} co-factors. The second motif (L,V)(V,L,A)(**N,D**)D(L,I,V)X(**S,T**)XXX**E** (often shorted as **NSE/DTE**) located on helix H, binds the third Mg^{2+} ion required for catalysis. [28] Variation of the second metal binding motif has been reported in some enzymes such as DCS from *Gossypium arboreum,* which possesses a second aspartate rich motif **DD**VA**E** on helix H[31], and (+)-germacrene D synthase from *Solidago canadensis,* that has a **ND**TY**D** motif instead. [32] In accordance with its importance, mutations in this region usually lead to altered substrates and/or to a decreased catalytic activity.

1.5.2   Reaction mechanism

The reaction of all sesquiterpene synthases is initiated by ionisation of the substrate FDP to generate a farnesyl cation, which can undergo either a 1,10-ring closure to form the *trans, trans*-germacradienyl cation (**37**), or a 1,11-cyclisation to form the *trans, trans*-humulyl cation (**38**), or no cyclisation at all. In addition, before PP_i ionisation, the enzyme-bound substrate FDP can be isomerised in the active site to the nerolidyl carbocation (**32**), a versatile intermediate in sesquiterpene synthase reactions that increases the variety of possible ring closure mechanisms for these catalysts.[33,3] In fact, **32** can undergo different cyclisations, such as 1,6-, 1,7-, 1,10- and 1,11-ring closures to form a bisabolyl cation **33**, cycloheptanyl cation **34**, a (*Z,E*)-germacradienyl cation **35** and a (*Z,E*)-humulyl cation **36**, respectively (Scheme 1.4). [28,26,25]
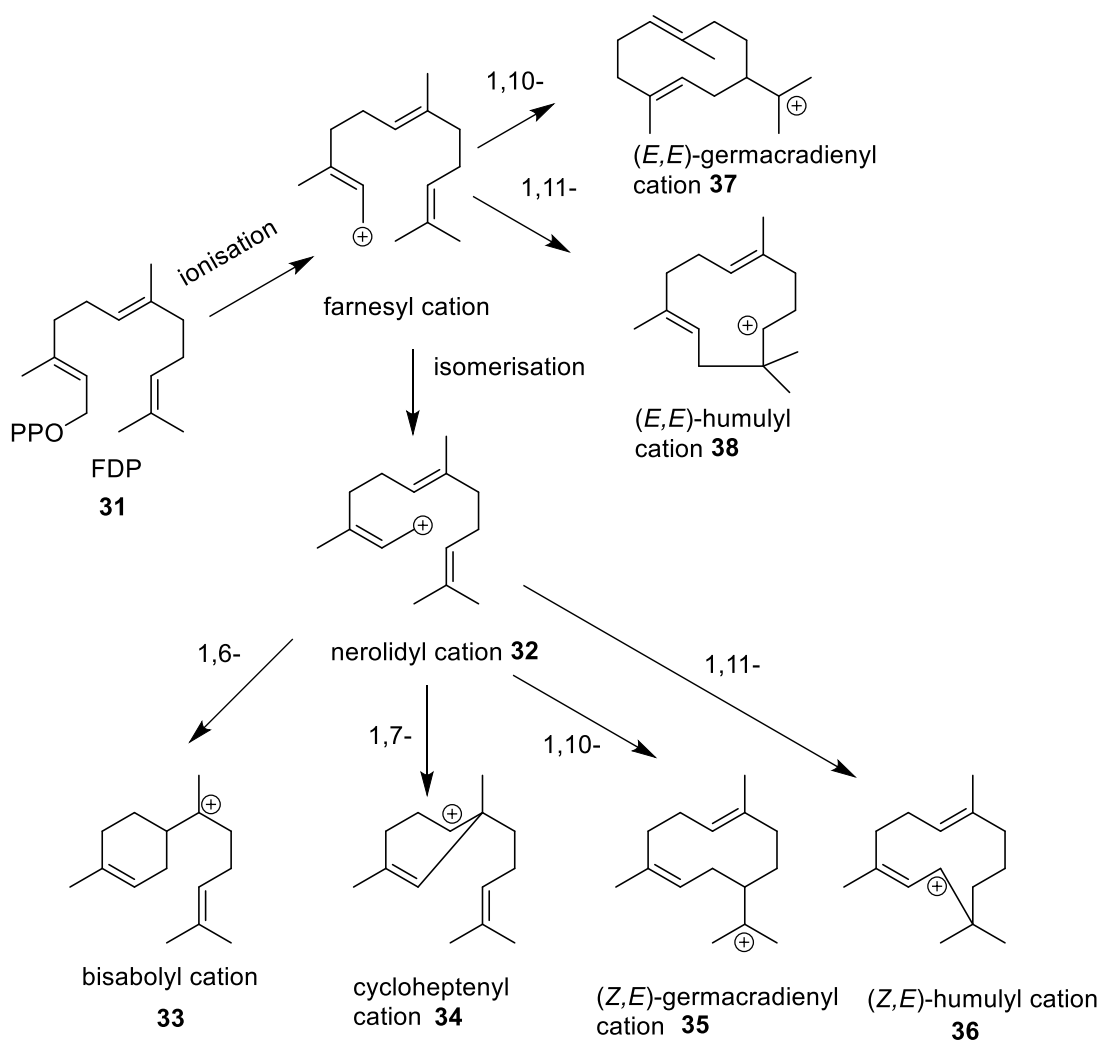
Scheme 1.4 Formation of farnesyl cation, nerolidyl diphosphate and the possible carbocation intermediates in the biosynthesis of sesquiterpenes.

All these carbocationic intermediates then undergo a multitude of subsequent reactions, which include hydride shifts, deprotonation to a neutral intermediate, secondary cyclisations and Wagner-Meerwein rearrangements to give the high structural diversity and multitude of products characteristic of the terpenoid natural products. [34]

1.6 Sesquiterpene synthases used in this study

1.6.1 Aristolochene synthase from *Penicillium roqueforti* (AS)

Aristolochene synthase from *Penicillium roqueforti* (AS) catalyses the cyclisation of FDP into the bicyclic hydrocarbon aristolochene. Further oxidations of aristolochene lead to the formation of many other molecules such as the mycotoxin PR-toxin **39** (Figure 1.6). [35]
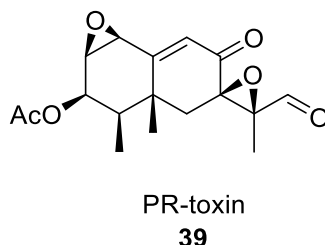
PR-toxin
39

Figure 1.6 Chemical structure of the mycotoxin PR-toxin.

AS adopts the class I α-helical terpene fold, with a conical hydrophobic active site surrounded by 6 α-helices connected by short polypeptide loops. It has the conserved aspartate rich motif $D^{115}DVIE$ on helix C on the upper part of the active site cleft.[36] The catalytic mechanism of AS has been extensively studied by site-direct mutagenesis[37,38,39,40,41], altered substrates[22,42,43] and mechanism based inhibitors.[44,45]
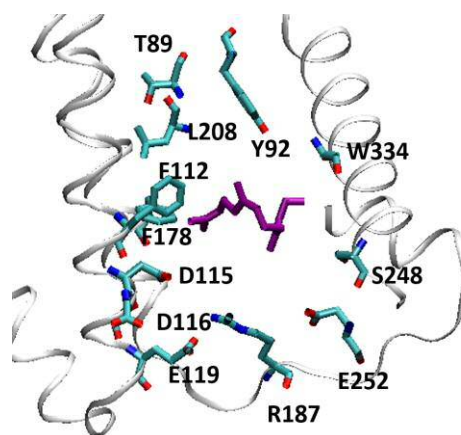
Figure 1.7 Cartoon representation of the AS active site with natural substrate FDP. Key active site residues are marked in black. FDP: purple; C: cyan; O: red; N: blue (1dgp.pdb).

Substrate binding cycle

Although several crystal structures of sesquiterpene synthases have been solved,[30,36,43,46–49] X-ray crystallographic studies with aristolochene synthase from *Aspergillus terreus* (AT-AS) first revealed the closed conformation while complexed with diphosphate and three magnesium ions.[30] Further experiments with AT-AS and fluorinated FDP analogues showed a series of independent structures revealing an array of binding interactions. Based on these structures, Shishova *et al.* [46] proposed a model for metal and substrate binding, and the enzyme conformational changes associated, necessary for the catalytic activity to proceed (Figure 1.8). In the active site, the initial binding of the substrate is directed by the molecular recognition of the diphosphate by hydrogen bond donors. The binding of one Mg^{2+} ion then follows or possibly occurs simultaneously, coordinating to the preorganised binding site structure and causing a reorientation of the diphosphate group. Binding of the second Mg^{2+} ion to the diphosphate group and to the first aspartate in the DDxxD motif causes more extensive conformational changes, triggering the active site closure. Finally, binding of the third magnesium ion completes the magnesium cluster. The two metal ions are coordinated to the first aspartate in the DDxxD motif, completing the conformational changes required for full active site closure and formation of the Michaelis-complex, which is binary complex formed after the initial recognition and capture of the substrate molecule by the enzyme. Opening of the active site and product release upon completion of the catalytic cycle is suggested to occur in the reverse sequence (Figure 1.8). Molecular dynamics simulations performed on AT-AS by van der Kamp *et al.*[50] strongly support the proposed binding cycle, and also revealed that the apoenzyme can adopt a range of conformations

from open to near-closed, but the binding of FDP and the second Mg^{2+} shifts the equilibrium to 'distinctly open conformations', inviting the further binding of the magnesium ions.
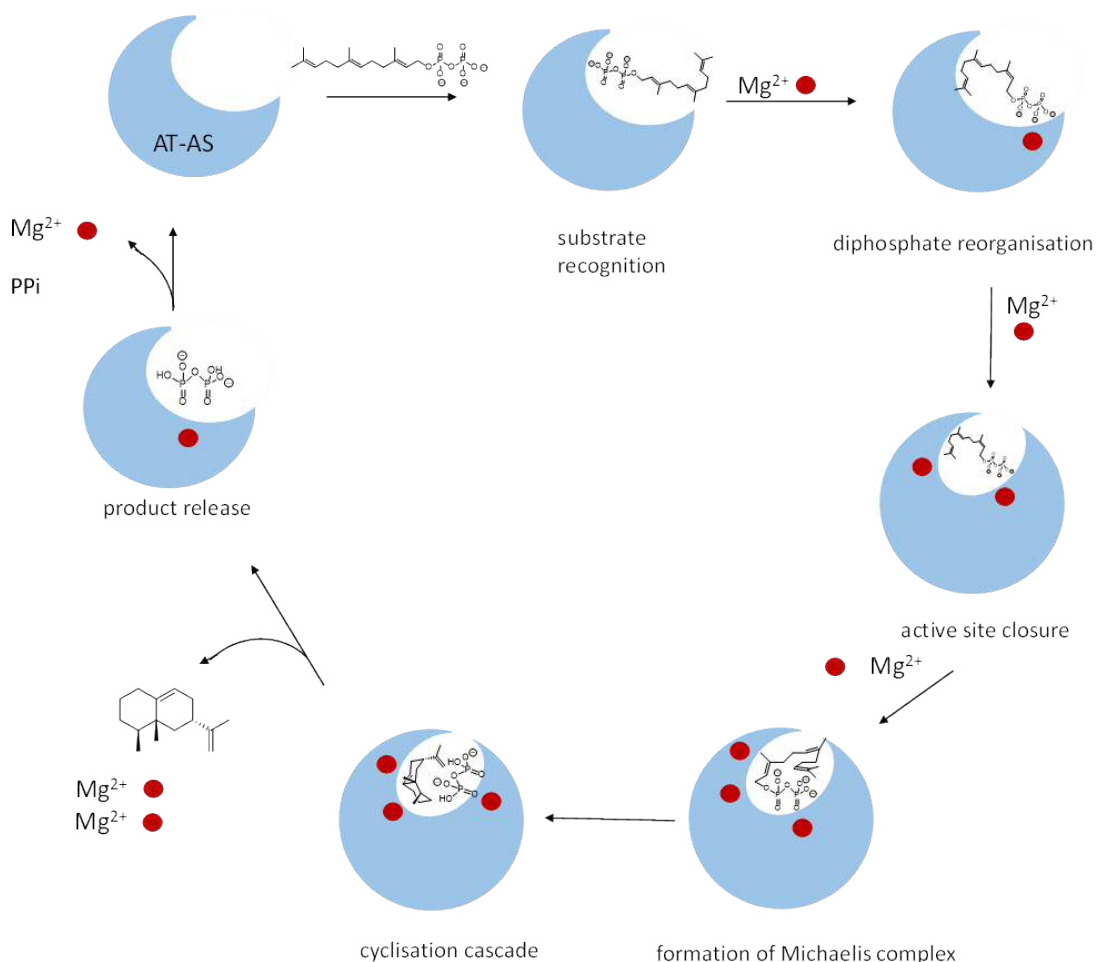
Figure 1.8 Model of metal binding and conformational changs of AT-AS.

Reaction mechanism

In the first step, FDP undergoes an initial 1,10-cyclisation, which occurs with inversion of configuration at C-1.[23] A subsequent loss of a proton the C12-methyl group leads to the formation of the intermediate germacrene A (**41**). Obtaining definitive evidence that germacrene A is an intermediate in the AS catalysed reaction was initially difficult as it had never been released by the active site of any sesquiterpene synthases. Several studies have been able to confirm the presence of germacrene A in the AS catalysis, most notably that of D. E. Cane and Y. S. Tsantrizos in 1996[43] and M. J. Calvert *et al.* in 2002. [51]

The intermediate **41** then undergoes a further cyclisation after it is protonated at the C6, C7- double bond, to form the bicyclic eudesmane cation (**42**). D. J. Miller *et*

22

al. demonstrated that this protonation occurs at the *Re*-face at C6 of germacrene A, and proposed Lys 206 as the acid/base involved. [52] A study by A. Faraldos *et al.* showed that the aza-analogue of the proposed intermediate eudesmane cation acted as a potent competitive inhibitor of AS, supporting the presence of **42** in AS catalysis. [44,45]

Once the eudesmane cation is formed, a 1,2-methyl migration and a 1,2-hydride shift occur, followed by a deprotonation on the H-8 *si* face, leading to formation of (+)-aristolochene (**45**) (Scheme 1.5) . [22]
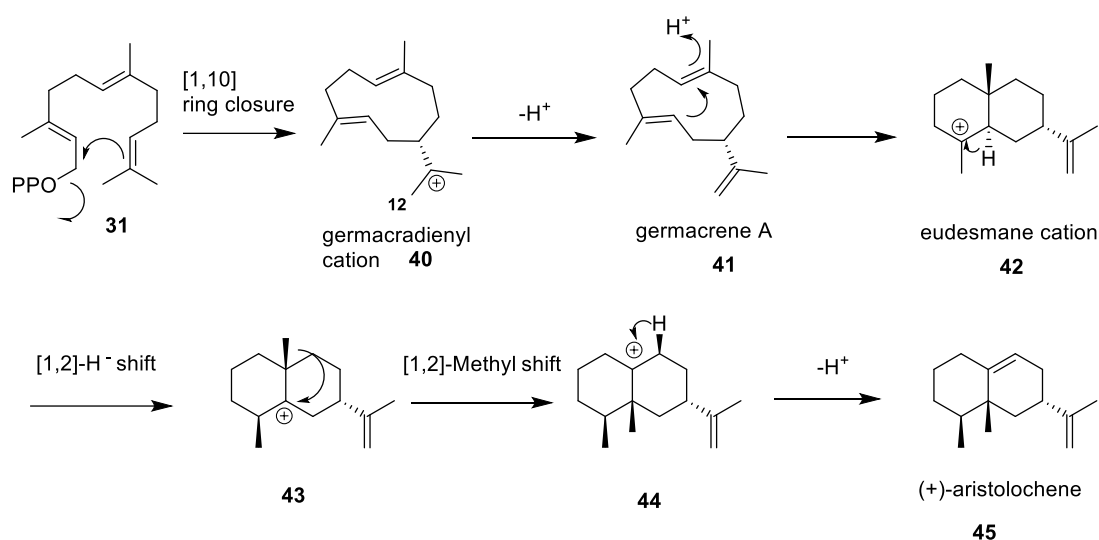
Scheme 1.5 AS catalysed biosynthesis of (+)-aristolochene.

1.6.2 Amorphadiene synthase (ADS)

Amorpha-4,11-diene synthase (ADS), more simply denominated amorphadiene synthase, is a sesquiterpene synthase from the plant *Artemisia annua,* that catalyses the cyclisation of FDP into amorpha-4,11-diene.[53] This particular cyclase has been intensively studied by medicinal chemists because the formation of amorpha-4,11-diene is the first step in the biosynthesis of the natural antimalarial drug artemisinin. Although a biosynthetic approach has been developed by Keasling and colleagues,[54–57] the isolation from plants remains to date the main source of the precious drug. [58]

Picaud and colleagues are the major contributors to the elucidation of the catalytic mechanism of ADS. [21,59] They proposed that the formation of amorpha-4,11-diene (**49**) occurs through the formation of the intermediate NDP (**46**), followed by 1,6-cyclisation and the formation of the bisabolyl cation **33** (Scheme 1.6).
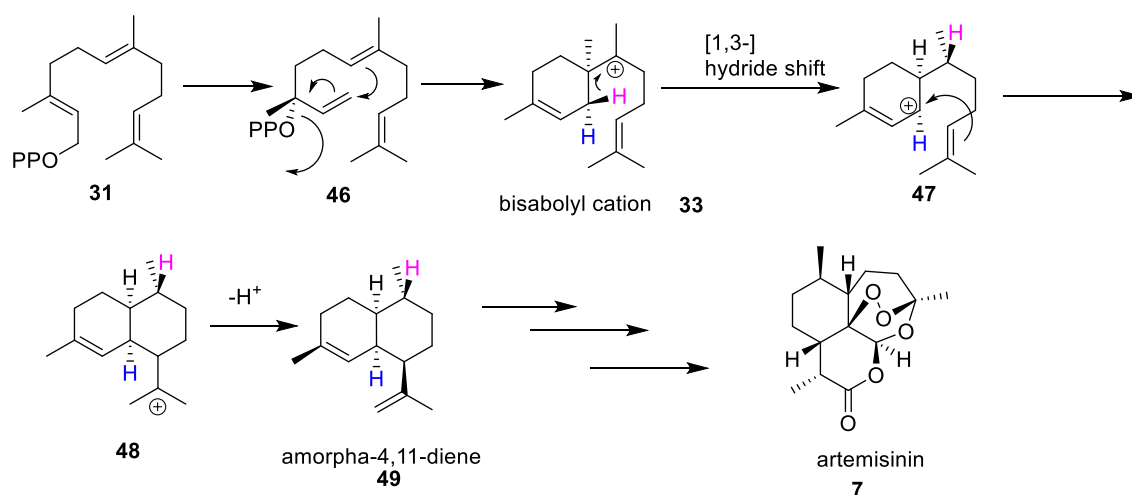
Scheme 1.6 ADS catalysed formation of amorphadiene, key intermediate in the biosynthesis of artemisinin

A subsequent hydride shift, a second ring closure and loss of a proton lead to amorpha-4,11-diene (**49**). Picaud and Soon-He performed single and double deuterated FDP experiments to determine the exact mode of action of ADS. GC-MS and NMR spectroscopic analysis of the products showed that only the *pro-S*-H on C1 of FDP is transferred on C6 during the 1,3-hydride shift while the *pro-R*-H remains at C1. [21] This outcome is also consistent with the initial 1,6-cyclisation, because in the case of an initial 1,10-cyclisation (e.g. aristolochene biosynthesis) and a following 1,3 hydride shift, the deuterium incorporated would have been found at C11 instead. [20]

The ability of ADS to convert GDP into a series of monocyclic monoterpenes supports the presence of the bisabolyl cation in amorphadiene biosynthesis (Figure 1.9), [59] as these compounds can be biosynthesised only though a 1,6 cyclisation closure.
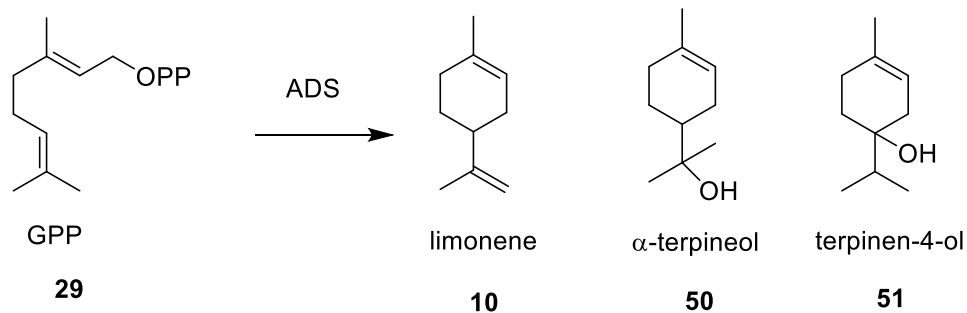
Figure 1.9 Products arising from ADS catalysed cyclisation of GPP.

1.6.3   δ-Cadinene Synthase (DCS)

δ-Cadinene synthase (DCS) (Figure 1.10) was isolated from the cotton tree (*Gossypium arboreum*) where it catalyses the cyclisation of FDP to the bicyclic product (+)-*δ*-cadinene (DCN).[60] The formation of (+)-*δ*-cadinene is the first committed step in the biosynthesis of gossypol (**15**), a phytoalexin produced by the plant as a defensive chemical against bacterial and fungal pathogens. [61,62]
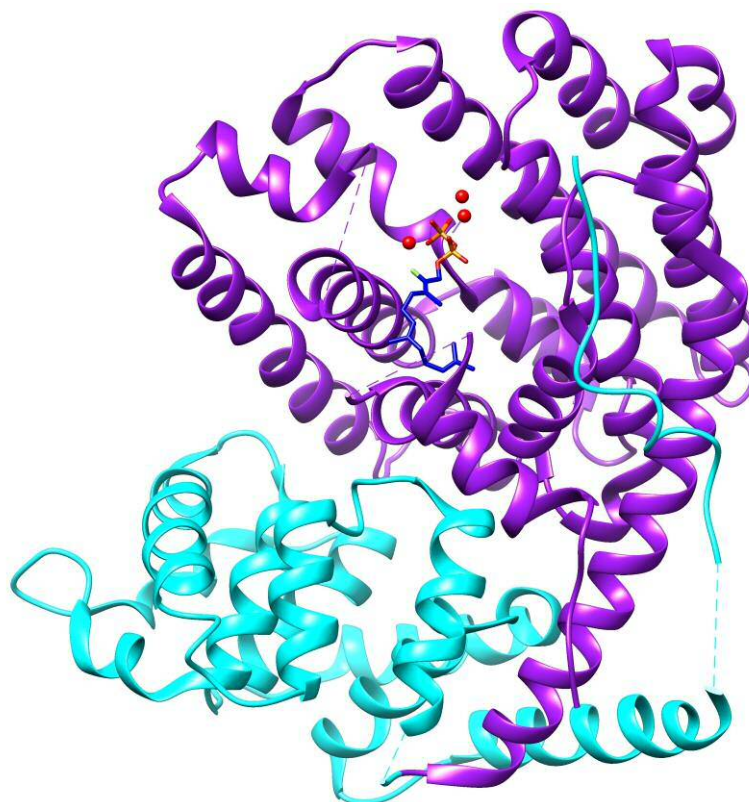
Figure 1.10 Ribbon representation of the crystal structure of DCS complexed with 2F-FDP (3g4f.pdb). Cyan: N-terminal domain; Purple: C-terminal domain. Red spheres: Mg+ cations. 2F-FDP: C = blue, O = red, P = yellow, F = green.

The catalytic domain is situated in the C-terminal subunit and it adopts an α-helical fold, typical of class I terpene synthases. It contains the conserved aspartate rich motif D^{307}DTYD^{311} on helix D. However, DCS is a unique sesquiterpene synthase as

it does not contain the characteristic NSE/DTE Mg^{2+} binding motif, but instead has a second aspartate rich motif $D^{451}DVAE^{455}$ on helix H.

Usually the NSE/DTE motif is a sign of distinction between terpenes synthases and chain elongation synthes, such as farnesyl diphosphate synthase. Consequently, the metal binding motif of DCS makes this cyclase unmatched in its genre. [31]

The first 250 amino acids of the β-domain form the N-terminal domain, of which the first 30 amino acids are involved in the active site closure.[31] In fact, although no catalytic activity seems to happen at the N-terminal segment, recent work from V. Gonzalez and colleagues demonstrated that this domain is essential for catalysis: [29] they showed that when the first 30 residues were removed from DCS, the catalytic efficiency of the cyclase was severely compromised.

Aspartate rich motif studies

To confirm the critical role of both aspartate rich motifs in metal binding, H. Gennadios *et al.* performed mutagenesis studies of DCS. [31] To test the $D^{307}DTYD^{311}$ motif, DCS-D307A, D308A, and D311A, were produced. Although all mutants produced DCN as the single product, it was impossible to determine kinetics data for D308A and D311A while D307A had a k_{cat} of 0.012 ± 0.001 s^{-1} and a K_M of 43 ± 16 μM, a very high value when compared with the wildtype K_M (3.2 ± 0.5 μM). This outcome is consistent with the theory that the aspartate rich motif is involved in the Mg^{2+} binding, essential for activating the diphosphate group and initiating catalysis. To investigate the importance of the unique second aspartate rich motif $D^{451}DVAE^{455}$, D451A, D452A and E455A mutants were designed. In this case, the first two mutants showed an activity comparable to the wildtype enzyme, while E455A mutations resulted in a very slow turnover. These experiments suggest that the second aspartate-rich motif in DCS may have a variable influence on the catalytic efficiency of this enzyme (Figure 1.11 and Table 1.2).
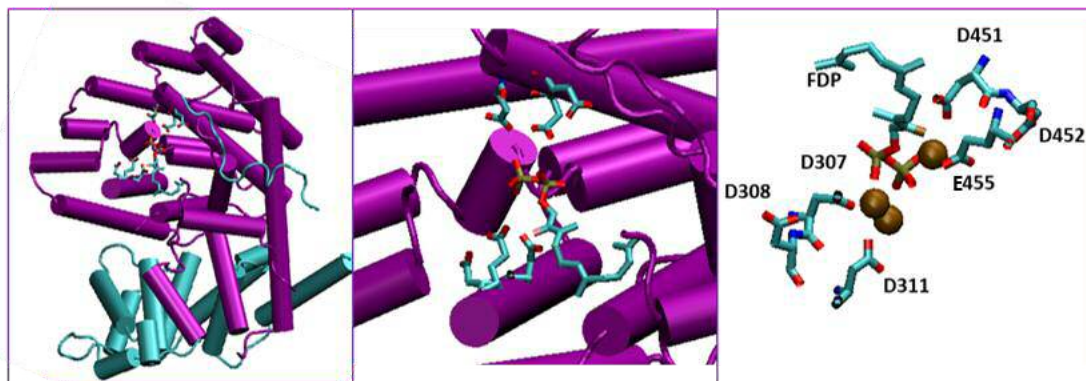
Figure 1.11 Left: cartoon representation of the co-crystal structure of DCS and FDP (3g4f.pdb), residues of interested are shown. Centre: zoom of the active site. Right: residues that were the object of the Gennadios studies.[31] Mg^{2+}: brown spheres. C=cyan, O= red, P= gold, N=blue, C-terminus: purple, N-terminus: cyan.

Table 1.2 Kinetics parameter of WTDCS and its mutants. [31] / denotes not measurable

Cyclase	k_{cat} (s^{-1})	K_M (μM)
WTDCS	0.010 ± 0.001	3.2 ± 0.5
DCS_D307A	0.012 ± 0.001	43 ±1 6
DCS_D311A	/	/
DCS_D308A	/	/
DCS_D451A	0.043 ± 0.001	2.4 ± 0.3
DCS_D452A	0.014 ± 0.001	3.1 ± 1.2
DCS_E455A	/	/

Mechanistic studies

Numerous scientists have attempted to fully elucidate the catalytic mechanism of DCS. Alchanati *et al.* suggested that nerolidyl dipshosphate (**46**), is an intermediate in the cyclisation of the natural substrate FDP into DCN. Incubation of DCS with the labelled substrate [4,4,13,13,13-^{2}H]-NDP (**^{2}H-46**) leads to the formation of [8,8,15,15,15-^{2}H]-DCN (**^{2}H-55**) (Scheme 1.7).[63]
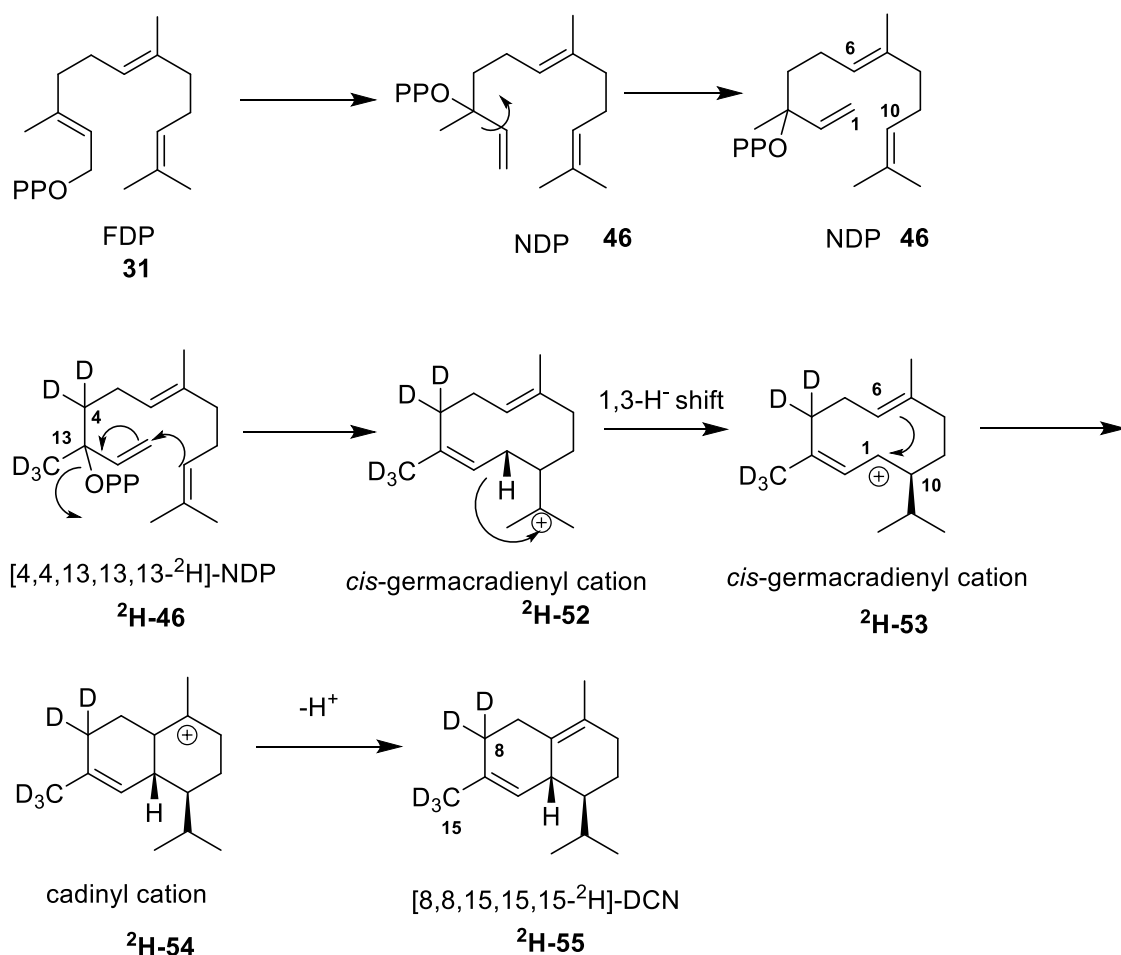
Scheme 1.7 Formation of the enzyme bound intermediate NDP (46, top) and DCS catalysed cyclisation of [4,4,13,13,13-²H]-NDP (46, bottom).

The mechanism proposed by Alchanati is shown in Scheme 1.7. The enzyme bound intermediate NDP (**46**) allows rotation about the C2,C3 σ-bond to secure the required optimal orbital alignment for a 1,10 ring closure to form the *cis*-germacradien-11-yl cation (**52**). After cyclization, a 1,3-hydride shift from C1 to C11 relocates the charge within the macrocycle giving rise to a relatively more stable cis-germacradien-1-yl cation (**53**). Subsequent 1,6-ring closure yields (+)-δ-cadinyl cation (**54**) and then δ-cadinene (**²H-55**) after loss of a proton at C6.

On the other hand, Arigoni suggested that the formation of DCN could also occur via the mechanism shown in Scheme 1.8, where there is no formation of the enzyme bound NDP. In this alternative pathway, a 1,10-cyclisation closure occurs via a direct displacement of the diphosphate moiety to yield the *trans,trans*-germacradienyl cation **56**, which then forms the key intermediate germacrene D (**57**) after a hydride

shift and deprotonation at C-13. [64] Then, a conformational change of **58** leads to its more reactive *trans*-conformer which is protonated at C13 to generate DCN.
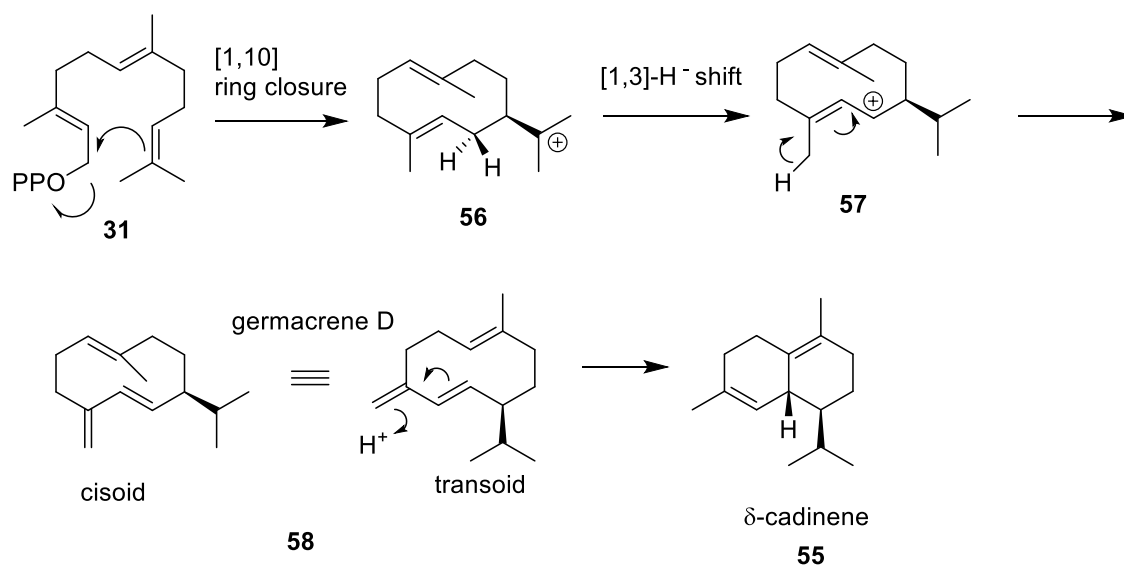
Scheme 1.8 Alternative catalytic mechanism of DCS proposed by Arigoni via germacrene D.

However, it is important to note that in the experiment conducted by Alchanati there is no loss of deuterium from the C13 of NDP, as no [8,8,15,15-^{2}H]-DCN was formed. This excludes the formation of the intermediate germacrene D during enzyme catalysis as suggested by Arigoni, and it is consistent with previous work by Davis *et al.* who reported no detection of ^{3}H-germacrene D during the conversion of ^{3}H-DCN into the phytoalexin 2,7-dihydroxycadalene (DHC).[65] Thus, the pathway depicted in Scheme 1.8 can be ruled out from the possible mechanisms used by DCS.

In addition, Benedict *et al.* confirmed the ability of DCS to turn over the compound NDP into DCN. Analysis of the labelling pattern of DCN formed from the deuterated FDP led to the conclusion that both (*E,E*)-FDP and (3*RS*)-NDP were equally used in the formation of DCN. These experiments also demonstrate that the (3*R*)-NDP is the only active enantiomer cyclised by DCS. [66]

The cyclisation of (3*R*)-[4,4,13,13,13-^{2}H]-NDP (**^{2}H-46**) to [8,8,15,15,15-^{2}H]-DCN (**^{2}H-55**) clearly supports the mechanism proposed by Alchanati and the formation of a cisoid allylic cation-diphosphate anion pair (**59**) which can undergo a 1,10 cyclisation. Furthermore, the capability of DCS to cyclase NDP into three more products: β-farnesene (**63**), α-bisabolol (**61**) and β-bisabolene (**62**) was demonstrated. β-Farnesene would arise from a deprotonation of **59**, while the formation of β-bisabolene and α-bisabolol introduced the possibility of the

intervention of the α-bisabolyl cation (**60**) during the cyclisation, therefore making a 1,6-cyclisation mechanism possible (Scheme 1.9).
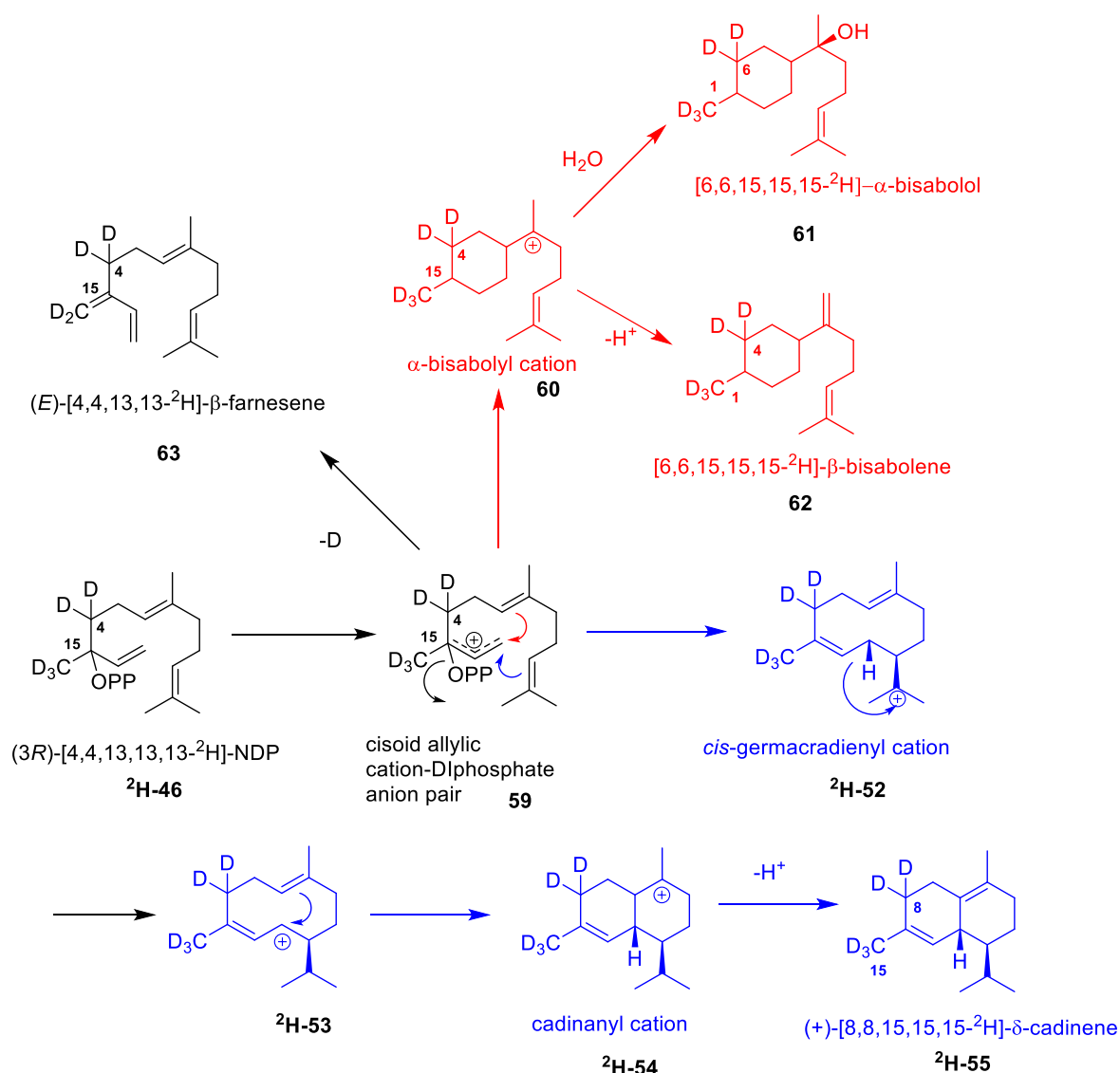
Scheme 1.9 Proposed reaction mechanisms for the cyclisation of [4,4,13,13,13-²H]-NDP proposed by Benedict *et al*. [66]

Faraldos *et al.* investigated the catalytic mechanism of DCS with the use of deuterated and fluorinated FDP analogues. Fluorine containing analogues of enzyme substrates have been shown to be instrumental in mechanistic investigations of terpene synthases, such as tobacco 5-epi-aristolochene synthase (TEAS) [67] and (*E*)-β-farnesene synthase (EBFS).[68] The small size of the fluorine atom does not seem to compromise active site binding, whereas its high electronegativity is known to inactivate fluorine containing double bonds towards protonation of the analogue and electrophilic alkylation. Moreover, the presence of the F is found to destabilise allylic cation intermediates.[69,70]

Enzymatic incubations with C2- and C10-fluorofarnesyl diphosphate analogues (**64**, **65** and **66**) led to the formation of 2F-helminthogermacrene A (**67**), 2F-germacrene A (**68**) and 10F-α-humulene (**69**) respectively as the single product in each case (Scheme 1.10). These results are consistent with the proposed 1,10-closure mechanism (Scheme 1.11, pathway A). In contrast, steady-state kinetic studies demonstrated that 6F-FDP (**70**) was a potent competitive inhibitor of DCS, and no 1,10-macrocyclation-derived products (**71-74**) were formed (Scheme 1.10). This observation is in accordance with the alternative 1,6-closure mechanism (Scheme 1.11, pathway B) since the destabilising effect of the 6-fluoro substituent towards the proposed 1,6-alkylation would cause the inability of DCS to turn over 6F-FDP (**75**).[49]

64

2F-helminthogermacrene A
67

65

2F-germacrene A
68

66

10F-α-humulene
69

DCS inhibition
(k_i= 2.4μM)

70

75

71

72

73

74
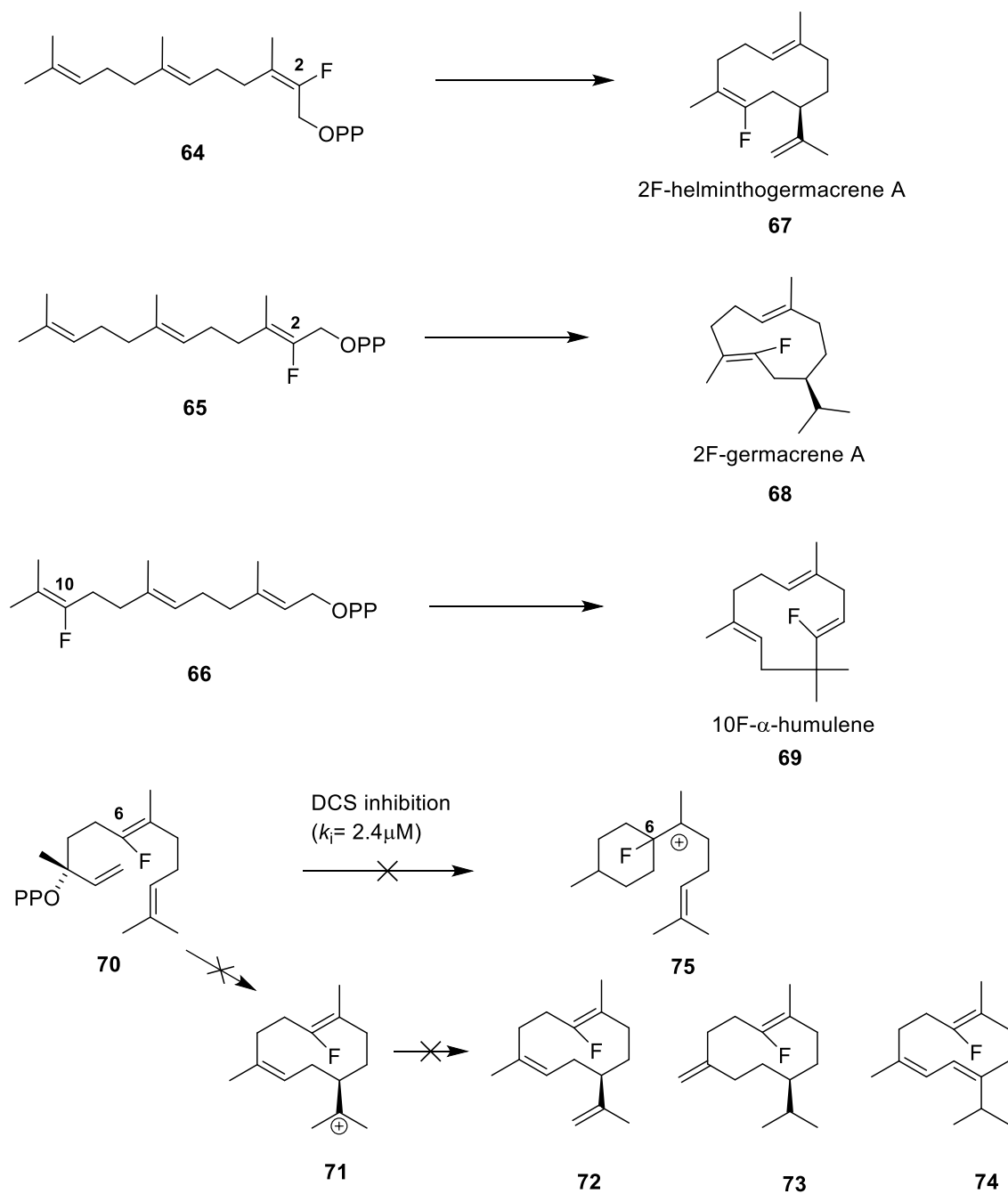
Scheme 1.10 Results of the incubations of fluorine containing FDP analogues with DCS.

31

46

46

1,10-ring closure
pathway A

1,6-ring
closure
pathway B

α-bisabolyl cation
33

[1,3]-H⁻shift

cis-germacradienyl cation
52

[1,3]-H⁻shift

75

[1,3]-H⁻shift

cis-germacradienyl cation
53

[1,5]-H⁻shift

76

cadinanyl cation
54

-H⁺

δ-cadinene
55
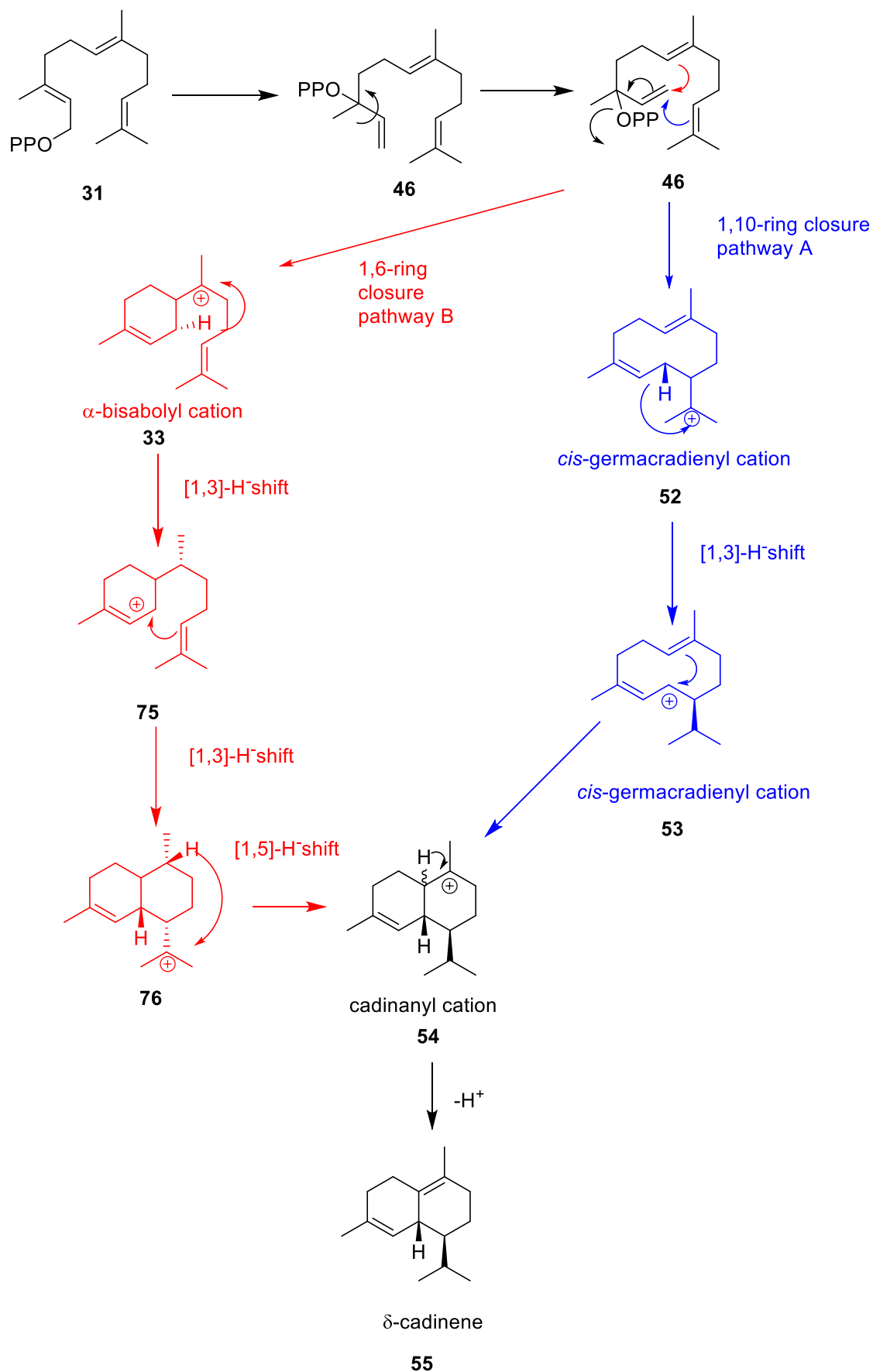
Scheme 1.11 Two possible cyclisation pathways for the formation of DCN. Blue, 1,10 ring closure; Red, 1,6 ring closure.

A. Faraldos *et al.* further investigated the possibility of either a 1,6- or a 1,10-cyclisation with the (2*Z*,6*E*)-FDP (**77**).[49] **77** is viewed as a preisomerised form of (*E,E*)-FDP, hence its ionisation should form a cisoid allylic cation anion pair ready to undergo the 1,10 cyclisation reactions cascade mechanism. GC-MS analysis of the pentane extractable products arising from incubation of DCS with **77** showed the formation of a first fraction corresponding to DCN and a second fraction corresponding to a 3:3:2 mixture of (*Z*)-γ-bisabolene (**78**), β-bisabolene (**59**) and α-bisabolene (**80**) (Scheme 1.12). The presence of these bisabolyl-derivated olefins in the pentane extract can be explained by the intervention of the α-bisabolyl cation in the DCS mechanism, therefore through a 1,6-cyclisation mechanism.
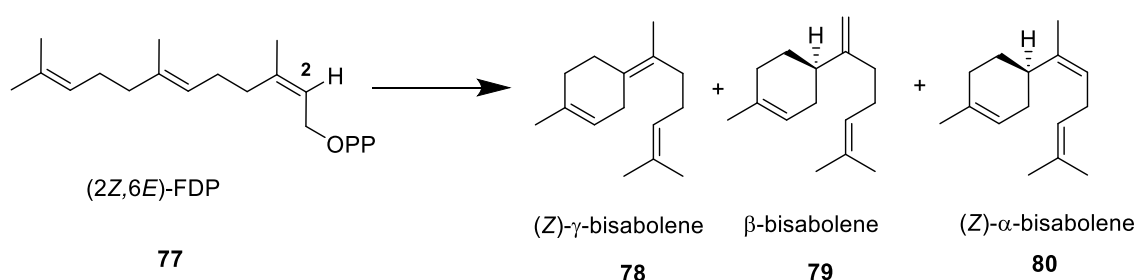
Scheme 1.12 Chemical structures of the products that arose from the incubation of DCS with (2*Z*,6*E*)-FDP.[49]

1.7 Aims of the project

The project is divided into two parts, both designed to investigate the enzymatic mechanism of DCS. The main part is focussed on inhibition studies of DCS with aza-analogues of putative carbocations, while the second part involves mutagenesis studies of the DCS active site. The two aims are described in detail below.

1.7.1 Main aim

Since examination of the catalytic mechanism of DCS using FDP analogues has failed, for the most part, to conclusively uncover the reaction mechanism followed by δ-cadinene synthase, the present investigation aims to provide alternative mechanistic evidence for the DCS-catalysed transformation of FDP to *δ*-cadinene, and hence, support either the 1,6- or 1,10-cyclisation mechanisms depicted in Scheme 1.11 (pathway B and A, respectively). The intrinsic cationic chemistry of terpene synthases makes the direct study of their mechanisms difficult. Although the highly unstable carbocationic intermediates cannot be isolated, it is possible to replace the sp^2 hybridised carbocationic carbon of a given carbocation or proposed

intermediate with a sp^3 hybridised nitrogen atom or a sp^2 hybridised iminium ions. Although the tetrahedral tertiary ammonium ions are inherently imperfect geometric analogues of the planar carbocations, these aza-terpenoids are thought to mimic the topological and electrostatic properties of carbocations generated by these enzymes. However, since they cannot be processed (turned-over) by the enzyme, they often act as tightly bound competitive (i.e. targeting the active site) inhibitors of terpene synthases. Several examples of the use of these type of analogues are reported in the literature. [45,71–76]

D. E. Cane and G. Yang have examined the reaction mechanism of trichodiene synthase, a sesquiterpene synthase responsible for the cyclisation of FDP in trichodiene. They performed inhibition studies of the synthase by the ammonium ion derivatives (*R*)- and (*S*)-**60** (Figure 1.12), which are thought to resemble the carbocation **33**, designed to be an intermediate in the cyclisation mechanism catalysed by trichodiene synthase.

(*S*)-   (*R*)-

aza-analogues of
α-bisabolyl cation

60

α-bisabolyl cation

33
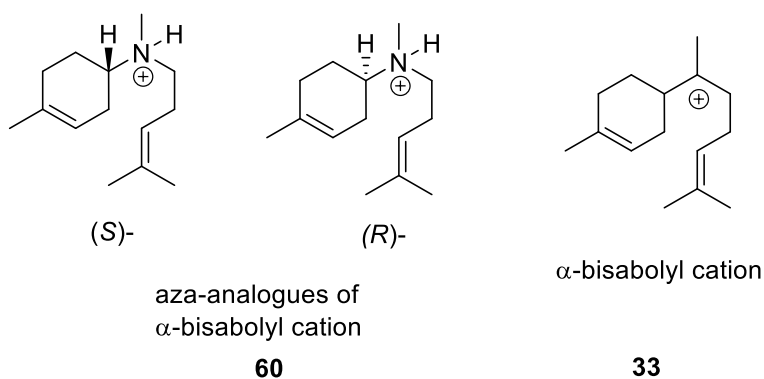
Figure 1.12 Chemical structures of the aza analogues used by D.E and G. Yang.

For the given enantiomeric aza analogues **60**, there was little discrimination by trichodiene synthase. In fact, both **(*R*)-** and **(*S*)-60** act as effective competitive inhibitors of trichodiene synthase, with a K_i of 0.51 ± 0.07 μM and 0.47 ± 0.07 μM respectively. These values are similar to the Michaelis-Menten constant K_M= 0.33 ± 0.04 μM for the natural substrate FDP, supporting the intermediacy of the proposed bisabolyl cation in the biosynthesis of trichodiene.

Another clear example of the use of aza-analogues to define the mechanistic mode of terpene synthases is the work of A. J. Faraldos *et al.* which helped elucidate the mechanism of AS through the use of aza-analogues of the putative intermediate

eudesmane cation. To confirm the existence of the eudesmane cation (Figure 1.13, **53**) as an intermediate in the biosynthetic pathway, the aza-analogues of **53** were synthesised (Figure 1.13, **81** and **82**). Inhibition studies with **82** indicated that this iminium salt is a potent competitive inhibitor of AS, with a K_i=0.35 ± 0.12 µM similar to the Michaelis-Menten constant K_M= 0.53 ± 0.21 µM. On the other hand, the abilities of iminium **81** to bind to the enzyme were more difficult to determine due to its elevated inhibition constant (K_i = 219 ± 17µM). These results indicated that the aza-analogue **82** is a good mimic of **53**, and support the intermediacy of eudesmane cation in the AS catalysis.[44]

eudesmane cation

42

imminium ions resembling eudesmane cation

81   **82**
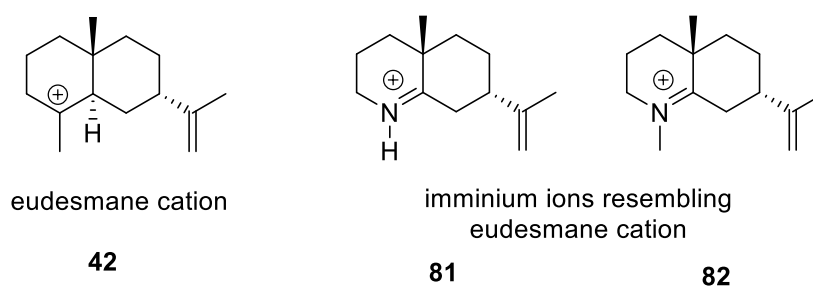
Figure 1.13 Structure of eudesmane cation and its aza-analogue.

Another example of the use of aza-analogues is seen in Taton's work where he and co-workers designed a series of nitrogen-containing compounds as analogues of the putative carbocations involved in the mechanism of the two plant enzymes 2,3-oxidosqualene cyclase (OSCC) and 2,3-oxidosualene-β-amyrin cyclase (OSβAC). Inhibition studies with these analogues showed that the compound **83** acted as a strong competitive inhibitor of the two enzymes, therefore, supporting the existence of carbocation **84** as the intermediate in the formation of oxidosqualene (Figure 1.14).[75]

oxidosqualene carbocation
aza-analogue
83

oxidosqualene cabocation
84
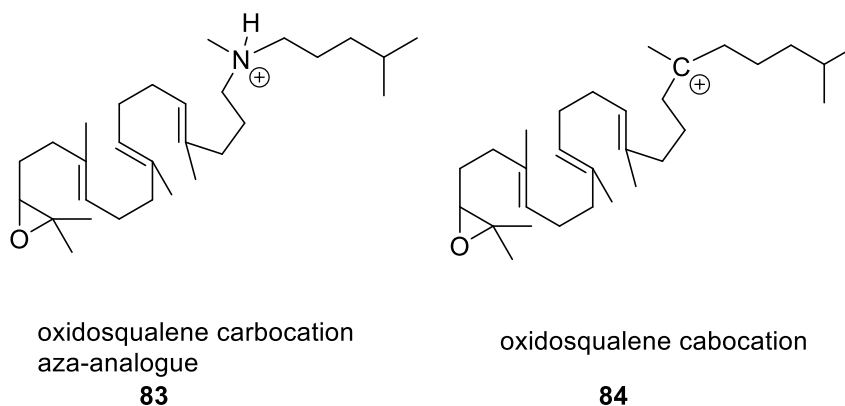
Figure 1.14 Chemical structures of the oxidosqualene carbocation thought to be involved in the synthesis of oxidosqualene, and its aza analogue.

Based on these considerations, the use of strategically designed aza-analogues should allow the disentanglement of some of the possible reaction mechanisms proposed for DCS. For example, if bisabolyl cation **33** is a reaction intermediate *en route* to δ-cadinene (**55**), the corresponding aza-analogue **60** (Figure 1.15) should be a potent competitive inhibitor of DCS. Likewise, the aza-analogue of the cis-germacrenyl cation (**85**) should bind tightly to the active site of DCS if the reaction involves an initial 1,10-cyclisation (Scheme 1.11, pathway A). It was expected that comparison of the inhibition constants and inhibition modes of these aza-analogues would generate conclusive mechanistic insights.

(S)-   *(R)-*

aza-analogues of   aza-analogue of
α-bisabolyl cation   cis-germacradienyl cation
60   **85**
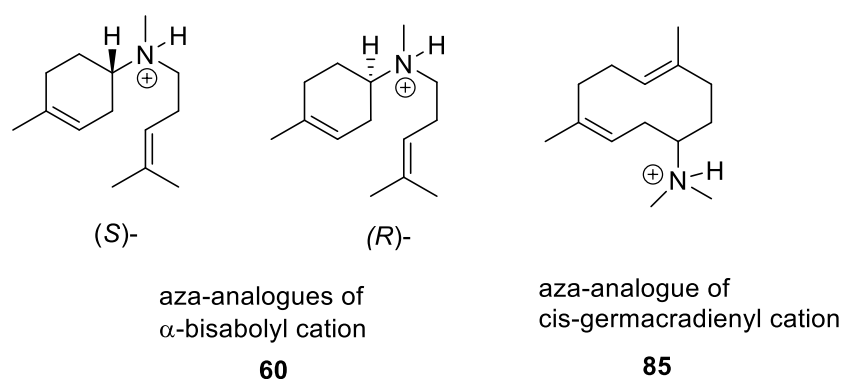
Figure 1.15 Aza analogues of bisabolyl cation and cis-germacradienyl cation targeted as mechanistic probes of DCS.

Therefore, the main objectives of this investigation were:

A) The synthesis of the aforementioned aza-analogues (Figure 1.15). To confirm that the aza-analogues **60** and **85** are good mimics of the putative α-bisabolyl cation (**55**) and cis-germacradienyl cation (**52**) respectively, these aza-compounds will be tested with ADS and AS as controls. As ADS is well known to undergo a 1,6- cyclisation mechanism, **60** will tightly bind the active site and act as potent inhibitors. On the other hand, **60** should not act as competitive inhibitors of AS, as its enzymatic mechanism involves a 1,10-cyclisation, therefore does not involve α-bisabolyl cation. An opposite outcome is expected from the inhibition studies of these two sesquiterpenes using **52**.

B) Kinetic evaluation of the synthesised aza-analogues with DCS after heterologous expression in *E. coli*.

1.7.2 Second aim

The second part of this project focused on defining the catalytic role of residue W279 of DCS. This amino acid was taken into consideration following Yoshikuni's studies of DCS in 2006. [32]

Interestingly, Yoshikuni and co-workers published a study where they explained how they engineered (+)-δ-cadinene synthase to produce germacradien-D-4-ol (GD4ol), a sesquiterpenoid synthetised by the class I sesquiterpene synthase germacradien-D-4-ol synthase from *Streptomyces citricolor,*[77] as the primary product through the error-prone PCR (EP-PCR) technique. Twenty-one clones producing DCN and GD4ol in different ratios were generated and reconstruction of the G-helix of DCS using site-directed saturation mutagenesis led to one specific mutant, DCS_N403P/L405H, which is capable of generating GD4ol *in vivo* up to 93%.

They proposed that the DCS-mediated formation of GD4ol **87** could occur when the active site is not completely shielded from the solvent. Hence, during catalysis, when the cis-germacradienyl cation is formed, instead of a 1,6 cyclisation, the delocalization of the positive charge could trigger a water attack at position 4 and therefore lead to the generation of GD4ol (Scheme 1.13).
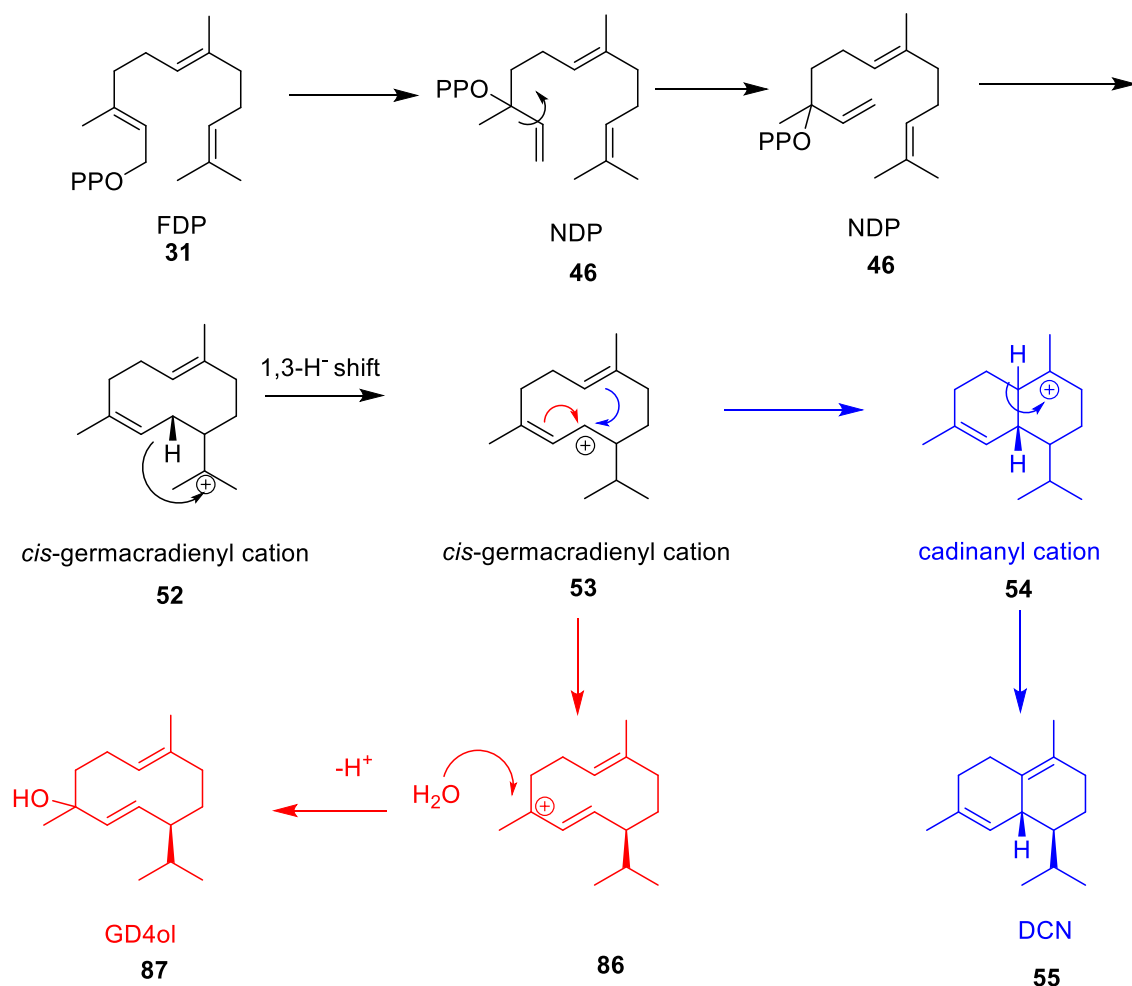
Scheme 1.13 Proposed cyclisation pathway for DCS to form DCN and GD4ol.

In Yoshikuni's investigation every mutation to the DNA that generated an active enzyme of interest occurred at a position coding for an amino acid in or near the G-helix, therefore they concluded that the G-helix plays an essential role in protecting the intermediate carbocation generated during the catalysis from the outer solvent.

Furthermore, the N-terminal domain of DCS in the β-domain has been shown to protect the active site from water, although no catalytic chemistry happens in this domain. In fact, in a study of Gonzalez *et al.*,[29] two truncated DCS variants were created, where the first 8 and 20 amino acids of the β-domain were deleted. Although the sesquiterpene synthases retained a reasonable enzyme activity, an increasing amount of GD4ol produced was observed. In addition, when the first 30 residues were removed from DCS, the catalytic efficiency of the cyclase was severely compromised, reaching 75% of the total GD4ol produced. The formation of this hydroxylated compound is likely to be a consequence of a premature quenching by water of the germacradienyl-1-cation (**86**) formed in the active pocket of DCS.

We were intrigued by the fact that no residues in the C-helix were described in Yoshikuni's investigation, probably due to the random saturation mutagenesis technique's limitation itself. Furthermore, there was no crystal structure of DCS available at the time and therefore this study was based on the homology model of DCS based on *epi*-aristolochene synthase from *Nicotiana tabacum*.

Analysis of the crystal structure of DCS, which was obtained by Gennadios and coworkers,[31] showed that Trp 279 is located at the C-helix, close to the G-helix, towards the bottom of the active pocket. Particularly, Trp 279 is oriented through the FPP in the same way as Y410 and L405 (Figure 1.16), two residues involved in the EP-PCR studies previously described[32] which are part of the hydrophobic core responsible for protecting the active site from the outer environment. The role of Trp 279 has not been elucidated yet, although its strategic location within the active site suggests that this residue may be ideally positioned to stabilise the possible carbocation intermediate formed during DCN biosynthesis.
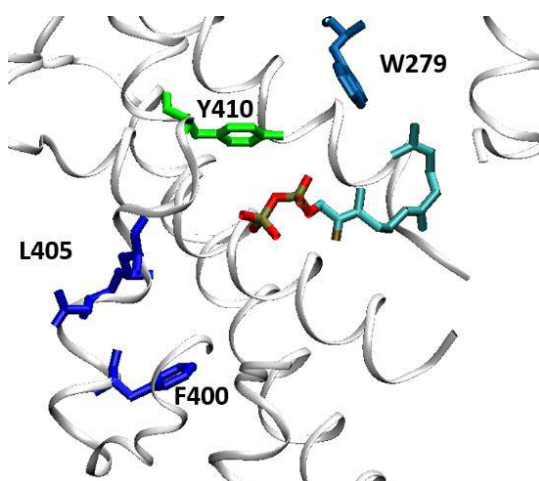
Figure 1.16 Cartoon representation of the DCS crystal structure with 2F-FDP (3g4f.pdb).[31] **Amino acids of interest are shown. 2F-FDP is colored as follows: C: cyan; P: brown; O: red; F: dark brown.**

Hence, lookijng at Yoshikuni and Gonzalez's work, the principle objective of the second part of the project was to investigate the importance and the role of the active-site aromatic residue Trp 279 by using site-directed mutagenesis (SDM) to produce and characterise several DCS_W279 mutants.

CHAPTER 2   Synthesis of Aza-analogues Mimicking the Bisabolyl Cation and the Germacradienyl Cation

2.1 Preface

This chapter describes the synthesis of the aza-compounds designed to be mimics of the proposed carbocationic intermediates in the catalytic mechanism of DCS. Each analogue was designed, synthesised and then used for the mechanistic investigation of DCS. As described in section 1.3.6 of Chapter 1, there are two mechanistic pathways that have been proposed for the formation of δ-cadinene (Scheme 2.1). The first pathway (Scheme 2.1, pathway A, blue) involves the formation of the intermediate *cis*-germacradien-11-yl cation (**52**), while the alternative pathway (Scheme 2.1, pathway B, red) involves formation of the α-bisabolyl cation (**33**). Inhibition studies of DCS with aza analogues that mimic the topological and electrostatic properties of two key carbocations involved in the proposed pathways would hopefully help to distinguish between the two possible mechanisms.
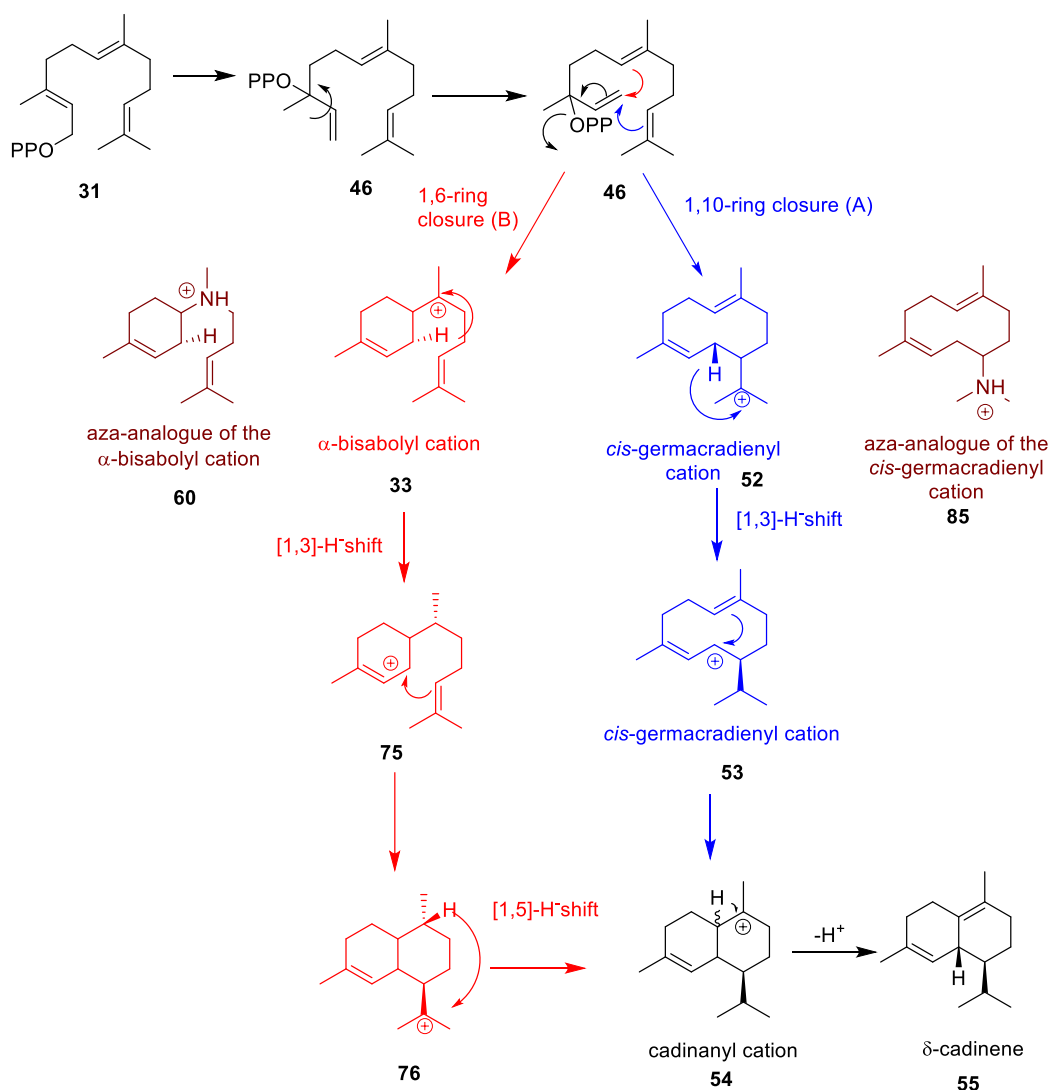
Scheme 2.1 Alternative pathways for the formation of DCN. The two different pathways and respective intermediates are blue and red. Aza-analogues designed to mimic the key intermediates are brown.

2.2 Synthesis of the (*R*)- and (*S*)- aza bisabolyl cations

Both enantiomers of the aza-analogue of the bisabolyl cation (**60**) have been previously prepared by Coates and co-workers[71] via an 11 step synthesis (Scheme 2.2, red and black).
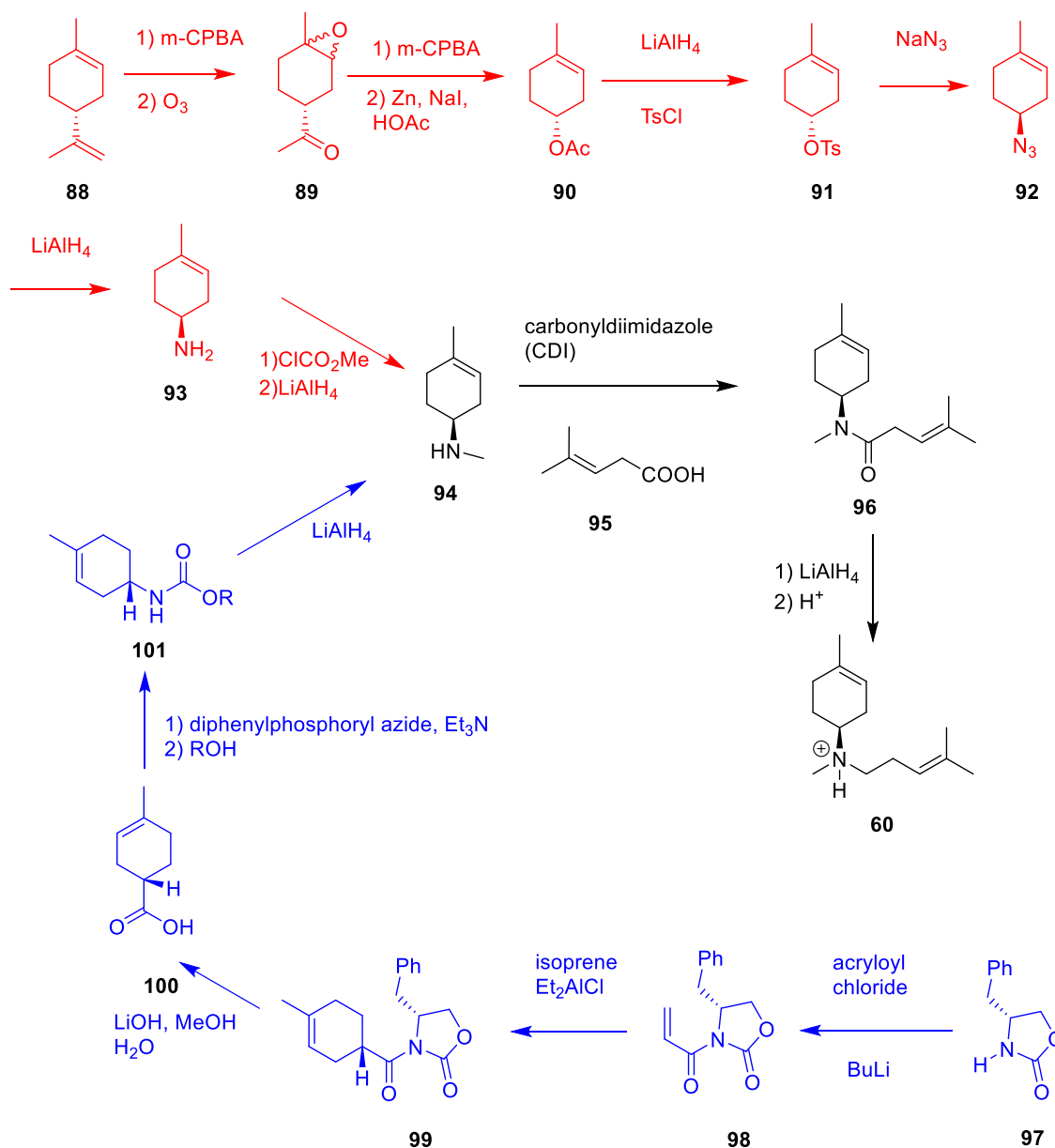
Scheme 2.2 Synthesis of the aza-cation mimicking the intermediate bisabolyl cation. Red: synthetic procedure developed by Coates. Blue: new proposed route. Black: common steps of the two pathways.

The first step of this synthesis is the protection of the cyclohexene double bond of **88** as an epoxide using 3-chloroperoxybenzoic acid (*m*-CPBA), followed by the oxidation with O_3. Following this sequence, a Bayer-Villiger oxidation of the resulting ketone gives acetate **90** after recovery of the cyclo hexene double bond using a combination of Zn and NaI in acetic acid. The acetate group of **90** was then

reduced with LiAlH₄. The resulting alcohol was transformed into a tosylate (**91**) in order to obtain a better leaving group for the next nucleophilic substitution reaction. The nucleophilic substitution of the tosylate **91** by azide proceeds with inversion of configuration, and introduces the nitrogen into the molecule, **92**. Then, a LiAlH₄ reduction followed by acylation and further reduction of **93** yielded amine **94**. The coupling of amine **94** with acid **95** followed by reduction of amide **96** yielded the final compound **60**.

The new synthetic procedures proposed in this work for the synthesis of the enantiomeric **(S)-** and **(R)-60** (Scheme 2.2, blue) requires 5 steps to get the enantiomerically pure amine **94**. This new approach involves an initial acylation of (*R*)- or (*S*)-4-benzyloxazolidin-2-one (**97**) with acryloyl chloride to get the chiral auxiliary **98**. The next step is the stereoselective Diels-Alder reaction of **98** and isoprene catalysed by Et₂AlCl (DEAC) in order to obtain the stereochemically pure adduct **99**. Following this, cleavage of the esteric bond yields acid **100,** which after the formation of the acyl azide intermediate, undergoes a Curtius rearrangement, followed by the attack of the alcohol added to the reaction, which should secure the presence of the nitrogen in the molecule and yield carbamate **101**. This is then reduced by LiAlH₄ to give amine **94**. After that, the synthesis finishes with the two same last steps (coupling with the acid **95** and reduction of amide **96**) previously developed by Coates (Scheme 2.2, black). The new proposed synthesis is more concise than that previously reported as it avoids the lengthy and for the most part inefficient protection/deprotection of the cyclohehexene 1,2-double bond of limonene, and the repetition of several LiAlH₄ reductions. Moreover, in the new pathway the use of ozone is avoided.

2.2.1 Optimization of the Diels-Alder reaction

Compound **98** is easily accessible by *N*-acylation of commercially available (*R*) or (*S*)-4-benzyloxazolidin-2-one (**97**) with acryloyl chloride. This reaction is known to occur with a reported 81% yield.[78] However, the best yield obtained in this project was 52%. The main difficulty of this *N*-acylation reaction is the need for absolutely dry conditions due to the use of *n*-butyl lithium (BuLi). In addition, the acyl chloride needed to be freshly distilled in order to obtain relatively high yields. Although these precautions were taken, the yield did not match the literature value.[11]

The second step towards the synthesis of the ammonium salt **60** involved the stereoselective Diels-Alder reaction of chiral auxiliary **98** with isoprene. Et$_2$AlCl,[78] [79] Yb(OTf)$_3$,[80] and AlCl$_3$ were used as catalysts for the [4+2] cyclisation and to promote stereoselectivity. Dichloromethane (DCM), dimethylformamide (DMF), and tedrahydrofuran (THF) were tested as solvents. The results arising from the different reaction conditions are shown in Table 2.1.

Table 2.1 Summary of the Diels-Alder reaction conditions. an= anhydrous.

entry	temperature/ time	solvent	catalyst (eq)	addition of the catalyst (min)	108 yield	108 $\alpha_D{}^{25}$
1	−78 °C, 30 min	an. DCM	Et$_2$AlCl (1.4)	slow (10)	27%	0
2	−78 °C, 30 min	an. DCM	Et$_2$AlCl (1.4)	fast (1)	21%	+72
3	−100 °C, 30 min	an. DCM	Et$_2$AlCl (1.5)	fast (2)	50%	+79
4	0 °C, 20 h	DCM	Yb(OTf)$_3$ (0.045)	slow (15)	/	/
5	r.t. 20 h	an. DCM	Yb(OTf)$_3$ (0.045)	slow (15)	12%	+59
6	0 °C one week	an.THF	Yb(OTf)$_3$ (0.045)	fast (2)	24%	+63
7	−116 °C, 30 min	an.THF	Et$_2$AlCl (1.4)	fast (2)	/	/
8	−100 °C, 30 min	an.THF	Et$_2$AlCl (1.4)	fast (2)	/	/
9	-78 °C, 3 h, r.t. 12 h	an. DCM	AlCl$_3$ (1)	fast (2)	60%	0

While the use of AlCl$_3$ gave rise to racemic Diels-Alder adduct **99** (entry 9, Table 2.1), the use of Yb(OTf)$_3$ gave the desired product only after a considerable amount of time (entry 6, Table 2.1). The use of dry dichloromethane as the solvent and DEAC as the catalyst added quickly at very low temperature [81] (entry 2 and 3, Table 2.1) led to the formation of **99** with excellent stereoselectivity (Figure 2.1, d.e. ≥ 95 and Figure 2.2, e.e. ≥ 95%).
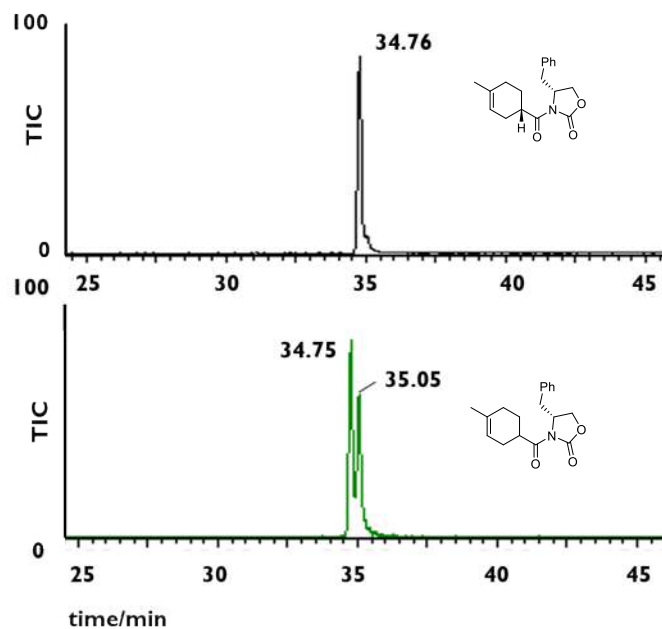
Figure 2.1 Gas-chromatogram of 99. Top: catalyst DEAC. Bottom: catalyst AlCl₃.
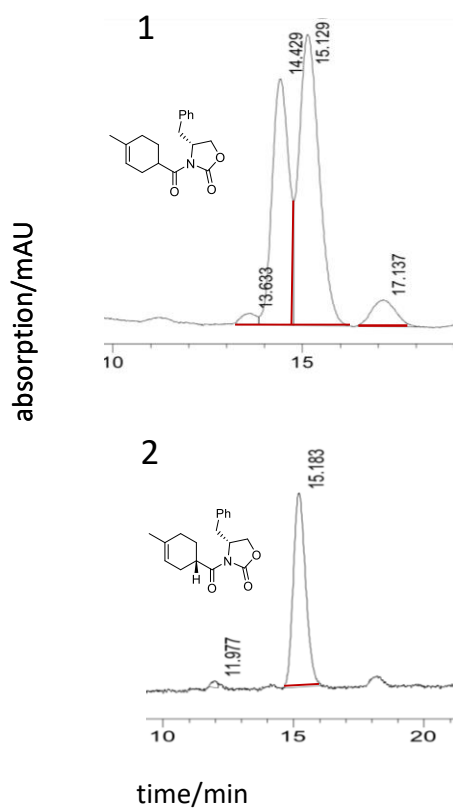
Figure 2.2 HPLC of 99 with chiral colum. Top: catalyst AlCl₃. Bottom: catalyst DEAC.

The reaction mechanism of the [4+2] cyclisation is shown in Figure 2.3 below.
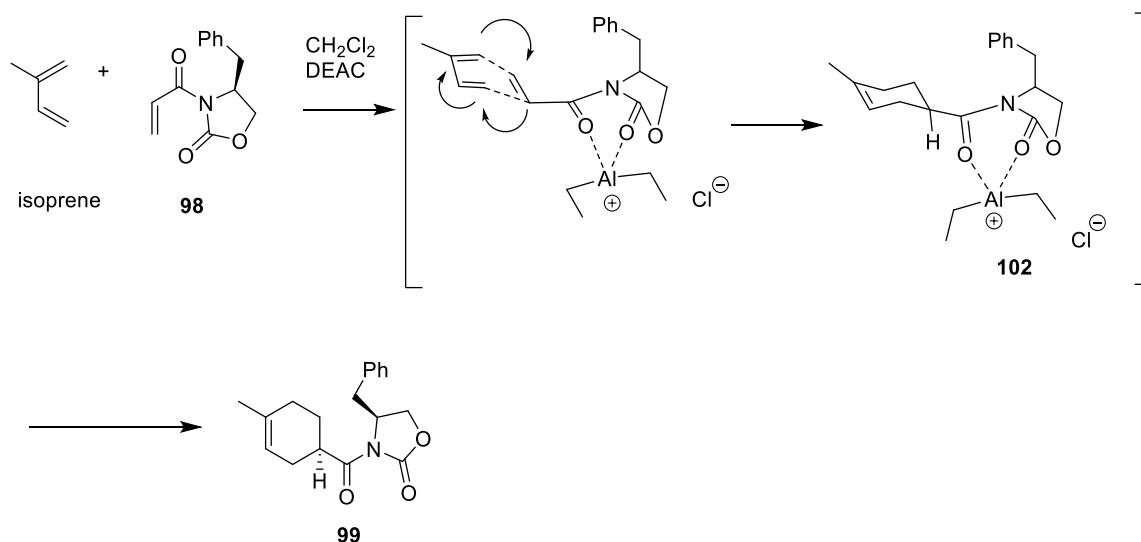
Figure 2.3 Diels-Alder reaction mechanism between 98 and isoprene with the formation of intermediate 102.

Despite several attempts at this reaction, a yield matching the literature value (81%)[79] was not achieved. Hence, to obtain a better yield, alternative methods were explored.

An alternative asymmetric Diels-Alder reaction (Scheme 2.3) can also be performed with very good yield and high d.e. using $TiCl_4$ as the catalyst and chiral pantolactone as the chiral auxiliary.[82,83]
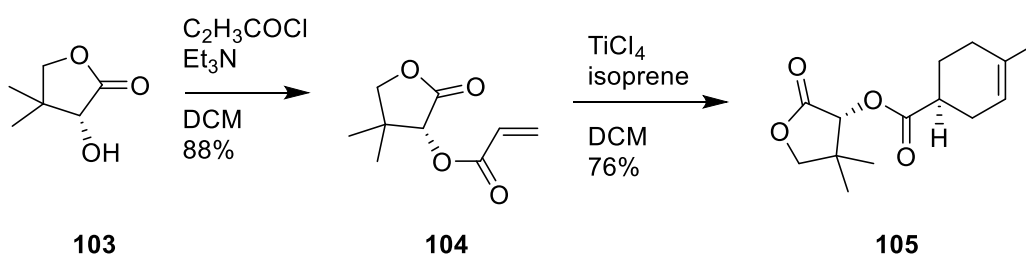
Scheme 2.3 Diels-Alder reaction using *R*-pantolactone (103) as the chiral auxiliary and $TiCl_4$ as the catalyst. [82,83]

This procedure is advantageous because $TiCl_4$ is a less toxic catalyst than DEAC, which generates toxic HCl gas on contact with water, therefore safer to use. Also, the new Diels-Alder reaction is preferable because it is easily controlled due to the relative higher temperatures needed (0 °C).

Although this new procedure appears to be more cost-effective since $TiCl_4$ is a less costly catalyst than DEAC, the *S*-enantiomer of pantolactone was found to be too expensive to be used in this synthesis. Therefore, only the *R*-pantolactone was used

in the synthesis of the *S*-aza-bisabolyl cation and a variety of reaction conditions for its use were screened. The results are summarised in Table 2.2.

Table 2.2 Diels-Alder reaction conditions and results obtained when (*R*)-pantolactone was used as the chiral auxiliary. d.e. = diasterosiomeric excess. Solvent used CH₂Cl₂/hexane 7:1

	TiCl₄ (eq.)	Isoprene (eq.)	T (°C)	Time (h)	Yield (%)	$\alpha_D{}^{25}$ (c=1, CHCl₃)	%d.e.
1	0.15	1.5	−24	5	/	/	/
2	0.1	4	−24	48	10	-49	99
3	0.1	3	−10	5	84	-51	97
4	0.5	1.3	0	3	80	/	/
5	0.1	3	−10	4	79	/	/

Performing the reaction at −24 °C (Table 2.2 entry 2) gave the Diels-Alder adduct **105** in excellent d.e. (99) but low yield (10%). It was found that by increasing the temperature to −10 °C (Table 2.2, entry 3), the formation of the product **105** was accomplished in high yield (84%) and excellent stereoselectivity, as confirmed by gas chromatography (Figure 2.4, left, d.e.= 97%) and chiral HPLC (Figure 2.5, e.e. = 92%) respectively.
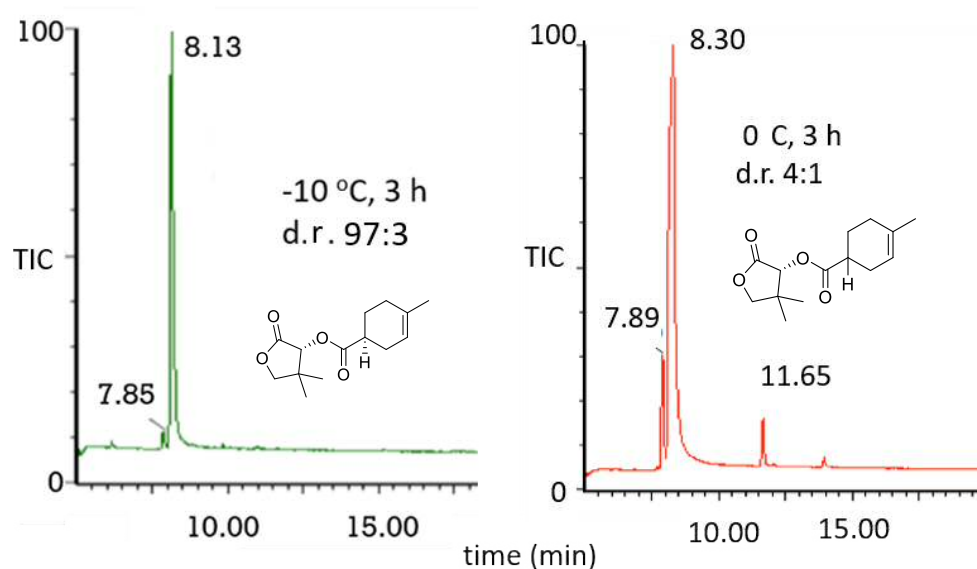
Figure 2.4 Gas chromatogram of Diels-Alder adduct 105 highlighting the formation of a major diasteroisomer. Reaction condition of table 2.2, left: entry 2; right: entry 3. Peak at 11.65 min is an impurity.
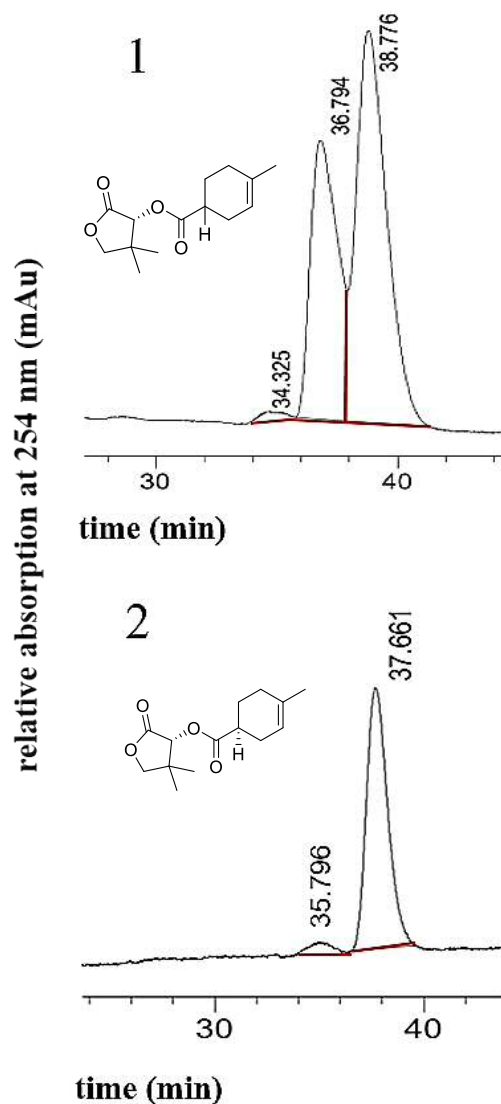
Figure 2.5 HPLC of 105 performed with chiral column. 1: racemic 105; 2: 105 obtained with the use of TiCl₄ at -10 °C (entry 3, table 2.2)

The ^{1}H NMR spectrum (300 MHz, CDCl$_3$) of **105** confirmed its structure, as evidenced by the absence of the doublet of doublets at δ_H = 6.63 and 5.96 ppm, indicative of the vinyl protons of the chiral dienophile **104** (Figure 2.6). Then, a multiplet at δ_H = 2.60 ppm, integrating for 1 proton corresponds to the hydrogen attached to the chiral carbon of the cyclohexene unit, (4, Figure 2.6, bottom) and two singlets at δ_H = 1.12 and 1.04 ppm integrating to 3 each correspond to the two methyl groups of the pantolactone group. Furthermore, a new signal corresponding to vinyl hydrogen of the cyclohexene ring was visible at δ_H = 5.28 ppm.
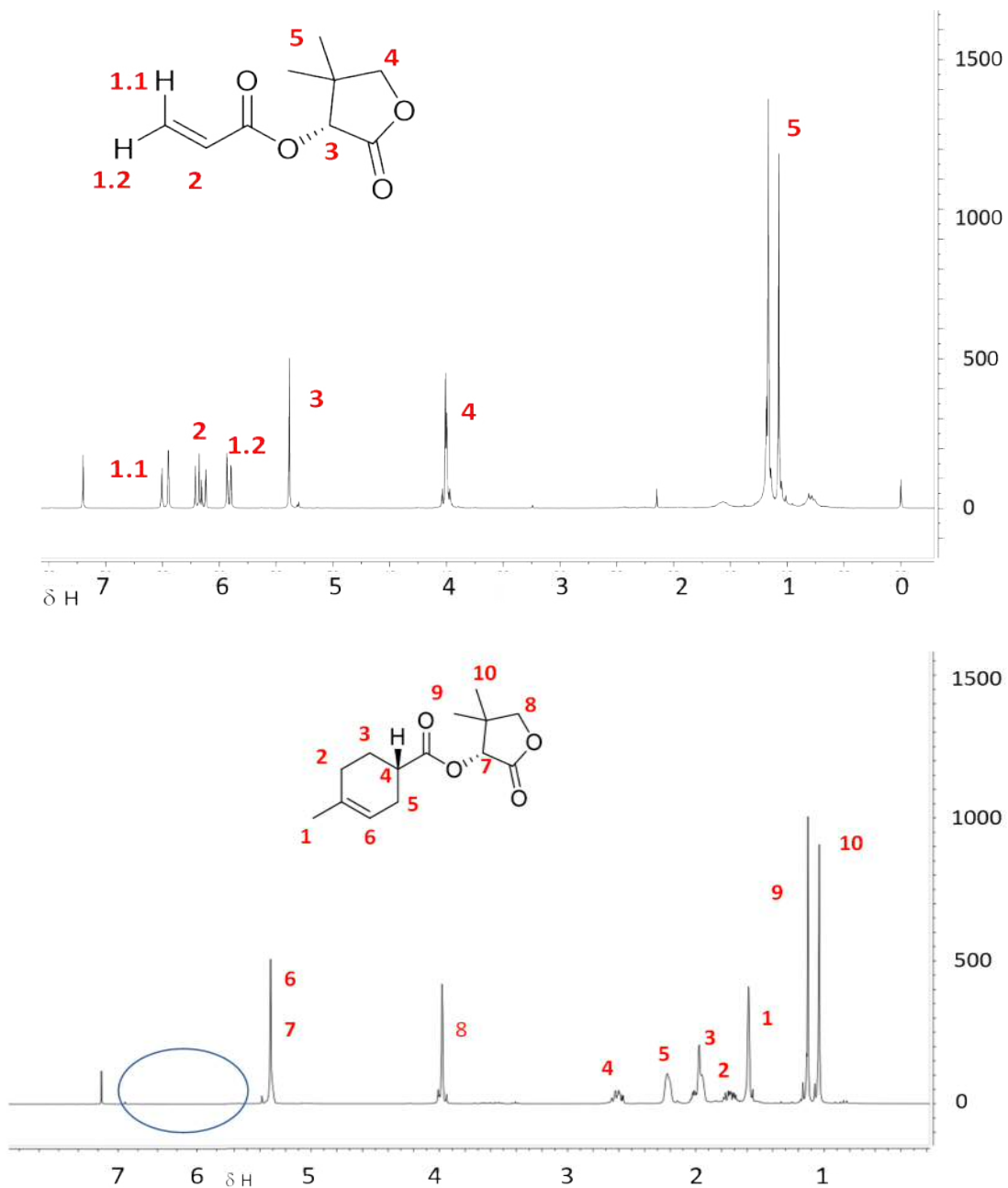
Figure 2.6 ^{1}H NMR spectrum (300 MHz, CDCl$_3$) of (top) 104 and (bottom) 105. The absence of the doublet of doublets indicative of the vinyl protons of 104 is outlined with a blue circle on the bottom spectrum.

2.2.2 Synthesis of methyl cyclohexene carboxylic acid (100)
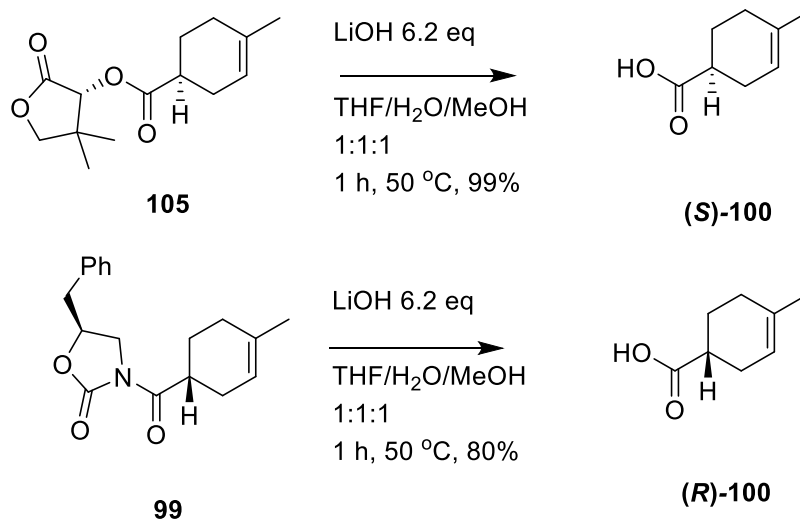
Scheme 2.4 Reaction conditions for the hydrolysis of Diels-Alder adducts 105 and 99.

The next synthetic step involved the saponification of the Diels-Alder adducts to yield acid **100** (Scheme 2.4). Treatment of compound **105** with LiOH (6.2 eq) in a 1:1:1 mixture of MeOH/THF/water for 1 h at 50 °C, followed by an acid/base work up yielded acid **(S)-100** in excellent yield (99%).

As the literature value of the optical rotation for the **(S)-100** with an e.e. of 99.7% is $\alpha_D = -107$ (95% EtOH, c=4)[14], the optical purity of **(S)-100** obtained during this work was 99%. The same saponification procedure was applied to compound **99**, which gave **(R)-100** with a slightly lower yield of 80%, but with an o.p. of 98.5. %

The ^{1}H NMR spectrum (300 MHz, CDCl$_3$) of **100** is in good agreement with data reported by Argenti *et al.* [64] The signal at $\delta_H = 5.32$ ppm corresponds to the vinyl proton of the cyclohexene ring, and a multiplet at $\delta_H = 2.46$ ppm is due to the H attached to the chiral carbon of the cyclohexene ring.
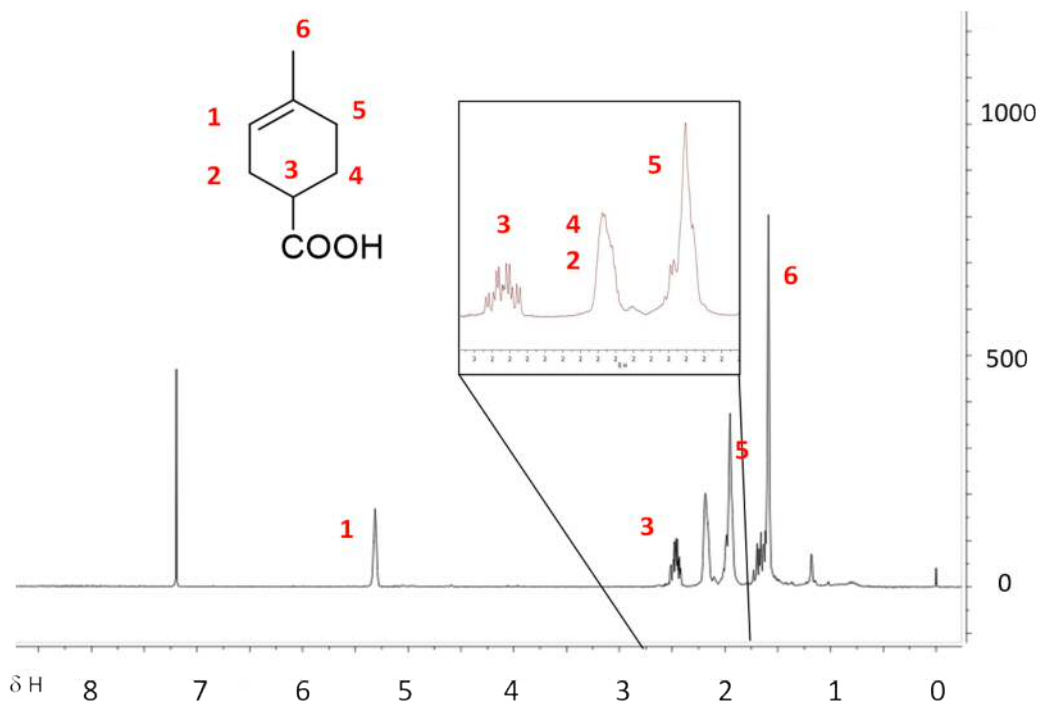
Figure 2.7 ^{1}H NMR spectrum (300 MHz, CDCl$_3$) of 100.

2.2.3 Synthesis of methoxybenzyl carbamate (113)
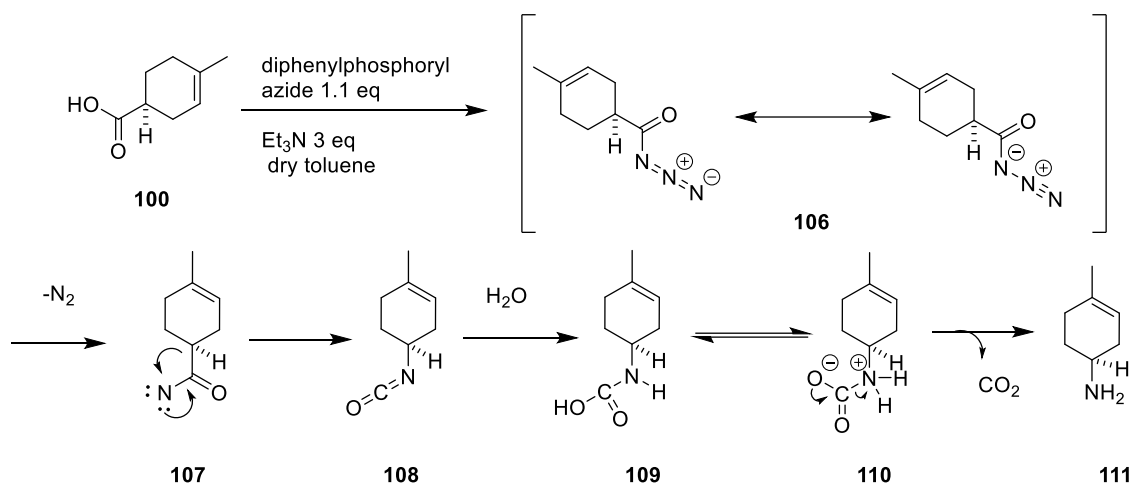
Scheme 2.5 Curtius rearrangement mechanism.
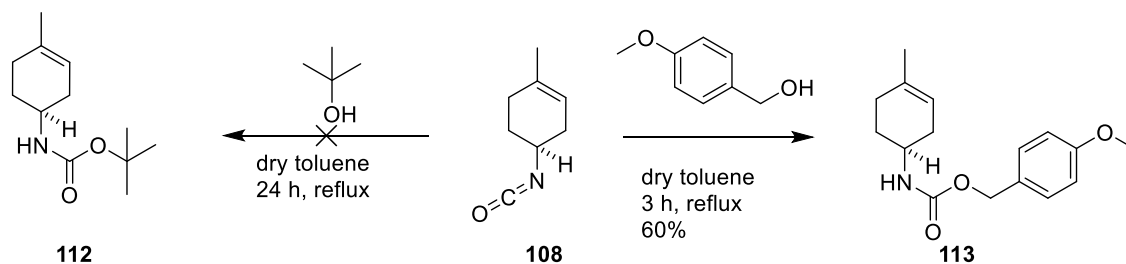
Scheme 2.6 Reactions of isocyanate 108 with *t*-butyl alcohol (left) and *p*-methoxybenzyl alcohol (right) to prevent the formation of amine 111 (scheme 2.5).

The fourth step involves a modified Curtius rearrangement of acid **100** to carbamates **112** or **113** (Scheme 2.5 and 2.6) This process introduces a nitrogen at the required position as a carbamate and will be positively charged in the final compound (**60**, Scheme 2.2). As shown in Scheme 2.5, the classic Curtius rearrangement yields *in situ* a highly unstable isocyanate **108**, which hydrolyses in the presence of water to carbamic acid (**109**). On warming, **109** decomposes to amine **111** and CO_2. The beauty of this reaction is that water can be replaced by an alcohol (p-methoxybenzyl alcohol or t-butyl alcohol in this case) to produce a stable carbamate. The fundamental mechanistic difference between our strategy for the introduction of the nitrogen into the target molecule and the approach used by Coates (S_N2 displacement of secondary tosylate),[71] is that this modified Curtius rearrangement preserves the original stereochemistry of the carboxylic acid used as the starting material, thus avoiding possible racemisation events that may occur in Coates synthesis as a consequence of possible mixed S_N1 and S_N2 displacements of tosylate **91** with an azide anion (Scheme 2.1, pathway A). The retention of stereochemistry in the Curtius rearrangement is possible because the sp^3 orbital of the migrating carbon migrates to one orbital to the other with a minimum amount of structural reorganisation: as it happens in 1,2- migration reactions, the large lobe of the sp^3 orbital is used so the new bond formed is on the same face of the migrating group, and therefore the stereochemistry is conserved.

The procedure first required reaction of carboxylic acid **100** with diphenylphosporyl azide (DPPA) in the presence of Et_3N at 110 °C for 3 h. As a result, an unstable isocyanate (**108**) formed by migration of the *exo* chiral alkyl group to the electron deficient sp-hybridised nitrogen atom of intermediate **107**. Initially, *t*-butyl alcohol was used as the nucleophile to trap the isocyanate *in situ* and protect the amine as a urethane (Boc-group) (**112**, Scheme 2.6). However, 24 h after addition of tBuOH at reflux temperature, TLC analysis of the reaction mixture showed only the presence of the isocyanate intermediate (**108**) which appeared as a red spot when the TLC was stained with CAM (ceric ammonium molybdate) solution. Consequently, 4-methoxybenzyl alcohol was used instead as the nucleophile (Scheme 2.6). TLC analysis in CAM solution of the reaction mixture after 12 h at reflux clearly showed the absence of the red spot corresponding to isocyanate **108** and the presence of a new compound that resulted to be carbamate

113. Purification by flash chromatography gave **113** in 60% yield. The formation of the carbamate was confirmed by ^{1}H NMR spectroscopy (300 MHz, CDCl$_3$) (Figure 2.8). The spectrum shows a triplet at δ_H = 7.22 ppm and a doublet at δ_H = 6.82 ppm corresponding to the aromatic portion of p-methoxybenzyl alcohol and a singlet at δ_H =4.95 ppm corresponding to the CH$_2$ attached to the carbamate group. This signal appears downfield in comparison with the ^{1}H NMR of p-methoxybenzyl alcohol, in which the same CH$_2$ signal appears at δ_H = 4.61 ppm. The singlet at δ_H = 3.74 ppm is due to the CH$_3$ of the methoxy group. Furthermore the multiplet at δ_H = 5.23 ppm corresponds to the vinylic proton, and the singlet at δ_H =1.57 ppm is due to the methyl group attached to the cyclohexene ring. Unresolved multiplets between 2.4-1.70 ppm correspond to the protons within the cyclohexene. The proton attached to the chiral centre in the ring also appears as an unresolved multiplet at δ_H = 2.3 ppm (Figure 2.8).
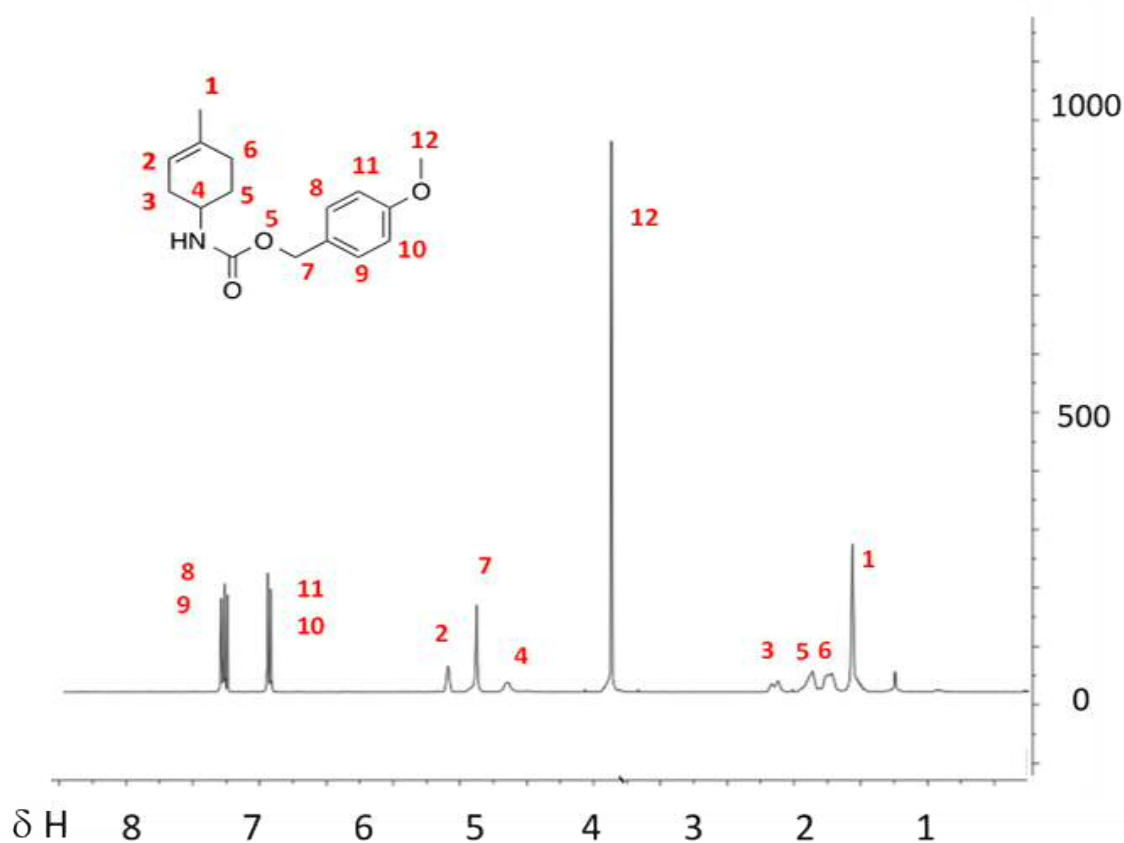
Figure 2.8 ^{1}H NMR spectrum (300 MHz, CDCl$_3$) of 113.

2.2.4 Synthesis of dimethylcyclohexenamine (94)
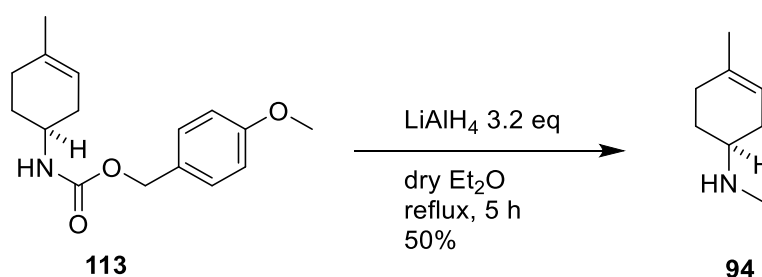
Scheme 2.7 Synthesis of 94.

Reduction of **113** with LiAlH$_4$ afforded the amine **94** in a modest yield. Due to the high volatility of amine **94**, some precautions, such as performing the work up at 0 °C, were necessary during the purification step by acid/base extractions. Also, the concentration *in vacuo* of the resulting etheral extracts after the work up required an unusually low temperature (5 °C). Under these conditions a yield of 50% was obtained for this reaction. The optical purity was 93% for **(S)-94** and 99% for **(R)-94.** The presence of the amine **94** was confirmed by ^{1}H NMR spectroscopy (300 MHz, CDCl$_3$). The signal corresponding to the proton attached to the nitrogen is absent, as it exchanges with the deuterium of the CDCl$_3$. For the same reason the signal at δ_H = 2.36 ppm corresponding to the CH$_3$ group attached to the nitrogen appears as a singlet, and not as a doublet. A multiplet signal at δ_H = 2.52 ppm is due to the proton attached to the chiral carbon. All signals corresponding to the p-methoxybenzyl alcohol are absent (Figure 2.9).
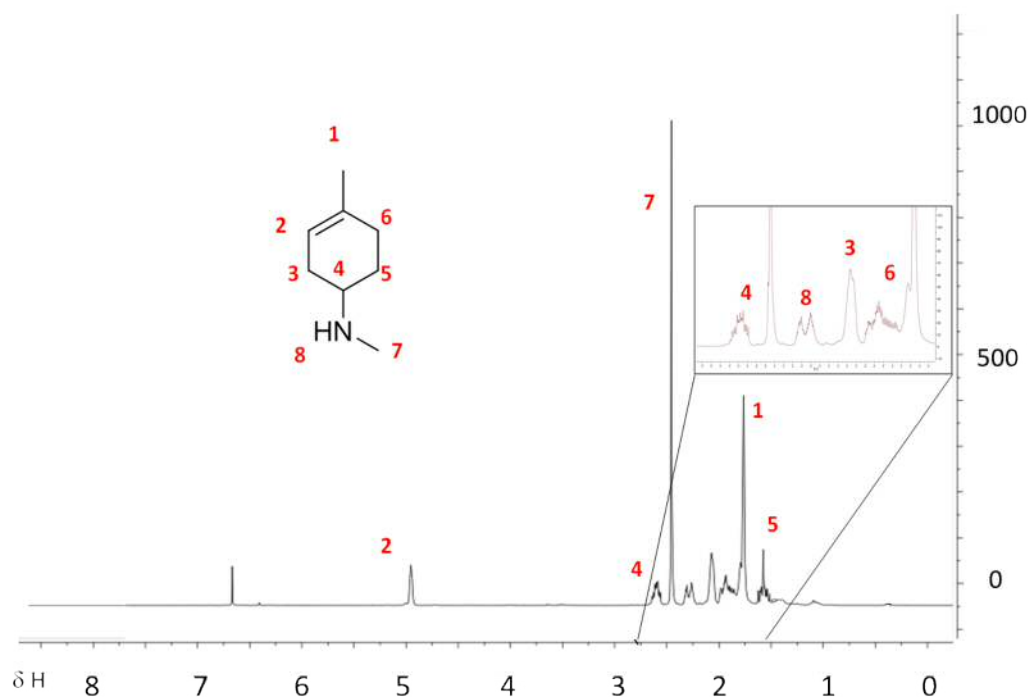
Figure 2.9 ^{1}H NMR spectrum (300 MHz, CDCl$_3$) of 94.

55

2.2.5 Synthesis of 4-methyl pentenoic acid (95)
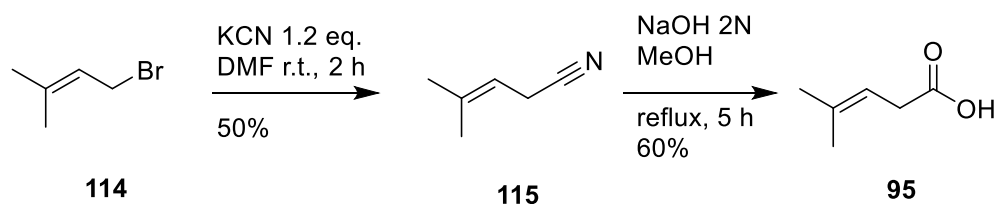
Scheme 2.7 Preparation of 4-methyl pentenoic acid 95.

4-Methyl pentenoic acid **95** was required as coupling partner for methyl amine **94** to generate cyclohexen-pentenamide **96**. It was prepared according to a literature procedure (Scheme 2.7). All the spectroscopy data for the isolated compound were in agreement with previously reported data.[10]

2.2.6 Synthesis of cyclohexen-pentenamide (96)
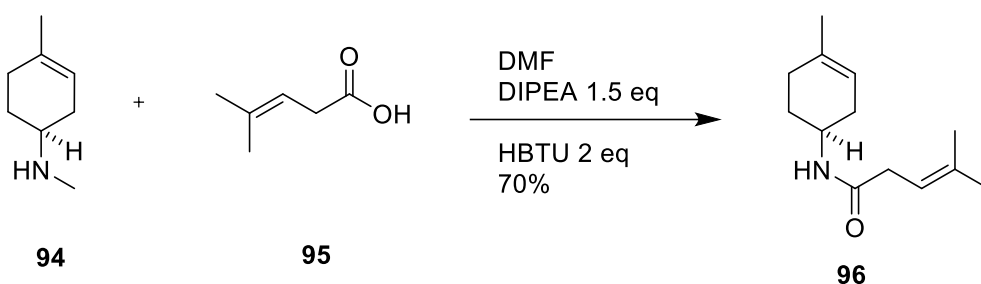
Scheme 2.8 Preparation of amide 96.

The synthesis of amide **96** involves coupling of 4-methyl pentenoic acid **94** with amine **95**. DIPEA and HBTU were used to activate the carboxylic acid towards the nucleophilic attack of amine **95**. The ^{1}H NMR spectrum for the product is complicated due to the slow rotation of the amide bond at room temperature. By ^{1}H-NMR (300 MHz, CDCl$_3$), amide **96** appears as a 1:1 mixture of *syn* and *anti* rotamers, due to a low-energy barrier between *cis* and *trans* configurations typical of amides.[9] The hydrogen on the chiral centre is strongly affected by amide bond rotation, making the two rotamers clearly distinguishable with resonances present at δ_H = 4.27 ppm and 5.03 ppm, both integrating to 0.5H. Likewise, the CH$_2$ group on the amide chain is split into two signals, each integrating to 1H (δ_H = 3.20 and 3.11 ppm). The protons on the methyl group adjoined to the nitrogen atom are also affected by this rotation, giving two singlets at δ_H = 2.10 and 1.95 ppm integrating to 1.5 H. Three

singlets integrating to 3Hs are discernible at δ_H = 1.66, 1.94 and 2.21 ppm corresponding to the three methyl groups not attached to nitrogen. Furthermore, the vinylic hydrogen connected to the cyclohexene ring and the one connected to the pentenamide chain are in chemically similar regions, so they are responsible for the multiplet at δ_H = 5.65-5.67 ppm which integrates to 2 protons (Figure 2.10). The optical purity was found to be 87% for **(S)-96** and 90% for **(R)-96**.
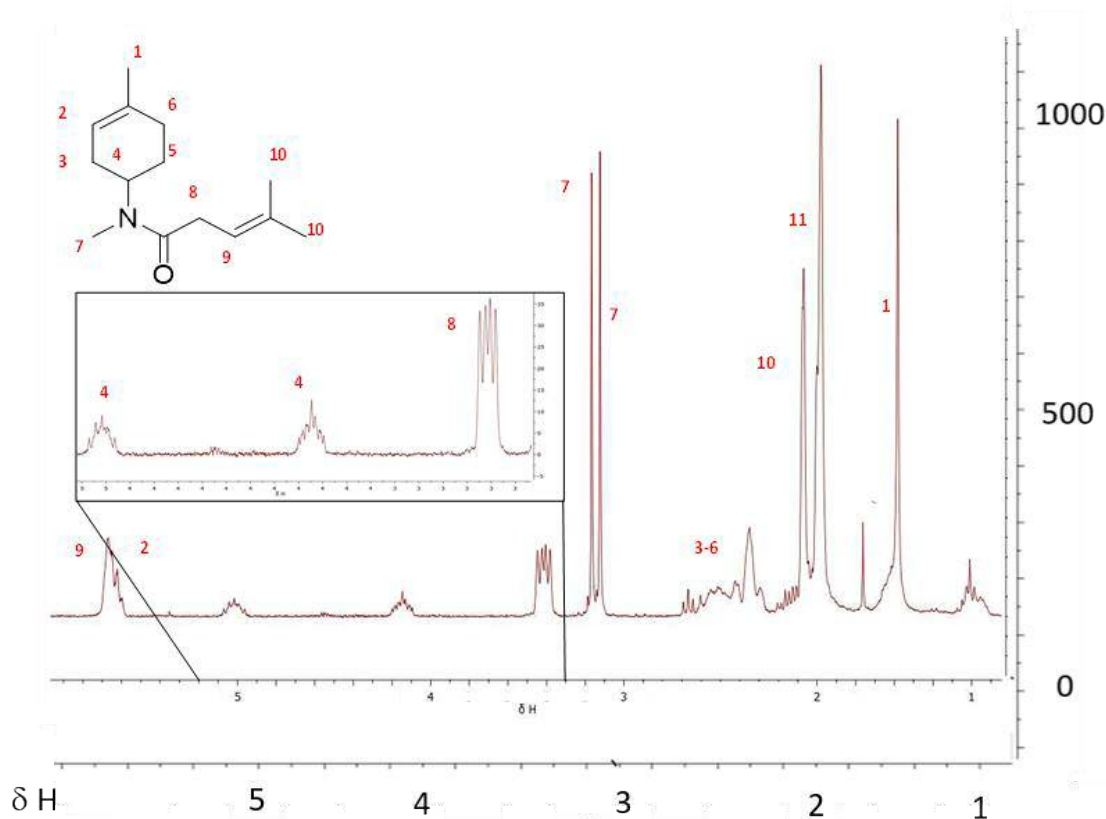
Figure 2.10 ¹H NMR spectrum (300 MHz, CDCl₃) of 96.

2.2.7 Synthesis of bisabolene aza-analogue 60

As for any aliphatic amine, it has been reported that the bisabolyl amine **116** is unstable if stored for long periods. To avoid degradation of **116**, the last step of the pathway was performed only when DCS was purified and tested for activity using its natural substrate farnesyl diphosphate.
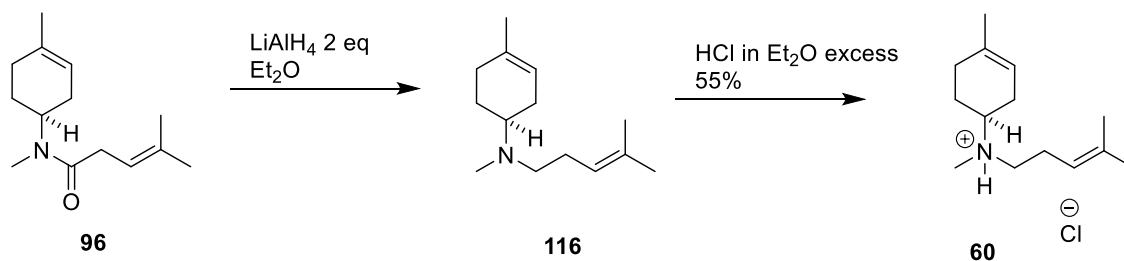
Scheme 2.9 Final preparation of the aza-analogue 60.

The last step of the synthesis of the aza-bisabolyl cation involves the reduction of the ketone group of amide **96** with LiAlH$_4$ to form the neutral **116**. The acid HCl was then used in order to protonate the nitrogen and form the ammonium ion of **60**. The optical purity for neutral **(S)-116** and **(R)-116** was found to be 98% and 99% respectively.

The ^{1}H NMR spectrum (300 MHz, CDCl$_3$) of **116** showed the presence of a triplet signal corresponding to the CH$_2$ next to the nitrogen (Figure 2.11). Furthermore, the ^{1}H NMR spectrum (300 MHz, CD$_3$OD) of **60** (Figure 2.12) clearly showed several downshifted signals when compared with the ^{1}H NMR spectrum of **116** (Figure 2.11) due to the influence of the counterion chloride and the protonated nitrogen.
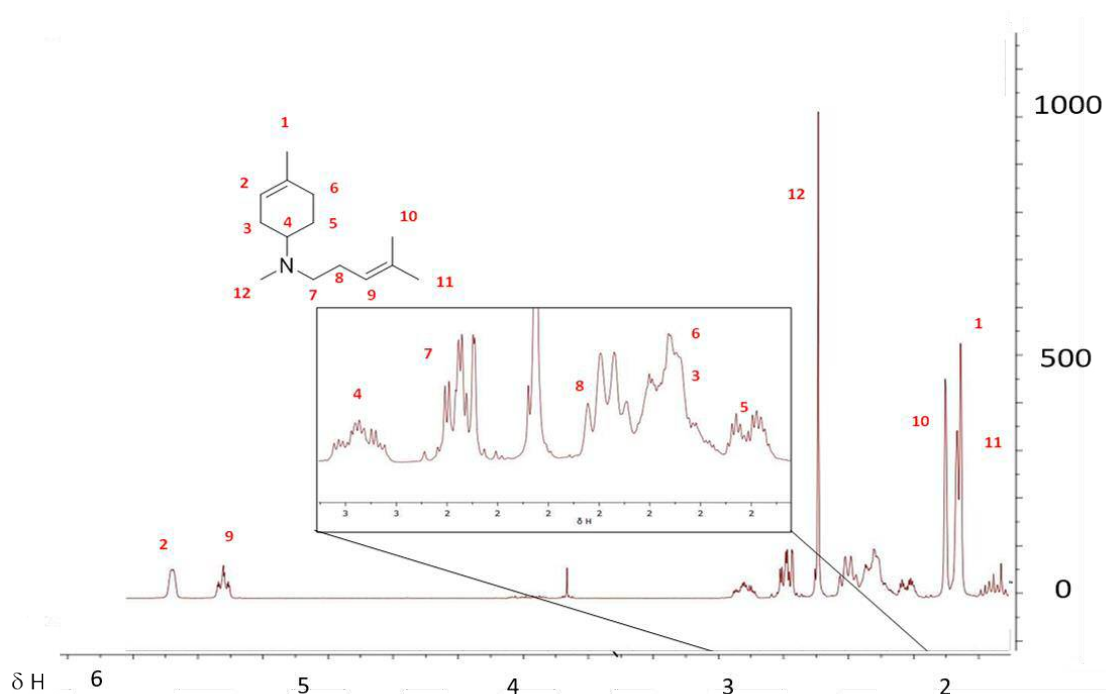
Figure 2.11 ^{1}H NMR spectrum (300 MHz, CDCl$_3$) of neutral 116.
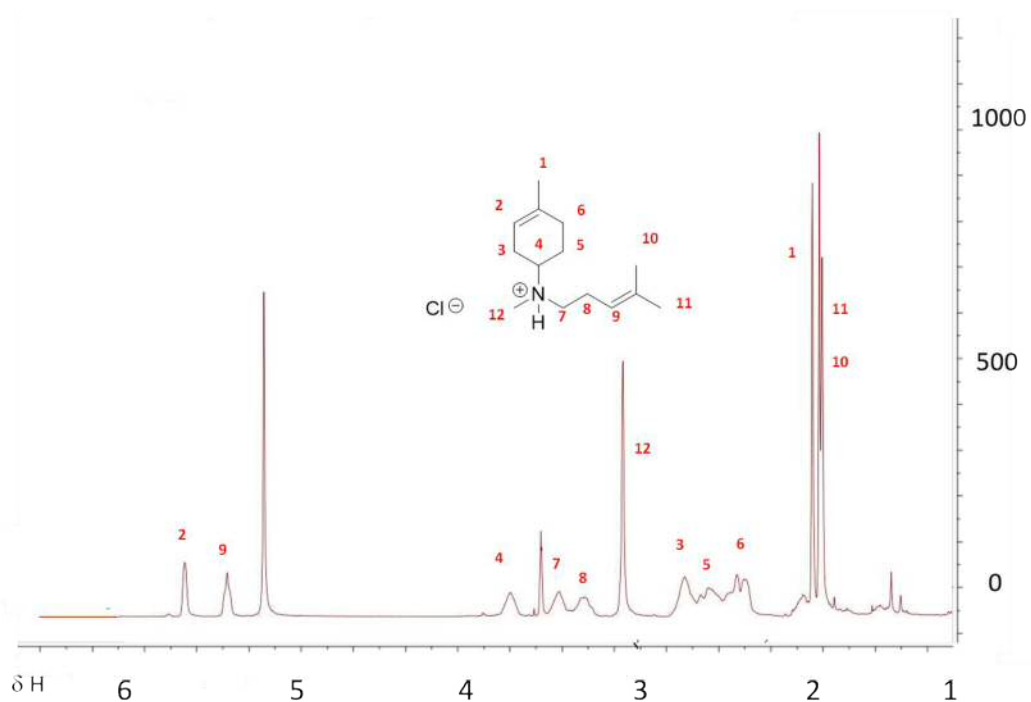
Figure 2.12 ^{1}H NMR spectrum (300 MHz, CD$_3$OD) of protonated 60.

In summary, a new, shorter, and elegant route to amine **(S)-** and **(R)-60** mimicking the bisabolyl cation **33** has been developed. The key problem was to find the right catalyst to induce the stereoselectivity in the Diels-Alder [4+2] cyclisation, and a new approach to introduce nitrogen into the molecule with the preservation of stereochemistry needed to be performed. The Evans auxiliary and R-pantolactone were used for the formation of **(R)-** and **(S)-60**, respectively. TiCl$_4$ and DEAC were used as catalysts to promote the stereoselectivity needed in order to obtain the S and R enantiomer, respectively.

2.3 Synthesis of the germacradien-11-yl aza-analogue (85)

The germacradien-11-yl-aza-analogue **85** (Scheme 2.1) has not been prepared prior to this work. Therefore, the first synthetic approach adopted aimed to produce the ten carbon analogue in its racemic form, with the intent to eventually optimise the synthetic route to obtain the two enantiomers.

In a previous work of Muto and colleagues,[84] germacrene B (**123**) was synthesised in seven steps, from (*E,E*)-farnesol to the cyclic intermediate (Scheme 2.10).

59
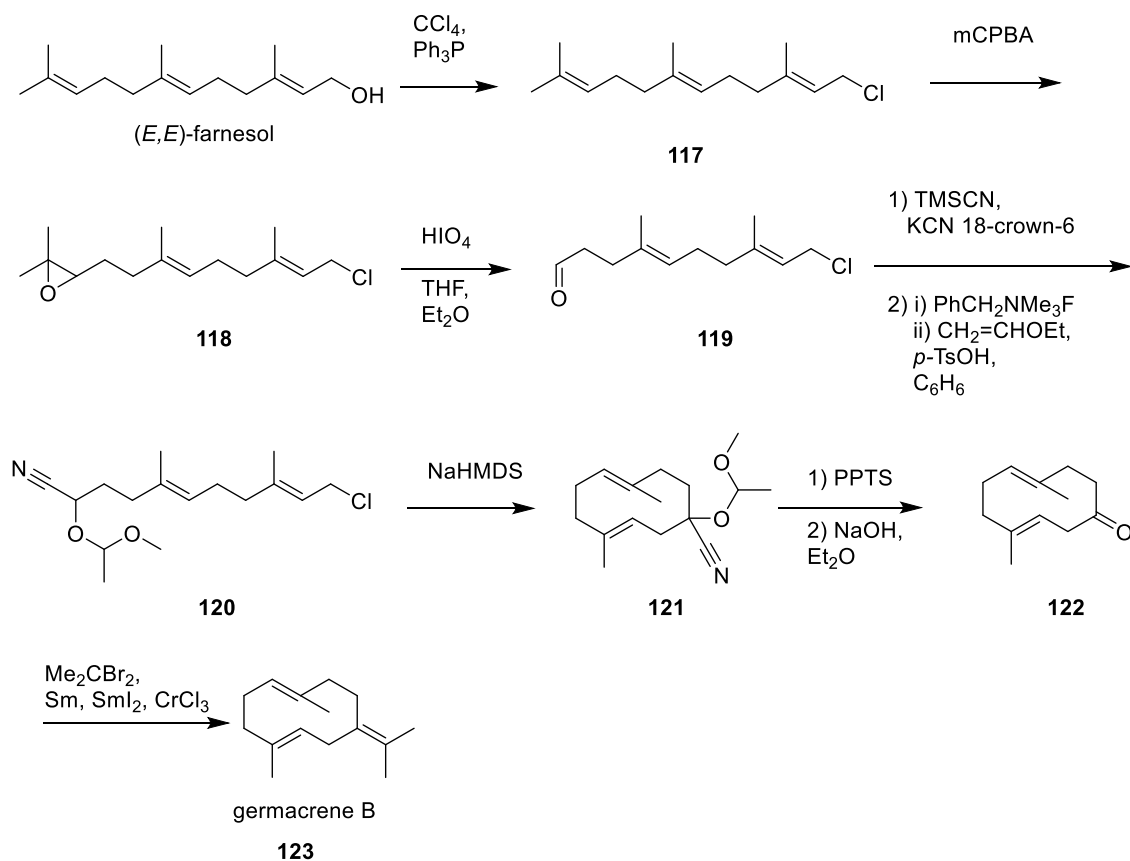
Scheme 2.10 Synthetic route to germacrene B, developed by Muto and colleagues.[84] **NaHMDS = sodium hexamethyldisilazide, PPTS = pyridinium *p*-toluenesulfonate TMSCN = trimethylsilyl cyanide.**

The treatment of farnesol with triphenylphosphine in carbon tetrachloride yielded the chloride **117**, which was epoxidised on the distal double bond with mCPBA to give **118**. Periodic acid was used to oxidatively cleave the epoxide to give aldehyde **119**, which was treated first with trimethylsilyl cyanide and potassium cyanide, and then with benzyltrimethylammonium fluoride to give the corresponding cyanohydrin, which was protected as the ethoxyethyl ether in order to give compound **120.** This was then cyclised to **121** with the use of sodium hexamethyldisilazide as base under high-dilution conditions. Removal of the protecting group with PPTS in methanol followed by the treatment with base yielded **122**, which was then treated with samarium and chromium halides to give the compound, germacrene B.

Muto reported that the final step of this synthesis could not be achieved with a conventional isopropylidenation, because the Wittig reaction caused a double bond migration, forming unwanted products. Therefore, the protocol developed by Utimoto was used instead.[85]

Inspired by this, the synthetic approach to generate the aza-analogue **85** of the germacradien-11-yl cation focused on the formation of ketone **122**, which should yield **85** after a reductive amination and acid treatment. The proposed synthesis is shown in Scheme 2.11.
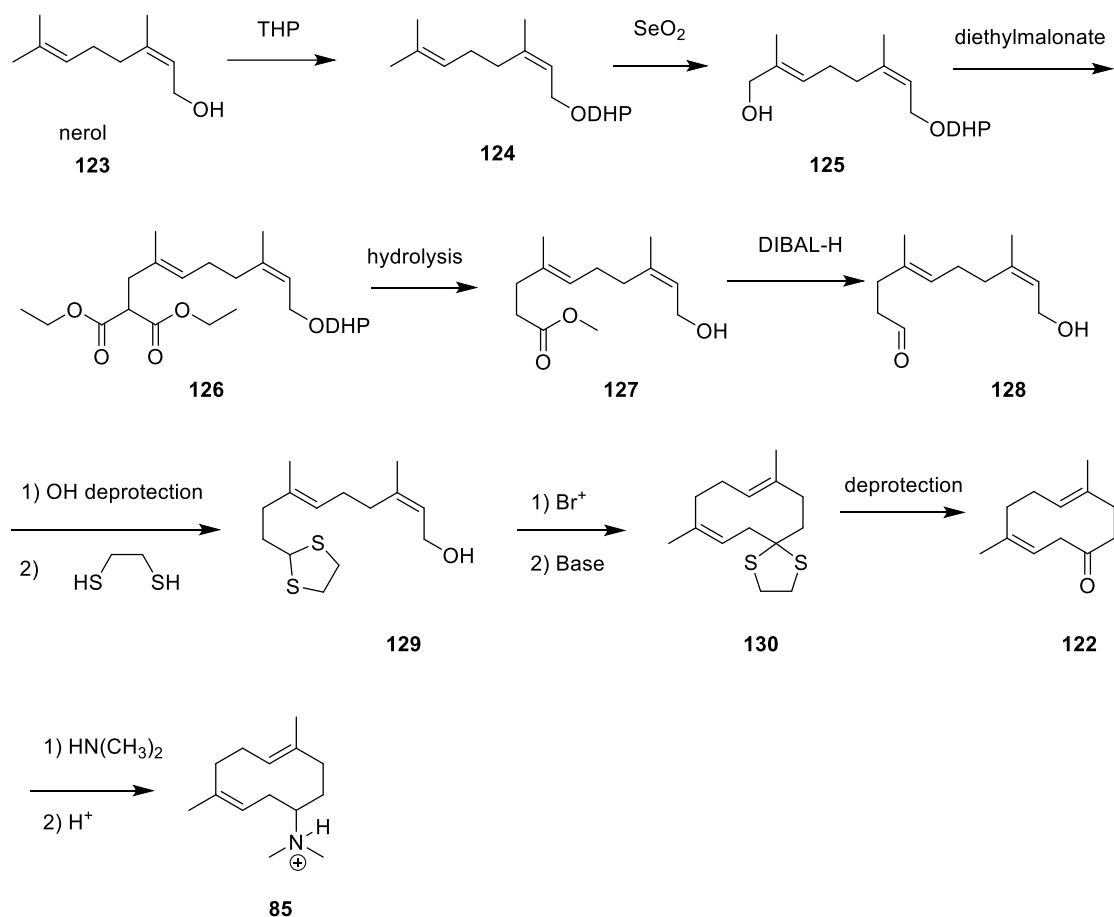
Scheme 2.11 Proposed synthetic approach for the formation of germacradien-11-yl-cation aza-analogue 85.

Nerol (**123**) was chosen as starting material because it possesses the *Z* stereochemistry to form the cyclic compound **85**. The first step of this synthesis is the protection of the hydroxy group of nerol, so the SeO_2 oxidation could be selectively performed without oxidation of the alcohol into an aldehyde. The new hydroxyl group is then substituted with a leaving group such as chloride or bromide. The resulting intermediate is reacted with diethylmalonate in order to elongate the carbon chain and yield diester derivate **126**, which is further hydrolysed to monoester derivate **127** first, and then reduced to the aldehyde **128**. The hydroxyl group is then deprotected, and the resulting alcohol is reacted with 1,3-dithioeth ane to form **129** and render the aldehyde proton more acidic, which should facilitate the next cyclisation to **130**. The next step of this protocol is the cyclisation of the

intermediate **129** to **130**, after the substitution with a better leaving group to facilitate the cyclisation reaction. This is a crucial step, as **129** could undergo intermolecular reactions and yield a polymer instead. This can be avoided using high dilution conditions so that intramolecular reactions are favoured instead. Once **130** is obtained, the deprotection of the ketone followed by a reductive amination and acid treatment should yield the desired cyclic aza- analogue **85**.

2.3.1   Synthesis of THP protected nerol (124)
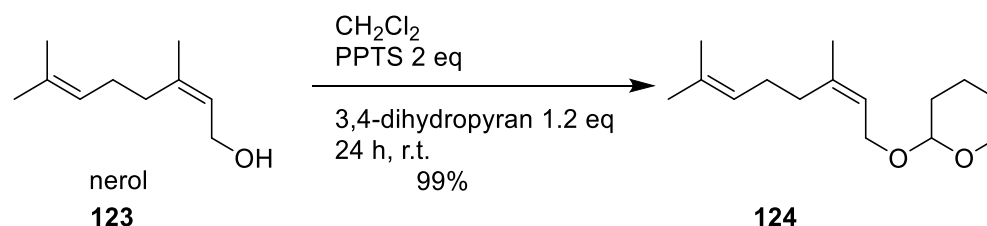
Scheme 2.12 Nerol protection condition using DHP as the protective group.

The first step of the synthesis was protection of the hydroxyl group of nerol using 3,4-dihydropyran. Despite the complex ^{1}H-NMR spectrum, the THP protection reaction was chosen due to the simple reaction conditions needed and high yield of the product. All the spectroscopy data for the isolated compound were in agreement with previously reported data. [86]

2.3.2   Synthesis of hydroxy THP protected nerol (125)
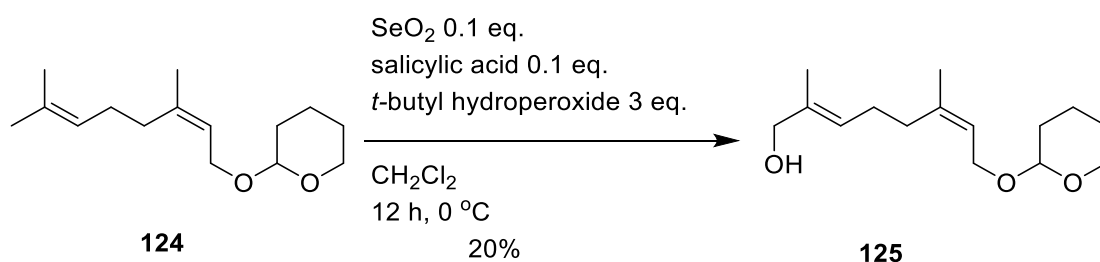
Scheme 2.13 Preparation of hydroxy THP-protected nerol 125.

The second step involved the allylic oxidation of **124** with the catalytic use of selenium dioxide. The limitation of this reaction is that the selenium dioxide is strong enough to completely oxidise **124** to the corresponding aldehyde. The formation of the reduced form of selenium and organoselenium byproducts was

avoided with the use of salicylic acid and *t*-butyl hydroperoxide, which regenerate the catalyst SeO$_2$ *in situ.* All the spectroscopy data for the isolated compound were in agreement with previously reported data. [86]

2.3.3 Synthesis of THP protected nerol chloride (132)
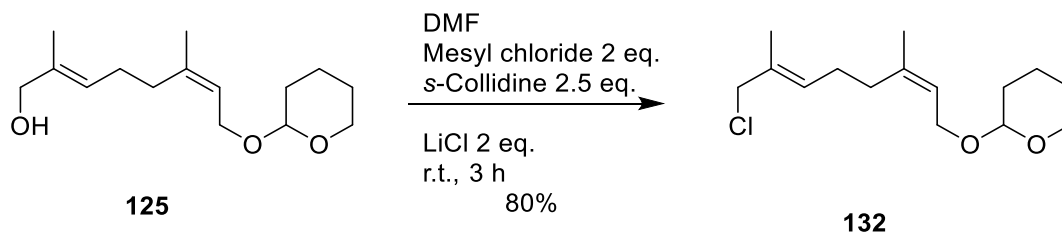
Scheme 2.14 Preparation of the alcohol 132.

A nucleophilic substitution was then performed using methanesulfonyl chloride and *s*-collidine. This reaction was necessary in order to substitute the hydroxyl group of **125** with a better leaving group to facilitate the next alkylation step. Chloride **132** was stable enough to silica for it to be purified by column chromatography, but it was used promptly for the next step or and stored at - 24 °C. As the alcohol **125** has a higher polarity than **132**, the formation of the chloride was easily confirmed by TLC analysis, using the solvent mixture hexane:EtOAc 4:1. In addition, the ^{1}H-^{13}C-HSQC spectrum (400 MHz, CDCl$_3$) of compound **132** showed a signal at δ_H = 52 ppm, corresponding to the carbon attached to the chloride. This confirms the presence of the chloride, as in the ^{1}H-^{13}C-HSQC spectrum (400 MHz, CDCl$_3$) of **132** reported in the literature.[86]

2.3.4 Synthesis of diethyl nerol malonate (126) and further steps

The chain elongation of the chloride **125** and the succeeding steps were not straightforward and presented several problems.

In order to get the diester **126** (Scheme 2.15), NaH was used as the base to deprotonate the alkylating reagent, diethyl malonate. Although this reaction did not present any problems, the separation of the diethyl malonate from the desired products was not achieved despite several different attempts. As purification by flash chromatography using a range of different solvent mixtures did not yield pure **126**, it was decided to proceed to the next step using the diester as the starting

material in its crude form. From here, several methods were attempted to obtain the aldehyde **128** (Scheme 2.15).
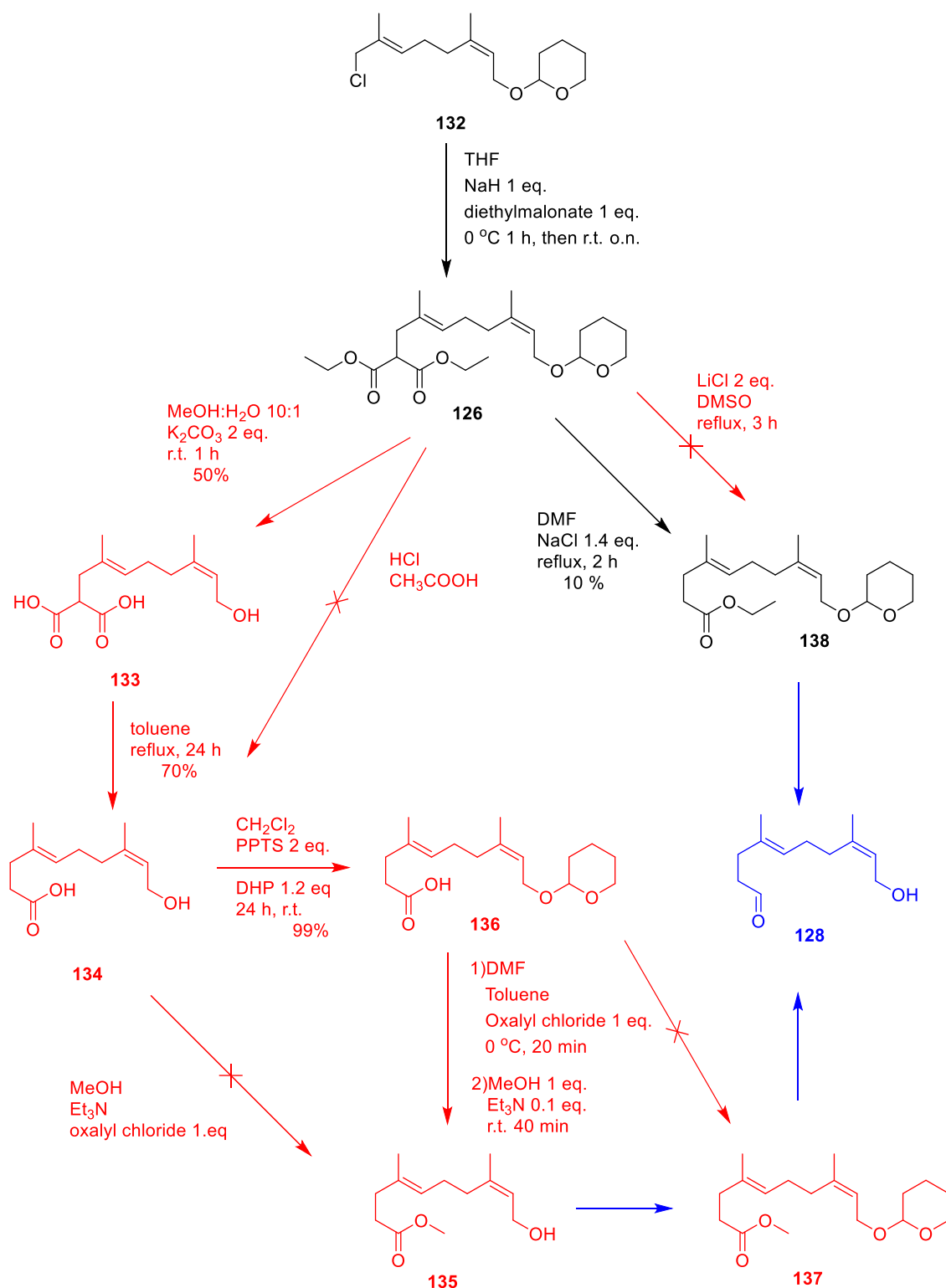
Scheme 2.15 Methodologies attempted for the synthesis of the aldehyde 128.

Following a literature procedure by Stritzke,[87] hydrolysis of **126** was performed using lithium chloride in DMSO. Unfortunately, the reaction did not yield the ethyl ester **128,** with starting material being recovered instead. Subsequently, following

a similar procedure by Fairlamb *et al.*,[88] NaCl in DMF was used instead and **128** was obtained. However, the 10% yield of **128** was low and so a different approach was taken.

Initially, acetic acid and HCl were used to obtain the carboxylic acid **134** from diester **126** in one step, following a procedure reported by Chong *et al*[89] . However, the ^{1}H NMR spectrum of the product showed no signals corresponding to the olefin protons, indicating the absence of the double bonds.

Finally, following Kaelz's saponification procedure,[90] the diester was hydrolysed with potassium carbonate in methanol, obtaining the diacid **133**, which was decarboxylated by heating to reflux to form the monoacid **134**.

Paddon and colleagues previously developed an esterification procedure aimed at generating a methyl ester from its corresponding carboxylic acid with the use of oxalyl chloride, methanol and catalytic amount of triethylamine.[54] Following Paddon's protocol, an attempt was made to prepare methyl ester **135** from the acid **134** in one step. Unfortunately, it was not possible to separate **134** from the starting material **133**, and the attempt to directly produce methyl ester **135** from impure **134** failed. Therefore, it was decided to protect **134** again and to perform the esterification on acid **136** instead, which yielded the unprotected monoester **135** in very low yield (8%).

Due to the increased number of steps required to produce **135**, and therefore **128**, also attributable to the labile nature of the THP group in the hydrolysis diester reaction (**136** to **135**), it was decided to start the synthesis from the beginning and change the nature of the protecting group. The acetyl protecting group was chosen. The protected compound neryl acetate is already commercially available, allowing the synthesis to start directly from the selenium oxide oxidation and therefore reduce the length of the synthesis by one step.

2.3.5 Synthesis of hydroxy nerol acetate (140)
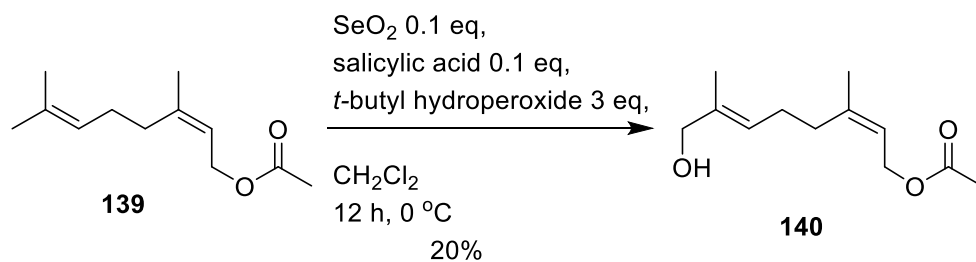
Scheme 2.16 Preparation of alcohol 140.

The oxidation of neryl acetate (**139**) was conducted using the same conditions employed to oxidise **124** to **125** (Scheme 2.13). As the alcohol **140** was obtained in low yield (20%), this reaction remained the limiting step of the whole synthesis. The formation of the alcohol was confirmed by NMR spectroscopic analysis. The ^{1}H NMR spectrum (400 MHz, CDCl$_3$) showed a doublet at δ_H = 4.93 ppm, which corresponds to the protons of the CH$_2$ attached to the acyl protecting group, and a singlet at δ_H = 4.32 ppm due to the CH$_2$ attached to the hydroxyl group. The signal corresponding to the olefinic protons are at δ_H = 5.79 ppm (Figure 2.13).
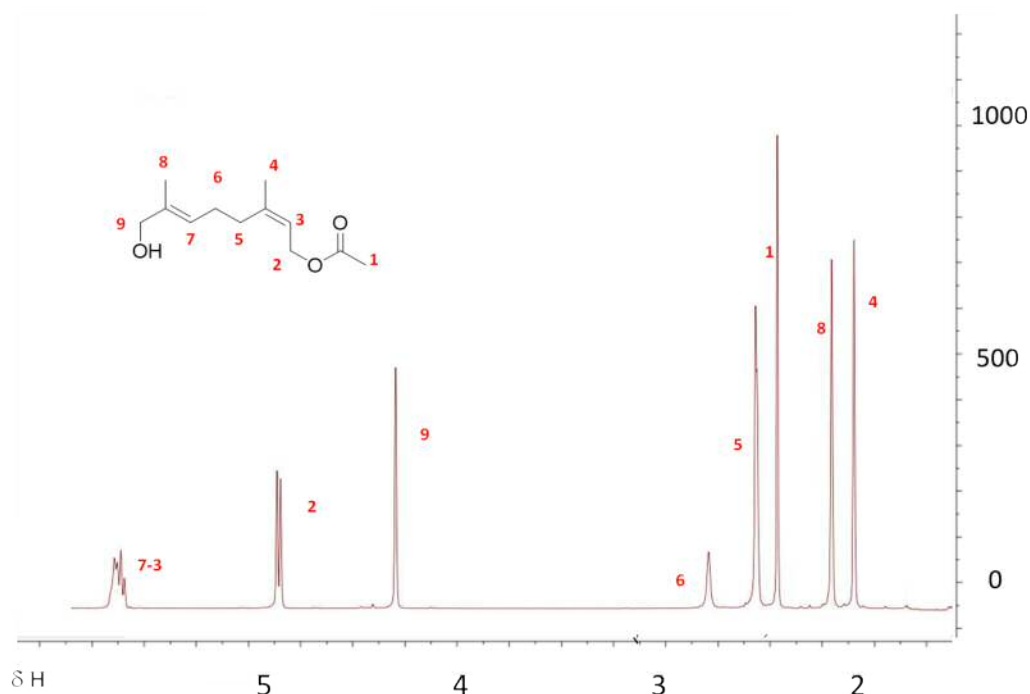
Figure 2.13 ^{1}H NMR spectrum (400 MHz, CDCl$_3$) of 140.

2.3.6 Synthesis of nerol bromide acetate (141)
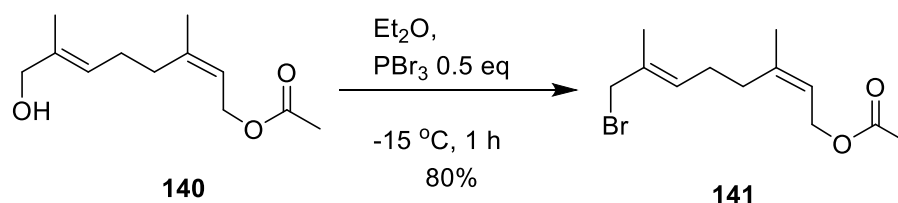
Scheme 2.17 Preparation of bromide 141.

In order to activate the alcohol **140** for the alkylation reaction and therefore to extend the terpenoid chain, the OH group was substituted with bromine, employing 0.5 equivalents of phosphorus tribromide at -15 °C in dry diethyl ether. As allyl bromide are reactive species, **141** was highly unstable to air, and it decomposed in time when stored at -20 °C for more than two days. Therefore, it was used promptly for the next step in its crude form.

2.3.7 Preparation of dimethylmalonyl adduct (142)

Two similar alkylating agents were used to alkylate bromide **141**: diethyl malonate and dimethyl malonate. In both cases sodium hydride was used as the base.

As found for chloride **132** (Scheme 2.15), when diethyl malonate was used, the purification of the final compound from the alkylating agent was not achieved despite several attempts. Although chemically similar, it was possible to obtain the pure diester when dimethyl malonate was used with **141** instead. The reaction conditions used are described in Scheme 2.18.
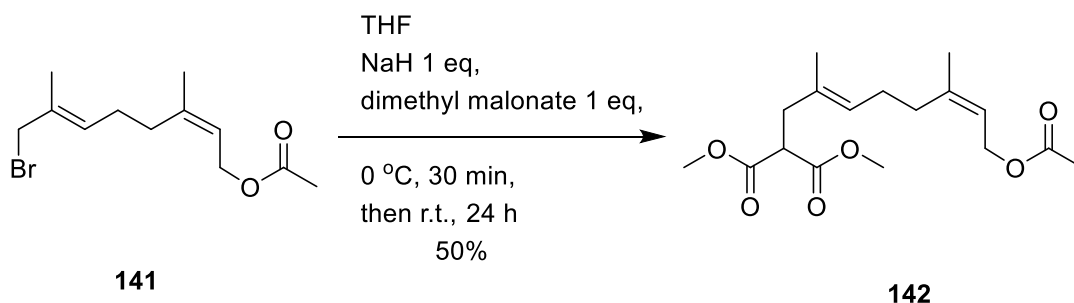
Scheme 2.18 Synthesis of alkylated malonate diester 142.

The formation of **142** was confirmed by the presence of a triplet signal integrating for 1 H at δ_H =3.85 ppm in the ^{1}H NMR spectrum (400 MHz, CDCl$_3$) corresponding to

the proton between the two methyl ester groups, and a singlet at δ_H = 4.12 ppm integrating for six protons corresponding to the two methyl groups of the diester portion of the molecule. Furthermore, the signal corresponding to the two protons on CH_2 attached to the diethyl malonate portion appeared upshifted at δ_H = 2.85 as a doublet, indicating the coupling to the adjacent protons on CH (Figure 2.14).
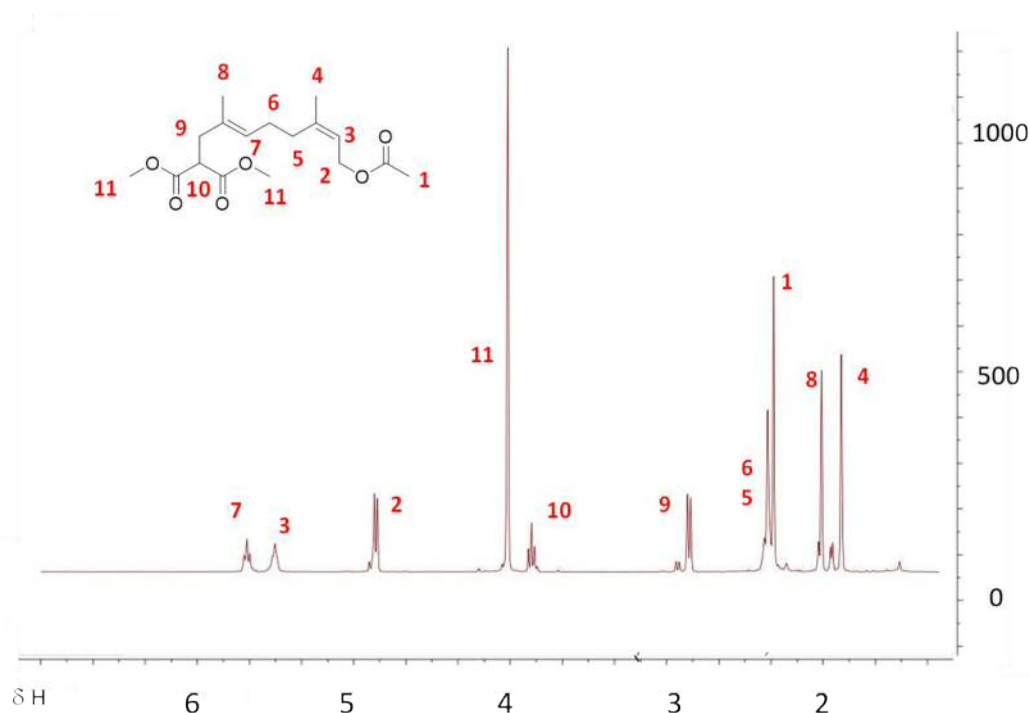
Figure 2.14 ^{1}H NMR spectrum (400 MHz, CDCl$_3$) of **142**.

2.3.8 Synthesis of nerol acetate monoester (143)

In order to hydrolyse diester **142** to the corresponding monoester **143**, the same reaction conditions previously used to convert the diester **126** to **138** (Scheme 2.15) were employed. **142** was treated with NaCl in DMF and heated to reflux, but the reaction did not yield **143**, and only starting material was recovered. Subsequently, following Stritzke's protocol instead,[87] the hydrolysis was performed using lithium chloride in DMSO. It is curious to note that previously the use of LiCl did not afford the hydrolysed compound **135**, this was only obtained using NaCl. The final reaction conditions used are described in Scheme 2.19 below.
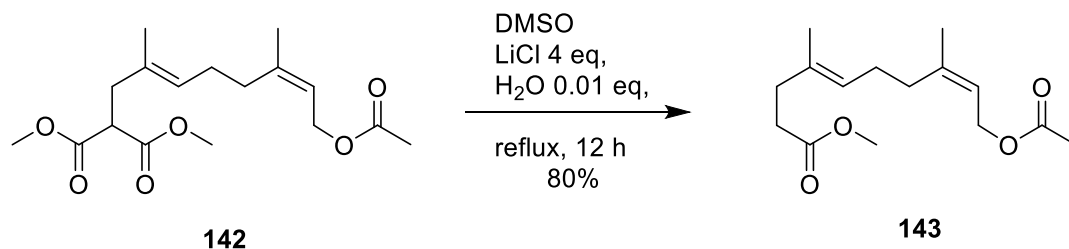
Scheme 2.19 Preparation of the monoester 143.

The formation of the monoester was confirmed by the presence of a triplet signals in the ^{1}H NMR spectrum (400 MHz, CDCl$_3$) at δ_H = 2.12 ppm integrating for 2H corresponding to the protons on the CH$_2$ attached to the methyl ester group. The signal corresponding to the methyl group at δ_H = 3.59 ppm integrates for only 3 protons, indicating the presence of only one methyl ester group in the molecule (Figure 2.15).
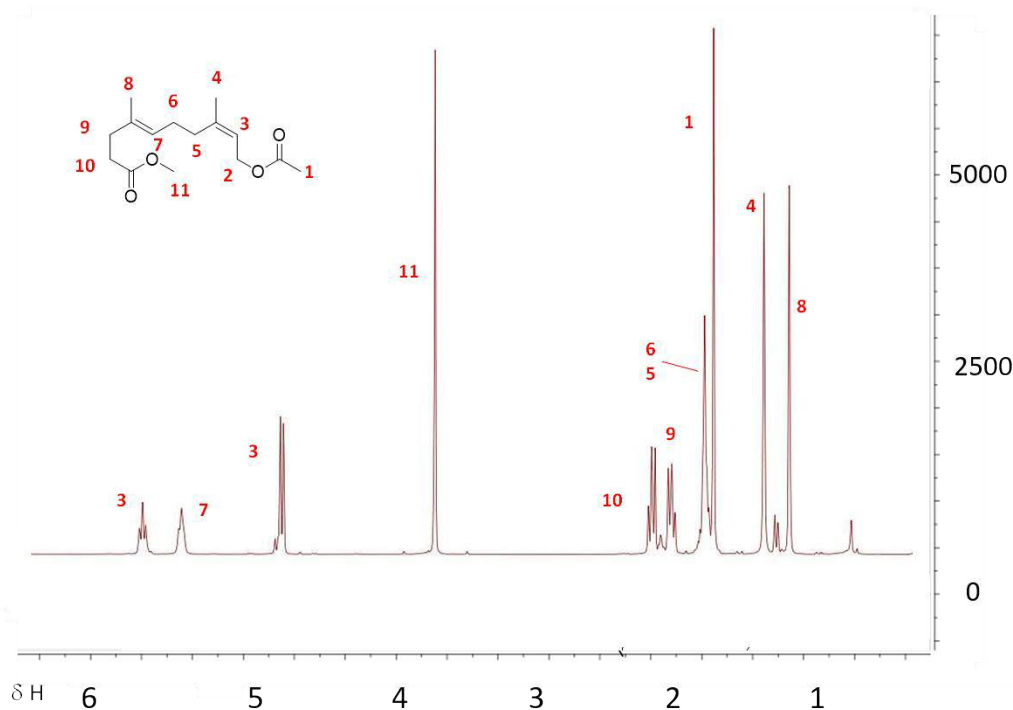
Figure 2.15 ^{1}H NMR spectrum (400 MHz, CDCl$_3$) of 143.

2.3.9 Synthesis of nerol aldehyde (149)

The synthesis of aldehyde **149** from monoester **143** was initially envisaged in 3 steps: 1) reduction of the ester functional group with the use of DIBAL-H in order to get the corresponding alcohol **146**; 2) oxidation of the hydroxyl group in order to yield aldehyde **148**; 3) removal of the acetal protecting group to obtain aldehyde **149** with the unprotected hydroxyl group (Scheme 2.20).

The DIBAL-H reduction was conducted at −78 °C, using initially 4 equivalents of reducing agent. Unfortunately, with these conditions, the unprotected alcohol **144** was obtained instead of the alcohol **146**, suggesting that less equivalents of DIBAL-H were needed in order to reduce only the ester functional group without also deprotecting the hydroxy group. Therefore, 2 equivalents of DIBAL-H were used, but again another compound was obtained instead of **146**. NMR analysis showed that the unprotected ester **145** was formed instead. In fact, in the ^{1}H NMR (400 MHz, CDCl$_3$) spectrum, the signal corresponding to the CH$_3$ of the acetyl protection was absent.
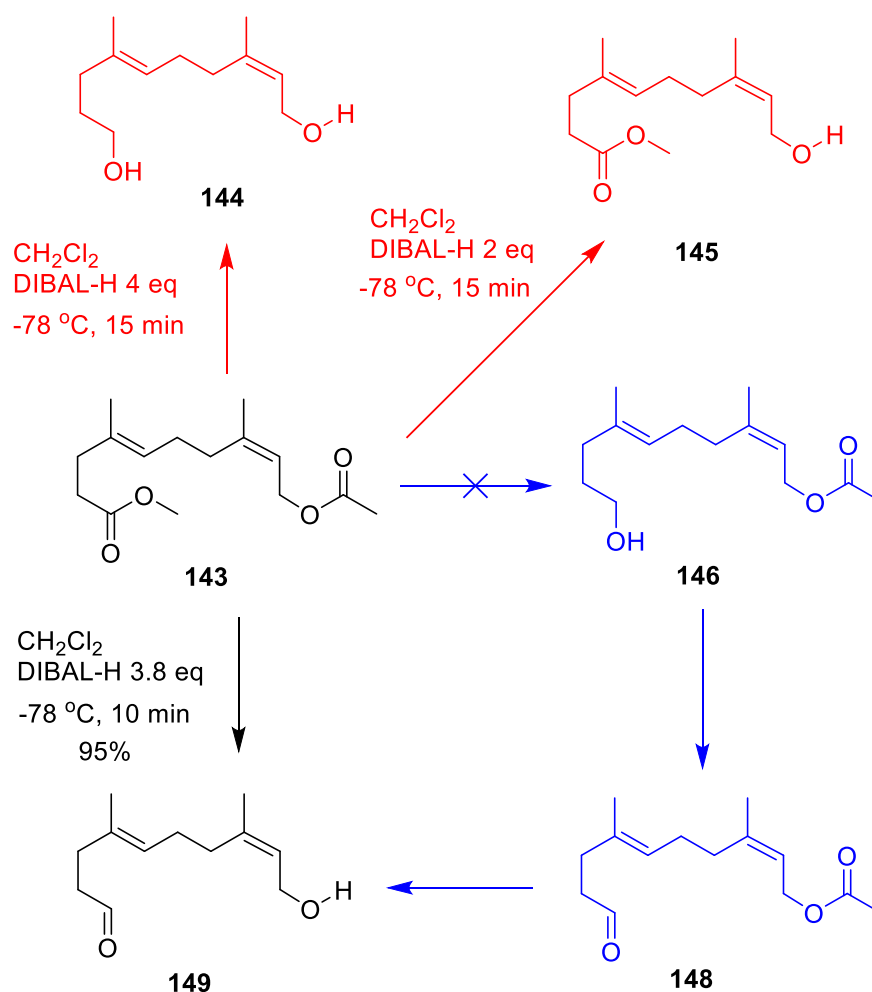
Scheme 2.20 Synthetic pathway for the formation of the aldehyde 149. Red: undesired products; Blue: initial proposed pathway; Black: final pathway for the synthesis of 149 in one step.

These two outcomes taken together indicate that the reducing agent DIBAL-H reduces the acetate first, and then the methyl ester. Consequently, employing between 2 and 4 equivalents of DIBAL-H, it should be possible to control the reaction and to obtain the aldehyde **149** directly. In addition, Mascall *et al.* managed to

successfully reduce the ethyl ester and the acetyl group within a complex molecule (Scheme 2.21, **150**), giving both aldehyde and alcohol, respectively, by performing a one step reaction involving of 3.8 equivalents of DIBAL-H. [91]
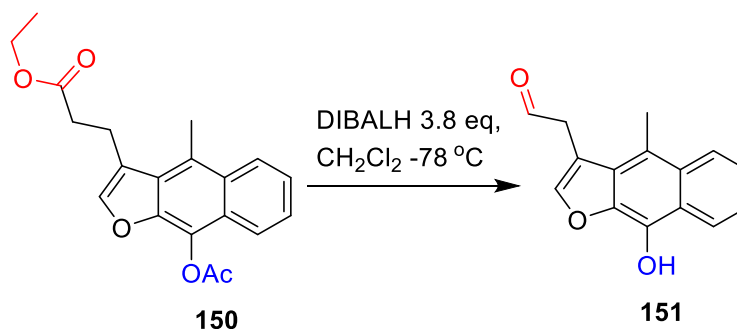
Scheme 2.21. Reduction condition used by Mascall and coworkers to obtain the compound 150 from 151 in one step using 3.8 equivalents of DIBAL.[91]

Inspired by Mascall's work, 3.8 equivalents of DIBAL-H were used to reduce **143**. The reaction was monitored by TLC, and quenched as soon as one product was formed, in order to avoid over-reduction. Finally, after reacting 10 minutes at – 78 °C, the reaction yielded the desired aldehyde **143** in very good yield (95%).

The formation of **143** was confirmed by NMR spectroscopic analysis. The ^{1}H NMR spectrum (400 MHz, CDCl$_3$) showed the unresolved signal at δ_H = 10.2 ppm integrating for 1 H corresponding to the aldehyde proton. Furthermore, the signal corresponding to the methyl acetate protecting group at δ_H = 1.98 was absent and a doublet at δ_H = 2.50 ppm integrating for 2H corresponds to the protons on the CH$_2$ attached to the OH. These two signals indicate that the acetyl protection group was absent.
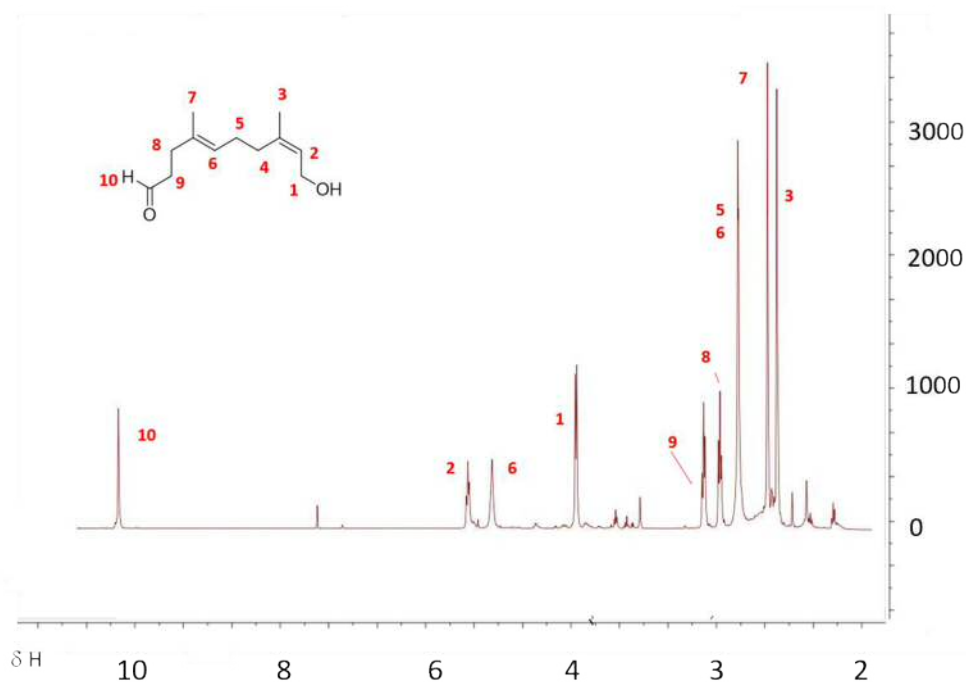
Figure 2.16 ¹H NMR spectrum (400 MHz, CDCl₃) of crude 149.

As the aldehyde was volatile, it was stored immediately in the freezer after the work-up without any further purification and used promptly once out of the freezer. The use of these reaction conditions allowed to control the DIBAL-H reduction in such a way that the desired aldehyde **149** was obtained in one single step, shortening the total synthesis of the aza-analogue **85** by two steps.

2.3.10 Synthesis of nerol dithiolane (164)

The next step of the synthesis involved the protection of the aldehyde with the 1,2-ethanedithiol. This step is necessary to make the aldehyde proton more acidic, and consequently to facilitate its deprotonation, and to promote the 10-C membered ring formation in the following cyclisation reaction. Following the work of Khan,[92] catalytic amounts of oven-dried NiCl₂ were used. The different solvent mixtures and reaction times used are described in Table 2.3, and the best reaction conditions found are described in entry 2.

Table 2.3 Reaction conditions used for the formation of 152. sm = starting material.
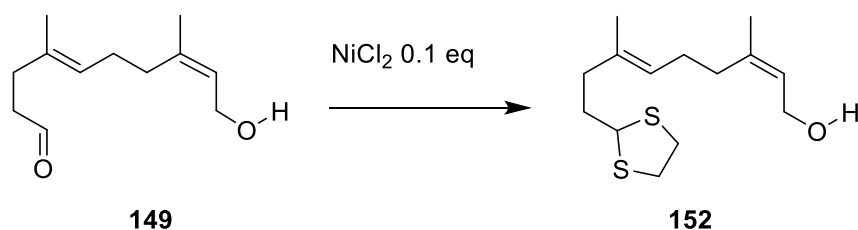
Entry	Solvent	Time (h)	152 Yield (%)
1	CH$_2$Cl$_2$	5	10
2	CH$_2$Cl$_2$	24	55
3	CH$_2$Cl$_2$:DMSO 5:1	5	0, sm recovered
4	CH$_2$Cl$_2$:DMSO 5:1	24	30
5	CH$_2$Cl$_2$:MeOH 10:0.5	5	0, sm recovered
6	CH$_2$Cl$_2$:MeOH 10:0.5	24	unknown major product
7	CH$_2$Cl$_2$:MeOH 5:1	5	unknown major product

CH$_2$Cl$_2$ was used as the solvent, with the addition of a small amount of a more polar solvent to enhance the solvation of the catalyst. However, when DMSO was added (Table 2.3, entry 3 and 4) the yield of the protection reaction was not increased nor the time reaction reduced. When methanol was added in small amounts (entry 5) only starting material was recovered. On the other hand, when it was left to stir for 24 h (entry 6) unknown product was formed as the major product. Again, when the amount of methanol added to the reaction mixture was increased (entry 7), the same unknown product was formed. NMR spectroscopic analysis did not allow to determine the exact chemical structure of the compound formed, but it suggested that the MeOH attacked the aldehyde function, with the possible formation of an acetal. Consequently, it was decided to run the reaction only in CH$_2$Cl$_2$ instead. The formation of **152** was achieved in 10% yield after 5 h, and in 55% yield after 24 h (entry 1 and 2 respectively).

The formation of the protected compound **152** was confirmed by NMR spectroscopic analysis. The ^{1}H NMR spectrum (400 MHz, CDCl$_3$) showed the presence of a multiplet signal at δ_H = 3.43-3.62 ppm integrating to 4 H corresponding to the dithiol protection. The triplet at δ_H = 4.78 ppm corresponds to the H attached on the CH between the two sulfurs. The quartet at δ_H = 2.25 ppm corresponds to the protons on CH$_2$ vicinal to the dithional protection.
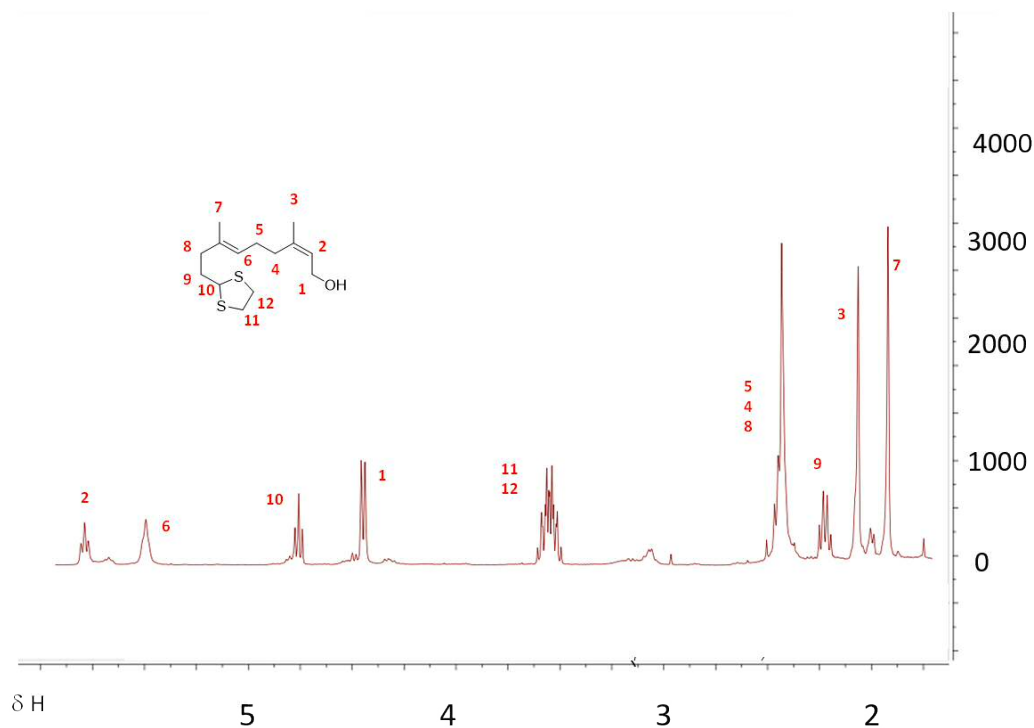
Figure 2.17 ^{1}H NMR spectrum (400 MHz, CDCl$_3$) of crude 152.

2.3.11 Synthesis of dimethyl dithiaspirotetradecadiene (153)

The crucial step of the synthesis of the aza analogue **85** is the formation of the 10-C cyclic compound **153** from the cyclisation of alcohol **152**. As described in scheme 2.10, Mutu *et al.* reported the formation of a 10-C membered ring terpenoid with the use of sodium hexamethyldisilazide (NaHMDS) as the base, and THF as the solvent. The difficulty of this reaction lies in the fact that the starting material (**153**) needs to be reactive, but not too much, so that only intramolecular reactions can take place and intermolecular reactions avoided. Therefore, to activate **152** towards the cyclisation, it was decided to form its corresponding chloride, with the use of methansulfonyl chloride, *s*-collidine and lithium chloride in DMF. Once the chloride was formed, it was slowly added over 12 h to a diluted solution of NaHMDS in THF so that the final concentration of the starting material in the reaction mixture was

0.018 M. High dilution conditions were necessary to avoid the formation of intermolecular polymerisation reactions. The various reaction conditions attempted are described below in Table 2.4.

Table 2.4 Reaction conditions used to prepare 153. The reaction conditions described in the table are referred to the second step of the reaction. s.m. = starting material recovered.
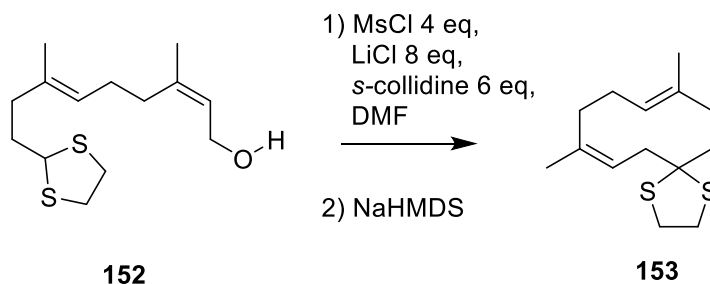
Entry	Solvent	Temp	Time/h	NaHMDS (eq)	Outcome
1	THF	r.t.	13	4.4	s.m.
2	THF	reflux	13	4.4	s.m. + unknown compound
3	THF	r.t.	24	6.6	s.m.
4	Et$_2$O	r.t.	13	4.4	s.m.
5	Et$_2$O	reflux	13	4.4	unknown compound
6	Et$_2$O	r.t.	24	4.4	s.m.

Unfortunately, none of the above trial reactions yielded the desired compound **153**. When THF was used as the solvent and the reaction left to stir at room temperature only starting material was recovered (entry 1 and 3, table 2.4). Increasing the amount of base did not improve the outcome. When the reaction was heated (entry 2, table 2.4), some starting material was recovered, but the formation of an unknown compound was observed. The ^{1}H NMR spectrum (400 MHz, CDCl$_3$) showed the presence of a triplet signal integrating for 2H corresponding to the CH geminal to the chloride group, therefore indicating that no cyclisation occurred. The exact chemical structure of the formed product was not determined. When diethyl ether was used as the solvent (entry 4, 5, and 6, table 2.4), starting material was only recovered at room temperature, but an unknown compound was formed when the

reaction was heated to reflux. Although it was not possible to assign a precise chemical structure to the compound formed, NMR analysis suggested again that no cyclisation occurred. It is important to note that when diethyl ether was used as the solvent, the unidentified product was formed more clearly than when THF was used. This may suggest that the use of THF as the solvent promotes the formation of side products.

Due to the end of the PhD timeline, it was not possible to explore the cyclisation reaction in more detail and to perform the remaining reactions needed to obtain the germacradien-11-yl cation aza-analogue **85**. Future work may include the use of different bases, the formation of a bromide intermediate, or the use of a more concentrated reaction environment. Once the spiro compound **153** is formed, the remaining steps, deprotection of the ketone group and reductive amination, should be straightforward.

Summary

This chapter covered the design and the development of a new enantioselective synthesis of the bisabolene aza-analogues **(S)-** and **(R)-60**, which was 4 steps shorter, more economic, and more efficient than the one described in the literature by Coates and colleagues.[71]

In addition, a synthetic route to obtain the racemic the germacradien-11-yl cation aza-analogue **85** was designed and, although there was not enough time to complete it, 6 out of 9 steps were achieved.

CHAPTER 3   **Positive and Negative Control of the Aza-bisabolyl Cation and Mechanistic Analysis of δ-Cadinene Synthase**

3.1 Amorphadiene synthase

As described in section 1.6.2, amorphadiene synthase from *Artemisia annua* (ADS) is a sesquiterpene synthase that catalyses the biosynthesis of bicyclic sesquiterpene amorphadiene. ADS has been shown to catalyse an intial 1,6-cyclisation of FDP (Scheme 1.6, Chapter 1). The formation of the α-bisabolyl cation **33** in the catalytic mechanism of ADS was confirmed by Picaud and colleagues.[21] The two enantiomers of the aza-analogue **60** are designed to mimic the bisabolyl cation intermediate **33** (Figure 3.1). Therefore they are expected to act as strong competitive inhibitors of ADS. Consequently, ADS inhibition studies with **(*S*)-60** and **(*R*)-60** were performed as a positive control.

(S)-   *(R)-*

aza-analogues of
α-bisabolyl cation   α-bisabolyl cation

60   **33**
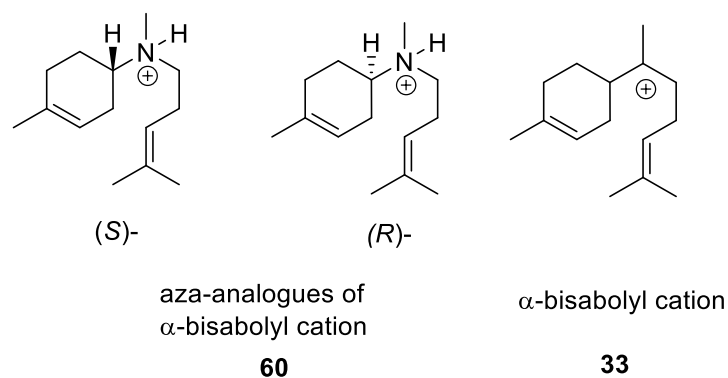
Figure 3.1 Chemical structures of the α-bisabolyl cation and its corresponding aza-analogues.

3.1.1 Characterisation of the wild-type amorphadiene synthase

ADS was produced and purified following the protocols described in the literature.[21,53,54]

Heterologous expression of ADS gene

A cDNA containing the gene encoding ADS from *Artemisia annua* was previously subcloned into the expression vector pET21d, and a hexa-histidine tag was introduced into the pET21d-ADS within the research group in order to simplify the ADS purification process. *E. coli* BL21(RP) cells were transformed with the resulting plasmid as described in section 6.1.7 and expressed following method A described in section 6.1.8: a single colony was picked from a plate prepared as stated in 6.1.7 and used to inoculate 100 mL of LB medium containing 200 μL of ampicillin solution at 50 mg/mL. This culture was incubated at 37 °C overnight with shaking at 150 rpm.

A portion (10 mL) of this stationary phase culture was then used to inoculate 500 mL LB medium containing ampicillin (50 µg/ml). This was then incubated at 37 °C with shaking at 150 rpm until the optical density reached 0.5 AU at 600 nm. IPTG (final concentration 0.4 mM) was added and the culture was allowed to grow for 6 h at 20 °C before being harvested by centrifugation at 4000 g for 10 minutes. The supernatant solution was decanted and the cell pellet was stored at - 20 °C until required.

ADS purification

The previously prepared pellet was allowed to defrost on ice and then resuspended in 20 mL of cell lysis buffer 1. Lysozyme (0.5 mg/mL) was added and the solution was stirred at 0 °C for 1 h before being lysed by sonication on ice. Thanks to the reducing agent and the detergent present in the cell lysis buffer 1, dithiothreitol (DTT) and Tween 20% respectively, ADS was found in the supernatant mixture, as judged by SDS-PAGE (Figure 3.2, lane 2). The lysate was directly purified using a Ni^{2+} NTA affinity column. Affinity resin with bound divalent nickel ions was used to coordinate the His-tag motif previously introduced to ADS. This resulted in ADS binding to the column, and the lysate and other proteins eluting through the column, as they do not have a His-tag. The protein was eluted by washing the column with a buffer containing a gradually increasing concentration of imidazole (from 5 to 300 mM). This enabled fractionation from the column with an excess of imidazole displacing the histidine residues, allowing the free proteins to elute from the column. ADS eluted with 60-100 mM imidazole in binding buffer, the fractions containing pure protein were analysed by SDS-PAGE (Figure 3.2). Those fractions containing the protein were then dialysed against dialysis buffer 1 and concentrated by Amicon™ ultrafiltration using a Millipore 30,000 MW cut off membrane.
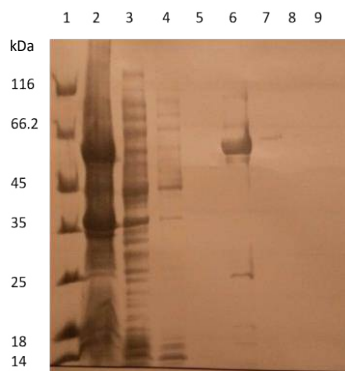
Figure 3.2 SDS-PAGE analysis of ADS purification. Lane 1: protein marker. Lane 2: supernatant after sonication. Lane 3: flow-through. Lane 4: cell lysis buffer with 5 mM of imidazole. Lane 5: cell lysis buffer with 20 mM of imidazole. Lane 6: cell lysis buffer with 100 mM of imidazole. Lane 7: cell lysis buffer with 100 mM of imidazole. Lane 8: cell lysis buffer with 300 mM of imidazole.

Analysis of the pentane extract products and kinetics studies

Analytical incubations of ADS and FDP were carried out to test activity of the purified ADS and to compare the product profile to those in reported literature.[21,86] 50 µL of purified enzyme was incubated with 1 µM of FDP in 250 µL of incubation buffer 2. The reaction was then overlaid with 500 µL of hexane and allowed to stir for 24 h. The GC-MS analysis of the pentane extract showed the presence of one major compound, with a molecular ion of m/z = 204. The mass spectrum of the enzymatic product, amorphadiene, corresponds well with what is reported in the literature (Figure 3.3). [21,86]
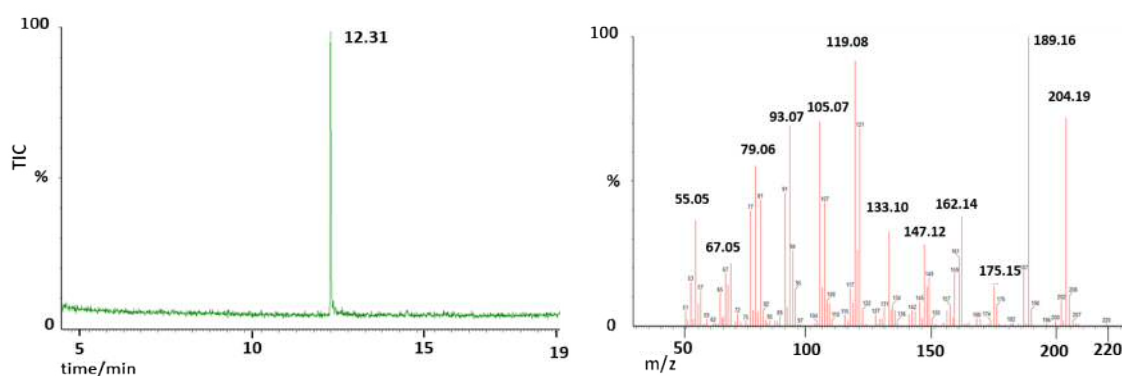
Figure 3.3 GC-MS of the pentane extractable products arising from the incubation of ADS with FDP. Left: gas chromatogram highlighting the formation of a single product; Right: mass spectrum of the compound eluting at 12.31 min.

3.1.2 `Steady state kinetics

The steady-state kinetic parameters for the reaction catalysed by ADS were measured using a radiolabelled-substrate assay commonly used with terpene synthases, which involves the incubation of a range of concentrations of [1-^{3}H]-FDP with a fixed concentration of enzyme for a defined length of time. The radio-labelled products were then extracted with hexane, and the radioactivity level measured through scintillation counting. The data were then fitted against the Michaelis-Menten equation, $V = (V_{max} [S])/(K_M + [S])$, to give k_{cat} and K_M (Section 6.1.15). K_M represents the Michaelis constant, which is equal to the substrate concentration at which the rate of the reaction is half of the V_{max}. k_{cat} is the catalytic constant, and measures the number of substrate molecules converted into products per unit of time. The enzymatic catalytic efficiency is defined by the ratio k_{cat} / K_M.

Incubation time, enzyme concentration and Mg^{2+} concentration in the incubation buffer are factors that influence the catalytic incubations, therefore each was optimised before performing steady state kinetics.

As sesquiterpene synthases catalyse the formation of mostly hydrophobic molecules, high concentration of sesquiterpenes in the reaction buffer will reduce the rate of the release of newly formed products from the enzyme active site.
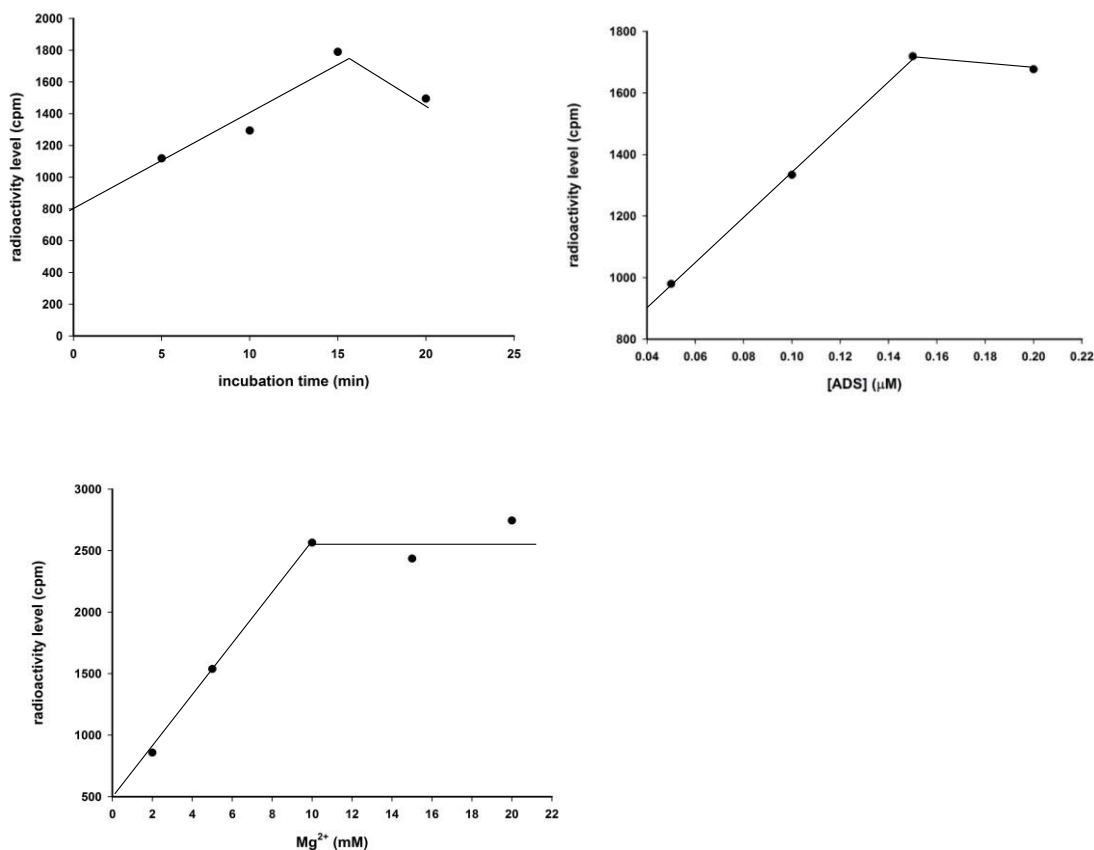
Figure 3.4 Graphs showing the radioactivity level of products formed by ADS plotted against: Top left: reaction time (0.1 μM of ADS, 12 μM FDP, 30 °C); Top right: ADS concentration (10 μM FDP, 10 min, 30 °C); Bottom left: Mg^{2+} concentration in kinetic buffer (12 μM FDP, 10 min, 30 °C, 0.1 μM ADS).

To determine the optimal reaction time, incubations were carried out with 0.1 μM of ADS, 12 μM [1-^{3}H]-FDP in incubation buffer 1 for variable amount of time. Initial rate was found to be linear with respect to time between reaction times of 1-15 min and so 10 min was chosen as the reaction time from then on (Figure 3.4, left).

To find the right enzyme concentration, incubations were set up with 12 μM [1-^{3}H]-FDP, for 10 min at variable protein concentration between 0.05 μM and 0.2 μM. The initial rate was found to be directly proportional to enzyme concentration between 0.05 and 0.15 μM and so a concentration of 0.10 μM ADS was chosen for future assays (Figure 3.4, center).

Finally, the bivalent magnesium cation is essential for sesquiterpene catalysis, but when it reaches saturation condition it interferes with the enzyme catalysis. Therefore, to find the ideal concentration of magnesium needed in the catalysis buffer, the incubations were prepared with 12 μM [1-^{3}H]-FDP, for 10 min at 30 °C, with a fixed ADS concentration of 0.1 μM and variable amount of magnesium ion in

the buffer. The initial radioactivity level was found to be directly proportional to Mg^{2+} concentration between 2 and 10 mM and so a concentration of 5 mM of Mg^{2+} was chosen for future assays (Figure 3.4, right).

Kinetic analysis of ADS was carried out following the protocol described in section 6.1.15, and incubating 0.1 μM of enzyme at 30 °C for 10 minutes. The kinetic parameters were calculated based on the average weighted mean of three independent experiments. The K_M was found to be 1.5 ± 0.15 μM, and the k_{cat} was found to be $2.19 \times 10^{-3} \pm 5 \times 10^{-5}$ s−1 (Figure 3.5). Both K_M and the k_{cat} were comparable with the literature data ($k_{cat} = 4.3 \times 10^{-3}$ sec−1, $K_M = 2.0$ μM)[21,86].
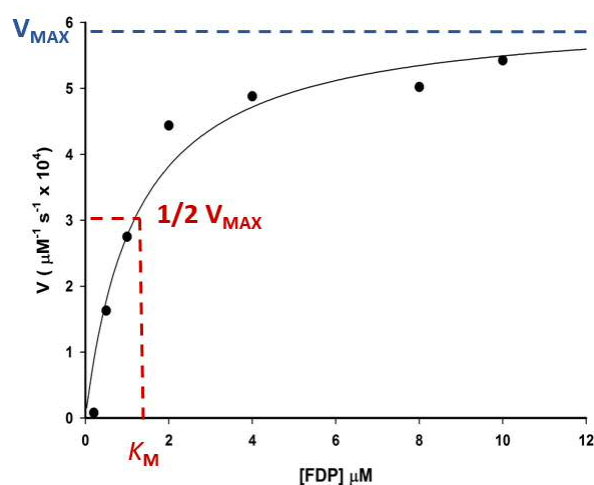
Figure 3.5 Representative Michaelis-Menten plot for the production of radiolabeled hexane extractable products from [1-³H]-FPP catalysed by ADS.

3.1.3 Inhibition studies of ADS with the α-bisabolyl cation aza-analogues

The method used to study the inhibition of ADS (and later on of AS and DCS) relied on the Lineweaver-Burk plot to determine the type of inhibition. This plot arises from taking the reciprocal of the Michaelis-Menten equation ($V = (V_{max} [S])/(K_M + [S])$ to give the following equation $[1/V = (1/V_{max}) + (K_M/V_{max} \times [S])]$. Therefore, a plot of $1/V$ against $1/[S]$ gives a straight line with the x-axis intercept at $1/K_M$, the y-axis intercept $1/V_{max}$ and the gradient K_M/V_{max} (Figure 3.6, left).
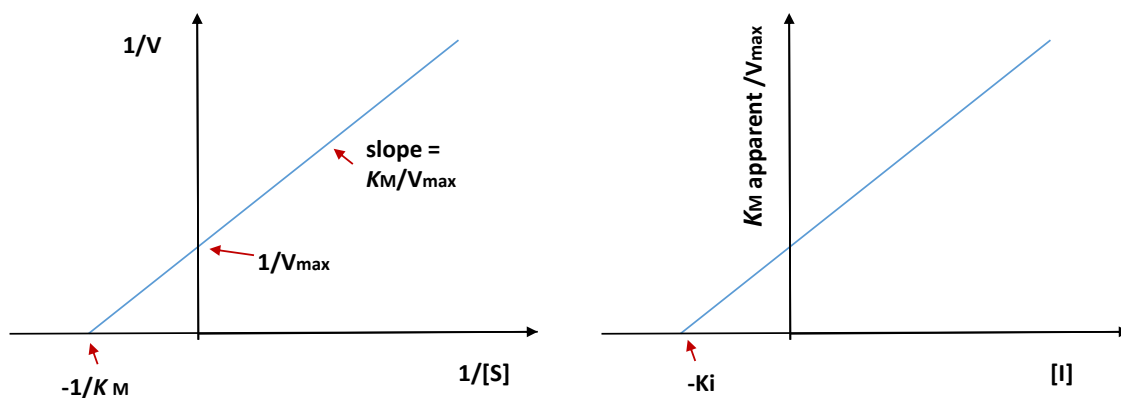
Figure 3.6 Left: Lineweaver-Burk plot; Right: plot of $K_M(\text{app})/V_{max}$ against [I] for the calculation of K_i.

Inhibition experiments comprised of a series of incubations, with increasing concentrations of inhibitor present, i.e. in each series the concentration of substrate is constant while concentration of inhibitor increases. The data was treated as described above to generate a Lineweaver-Burk plot and to illustrate graphically the inhibition mode. The K_i was then calculated fitting the Michaelis-Menten equation, where K_M (apparent) = K_M (1 + [I]/K_i), therefore, a plot of $K_M(\text{app})/V_{max}$ against [I] gives a straight line with the x-axis intercept at – K_i (Figure 3.6, right).

Inhibition studies were run following the protocol previously reported in section 6.1.16. The optimised condition previously found for ADS were used. Following previous inhibition studies on sesquiterpenes,[49] the concentrations of the (*S*)-aza bisabolyl cation (**S-60**) used for each series of reactions were 5, 10 and 15 μM (Figure 3.7).

Figure 3.7 Representative Michaelis-Menten plot for the production of radiolabeled product by: Black, ADS; Red, ADS + 5 μM (*S*)-60; Blue, ADS + 10 μM (*S*)-60, Green, ADS + 15 μM (*S*)-60.

The Lineweaver-Burk plot (Figure 3.8, top) shows the lines intercepting above the x axis and on the y axis, indicating a competitive inhibition mode, which is typically found with terpene synthases and aza-analogues. **(S)-60** inhibits ADS albeit with reduced binding affinity, ($K_{i=}$ 25 ± 5 μM) (Figure 3.8, bottom), when compared to the natural substrate FDP (2.0 μM).

Figure 3.8 Top: representative double-reciprocal plot (left) and zoom section of y-intercept (right) of the inhibitions data of ADS by (S)-60. Black, ADS; Red, ADS +5 μM of (S)-60; Blue, ADS + 10 μM (S)-60; Green, ADS + 20 μM (S)-60. Right: Plot of K_M(app) / V_{max} against [I] for the calculation of K_i.

Measurement of the inhibition of ADS by **(S)-60** was repeated in presence of 250 μM of PP$_i$ as it was previously demonstrated that the PP$_i$ leads to a considerably stronger enzymatic interaction for aza-inhibitors.[45,71] As the cation mimic may require PP$_i$ as a partner to enter and bind the enzyme active site effectively, the presence of PP$_i$ in the incubation reactions might lead to a more tightly bound active site carbocation/diphosphate ion pair.[45,30,46,93,94,71] The Michaelis-Menten plot clearly shows that the addition of PP$_i$ had a synergistic effect on the overall inhibition (Figure 3.9).
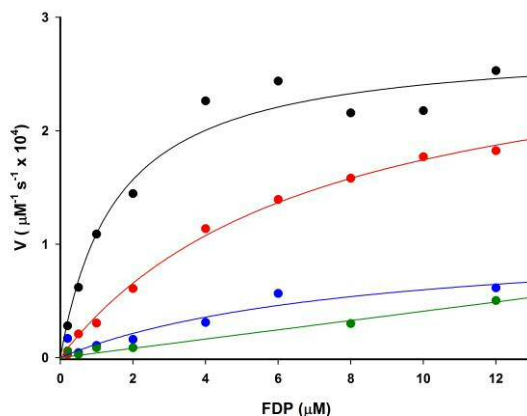
Figure 3.9 Representative Michaelis-Menten plot for the production of radiolabeled product by: Black, ADS; Red, ADS + 5 μM (*S*)-60; Blue, ADS + 10 μM (*S*)-60; Green, ADS + 20 μM (*S*)-60. For each series of reaction a fixed concentration of 250 μM of PP$_i$ was added.

The double-reciprocal plot (Figure 3.10) shows the lines intercepting exactly nor at the y axes nor at the x axes, indicating a mixed inhibition mode. This type of inhibition is rare in systems such as terpene synthases, where there is a single binding site. Due to the absence of any secondary regions for binding, the explanation for mixed inhibition remains difficult. More likely, taking in consideration 10% of error, typical of the radioactive kinetic inhibition assay, the Lineaweaver-Burk plot might indicate a competitive inhibition mode.
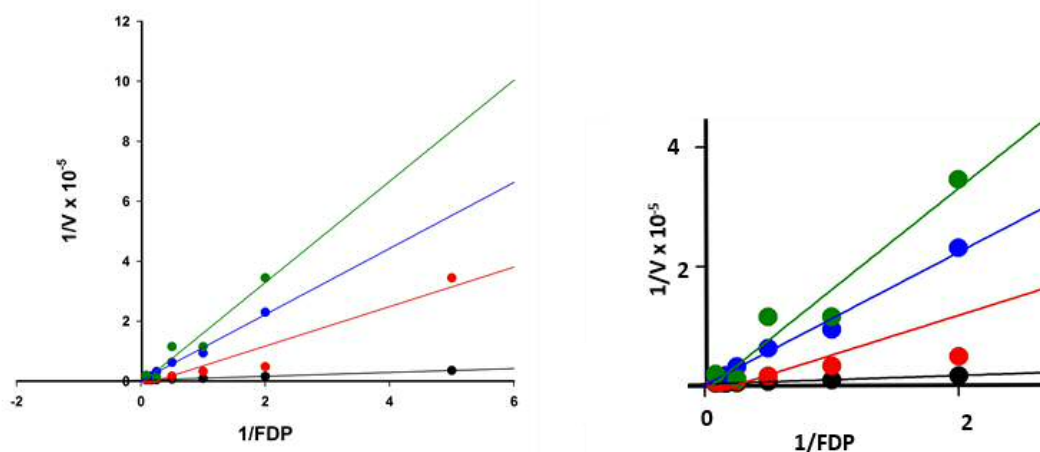
Figure 3.10 : Representative double-reciprocal plot (left) and zoom section of y-intercept region (right) of the inhibitions data of (*S*)-60. Black, ADS; Red, ADS +5 μM of (*S*)-60; Blue, ADS + 10 μM (*S*)-60; Green, ADS + 20 μM (*S*)-60. Right: detail zoom of reciprocal plot. For each series of reactions a fixed concentration of 250 μM of PP$_i$ was added.

Plotting the K_M apparent on V_{max} against the concentration of inhibitor used, **(*S*)-60** was found to be a potent inhibitor of ADS in the presence of PP$_i$, with a K_i of 1.5 ± 0.5

µM (Figure 3.11), which is 10-fold lower than the K_i obtained without PP_i and comparable to the K_M for FDP. This outcome demonstrates again how the presence of PP_i facilitates the entrance of the aza-analogue into the enzyme active site, hence lowering the K_i value for the inhibitor.
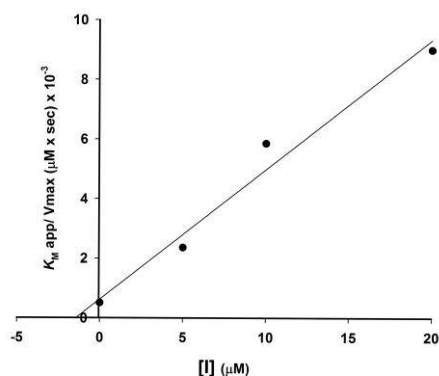
Figure 3.11 Plot of K_M(app) / V$_{max}$ against [I] for the calculation of K_i of (*S*)-60 in the presence of 250 µM PP$_i$.

Similar results were obtained when the *R* enantiomer of **60** was used to inhibit the reaction catalysed by ADS. The Michaelis-Menten plot (Figure 3.12) showed a small decrease of the V$_{max}$ with increasing concentration of the inhibitor.
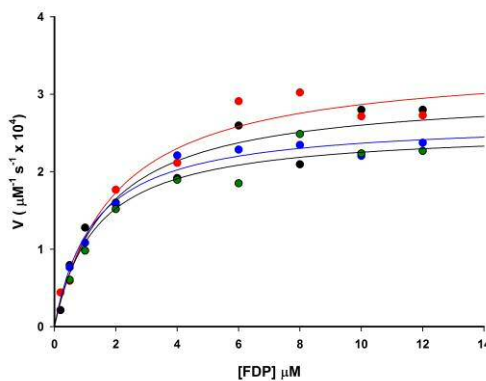
Figure 3.12 Representative Michaelis-Menten plot for the production of radiolabeled product by: Black, ADS; Red, ADS + 5 µM (*R*)-60; Blue, ADS + 10 µM (*R*)-60; Green, ADS + 15 µM (*R*)-60.

Analysis of the Lineweaver-Burk plot of the inhibition data of ADS with **(*R*)-60** did not lead to a firm conclusion (Figure 3.13). Despite several independent sets of experiments, the inhibition mode could not be determined. The Lineweaver-Burk plot showed some lines intercepting before the y-axis and above the x-axis, indicating a difference in V$_{max}$ and an effect on K_M, therefore a mixed inhibition, and other lines intercepting on the y-axis, indicative of a competitive inhibition.
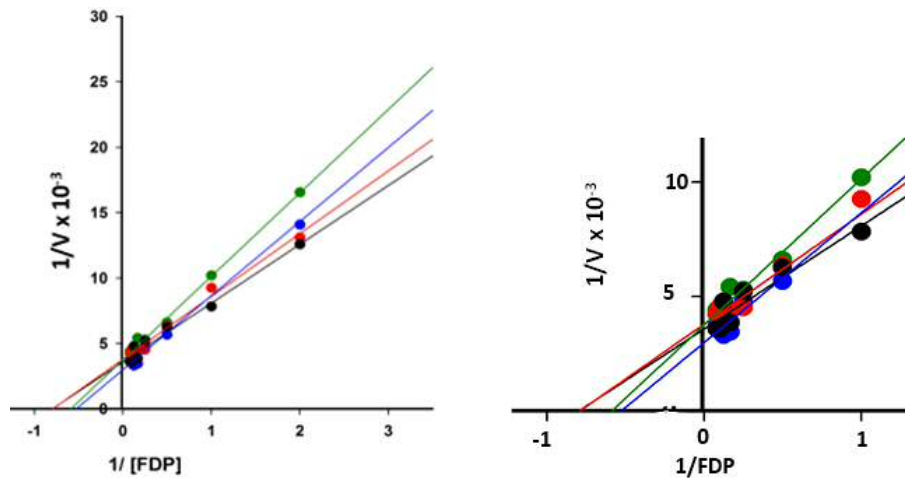
Figure 3.13 Representative double-reciprocal plot (left) and zoom section of the y-axis intercept region (right) of the inhibitions data of (*R*)-60. Black, ADS; Red, ADS + 5 μM of (*R*)-60; Blue, ADS + 10 μM (*R*)-60; Green, ADS + 15 μM (*R*)-60.

(*R*)-60 is a moderate inhibitor of ADS, showing a K_i of 50 ± 17 μM (Figure 3.14), which is an order of magnitude higher than the Michaelis-Menten constant for FDP (2 μM).
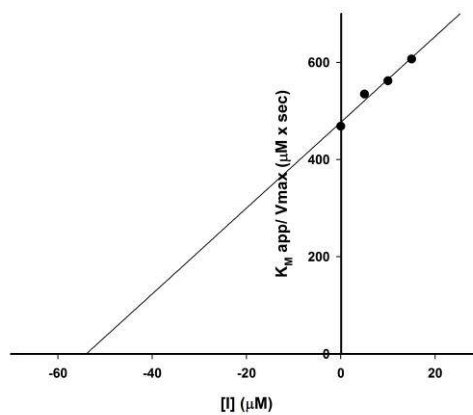
Figure 3.14 Representative plot of K_M(app) / V_{max} against [I] for the calculation of K_i of (*R*)-60.

When the inhibition experiments were repeated with the addition of PP$_i$, the Michaelis-Menten plot showed a significant reduction of the V_{max} value when 0.4 μM of **(*R*)-60** were added to the reaction mixture (Figure 3.15), indicative of a strong enzyme inhibition.
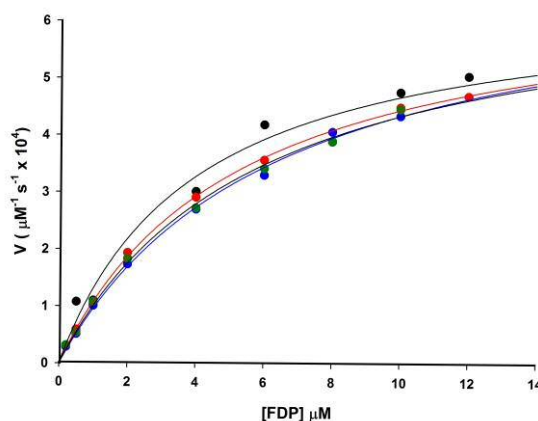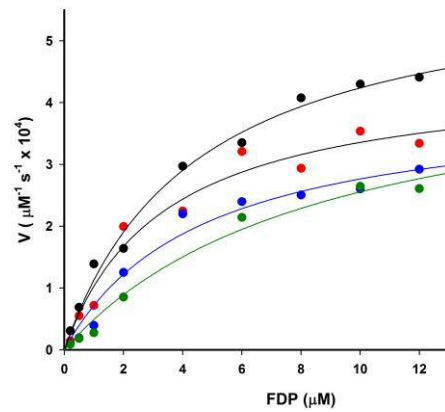
Figure 3.15 Representative Michaelis-Menten plot for the production of radiolabeled product by: Black, ADS; Red, ADS +0.4 μM of (*R*)-60; Blue, ADS + 1.2 μM (*R*)-60; Green, ADS + 2.5 μM. (*R*)-60. For each series of reaction a fixed concentration of 250 μM of PP$_i$ was added.

The double-reciprocal plot Lineweaver-Burk showed a competitive inhibition mode, as the lines cross at the y-axis (Figure 3.16, top), indicating that **(*R*)-60** competes with FDP for binding ADS active site.

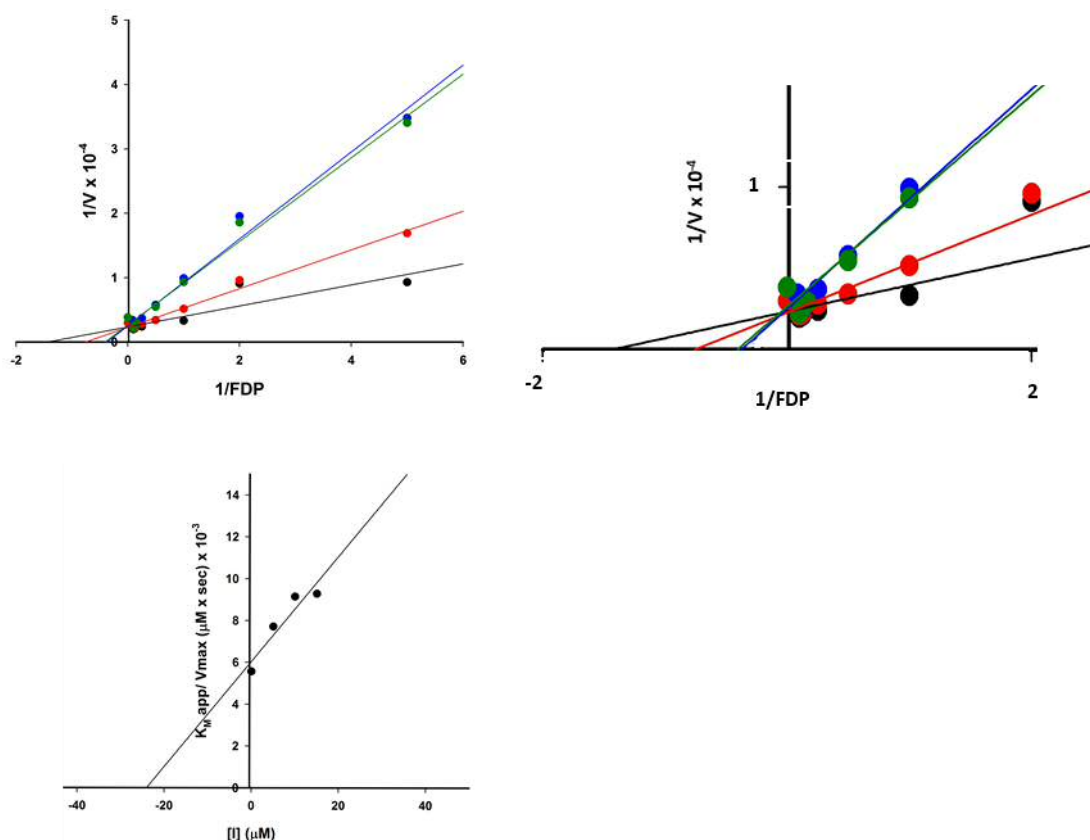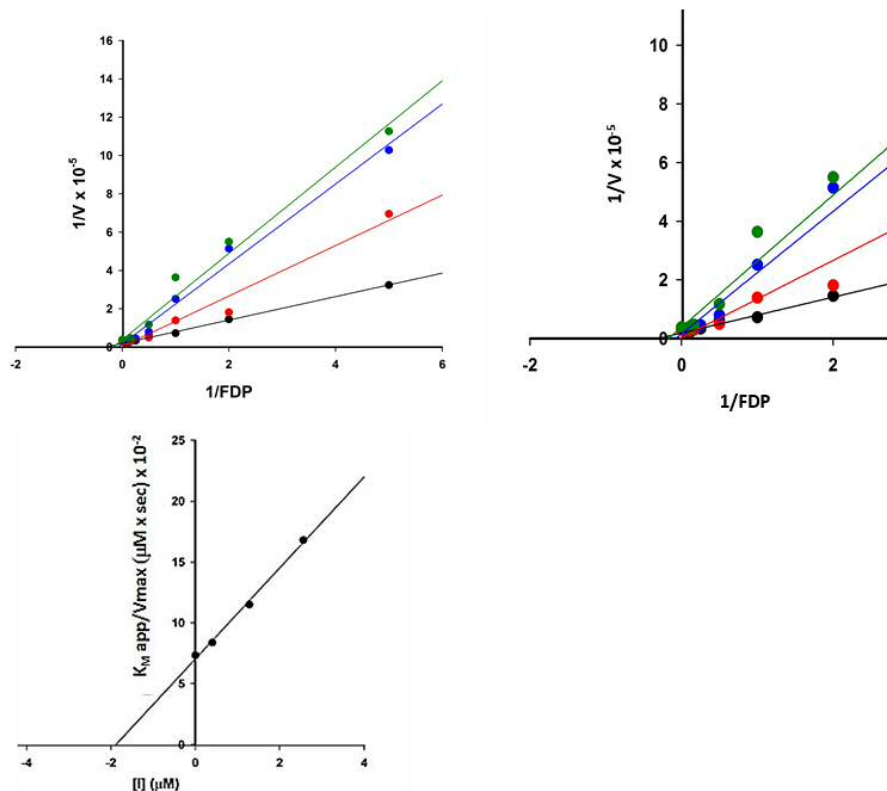**Figure 3.16 Representative double-reciprocal plot (top left) and zoom section of y intercept (top right) of the inhibitions data of (*R*)-60. Black, ADS; Red, ADS +0.4 μM of (*R*)-60; Blue, ADS + 1.2 μM (*R*)-60; Green, ADS + 2.5 μM (*R*)-60. For each series of reaction a fixed concentration of 250 μM of PP$_i$ was added. Bottom: Representative plot of K_M(app)/ V_{max} against [I] for the calculation of K_i.**

These results demonstrated that **(R)-60** tightly binds ADS active site in the presence of PP$_i$, giving a K_i of 3.7 ± 1.9 μM (Figure 3.16, bottom), a value which is comparable with the Michaelis-Menten constant of ADS for the natural substrate FDP.

Analysing the inhibition data obtained for ADS, which are summarised in Table 3.1, it can be concluded that both the R- and S- enantiomer of the aza-carbocation **60** act as moderate competitive inhibitors of ADS. The addition of PP$_i$ (250 μM) led to a considerably stronger enzymatic inhibition, lowering the two inhibition constants by one order of magnitude**.** These results are likely to be a consequence of favorable electrostatic interaction between the positively charged aza-analogues and an active site bound diphosphate.

Table 3.1 ADS Kinetics inhibition data for aza-analogues of α-bisabolyl cation (93) ADS K_M= 2.00 ± 0.15 μM k_{cat}= 1.19x10^{-2} ± 52x10^{-5} s^{-1}.

Inhibitor	+250 PP$_i$ (μM) K_i (μM)	K_i (μM)
(S)-60	1.5 ± 0.5	25 ± 5
(R)-60	3.7 ± 1.9	50 ± 17

The fact that both enantiomers of **60** acted as competitive inhibitor of the enzyme shows that they are able to compete with the natural substrate FDP for entering the active site, tightly bind to it and interfere with the ADS-catalysed amorphadiene formation. As these aza-compounds cannot be turned over by ADS, these kinetics results support the intermediacy of **33** in the biosynthesis of amorphadiene. This outcome is partially in agreement with Picaud's previous studies.[21] He used deuterated farnesyl phosphate and deuterium exchange experiments to suggest that the R-enantiomer of the bisabolyl cation is the sole intermediate formed in the biosynthesis of amorphadiene. Based on this consideration, only the R-aza analogue **60** should have been able to enter and bind to ADS active site, therefore acting as a competitive inhibitor. The fact that both enantiomers of **60** are equally effective as ADS inhibitor is consistent with a flexible model of sesquiterpene synthase active site, according to which an active site can accommodate a variety of intermediates of varying shape and charge distribution without being rigidly complementary to a

single intermediate or transition state species. This model is also consistent with D.E. Cane's work.[71] He found that both enantiomers of the aza-analogue **60** were able to equally inhibit trichodiene synthase.

3.2 Aristolochene synthase

As described in section 1.6, aristolochene synthase from *Penicillin roqueforti* (AS) is a sesquiterpene cyclase that catalyses the formation of the bicyclic hydrocarbon (+)-aristolochene. As AS has been intensively studied in the past, its catalytic mechanism is well known and was described in scheme 1.5, Chapter 1. Taking into consideration that a 1,10-cyclisation mechanism does not involve the formation of the α-bisabolyl cation **33** (Scheme 3.1) which must to be formed in a 1,6 cyclisation instead, if the aza-analogue **60** is a good mimic of **33**, then its enantiomers should not be able to enter the AS active site and act as a competitive inhibitor. Therefore, AS inhibitions studies with both **(S)-60** and **(R)-60**, were performed as a negative control.
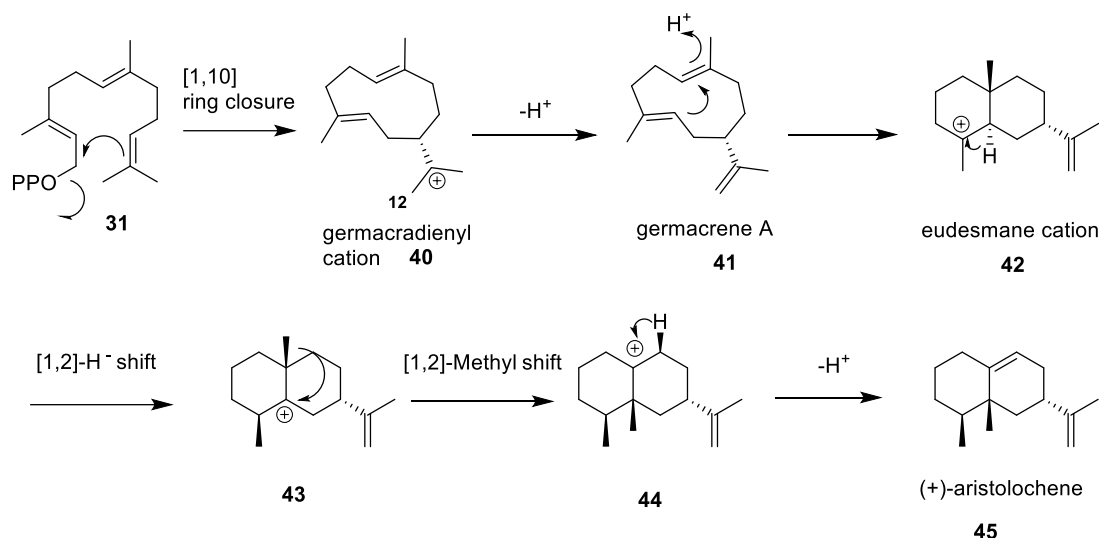
Scheme 3.1 AS mediated mechanism showing the germacradienyl cation 40 as the key intermediate in the aristolochene formation.[21]

3.2.1 Characterisation of wild-type aristolochene synthase

AS was produced following the protocols previously described in the literature.[22,23,36,38–42,45,46,50]

Expression and purification

A cDNA coding for AS from *Penicillum roqueforti* was previously subcloned into the expression vector pET21 in our lab. *E. coli* BL21(DE-3) cells were transformed with the resulting plasmid as described in section 6.1.7. A single colony was picked from a plate prepared as stated in 6.1.7 and used to inoculate a solution of LB medium (100 mL) containing 0.3 mM ampicillin. This culture was incubated at 37 °C overnight with shaking at 150 rpm. A portion (10 mL) of this stationary phase culture was then used to inoculate 500 mL LB medium containing ampicillin. This culture was incubated at 37 °C with shaking at 150 rpm until the optical density reached 0.5 AU at 600 nm. Isopropyl β-D-1-thiogalactopyranoside (IPTG) was added (0.5 mM) and the culture was left to grow for 6 h at 20 °C before being harvested by centrifugation. The supernatant solution was decanted and the cell pellet was stored at −20 °C until required.

A cell pellet was allowed to defrost on ice, resuspended in cell lysis buffer 2 (section 6.1.6), and lysed by sonication on ice. Sonication causes the fragmentation of the cells, which were centrifugated to separate the cells fragments from the supernatant solution. Since AS was found in the inclusion bodies, as judged by SDS-PAGE (Figure 3.17, lane 2), the lysate was centrifuged and the supernatant solution discarded. The pellet was then resuspended in cell lysis buffer and a basic extraction method was performed to extract the protein from inclusion bodies by unfolding and refolding the protein's tertiary structure. The procedure consists initially of resuspending the pellet in cell lysis buffer 2, then increasing the pH of the stirred suspension to ~12 with the addition of 1 M NaOH to solubilise the protein. The solution was left to stir for 30 min in ice. Then, β-mercaptoethanol (final conc. 5 mM) was added and the pH was adjusted to 8 by addition of 1 M HCl. After stirring for a further 30 min at 0 °C the solution was centrifuged at 30.000 g for 30 min. The pellet was discarded, the remaining AS protein solution was purified using a diethylaminoethyl anion exchange column (DEAE-cellulose, 75 mL), containing positively charged diethylaminoethanol groups that bind negatively charged proteins. Positively charged or neutral impurities flowed through the column and were discarded. Elution of AS was accomplished by increasing the NaCl concentration in the cell lysis buffer 2 used to wash the column, as the chloride ions compete for binding to the tertiary ammonium groups of the DEAE resin and displace AS. The salt concentration was increased until baseline absorbance (at 280 nm) was observed. SDS-PAGE analysis of the eluted fractions from the DEAE anion exchange column

absorbing at 280 nm allowed identification of fractions containing the protein corresponding to the correct molecular weight of AS (64 kDa) (Figure 3.17). These fractions were then pooled together and dialysed against dialysis buffer 2 at 0 °C to remove excess NaCl. The protein was then concentrated by Amicon™ ultrafiltration using a Millipore 30,000 MW cut-off membrane. Enzyme concentration was determined by the method of Bradford.[95]
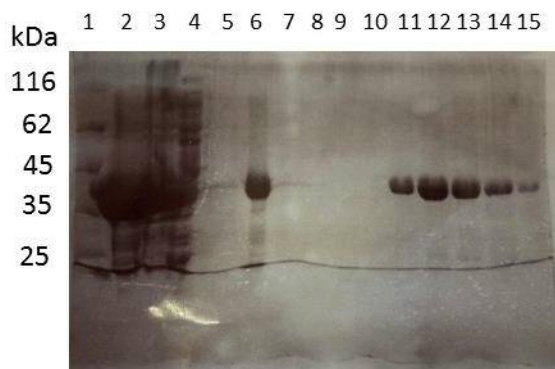
Figure 3.17 SDS-polyacrylamide gel showing PR-AS purification. Lane 1: protein marker. Lane 2: pellets after base extraction. Lane 3: supernatant after base extraction. Lane 4: flow-through fraction from the DEAE anion exchange column. Lane 6: fraction from the DEAE anion exchange column containing aggregated AS. Lane 5-15: eluent fractions from the DEAE anion exchange elution.

Analysis of the pentane extract products

Analytical incubations of AS and the natural substrate FDP were carried out to test the activity of the purified AS and to compare the product profile to that reported in the literature. 50 μL of purified enzyme were incubated with 1 μM of FDP in 250 μL of incubation buffer 2. The reaction was then overlaid with 500 μL of hexane and left to stir for 24 h. GC-MS analysis of the pentane extracts showed the presence of one major compound, with a molecular ion of m/z = 204. The mass spectrum of the sesquiterpene product, aristolochene, was in agreement with what is reported in the literature (Figure 3.18).[22,23,36,38–42,45,46,50–52,67]
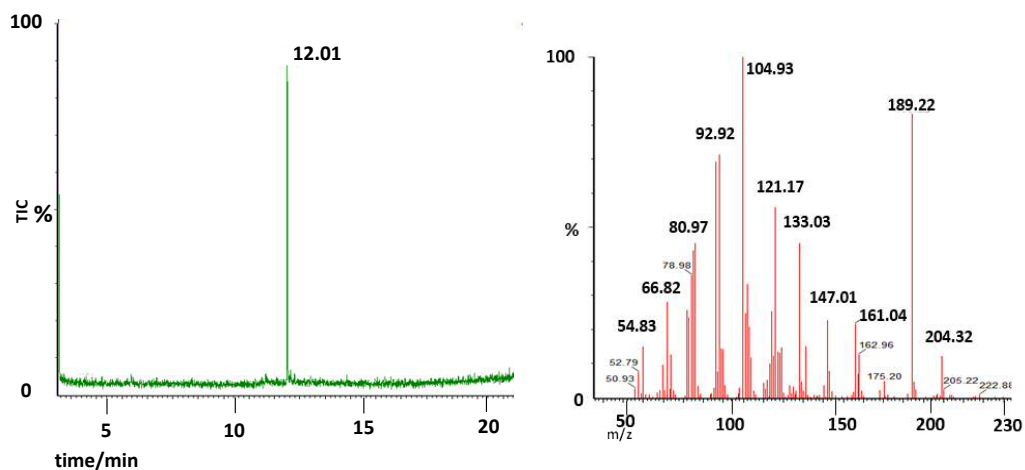
Figure 3.18 GC-MS of the pentane extractable products arising from the incubation of AS with FDP. Left: gas chromatogram highlighting the formation of a single product; Right: mass spectrum of the compound eluting at 12.01 min.

3.2.2 Steady state kinetics

To determine the optimal reaction time, incubations were carried out with 0.1 μM of AS, 10 μM [1-^{3}H]-FDP in incubation buffer 2 for variable amount of time. Initial rate was found to be linear with respect to time between reaction times of 5-20 min and so 10 min was chosen as the reaction time from then on (Figure 3.19, left).
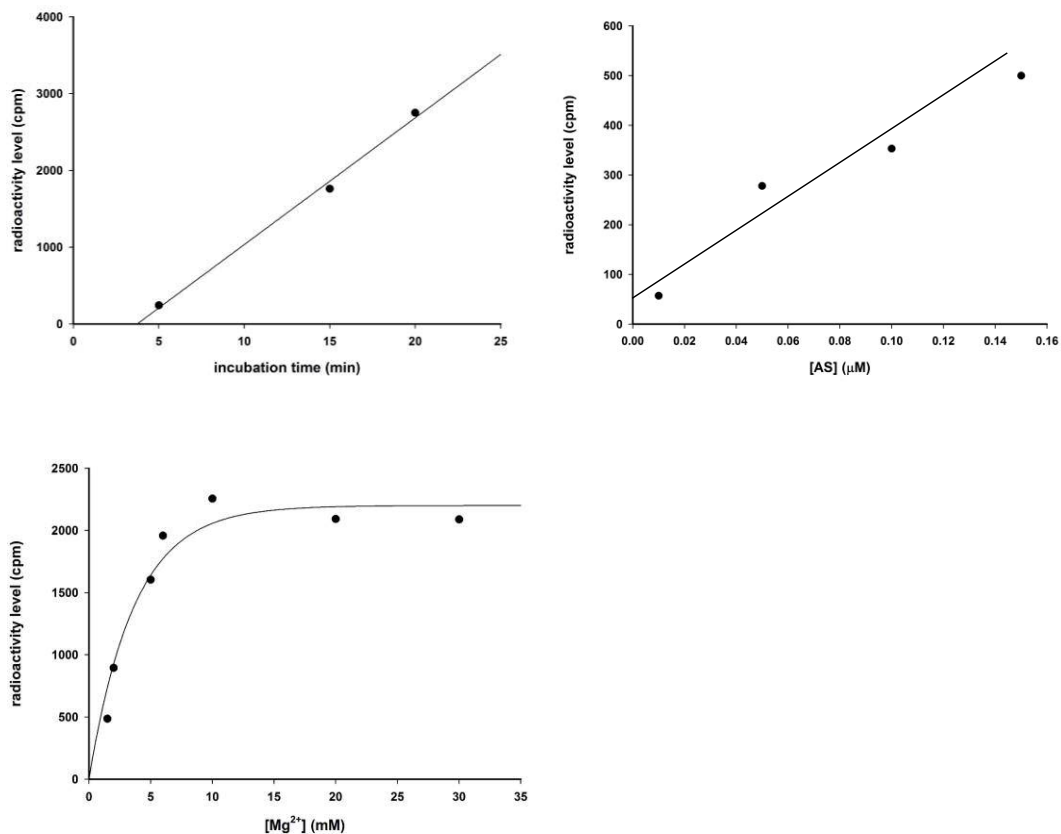
Figure 3.19 Graphs showing radioactivity level in hexane extractable products formed by AS plotted against: Top left: reaction time (0.1 μM of AS, 10 μM FDP, 30 °C); Top right: enzyme concentration (10μM FDP, 10 min, 30 °C); Bottom left: magnesium ion concentration in the buffer (0.1 μM of AS, 10 μM FDP, 30 °C).

An assay to find the optimal concentration of the enzyme incubations was carried out. Incubations were prepared with 10 μM [1-^{3}H]-FDP, for 10 min at variable enzyme concentration in the incubation buffer 2. The initial rate was found to be directly proportional to enzyme concentration between 0.01 and 0.16 μM and so a concentration of 0.10 μM of AS was chosen for future assays (Figure 3.19, center).

To determine the optimal magnesium concentration in the catalysis buffer, incubations were carried out with 10 μM [1-^{3}H]-FDP, 0.1 μM of AS for 10 min, with variable and increasing concentration of magnesium (Figure 3.3, left). The initial rate was found to be directly proportional to Mg^{2+} between 1 and 6 mM and so a concentration of 5 mM of was chosen for future assays. The optimal conditions found for kinetics assay (10 min, [AS]=0.1μM, Mg^{2+}=5 mM) were in agreement with literature values.[22,23,36,36,38–42,45,46,50–52,67]

Kinetic analyses were then carried out as described above and following the protocol described in section 6.1.15, and incubating 0.1 μM of enzyme at 30 °C for 10 minutes. k_{cat} and K_M, calculated as a mean from three independent experiments, were found to be $1.00 \times 10^{-2} \pm 2 \times 10^{-4}$ sec^{-1} and 2.01 ± 0.41 μM, respectively (Figure 3.20). Both K_M and the k_{cat} were comparable with the literature data [39] ($k_{cat} = 3 \times 10^{-2} \pm 2 \times 10^{-2}$ sec^{-1}, $K_M = 2.3 \pm 0.5$ μM). The catalytic efficiency was calculated to be $4.13 \times 10^{-3} \pm 1.9 \times 10^{-4}$ μM^{-1} sec^{-1}.
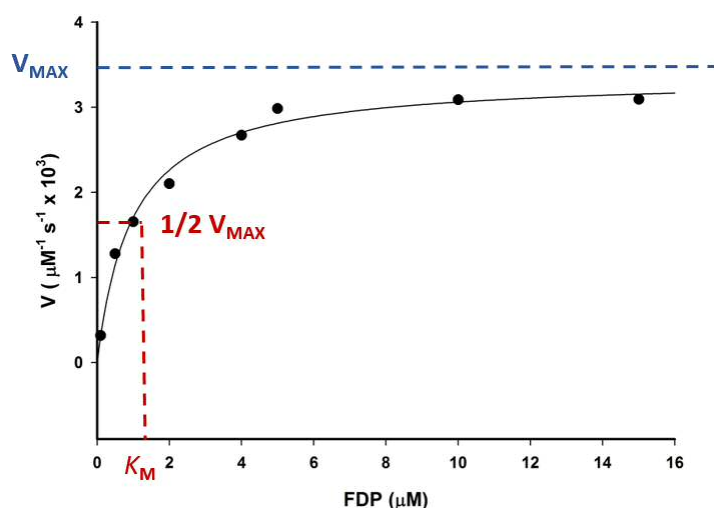
Figure 3.20 Representative Michaelis-Menten plot for the production of radiolabeled hexane extractable products from [1-³H]-FDP catalsyed by AS.

3.2.3 Inhibition of AS catalysed reaction the α-bisabolyl cation aza-analogues (60)

Inhibition studies were performed following the protocol described in section 6.1.16, and using the optimal condition previously found for AS. Following the literature work,[45] the chosen concentration of the *S*-aza bisabolyl cation **60** used for each series of reactions were 0, 50, 100, 150 μM (Figure 3.21).
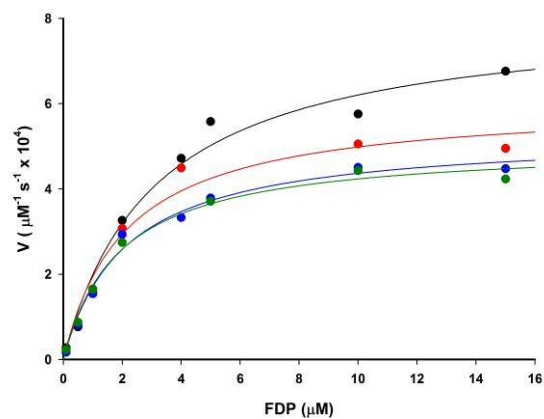
Figure 3.21 Representative Michaelis-Menten plot for the production of radiolabeled product by: Black, AS; Red, AS + 50 μM of (*S*)-60; Blue, AS + 100 μM (*S*)-60; Green, AS + 150 μM (*S*)-60.

(*S*)-60 proved to interact with AS rather poorly when compared to the tight binding of FDP (K_M =2.42 ± 0.11 μM). In fact, its elevated inhibition constant, (K_i = 295 ± 15 μM, Figure 3.22, bottom), made it difficult to determine the affinity of (*S*)-60 for the enzyme and its inhibition mode.
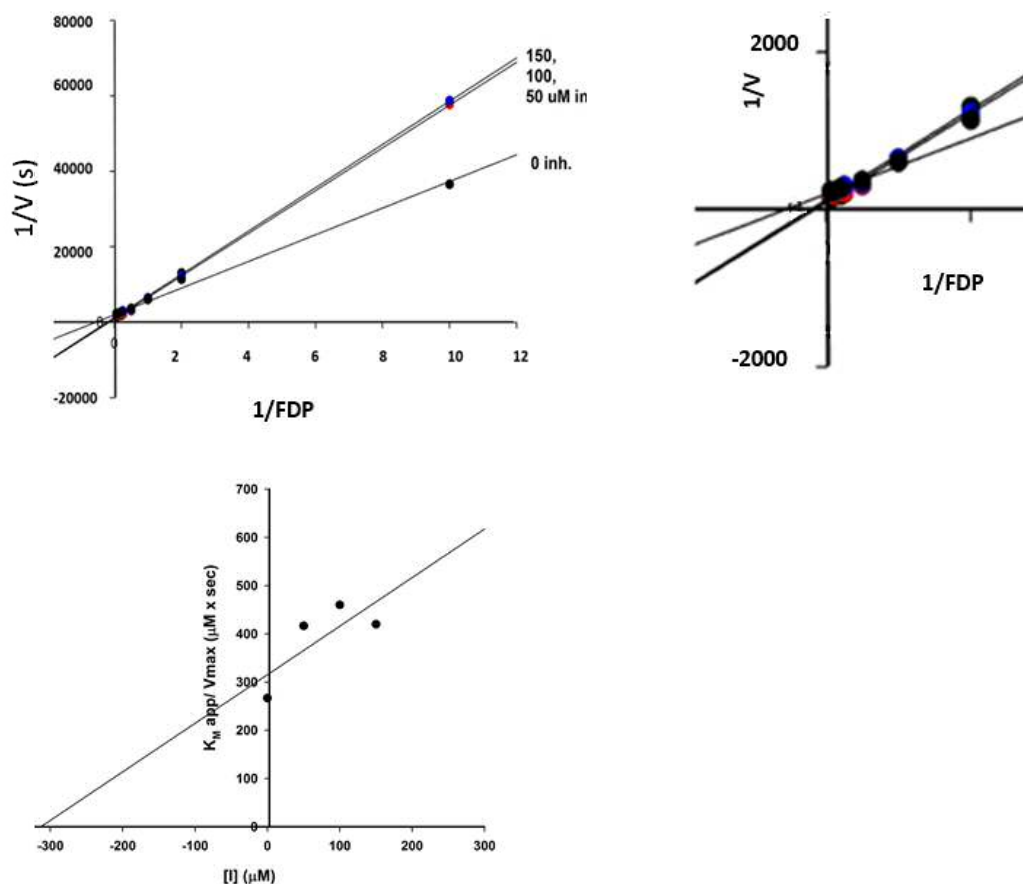
Figure 3.22 Top left: representative double-reciprocal plot of the inhibitions data of AS with (*S*)-60. Right: zoom section of y intercept region. Bottom left: Representative plot of K_M(app) / V$_{max}$ against [I] for the calculation of K_i.

The Lineweaver-Burk plot (Figure 3.22, top) shows the lines intercepting slightly before and above the x axis, suggesting that it is a mixed inhibitor. In terpene synthases, mixed inhibitors are quite rare and difficult explanation, as they have only a single binding site.

Measurements of the inhibition of AS by **(*S*)-60** were repeated in the presence of 250 μM of PP$_i$. Although the Michaelis-Menten plot obtained showed that the addition of PP$_i$ affected the inhibition, as the V$_{max}$ of AS decreased with increasing concentration of the inhibitor (Figure 3.23), it was not possible to determine the inhibition mode despite carrying out several sets of experiments.
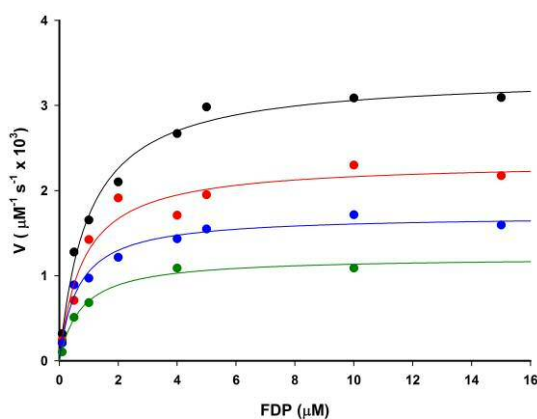
Figure 3.23 Representative Michaelis-Menten plot for the production of radiolabeled product by: Black, AS; Red, AS + 50 μM of (*S*)-60; Blue, AS + 100 μM (*S*)-60; Green, AS + 150 μM (*S*)-60. For each series of reaction a fixed concentration of 250 μM PP$_i$, was added.

The Lineweaver-Burk plot (Figure 3.24) shows the lines not intercepting either at the y- or at the x-axis, indicating a difference in both V$_{max}$ and K_M, indicative of mixed inhibition.
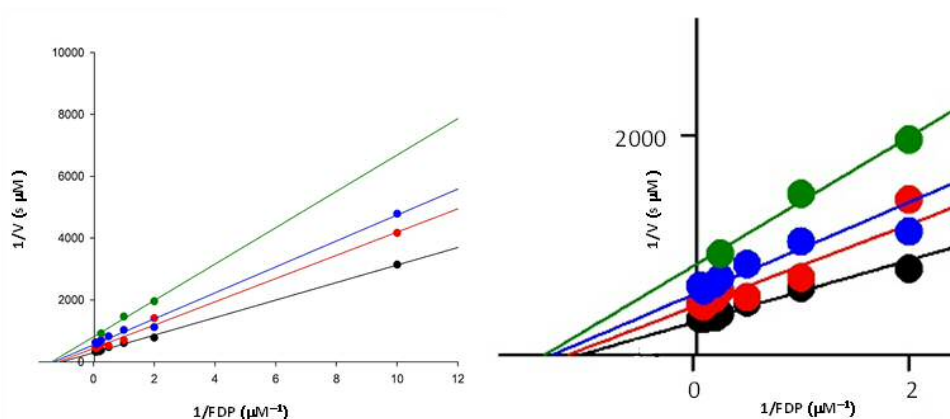
Figure 3.24 Representative double-reciprocal plot (left) and its zoom of y-intercept (right) of the inhibitions data of (*S*)-60. Black, (*S*)-60= 0; Red, (*S*)-60= 50 μM; Blue, (*S*)-60= 100 μM; Green, (*S*)-60= 150 μM. For each series of reactions a fixed concentration of 250 μM PP$_i$ was added.

When the slopes of the double-reciprocal plot lines were plotted against the inhibitor concentration (Figure 3.25), **(*S*)-60** was found again to be a weak inhibitor of AS in the presence of PP$_i$, with a K_i of 255 ± 23 μM, which is high compared with the K_M 2.42 ± 0.11 μM for the natural substrate FDP.
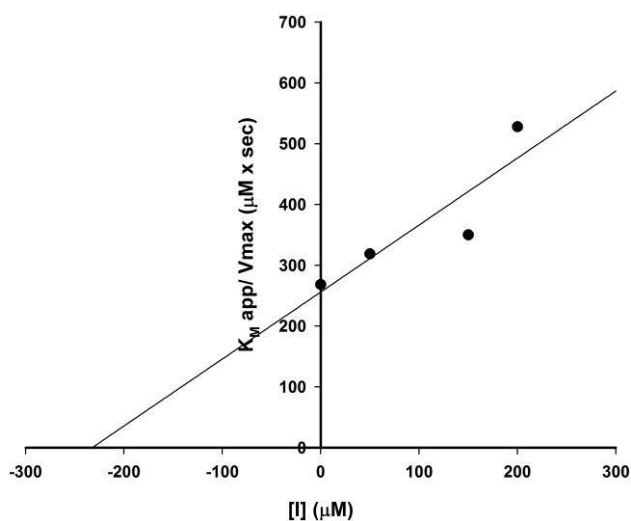
Figure 3.25 Representative plot K_M(app) / V$_{max}$ against [I] for the calculation of K_i of (*S*)-60 in the presence of PP$_i$.

Similar results were obtained when the (*R*)-enantiomer of **60** was used to inhibit the reaction catalysed by AS. The Michaelis-Menten plot showed a small decrease of V$_{max}$ with increasing concentration of **(*R*)-60** (Figure 3.26).
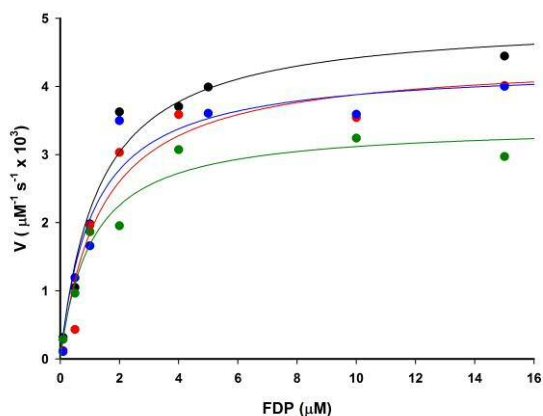
Figure 3.26 Representative Michaelis-Menten plot for the production of radiolabeled product by: Black, AS; Red, AS + 50 μM of (*R*)-60; Blue, AS + 100 μM (*R*)-60; Green, AS + 150 μM (*R*)-60.

The Lineaweaver-Burk plot (Figure 3.27, top) again suggested a competitive mode of inhibition, as the lines crossed, within the error, on the y-axis, but as the K_i was found to be 3 orders of magnitude higher (489 ± 62 μM) than the K_M for FDP (2.3 ± 0.5 μM), it can be said that **(*R*)-60** is not an effective mimic of an on-path intermediate generated during the catalytic cycle of AS.
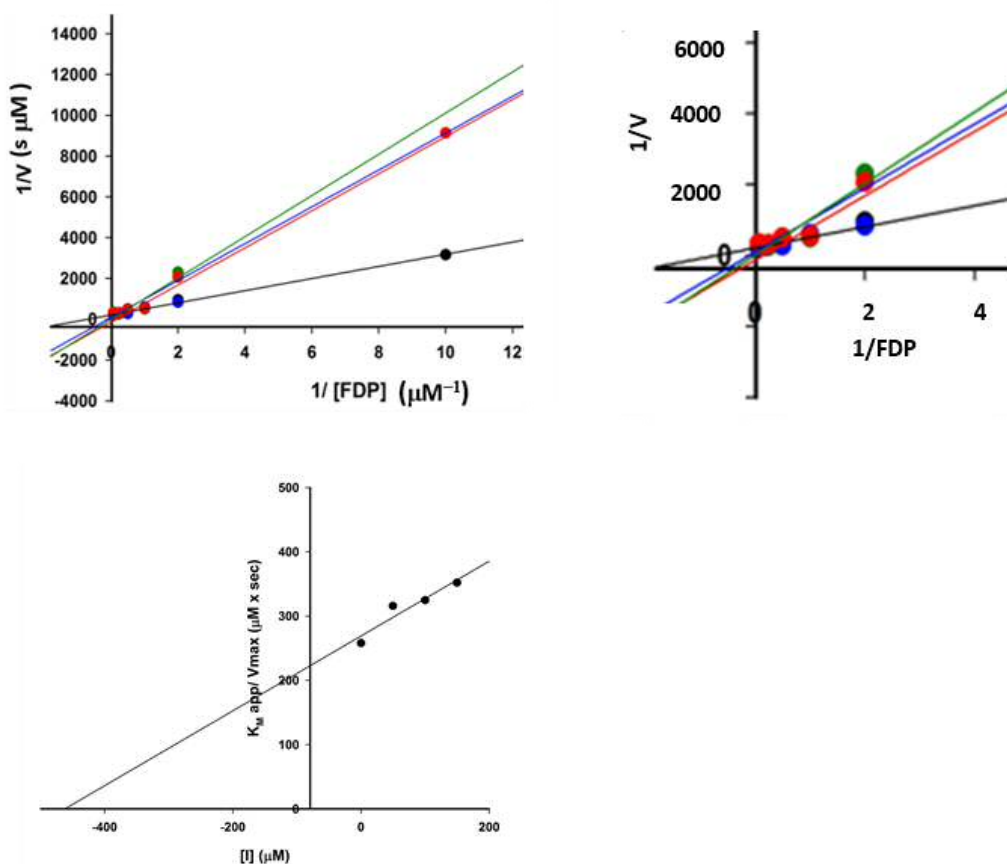
Figure 3.27 Top: representative double reciprocal plot (left) and zoom section of y intercept region (right) of the inhibition data of AS with (*R*)-60. Black, AS; Red, AS + 50 μM (*R*)-60; Blue,

When PP_i was added to the inhibition incubations, interpretation of the kinetics data obtained was not straightforward. The Michaelis-Menten plots obtained from several individual sets of experiments did not show a linear relationship (Figure 3.28).
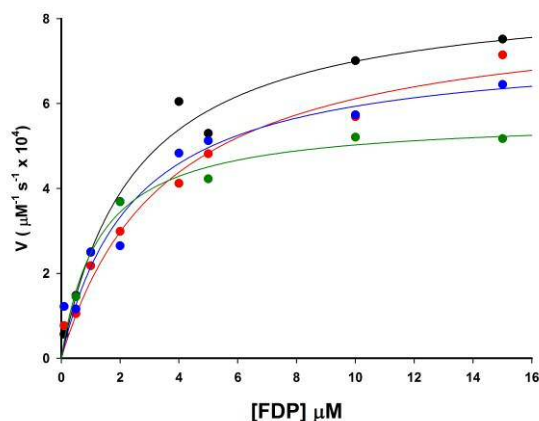
Figure 3.28 Representative Michaelis-Menten plot of: Black, AS; Red, AS + 50 μM of (*R*)-60; Blue, AS + 100 μM (*R*)-60; Green, AS + 150 μM (*R*)-60. For each series of reaction a fixed concentration of 250 μM of PP_i was added.

The Lineweaver-Burk double-reciprocal plot suggested again a mixed type of inhibition, as the lines cross before the y axis and above the x axis (Figure 3.29, top). As the **(*R*)-60** K_i was found to be 489 ± 62 μM (Figure 3.29, bottom), which is a rather high value when compared with FDP, indicating that **(*R*)-60** is not capable to act as an AS inhibitor in the presence of PP_i.
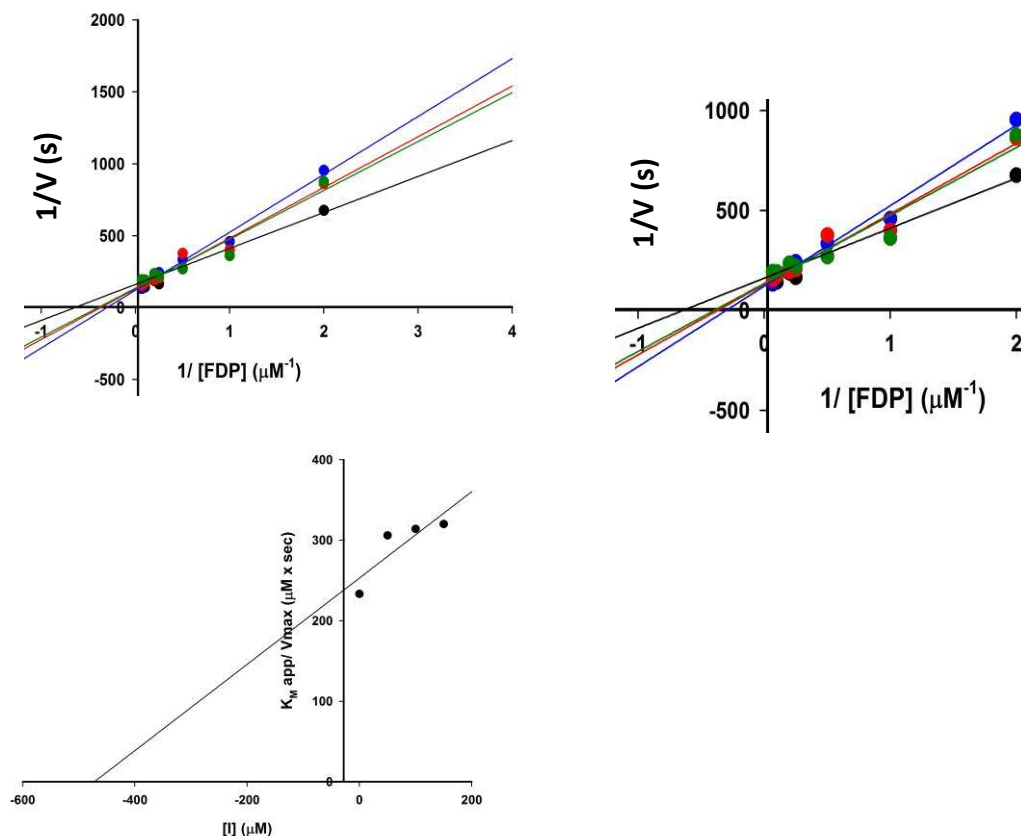
Figure 3.29 Top: representative double-reciprocal plot (letf) and zoom section of y intercept region (right) of the inhibition data of AS with (*R*)-60. Black, AS; Red, AS + 50 μM of (*R*)-60; Blue, AS + 100 μM (*R*)-60; Green, AS + 150 μM (*R*)-60. For each series of reactions a fixed concentration of 250 μM of PP$_i$ was added. Bottom: plot of K_M(app) / V_{max} against [I] for the calculation of K_i of (*R*)-60 in the presence of 250 μM PP$_i$.

The inhibition data obtained are summarised in table 3.2 below.

Table 3.2 AS Kinetics inhibition data for aza-analogues of α-bisabolyl cation (60). AS K_M= 2.42 ±11 μM k_{cat} = 1x10^{-2} ± 2x10^{-5} s^{-1}.

Inhibitor	+250 PP$_i$ (μM) K_i (μM)	K_i (μM)
(*S*)-60	255 ± 23	295 ± 15
(*R*)-60	489 ± 62	472 ± 48

Although the exact inhibition mode could not be determinated, these results show that both enantiomers of the designed aza-analogue of the α-bisabolyl cation (**60**) bind weakly to the enzyme, consequently, they do not significantly interfere with AS-mediated aristolochene formation. This outcome is consistent with previous

studies on the catalytic mechanism of AS, as the α-bisabolyl cation **33** is not an intermediate in the biosynthesis of aristolochene and it can be said that these aza-analogues do not accurately resemble any possible intermediate carbocation involved in the AS cyclisation mechanism.

Taking the ADS and AS kinetics inhibition data all together, it can be concluded that the designed aza-analogues are a good mimic of the intermediary α-bisabolene carbocation **33**, and they can be useful tools to gain more information about the potential intermediacy of **33** in the DCS-mediated cadinene biosynthesis.

3.3 δ-Cadinene synthase (DCS)

As described in section 1.6.3, a considerable amount of effort has gone into determining the catalytic mechanism of δ-cadinene synthase, but unfortunately it was not possible to establish the exact enzymatic mechanism used by DCS to form DCN. This section will initially describe the characterisation of WT DCS and the optimisation of its purification protocol. Finally, the enzymatic inhibitions studies with the previously synthesised aza-analogues **(R)- and (S)-60** will be shown in order to give further evidences towards a 1,6- or a 1,10-cyclisation reaction.

3.4 Characterisation of the wild-type δ-cadinene synthase

WT-DCS was produced as previously described in the literature.[31,49]

3.4.1 Purification

A cDNA of WT-DCS from *Gossypium arboreum* was previously subcloned into the expression vector pET21d by Dr. S. Taylor. *E. coli* BL21(DE-3) cells were transformed with the resulting plasmid as described in section 6.1.7 and the cDNA expressed following method B described in Chapter 6, section 6.1.8: a single colony was picked from a plate prepared as stated in 6.1.7 and used to inoculate a solution of LB medium (100 mL) containing 0.3 mM ampicillin. This culture was incubated at 37 °C overnight with shaking at 150 rpm. A portion (10 mL) of this stationary phase culture was then used to inoculate 500 mL LB medium containing 0.3 mM ampicillin. This culture was incubated at 37 °C with shaking at 150 rpm until the optical density reached 0.5 AU at 600 nm. IPTG was added (0.5 mM) and the culture

was left to grow for 6 h at 20 °C before being harvested by centrifugation. The supernatant solution was decanted and the cell pellet was stored at −20 °C until required. Raw WT-DCS was purified following the protocol depicted in the literature[49] and described in section 6.1.9, method B. A cell pellet was allowed to defrost on ice, resuspended in cell lysis buffer 2 and lysed by sonication on ice. Since DCS was found in the inclusion bodies, as judged by SDS-PAGE, the lysate was centrifuged and the supernatant solution discarded. The pellet was then resuspended in cell lysis buffer and a basic extraction method was performed as previously described. The solution was then centrifuged at 30.000 g for 30 min. The pellet was discarded, and the remaining DCS protein solution was purified by DEAE column following the same procedure previously used to purify AS. The eluent fractions absorbing at 280 nm were analysed by SDS-PAGE (Figure 3.30), and those containing protein of the expected molecular weight (66.4 kDa) were pooled together and dialysed against dialysis buffer 2 at 0 °C to remove the excess of NaCl used to elute the enzyme. The protein was then concentrated by Amicon™ ultrafiltration using a Millipore 30,000 MW cut-off membrane. Enzyme concentration was determinate by Bradford assay.[95]
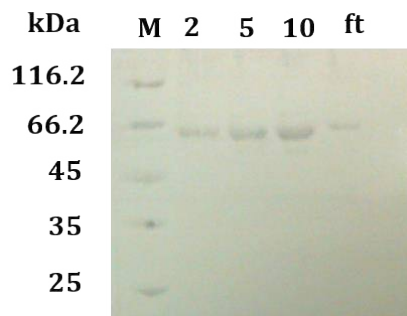
Figure 3.30 SDS-polyacrylamide gel of pure WT-DCS. (M): protein marker; (2): 2 μL; (5) 5 μL; (10) 10 μL of a 0.1 μM solution of pure protein. (ft): flow through of Amicon.

3.4.2 Analysis of the pentane extract products

Analytical incubations of DCS and FDP were carried out to test activity of the purified DCS and to compare the product profile to those in reported literature.[49] 50 μL of 0.1 μM solution of purified enzyme were incubated with 1 μM of FDP in 250 μL of incubation buffer 2. The reaction was then overlaid with 500 μL of hexane and and allowed to stir for 24 h. The GC-MS analysis of the pentane extract showed the presence of one major compound, with a molecular ion of m/z = 204. The mass

spectrum of the enzymatic product, DCN, corresponds well with that reported in the literature (Figure 3.31). [49]
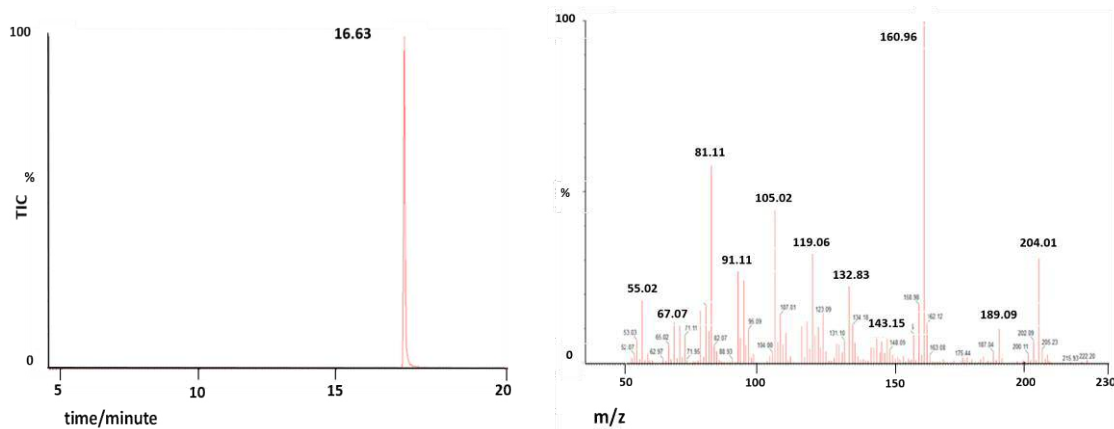
Figure 3.31 GC-MS of the pentane extractable products arising from the incubation of DCS with FDP. Left: gas chromatogram highlighting the formation of a single product; Right: mass spectrum of the compound eluting at 16.63 min

For the reasons mentioned in section 3.1.2 , kinetics studies were required in order to determine the optimal reaction time and enzyme concentration to be used in inhibition studies (Figure 3.32).
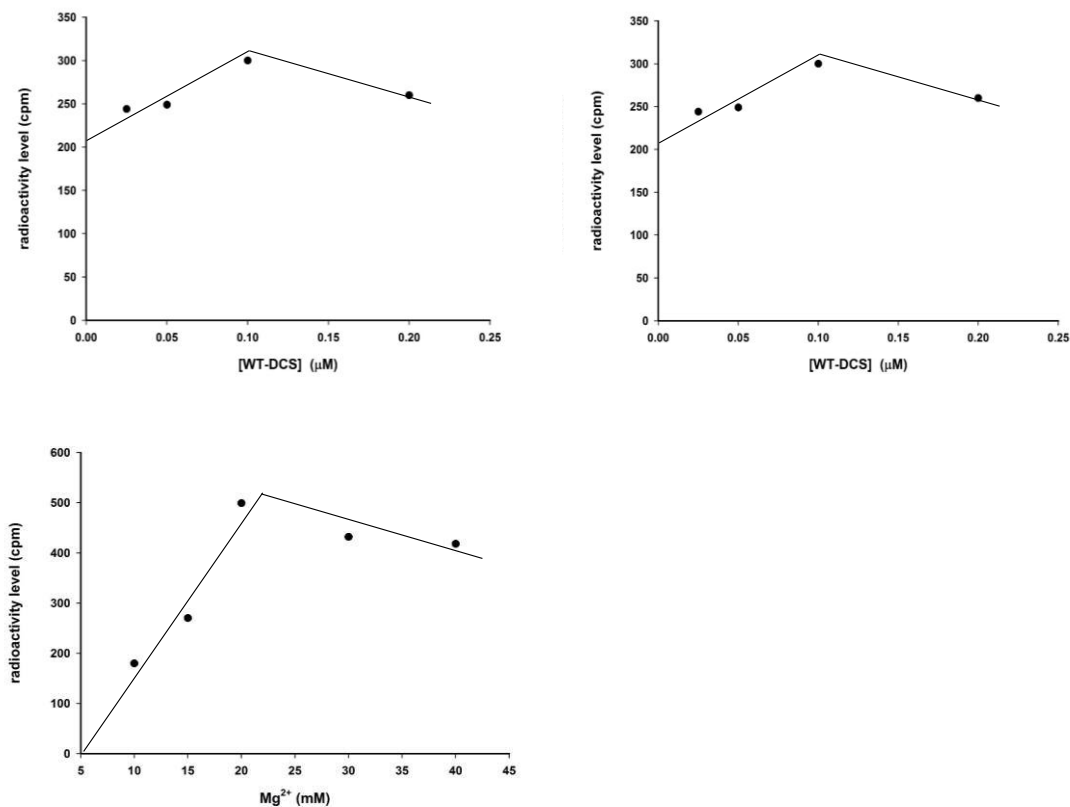
Figure 3.32 Plots of radioactivity level (counts per minute) of radiolabelled product formed by DCS against: Top left: reaction time (0.1 μM of WT-DCS, 10 μM FDP, 30 °C); Top right: WT-DCS concentration (10 min, 10 μM FDP, 30 °C); Bottom left: Mg²⁺ concentration in the incubation buffer 3 (0.1 μM of WT-DCS, 10 μM FDP, 30 °C 10 min).

Kinetics analyses were carried out following the protocol described in section 6.1.15, and incubating 0.1 μM of enzyme at 30 °C for 10 minutes. Based on the first attempt (Figure 3.30) the K_M was found to be 7.74 μM, which is comparable to the values reported in literature (5-9 μM). On the other hand, the k_{cat} was found to be 1×10^{-3} s^{-1}, ten times less than the literature value (1×10^{-2} s^{-1}).[49]
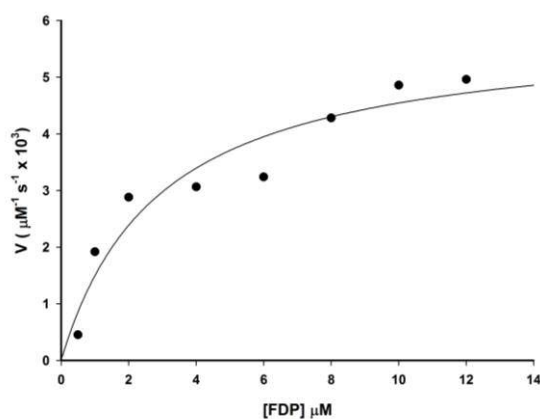
Figure 3.33 Representative Michaelis-Menten plot for the production of radiolabeled hexane extractable products from [1-³H]-FPP catalysed by WT-DCS.

Although the first attempt to perform kinetic studies was successful, subsequent attempts gave only background counts (0-50 cpm) by scintillation counting, even though the GC-MS analysis of the hexane extract of the incubation of DCS with FDP showed the peak corresponding to DCN. An instability of the protein was suspected, so fresh DCS was prepared and purified (as previously described) and used promptly for the kinetic assay. Unfortunately, again only background levels of activity were detected once more.

A series of kinetics studies were performed changing one parameter at the time: the buffer, the [1-³H]-FDP, and the DCS, all of them freshly prepared and used. After negative results, also the operator was changed in order to exclude a human error, but again only background radioactivity was detected.

A control kinetics experiment using freshly prepared aristolochene synthase was performed successfully and the data obtained were consistent with data reported in

the literature.[45] This confirmed the inactivity of DCS, and an instability of the protein was suspected. Although the DCS purification and expression protocol described above have been successfully performed before,[31,49] it was not possible to reproduce it in our lab this time.

3.5 Developing a new purification protocol

One of the key steps in the protein purification protocol is the base extraction, where the protein is brought to pH 12 and then back to pH 8. This step is necessary because WT-DCS is produced (with the conditions previously described in the literature [49]) as an insoluble protein, found in the inclusion bodies in the pellets. At pH 12, DCS is soluble and it has a net negative charge. This net charge increases the solubility of DCS and other proteins present in the lysate by creating attractive interactions with water molecules and by the repulsion of like-charged proteins. The pH is then brought back to 8, so other proteins present in the lysate precipitate and the buffer pH is restored. As this is a step where the protein is unnaturally unfolded and folded again by the change of pH, it was speculated that the conditions used in the base extraction were too harsh for the protein to refold correctly and regain catalytic activity.

To better understand if the basic extraction was responsible for the instability of WT-DCS, a series of changes in the expression and purification procedure were made in order to get soluble WT-DCS naturally folded by *E. coli* and avoid the base extraction step.

3.5.1 Use of different buffers

Different attempts were made to increase the solubility of the protein. The use of detergent containing cell lysis buffer (50 mM Tris, 500 mM NaCl, 20 mM β-mercaptoethanol, 10% v/v glycerol, 1% Tween™, pH 8) [67] and Mg^{2+} containing cell lysis buffer (20 mM Tris, 5 mM EDTA, 5 mM β-mercaptoethanol, pH 8, 5 mM $MgCl_2$) did not increase the solubility of DCS, as the enzyme was found in the pellets inclusion bodies again.

3.5.2 Production of a less concentrated protein

Another strategy to make soluble protein was to decrease the quantity of IPTG used to induce the *E. coli* cells, and consequently to grow them more slowly (overnight at

20 °C instead of 4 h at 37 °C). Following these changes to the protocol, *E. coli* should produce less recombinant protein, and therefore WT-DCS might not precipitate, making the base extraction procedure unnecessary.

The previous large scale protocol was then followed (Section 6.1.8, method B) but 0.1 mM IPTG was used instead of 0.5 mM, and then the culture was allowed to grow for 16 h at 20 °C before being harvested by centrifugation at 4000 *g* for 10 minutes. The supernatant solution was discarded and the pellet was re-suspended in the cell lysis buffer, sonicated and harvested again as previously described. Finally, SDS-PAGE analysis of the pellets and the supernatant solution confirmed the presence of DCS in the solution fractions (Figure 3.34).
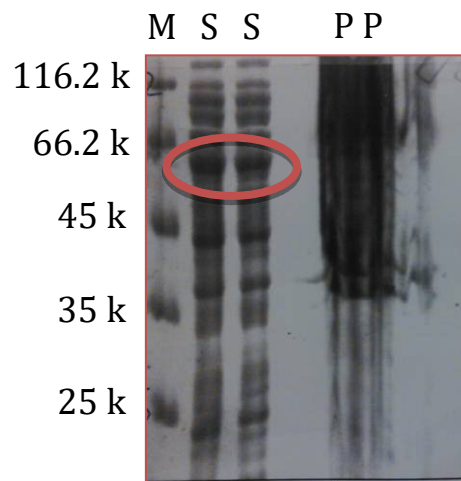
Figure 3.34 SDS-Polyacrylamide gel of (S): lysate; (P): pellets obtained after sonication; (M): molecular weight markers.

The base extraction step was hence unnecessary and lysate was then loaded directly onto a DEAE-cellulose column as described in Section 6.1.9, method B. Since no base extraction was now being carried out, the cell lysate may have been too complex due to the higher level of impurities, preventing binding of the desired protein to the cationic resin. Consequently, DCS purification by anion exchange DEAE-cellulose was unsuccessful. (Figure 3.35)
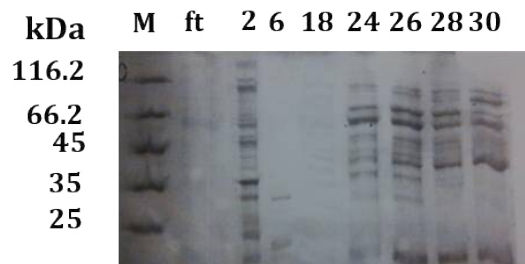
Figure 3.35 SDS-Polyacrylamide gel of (M): protein marker; (FT): flow through; (2-30): DEAE column fractions.

3.5.3 Introduction of a His-tag at the C-terminus

To solve the purification issue of soluble DCS, a His_6 tag was introduced at the C-terminus of the protein by PCR (Polymerase Chain Reaction). To bring the His-tag coding sequence of pET21d in-frame with the DCS sequence, a single nucleotide deletion was necessary. The Quickchange site-directed mutagenesis kit was used to introduce the deletion. The following primers were designed to delete a thymidine in the stop codon:

DCS_Histag_fw   **5'-GAACCAATTG CACTTGAGGA TCCGAATTC-3'**

DCS_Histag_rv   **5'-GAATTCGGAT CCTCAAGTGC AATTGGTTC-3'**

PCR procedure**:** sterile H_2O (39 µL), Pfu-polymerase buffer (5 µL), dNTPs (1 µL, 10 mM), 2 µL of forward and reverse primers 0.1 mM, 1 µL template DNA 0.01 pmol and 1 µL Pfu-polymerase (2.5 U/µL) were added to a PCR tube and followed PCR protocol (Table 7.3). The parental DNA was digested with 1 µL *Dpn*I (10 U/µL) for 1 h at 37 °C. The reaction was cooled on ice before transformation into XL1-Blue *E. coli* cells. Mutations were confirmed by DNA sequence analysis using Eurofins MWG Operon's DNA sequencing service.

DCS_His_6 was then prepared as previously described but using the newly cloned cDNA, and to optimise the expression procedure several test expressions were carried out varying the temperature, the length of large scale incubation, and the amount of IPTG used as described in Section 6.1.8. The best protein expression was achieved when 0.3 mM IPTG was used, and when the culture was left to grow for 12 h at 20 °C.

Due to the presence of the hexahistidine tag, DCS_His$_6$ could be purified through the use of the Amintra NTA (Nitrilotriacetic acid) Ni^{2+} column (Expedeon^{LTD}), which required less time and the use of fewer reagents when compared with the DEAE column purification method. The procedure followed is the same used to purify ADS, and described in Section 6.1.9, Method C. DCS_His$_6$ eluted with 60-100 mM imidazole in the binding buffer, the column fractions were analysed by SDS-PAGE (Figure 3.36), and those containing pure DCS_His$_6$ were dialysed against dialysis buffer 2 at 0 °C to remove the excess of imidazole used to elute the enzyme and concentrated by Amicon™ ultrafiltration using a Millipore 30,000 MW cut-off membrane. Enzyme concentration was determined by Bradford assay.[95]
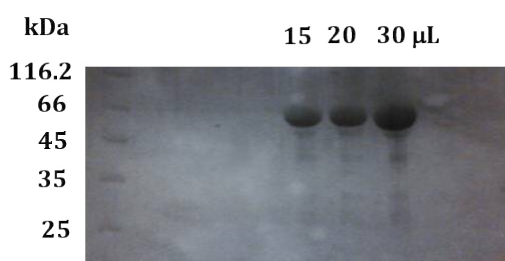
Figure 3.36 SDS-polyacrylamide gel of pure concentrated DCS_His$_6$. (M): protein marker; (15): 15 μL; (20) 20 μL (25) 25 μL of 200 μM purified DCS_His$_6$.

3.6 Characterisation of DCS_His$_6$

3.6.1 Analysis of the pentane extractable products

DCS_His$_6$ activity was determined by incubation of the protein with FDP as described in section 6.1.11. GC-MS analysis (Figure 3.37 and 3.38) showed the formation the δ-cadinene, alongside with a small production of germacradien-4-ol (GD4ol) (≤ 10%).
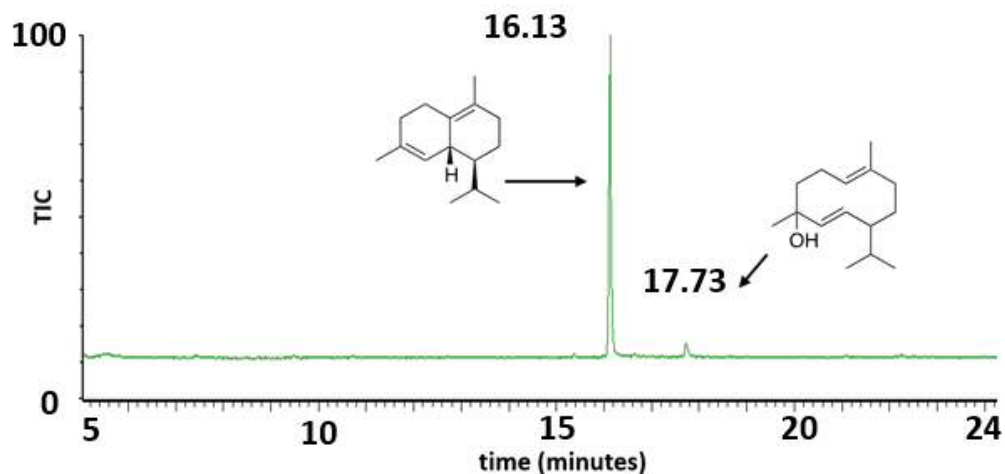
Figure 3.37 Gas chromatogram of DCN and GD4ol produced by incubation of DCS_His₆ with FDP.

These products were identified by comparison with the GC-retention times and the mass spectra of authentic products arising from incubation of FDP with WT-DCS and WT-GdolS reported in the literature.[49,96] These results suggest that the hexahistidine tag slightly perturbs the ordered closed conformation that DCS adopts when bound to the substrate. This is consistent with the hypothesis that a precise series of loop movements must occur to effect closure of the active site of DCS or water can ingress and quench the intermediate carbocations.
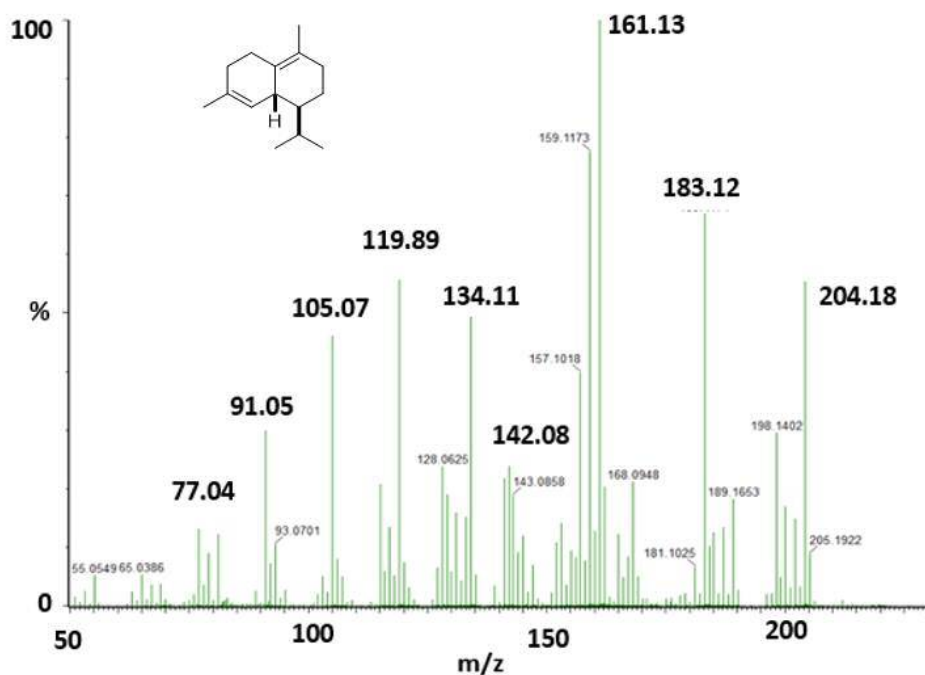
Figure 3.38 MS of GD4ol produced by incubation of DCS_His₆ with FDP.

3.6.2 Size exclusion chromatography

Size exclusion chromatography was used to determine if DCS_His$_6$ exists as a monomer, a dimer or as multi-subunit complex in solution. A Superdex 75 10/300 GL column was calibrated with a solution of standards (BIO-RAD gel filtration standard solution) containing proteins of known molecular weight (Figure 3.39). Comparing the retention volumes of the standards with the DCS_His$_6$ showed that DCS_His$_6$ existed as a monomer. Furthermore, the straight-line graph obtained from the equation extrapolated by plotting the log$_{10}$ of the standards molecular weights against the retention volumes obtained gave an estimation of the DCS_His$_6$ molecular weight. Using the linear best-fit equation shown in Figure 3.39, right below, DCS_His$_6$ molecular weight was estimated to be 60256 ± 2846 compared to the real weight of 66000, hence showing that exists as a monomer in solution.
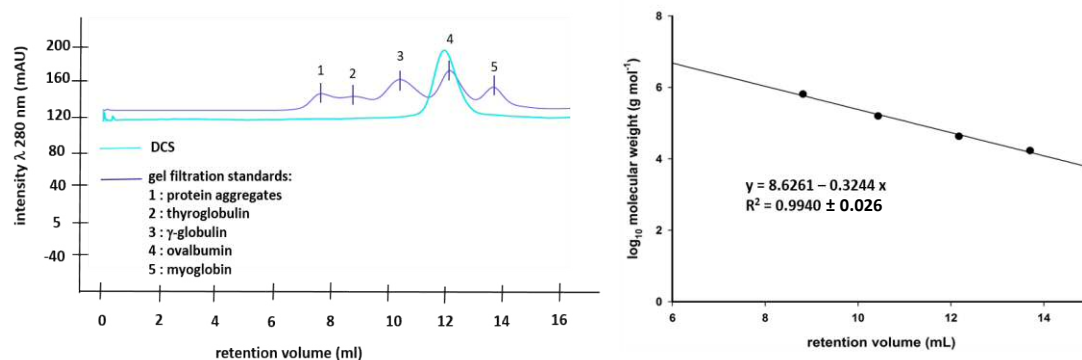
Figure 3.39 Left: overlaid size exclusion chromatogram of DCS_His$_6$ and the proteins contained in the BIO-RAD standard solution: thyroglobuline (MW = 670000), γ-globulin (MW = 158000), ovoalbumin (MW = 44000), and myoglobin (MW = 17000). Right: calibration curve of retention volumes against log$_{10}$ of the molecular weights.

3.6.3 CD spectroscopy

Previous investigation of the crystal structure and CD spectroscopy of WT-DCS revealed an overall α-helical fold (Figure 1.10).[31] CD spectra of DCS_His$_6$ were recorded to confirm that no change in the secondary structure of the protein appeared after the introduction of the 6-histidine tag. The spectra were recorded from 190 to 360 nm following the procedure described in Section 6.1.14, Chapter 6. The CD spectra obtained (Figure 3.40) displayed the two minima at 208 nm and 222 nm, distinctive of an α-helical secondary structure, confirming that the hexahistidine tag did not affect the protein α-helical fold. Furthermore, the spectra recorded in the pH values of 7 and 8, DCS_His$_6$ did not show significant changes,

confirming the stability of the protein in this pH range. Therefore, the future steady state kinetics were determined using the same range of pH in the kinetic buffer.
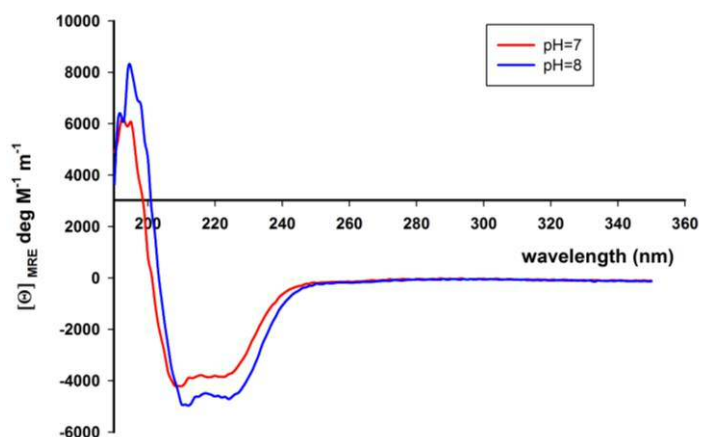
Figure 3.40 CD spectra of DCS_H$_6$ at: red, pH 7; blue, pH 8.

3.6.4 Stability studies

To determine the stability of DCS_His$_6$ once purified, the enzyme was stored at −20 °C with 10% of glycerol for 10 days, and at −20 °C,−80 °C for 10 days, and analysed by GC_MS. Analysis of hexane extract of the incubations with FDP showed an increased amount of the alcohol GD4ol formed. In addition, GC spectra showed the formation of a third product (eluting at 12.77 minutes) that appears to be an acid catalysed dehydration product of GD4ol (Figure 3.41).
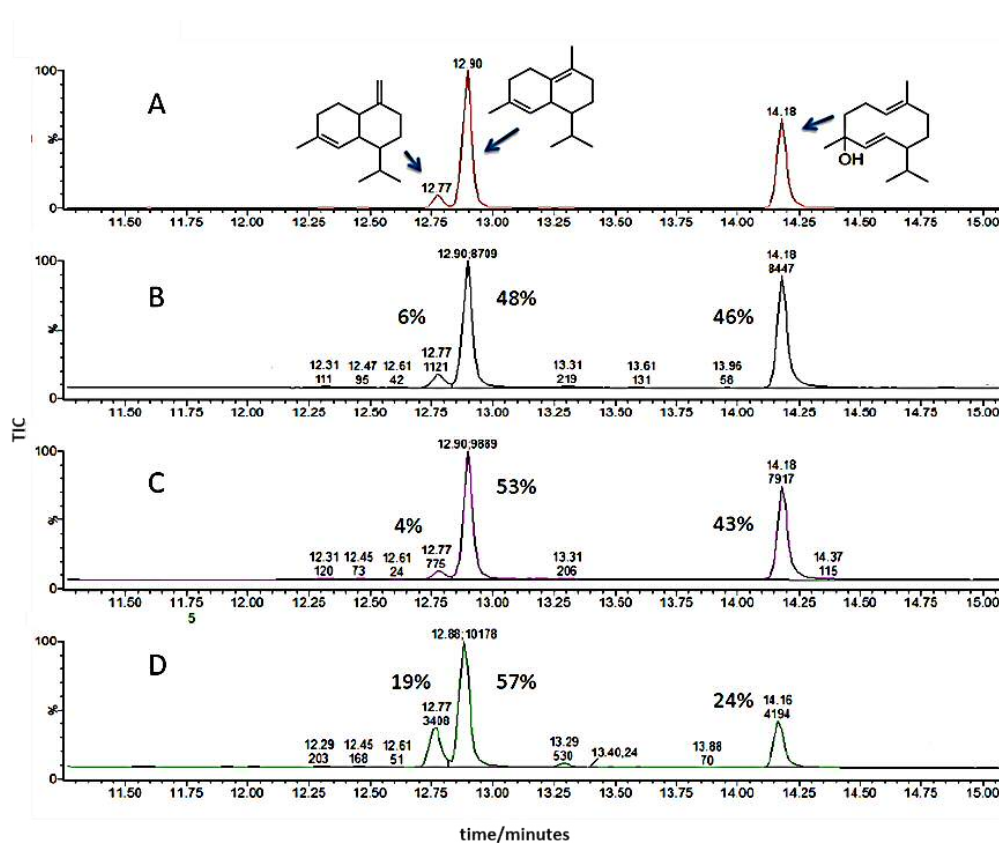
Figure 3.41 GC-MS analysis of the pentane extractable products arising from the incubation of DCS_His$_6$ with FDP after 10 days. A : peaks corresponding to 203-205 MW. B: DCS_His$_6$ stored at −20 °C; C: DCS_His$_6$ stored at − 80 °C; D: DCS_His$_6$ stored at −20 °C with 10% glycerol.

Furthermore, also when lyophilised, the protein proved to be unstable. DCS_His$_6$ was lyophilised and stored as a powder at −20 °C for a week. After being resolubilised in dialysis buffer 2, an incubation with the substrate FDP was performed. GC-MS analysis demonstrated the formation of GD4ol as the major product, suggesting a mis-folding of the protein and/or an increased amount of water into the active site. In addition, the spectra showed the presence of acid catalysed dehydration product of GD4ol, and three extra products, of which chemical structures could not be determined (Figure 3.42).

114
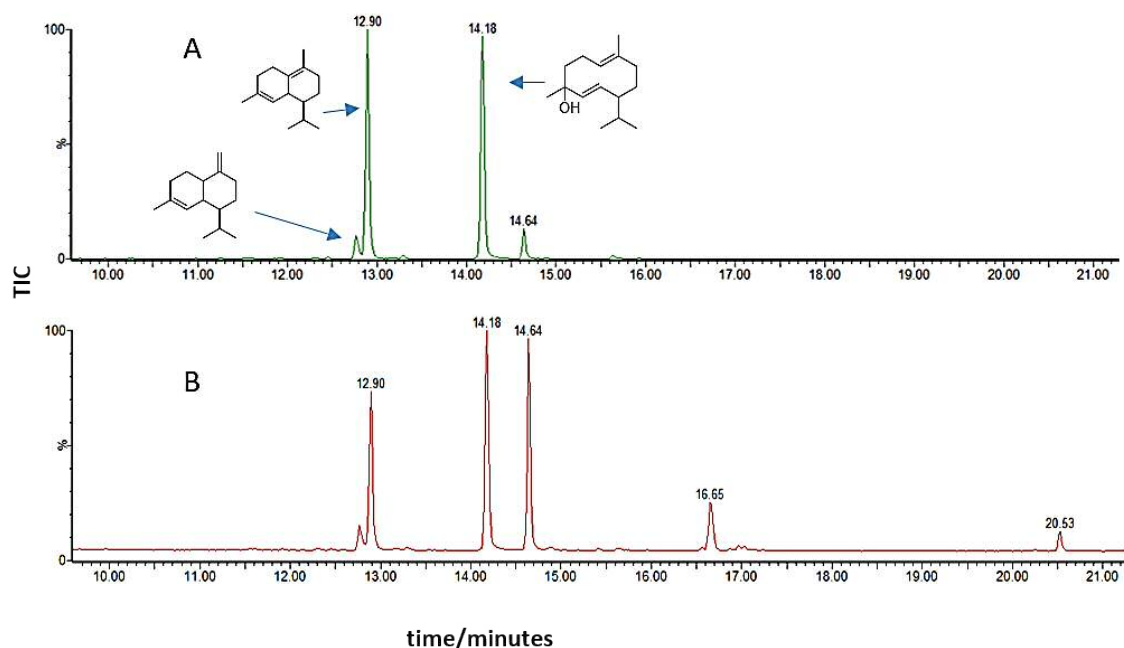
Figure 3.42 Gas chromatogram of the pentane extractable products arising from the incubation of DCS_His$_6$ with FDP. A: peaks corresponding to 203-205 MW. B: DCS_His$_6$ stored at −20 °C as a powder.

As DCS_His$_6$ was unstable when stored for 10 days, it was decided to express and purify fresh protein each time, and to use it for steady state kinetics and inhibition study promptly after purification.

3.7 Steady state kinetics

As for previous enzymes used in this work, kinetic analyses of DCS_His$_6$ were performed in order to establish the optimal assay conditions. Incubations with fixed enzyme concentration (0.1 µM) and fixed [1-^{3}H]-FDP (10 µM) were carried out for 10 min at variable concentration of Mg^{2+} in the incubation buffer (Figure 3.43, top left). The initial rate was found to be directly proportional to Mg^{2+} concentration between 10 mM and 20 mM. A concentration of 15 mM of Mg^{2+} was then chosen for future assays.

To find the optimal concentration of the enzyme, incubations were carried out with 10 µM [1-^{3}H]-FDP, for 10 min at variable enzyme concentration in the standard incubation buffer. The initial rate was found to be directly proportional to enzyme

concentration between 0.05 and 0.30 μM, so a concentration of 0.10 μM of DCS_His$_6$ was chosen for future studies (Figure 3.43, top right).

Finally, to determine the optimal reaction time, incubations were carried out with 0.1 μM of DCS_His$_6$, 10 μM [1-^{3}H]-FDP in incubation buffer for variable amount of time. Initial rate was found to be linear with respect to time between reaction times of 5-15 min and so 10 min was chosen as the reaction time for the kinetic experiments (Figure 3.43, bottom left). These best conditions were found to be very similar to those previously found for WT_DCS. [49]
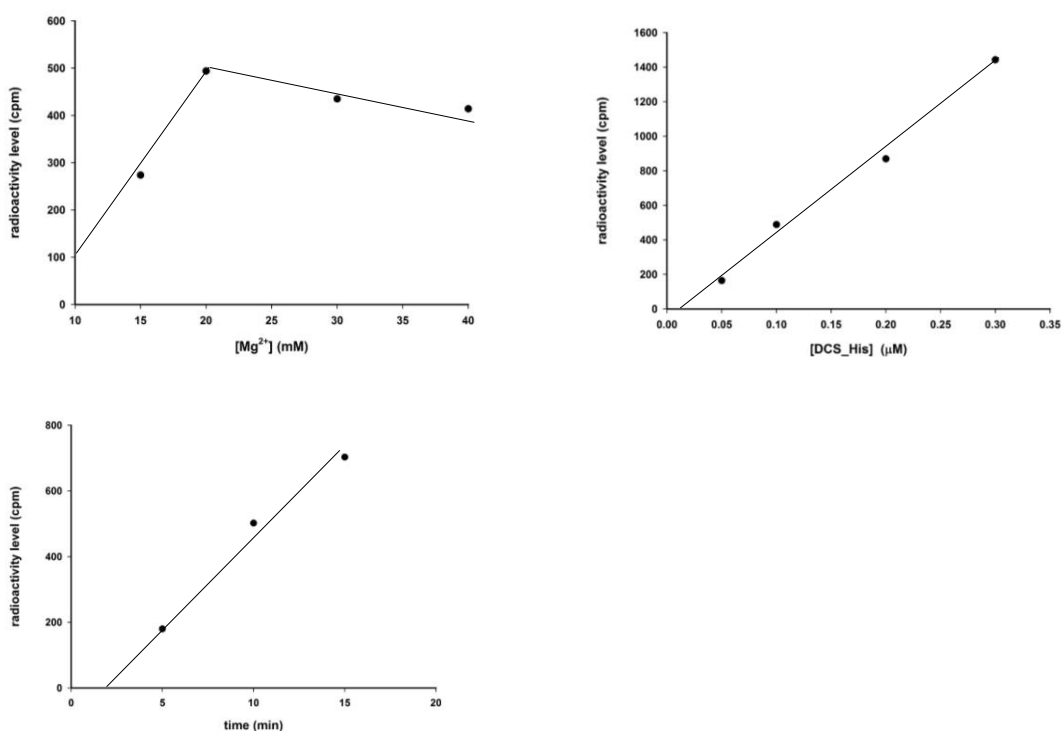
Figure 3.43 Kinetics analysis of DCS_His$_6$. Plot of radioactivity level of radiolabelled products formed by DCS against: Top left: Mg^{2+} concentration in the kinetic buffer (0.1 μM of DCS, 10μM FDP, 10 min); Bottom left: time course (0.1 μM of DCS, 10μM FDP); Top right: enzyme concentration (10μM FDP, 10 min).

The conditions of 15 mM of Mg^{2+} in the kinetic buffer, 10 min reaction time and 0.10 μM of enzyme inhibition were used to carry out steady state kinetics of DCS_His$_6$. The K_M and k_{cat} were calculated as the average weighted mean of three separate experiments, and were found to be 0.58 ± 0.11 μM and 1.26 × 10^{-3} ± 5 × 10^{-6} sec^{-1} respectively (Figure 3.44).
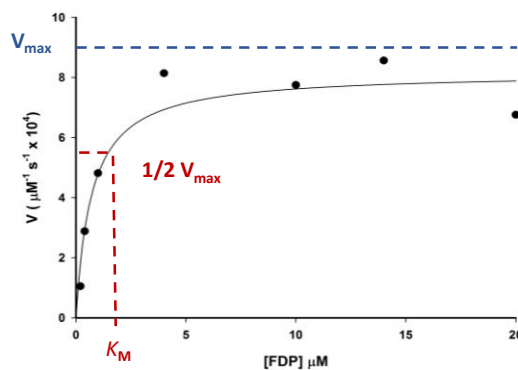
Figure 3.44 Representative Michaelis-Menten plot for the production of radiolabeled hexane extractable products from [1-^{3}H]-FDP catalysed by DCS-His$_6$.

Although the k_{cat} value found for DCS-His$_6$ is ten times smaller than for WT-DCS (1x10^{-2} s^{-1}), the introduction of the hexahistidine-tag gave rise to an enzyme with overall catalytic efficiency (k_{cat}/K_M) of 2.17 × 10^{-3} ± 4 ×10^{-3} s^{-1} µM^{-1}, which is identical, within experimental error, to WT-DCS (k_{cat}/K_M 3.1 × 10^{-3} ± 5.6 ×10^{-3} s^{-1} µM^{-1}).

3.7.1 Inhibition of DCS-His$_6$ by the α-bisabolyl cation aza-analogues

Inhibition studies were performed following the protocol previously used to inhibit ADS and AS, and described in section 6.1.16. Following previous inhibition protocol in the literature,[49] the concentrations of the (*S*)-aza bisabolyl cation used for each series of reactions were 40, 120 and 200 µM (Figure 3.45).
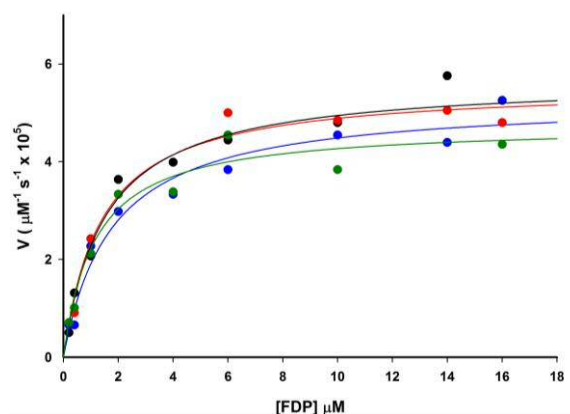
Figure 3.45 Representative Michaelis-Menten plot for the production of radiolabeled product by: Black DCS_His$_6$; Red, DCS_His$_6$ + 40 µM (*S*)-60; Blue, DCS_His$_6$ + 120 µM (*S*)-60, Green, DCS-His$_6$ + 200 µM (*S*)-60.

The Lineweaver-Burk reciprocal plot of the data obtained (Figure 3.46, top) shows the lines the intercepting on the y-axis, indicating clearly that this compound is a competitive inhibitor. In addition, **(S)-60** proved to be a weak inhibitor, with a K_i of 273 ± 77 μM (Figure 3.46, bottom), which is a value almost three orders of magnitude higher than the DCS_His$_6$ K_M for the natural substrate FDP (0.58 ± 0.11 μM). This outcome indicates that **(S)-60** is able to enter the active site but it does not have a high affinity for DCS.
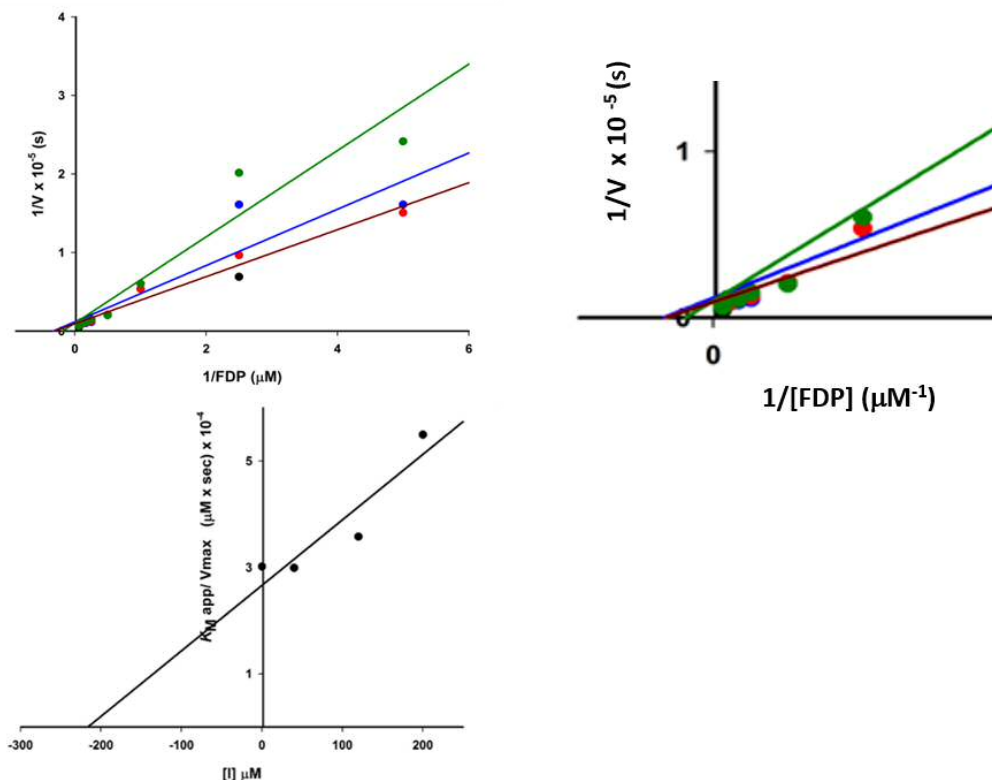
Figure 3.46 Top: representative double-reciprocal plot (right) and zoom section of y intercept section (left) of the inhibitions data of DCS-His$_6$ with (S)-60. Black, DCS-His$_6$; Red, DCS-His$_6$ + 40 μM (S)-60; Blue, DCS-His$_6$ + 120 μM (S)-60, Green, DCS-His$_6$ + 200 μM (S)-60. Bottom: Representative plot of K_M(app) / V$_{max}$ against [I] for the calculation of K_i.

DCS_His$_6$ inhibitions with **(S)-60** were repeated in presence of 250 μM of PP$_i$. Initially, the incubations were performed using the concentrations of **(S)-60** previously used (40, 120 and 200 μM) without the PP$_i$ addition. The Michaelis-Menten plot obtained showed no catalytic activity when 40 μM were added to the incubation reactions, indicating strong enzyme inhibition properties by **(S)-60** in the presence of PP$_i$. Hence, the incubations were repeated with lower concentrations of **(S)-60**, 0.8, 2.8 and 6 μM, in order to obtain a clear Michaelis-Menten graph and to consequently calculate the K_i (Figure 3.47).
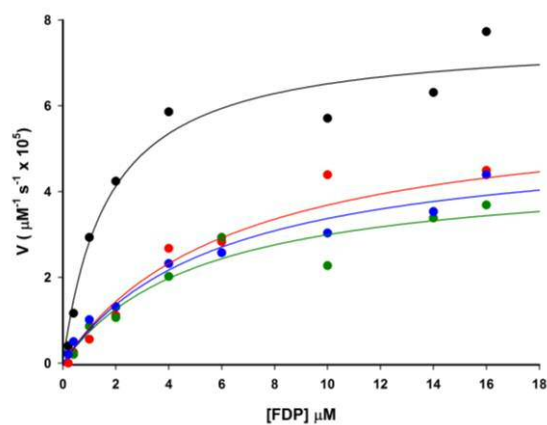
Figure 3.47 Representative Michaelis-Menten plot for the production of radiolabeled product by: Black, DCS_His$_6$; Red, DCS_His$_6$ + 0.8 μM (*S*)-60; Blue, DCS_His$_6$ + 2.8 μM (*S*)-60; Green, DCS_His$_6$ + 6 μM (*S*)-60. For each series of reaction 250 μM of PP$_i$ was added.

The double-reciprocal plot of the data obtained (Figure 3.48, top) showed, within the 10% error, the lines intercepting on the y axis, indicating a competitive mode of inhibition. In addition, **(*S*)-60** was found to be a strong inhibitor of DCS-His$_6$ in the presence of the PP$_i$. In fact, based on three independent measurements, the K_i value was found to be 3.44 ± 1.43 μM (Figure 3.48, bottom).
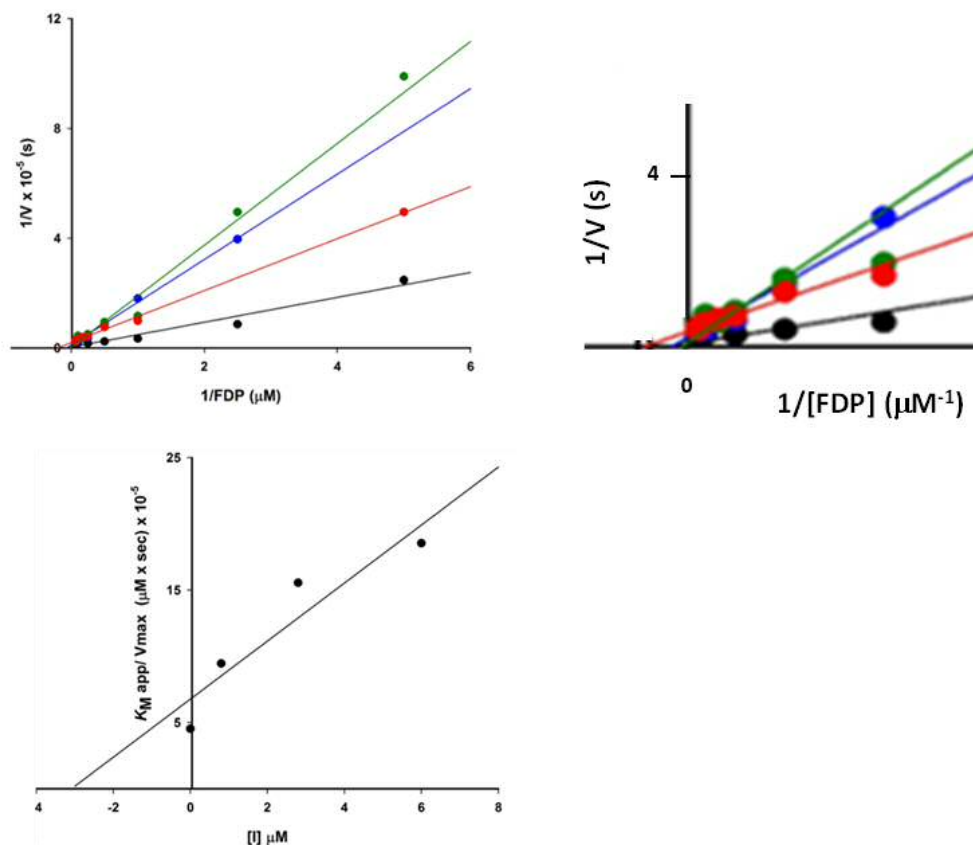
Figure 3.48 Representative reciprocal plot (top left) and zoom section of y intercept (top right) of the inhibitions data of DCS-His$_6$ with (*S*)-60. Black, DCS_His$_6$; Red, DCS_His$_6$ + 0.8 μM (*S*)-60; Blue, DCS_His$_6$ + 2.8 μM (*S*)-60; Green, DCS_His$_6$ + 6 μM (*S*)-60. For each series of reactions a fixed concentration of 250 μM PP$_i$. was added. Bottom: representative plot of K_M(app) / V$_{max}$ against [I] for the calculation of K_i.

This outcome is consistent with the results previously obtained in this work when ADS inhibition studies were performed, where the addition of PP$_i$ in the incubation reactions had a synergic effect on the overall inhibition, lowering the **(*S*)-60** K_i value for DCS-His$_6$ from 25 ± 5 μM to 1.5 ± 0.5 μM. It is important to note that the **(*S*)-60** K_i value for DCS-His$_6$ decreased by two orders of magnitude in presence of the PP$_i$ indicating once again that the inorganic diphosphate plays an active role in the inhibition process. The presence of the PP$_i$ in the reaction mixture means the formation of a cation-anion pair in the enzyme active site, which resembles the Michaelis complex and therefore increases the binding affinity to the active site.

Furthermore, the fact that **(*S*)-60** is a competitive inhibitor of the cyclase DCS_His$_6$, is strong evidence for the 1,6-cyclisation mechanism, providing evidences for the

formation of the *S*-enantiomer of the bisabolyl cation in the active site during the biosynthesis of DCN.

In a second set of experiments, the **(*R*)-60** inhibition properties were evaluated. Initially, 40, 120, and 200 μM of **(*R*)-60** were used to inhibit the sesquiterpene synthase (Figure 3.49).
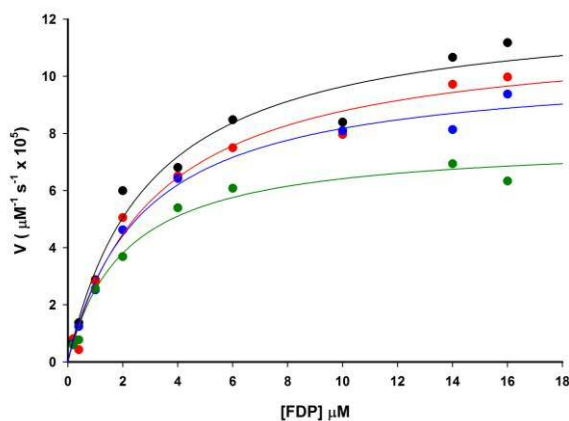
Figure 3.49 Representative Michaelis-Menten plot for the production of radiolabeled product by: Black DCS_His$_6$; Red, DCS_His$_6$ + 40 μM (*R*)-60; Blue, DCS_His$_6$ + 120 μM (*R*)-60, Green, DCS_His$_6$ + 200 μM (*R*)-60.

(*R*)-60 proved to be a very weak inhibitor of DCS-His$_6$ as the K_i found was high, 1.7 + 0.3 mM (Figure 3.50, top) when compared to DCS-His$_6$ K_M. In fact, this value is 1000 times higher than the DCS-His$_6$ K_M for the FDP (0.58 ± 0.11 μM), which indicates that the (*R*) enantiomer of the aza-bisabolyl cation **60** has a weak binding affinity for the enzyme active site. This outcome demonstrated the enantioselectivity of the enzyme, supporting the presence of only the (*S*)-enantiomer of the bisabolyl cation in the catalytic pathway.
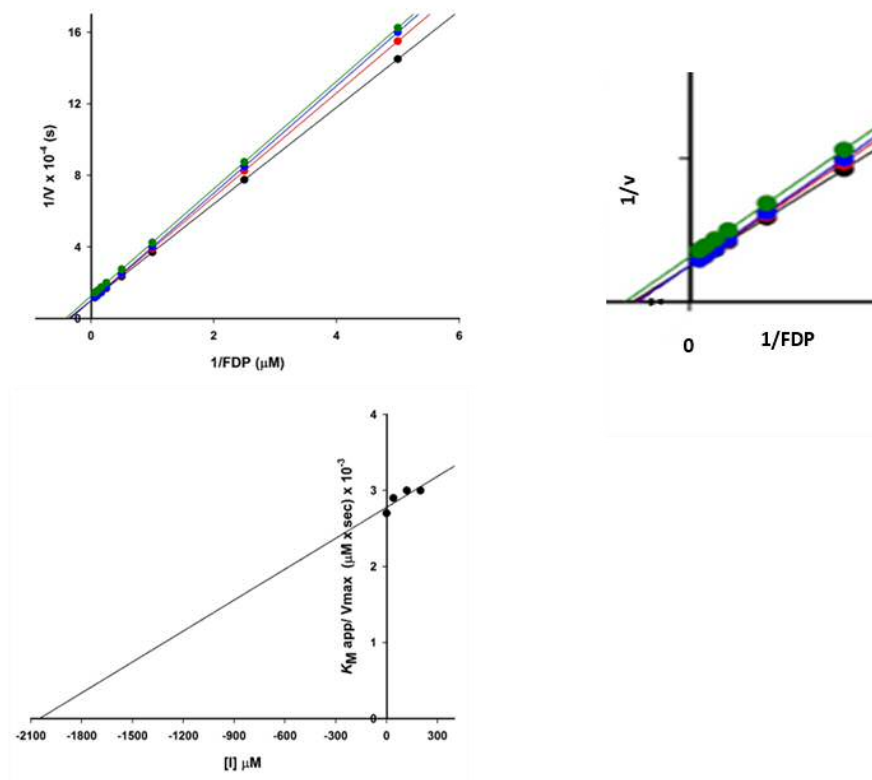
Figure 3.50 Representative reciprocal plot (top left) and zoom section of y intercept (top right) of the inhibitions data of DCS-His$_6$ with (R)-60. Black, DCS_His$_6$; Red, DCS_His$_6$ + 40 μM (R)-60; Blue, DCS_His$_6$ + 120 μM (R)-60, Green, DCS_His$_6$ + 200 μM (R)-60. Bottom: representative plot K_M(app) / V$_{max}$ against [I] for the calculation of k$_i$.

DCS_His$_6$ inhibitions with **(R)-60** were repeated in presence of 250 μM of PP$_i$. Unexpectedly, when running the inhibition assay, no catalytic activity was observed in the presence of 40 μM of **(R)-60**. After two sets of experiments, where the concentration of the inhibitor used were decreased constantly, 0.8, 2.4 and 5.6 μM of **(R)-60** were eventually used in the kinetics assay and in the calculation of the K_i (Figure 3.51).
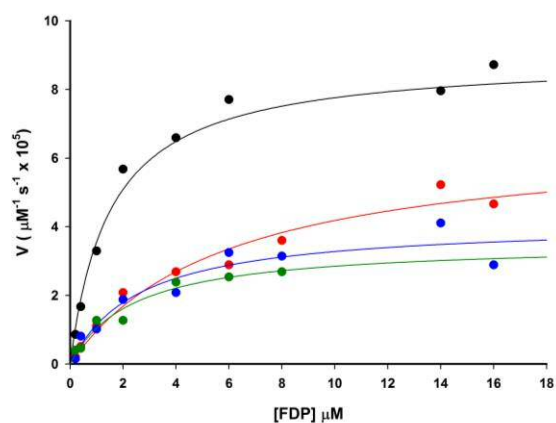
Figure 3.51 Representative Michaelis-Menten plot for the production of radiolabeled product by: Black, DCS-His$_6$; Red, DCS-His$_6$ + 0.8 μM (R)-60; Blue, DCS-His$_6$ + 2.4 μM (R)-60; Green, DCS-His$_6$ + 5.6 μM (R)-60. For each series of reaction a fixed concentration of 250 μM of PP$_i$ was added.

The Lineweaver-Burk plot of the data obtained (Figure 3.52, top) shows the lines intercepting on the y-axis, indicating clearly that this compound is a competitive inhibitor. Furthermore, the presence of external PP$_i$ enhances the inhibition properties of **(R)-60**, lowering the K_i from the order of millimolar to the order of micromolar. In fact, based on three independent experiments, the K_i was found to be 2.5 ± 0.5 μM (Figure 3.52, bottom), which is a close value to the DCS-His$_6$ K_M for the natural substrate FDP (0.58 ± 0.11 μM). This outcome indicates that **(R)-60** is able to inhibit the DCS-catalysed formation of DCN only in the presence of the inorganic diphosphate.
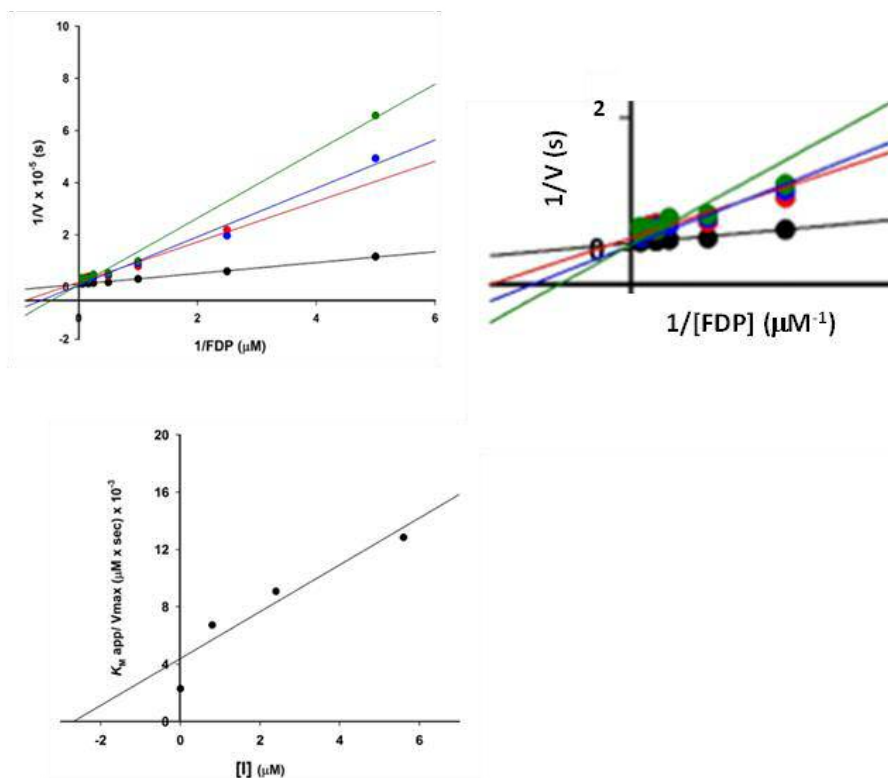
Figure 3.52 Representative reciprocal plot (top left) and zoom section of y intercept (top right) of the inhibitions data of DCS-His$_6$ with (*R*)-60. Black, DCS_His$_6$; Red, DCS_His$_6$ + 0.8 μM (*R*)-60; Blue, DCS_His$_6$ + 2.4 μM (*R*)-60; Green, DCS_His$_6$ + 5.6 μM (*R*)-60. For each series of reactions a fixed concentration of 250 μM of PP$_i$ was added. Bottom: representative plot of K$_M$ app / Vmax against [I] for the calculation of K_i of (*R*)-60 in the presence of 250 μM PP$_i$.

3.8 Summary and conclusion

WT-DCS cDNA was expressed and purified following the protocols previously developed in our laboratory, but the protein showed poor to no activity. The base extraction step in the WT-DCS purification protocol was suspected to be the cause of the inactivity of the protein. Therefore, a new expression protocol was developed in order to obtain soluble protein. A hexahistidine tag was introduced into the C-terminus of DCS, to facilitate and speed up the purification process. Analysis and characterisation of DCS_His$_6$ confirmed the conservation of the α-helical secondary structure typical of the sesquiterpene synthases, and although DCS_His$_6$ resulted to be unstable when stored with the main methodology widely used, steady state kinetics showed DCS_His$_6$ to be an active enzyme with an overall catalytic efficiency comparable to WT-DCS.

The aza-analogues of the bisabolyl cation previously designed and synthesised were incubated with DCS_His$_6$ to get an understanding of its mechanistic mode and gain

124

evidence towards a 1,6 or a 1,10-cyclisation mechanism. The kinetic inhibition data are summarised in Table 3.3 below.

Table 3.3 DCS_His$_6$ Kinetics inhibition data for aza-analogues of α-bisabolyl cation (60). DCS_His$_6$, K_M= 0.58 ± 11 μM; k_{cat} = 1.260 x 10^{-3}± 5 x 10^{-6} s^{-1}.

Inhibitor	+250 PP$_i$ (μM) K_i (μM)	K_i (μM)
(S)-60	1.5 ± 0.5	25 ± 5
(R)-60	2.5 + 0.5	1700 + 300

Both the aza analogues were found to be competitive inhibitors of DCS-His$_6$ in the presence of PP$_i$. These observations would be difficult to explain assuming that DCS catalyses an initial 1,10-cyclisation of FDP (Scheme 3.1, blue). The ability of **60** to enter the enzyme active site and to act as a competitive inhibitor is evidence for the 1,6-cyclisation pathway previously proposed (Scheme 3.1, red), and it demonstrates that the DCS-catalysed formation of the sesquiterpene DCN is a cyclisation mechanism that involves the formation of the α-bisabolyl intermediate. The presence of a sp^3 hybridised nitrogen atom in **60** and therefore the absence of the empty π orbital would then explain the inability of DCS to use **60** as a substrate.
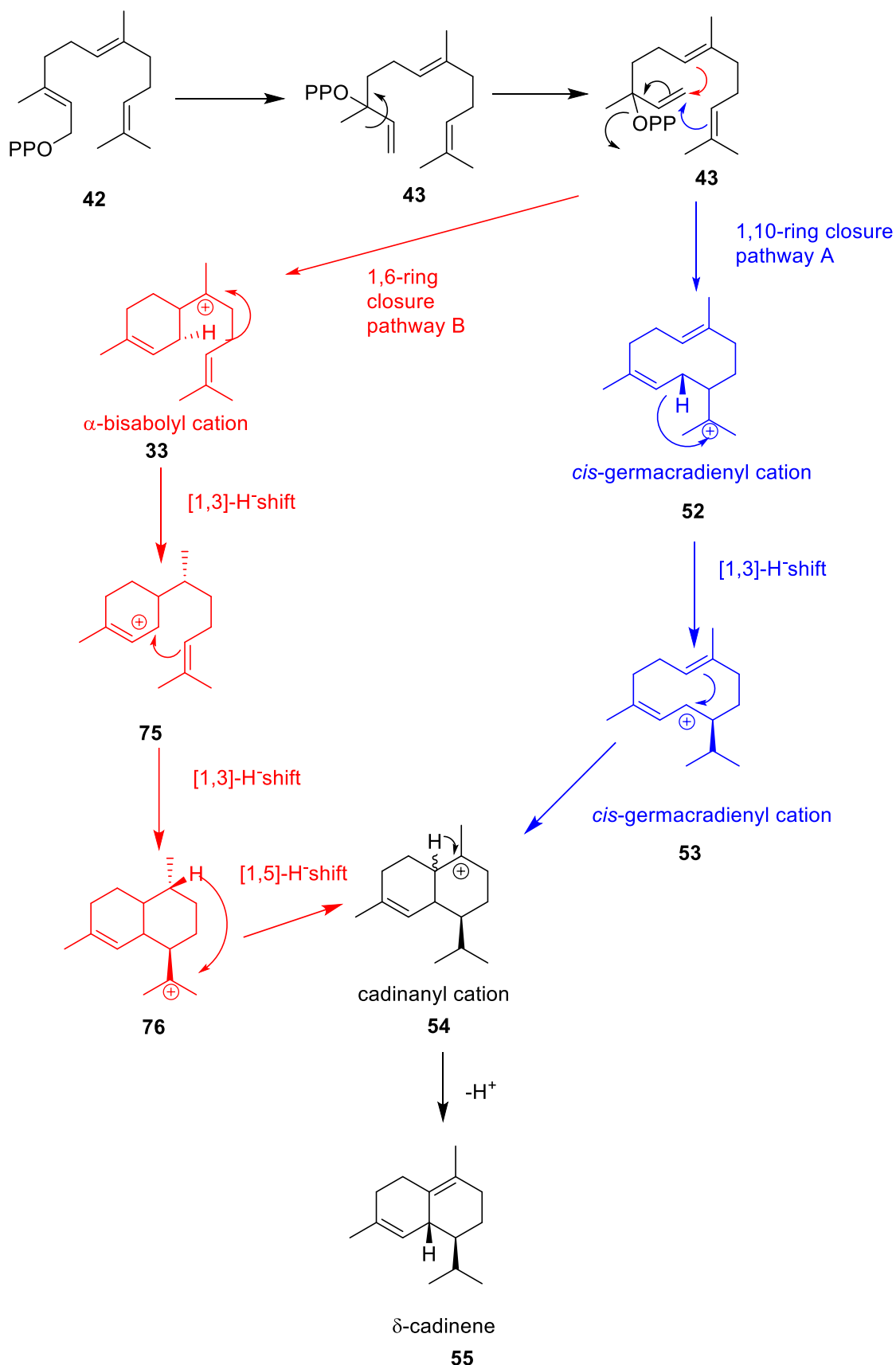
Scheme 3.2 1,6-(red) and 1,10-(blue) cyclisation mechanism proposed for the formation of DCN.

In addition, the fact that the presence of the inorganic diphosphate in the enzymatic inhibition assay led to a lower k_i and a more tightly bound active site

carbocation/diphosphate ion pair. These results are consistent with previous work reported in literature.[45,71,93,94] In fact, it is thought that the $[Mg_2]^{3+}$- PP_i complex formed during catalysis may lead to a favorable electrostatic and/or bonding interaction between the positively charged bisabolyl aza-analogue and the PP_i present in the DCS active site. It could be that the PP_i act as a general base/acid in the protonation step that leads to the cyclisation of **44** to **82** (Scheme 3.2), stabilising the bisabolyl cation itself.

The evidence that **(R)-60** acts as a weak inhibitor in the absence of the PP_i is more difficult to explain. A. J. Faraldos *et al.*[49] suggested that, in the DCS active site pocket, the (3*R*)-nerolidyl diphosphate chain is ideally positioned to ensure the formation of the α-bisabolyl cation with an *R* configuration at C6. The C1->C7 hydride shift from **33** to **76** then occurs to the same C7 Si face of **33**, therefore a **(7R)-75** formation is expected (Scheme 3.3).
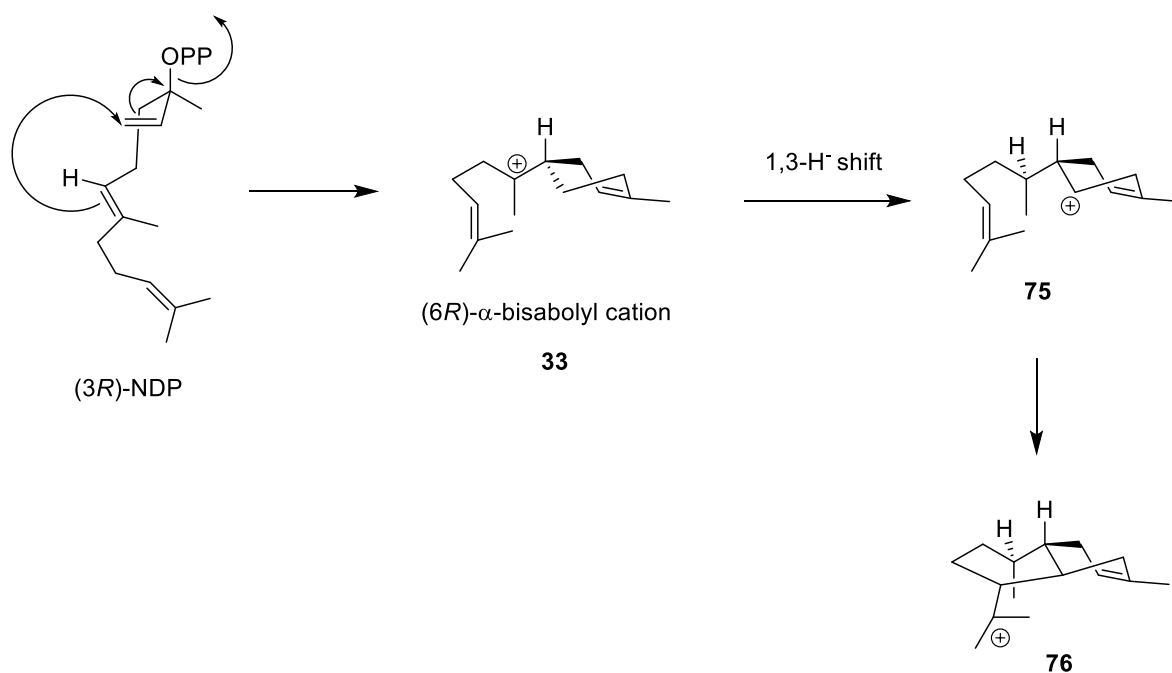
Scheme 3.3 DCS-catalysed formation of the (6*R*)-α-bisabolyl cation and its conversion into the carbocation (7*R*)-75 and the (7*R*)-76 then, proposed by Faraldos *et al.*[49]

Based on this previous work,[61] the **(R)-60** should mimic better the α-bisabolyl cation, and therefore act as competitive inhibitor with higher binding affinity when compared with the *S*-enantiomer. On the other hand, based on the results obtained during this project, it is proposed that DCS is able to synthesise DCN through the formation of the α-bisabolyl cation with *S* configuration at C6, therefore the

stereochemistry of the bisabolene intermediate itself it is not essential for the formation of the **(7R)-52**, as the 1,3 hydride shift could occur at both *Si* face and *Re* face of **33**.

Moreover, the evidence that both enantiomers of the inhibitor are equally effective in the presence of PP_i is consistent with a permissive model of cyclase active site structure, according to which an active site should accommodate a variety of rearranged intermediates of different shape and charge distribution without being rigidly complementary to a single intermediate. [71]

CHAPTER 4   **DCS Mutagenesis Investigation**

4.1 Preface

Although the full mechanism of DCS is not yet established, it was hypothesised that, similarly to the formation of other sesquiterpenes, the cyclisation of δ-cadinene occurs through the formation of several carbocations generated in its active site. [49] It has been previously described how the aromatic π-system of a residue located in the active site of sesquiterpene synthases can stabilise the positive charges formed during catalysis and protect the reactive carbocations from other quenching mechanisms.[77,38,40,41] Mutagenesis experiments designed to decipher the catalytic mechanism of PR-AS have shown that the aromatic residues Phe 178,[37] Trp 334[40] and Tyr 92[51] contribute to the stabilisation of the carbocations and therefore promoting the formation of aristolochene as the main product.

Yoshikuni *et al.* engineered DCS to form of the sesquiterpene GD4ol as the primary product.[32] They achieved this by producing a DCS-CAT (chloramphenicol acetyltransferase) fusion protein to exclude nonsense mutants and/or insoluble proteins, and to perform a dual-activity screen on it. They then used error-prone PCR (EP-PCR) to create twenty-one clones which formed GD4ol and DCN in different ratios. More specifically, DCS-N403P/L405H generates GD4ol as the major product (93%). They proposed that the DCS-mediated formation of GD4ol occurred via a 1,10-cyclisation closure when the active site is not completely shielded from the outer solvent. Therefore, during catalysis, when the *cis*-germacradienyl cation is formed, the delocalisation of the positive charge could trigger a water attack in position 4 and therefore could lead to the generation of GD4ol (Scheme 4.1).
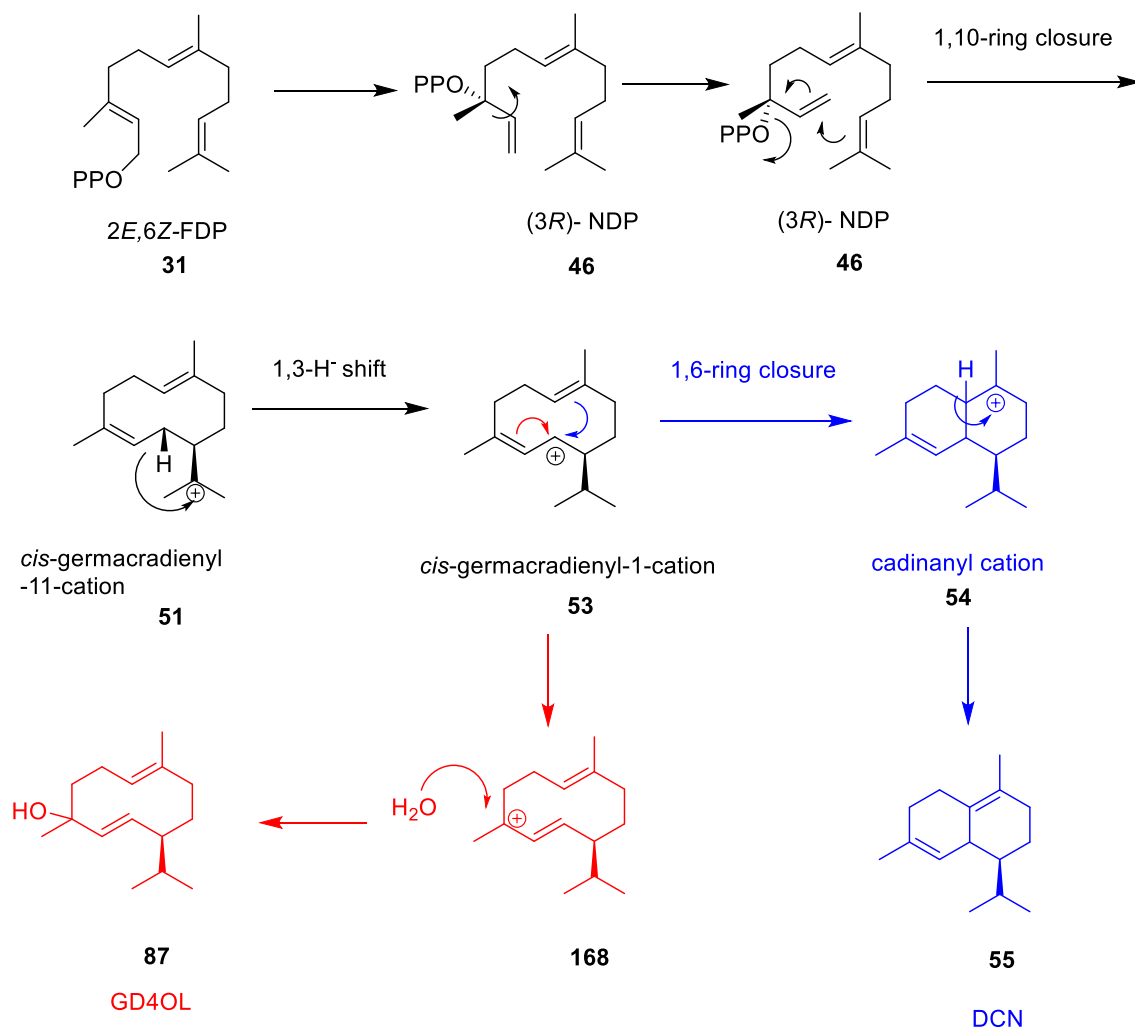
Scheme 4.1 Formation of the alcohol GD4ol proposed by Y. Yoshikuni.[32]

All the mutations described in Yoshikuni's experiments occurred at the G-helix, so they concluded that the amino acids situated in this particular helix play an important role in shielding the outer solvent from entering the active site and therefore quench the intermediate carbocations.

Analysis of the X-ray structure of DCS showed that aromatic amino acids W279 and Y410 are closer to the FDP isoprenyl chain and on the opposite side of the active site contour relative to N403 and L405 (Figure 4.1). W279 is on the C-helix of DCS and within 7 Å of Y410 just below the G2 helix and towards the bottom of the active site.
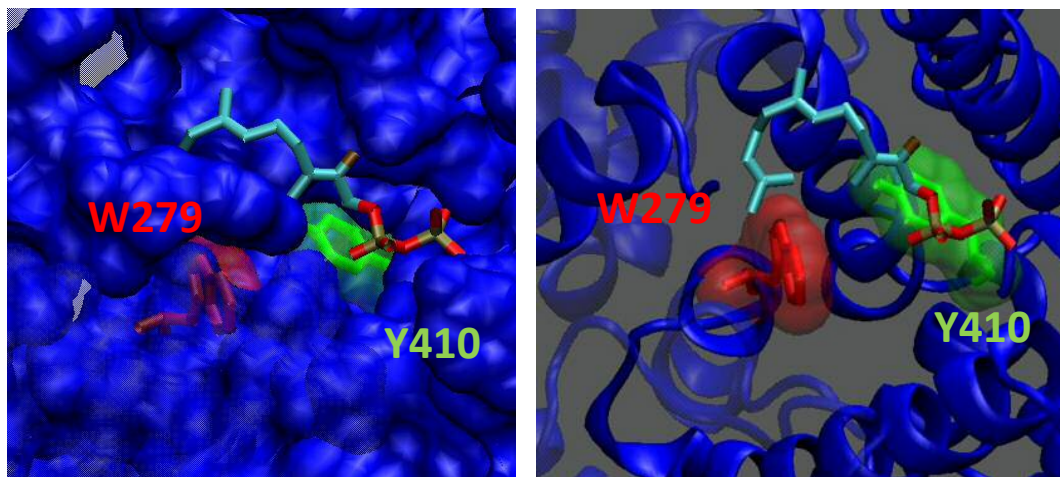
Figure 4.1 Surface (right) and ribbon (left) representations of the crystal structure of DCS active site (3g4f.pdb).[31] **Amino acids of interest of this study are shown. Red: W279, Green Y410, 2F-FDP is colored as follows: C: cyan; P: brown; O: red; F: dark brown.**

These two residues are ideally placed not only to stabilise carbocationic intermediates during the formation of DCN but also to form hydrophobic interactions that might help control the active site conformation of the natural substrate FDP and mediate active site closure and opening.

Site direct mutagenesis (SDM) has been successfully used to engineer other sesquiterpene synthases to produce altered products. A clear example is the work carried out on germacrene A synthase from *Solidago canadensis*. A single mutation in the active site (G402A) drastically changed the product profile of this cyclase, producing α-humulene instead of germacrene A.[96]

Taking Yoshikuni's work in mind, we report site direct mutagenesis studies of DCS, targeting the residue W279, showing the importance of this amino acid in shielding the active site from the solvent. Furthermore, we describe how a single amino acid mutation in the active site of DCS led to an enzyme that produces GD4ol up to 90%.

4.2 Expression and purification of active site mutants

To assess the importance of Trp 279 in the desolvatation of the active site, the following mutants were generated by site-directed mutagenesis from DCS_His$_6$: W279E, W279D, W279Q, W279M, W279L, W279Y and W279A. The designed primers used to construct the active site mutants and the procedure used are described in section 6.1.17. The presence of the desired mutation was confirmed by DNA sequencing.

Once the DCS_His$_6$ mutants were obtained, their heterologous expression in *E. coli* and purification were achieved following the same protocols previously developed for DCS_His$_6$ and described in Section 6.2.3.

4.3 CD spectroscopy

CD spectra of DCS_His$_6$ mutants were recorded to confirm that no change in the secondary structure of the protein appeared after the introduction of the active site mutations. Although the different amplitudes recorded may imply a partial misfolding, the CD spectra recorded from 190 to 360 nm, contained the two minima at 208 nm and 222 nm, distinctive of an α-helical secondary structure, confirming that each mutant maintained the protein α-helical fold (Figure 4.3).
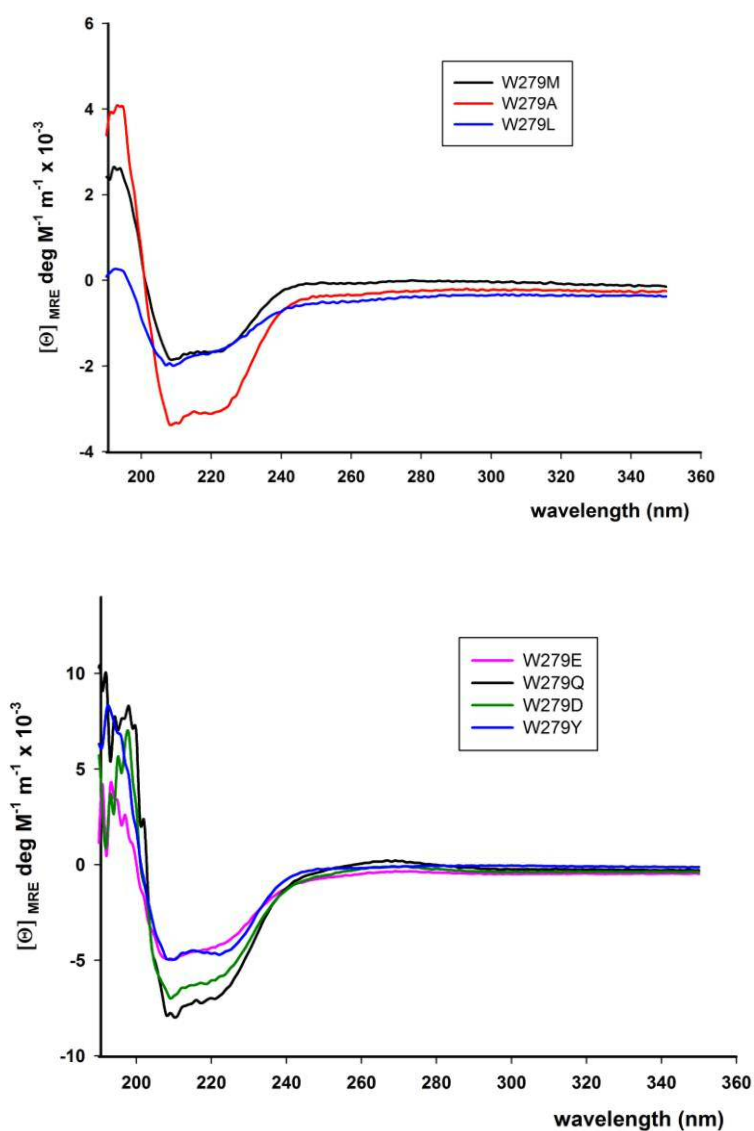
Figure 4.2 CD spectra of top: W279M, W279A, W279L; bottom: W279E, W279Q, W279D, and W279Y DCS_His$_6$.

4.4 Analysis of the sesquiterpene products and kinetics studies

The activity of DCS-His$_6$ mutants was determined by incubation of the protein with FDP as described in section 6.1.11. The GC-MS analysis of the pentane extractable products showed the formation of the two sesquiterpene DCN and GD4ol in variable ratios (Figure 4.4). These products were identified by comparison of the GC-retentions and the mass spectra with those of the product formed by WT_GD4olS and WT_DCS respectively.
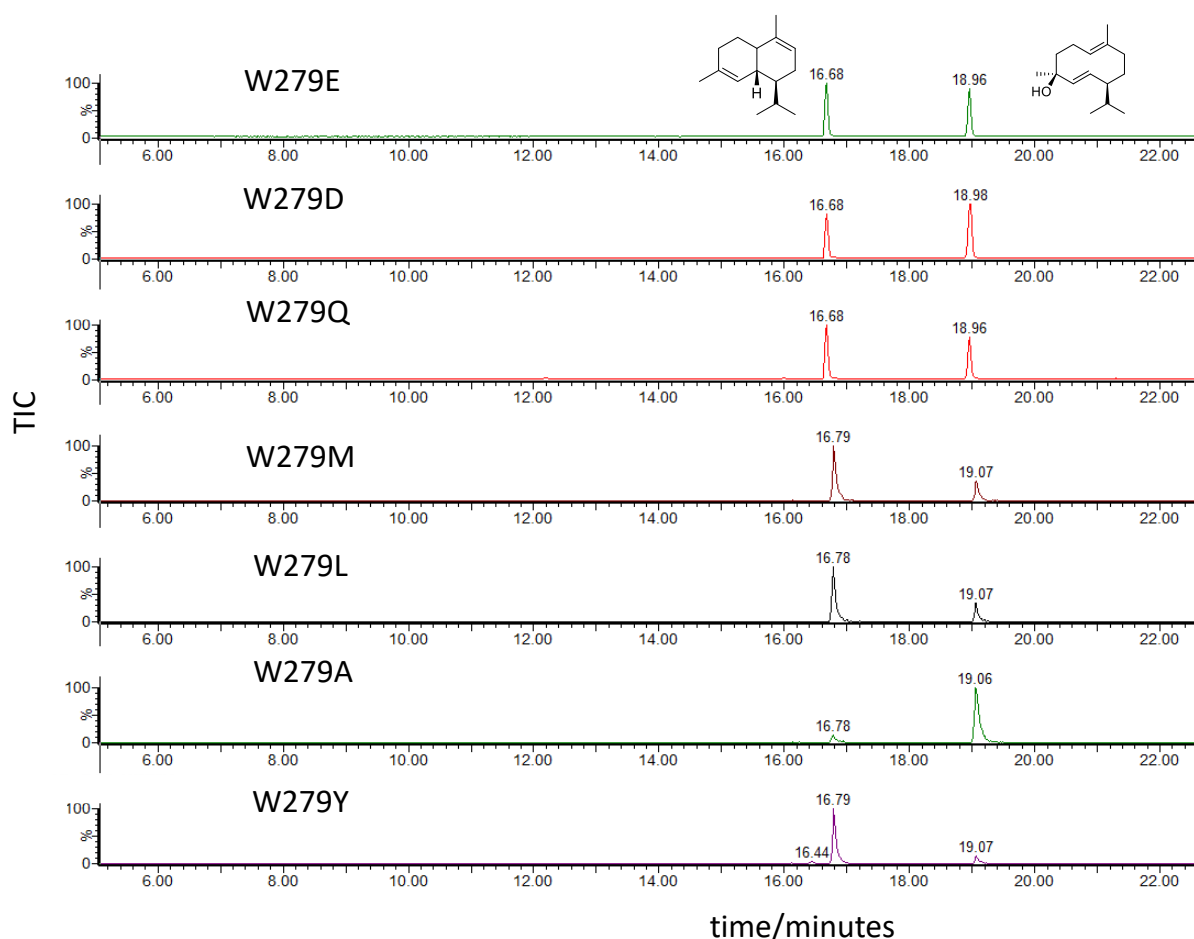
Figure 4.3 Gas chromatograms of the pentane extract products of the incubation of FDP with DCS_His$_6$ mutants.

All the kinetics studies of the DCS_His$_6$ mutants produced were performed following the same procedure used for DCS_His$_6$ and described in section 6.1.15.

Initially, W279 was mutated into Ala to assess whether the important role of Trp279 is due to its size and to its hydrophobic properties. Unexpectedly, the product distribution changed considerably: mutant W279A produced GD4ol as the main product, with a DCN:GD4ol ratio approximately of 9:1. This ratio is inverted when compared to that of DCS_His$_6$. Based on three independent measurements, W279A

134

k_{cat} and K_M values were found to be $3.12 \times 10^{-3} \pm 9.22 \times 10^{-6}\,s^{-1}$ and $2.23 \pm 0.51\,\mu M$ respectively (Figure 4.5). The k_{cat} found for W279A is comparable to the DCS_His$_6$ k_{cat} ($1.26 \times 10^{-3} \pm 5.73 \times 10^{-6}$), demonstrating that removal of the hydrophobic bulky residue in position 279 allowed the outer water to come in, reasonably by creating an empty tunnel in the active site, and quenching the germacradienyl-1-cation in position 4 without interfering with the overall catalytic efficiency.
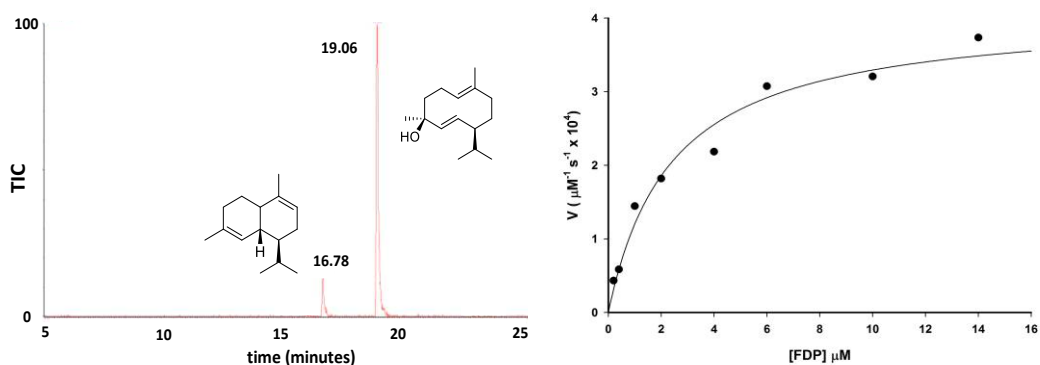
Figure 4.4 Left: Gas chromatogram of the pentane extractable products arising from the incubation of W279A with FDP; Right: representative Michaelis-Menten plot for the production of radiolabeled hexane extractable products from [1-³H]-FPP catalysed by DCS_W279A.

The van der Waals volume is a measure of atomic or molecular volume. This property, which is directly related to the van der Waals radius, is defined as the volume occupied by an individual atom, or by all atoms of a molecule.[97] As the protein folding is also a consequence of intermolecular forces, the removal of W279 van der Waals volume from the active site should favor the unfolding of DCS, allowing water ingress and carbocation quenching.

Therefore, to address the question whether the formation of the alcohol as main product is due to the residue volume, or it is due to the hydrophobic interactions with other residues in the active site, W279 was changed into tyrosine, another aromatic residue, but with a slightly smaller van der Waals volume.

It was found that W279Y DCS-His$_6$ was a reasonably functional synthase when compared to wild type with a k_{cat} and K_M of $7.32 \times 10^{-4} \pm 1.27 \times 10^{-5}\,s^{-1}$ and $4.28 \pm 0.7\,\mu M$ respectively (Figure 4.6). The quantity of GD4ol produced by W279Y was only 7% higher than the one produced by DCS_His$_6$. Furthermore, it was observed

the formation of another product eluting at 16.44 (Figure 4.6 left), which chemical structure could not be determined.
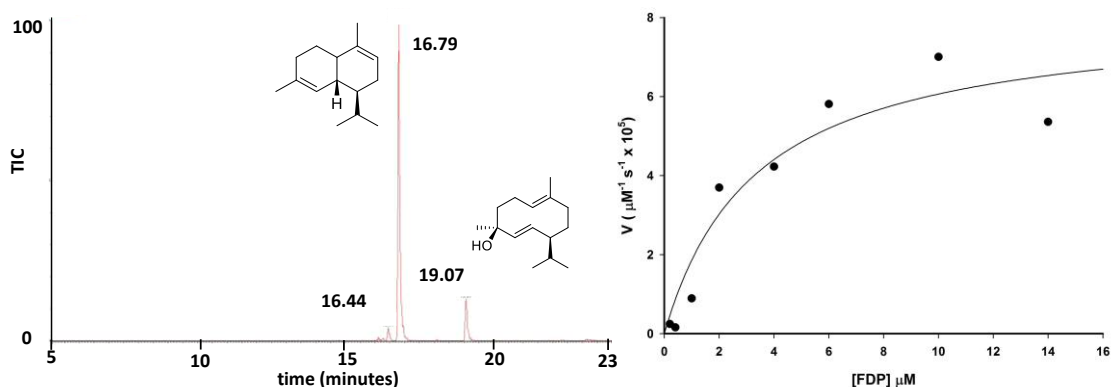
Figure 4.5 Left: Gas chromatogram of the pentane extractable products arising from the incubation of W279Y with FDP; Right: representative Michaelis-Menten plot for the production of radiolabeled hexane extractable products from [1-³H]-FPP catalysed by DCS_W279Y.

On the other hand, when W279 was changed with methionine and leucine, two amino acids with similar hydrophobic chain but with less van der Waals volume when compared with tryptophan, the amount of alcohol formed increased to 35% and 32% respectively. The product distributions generated by these mutants indicated that replacing the aromatic residue in position 279 with non-aromatic amino acids strongly compromised the formation of DCN as the single product. This outcome suggested that π system of tryptophan 279 could be involved in shielding the active site from the outer solvent, preventing the water attack at the intermediate *cis*-germacradienyl cation in the same way as Phe 178 does in aristolochene synthase.[37] W279M showed a k_{cat} of $1.09 \times 10^{-3} \pm 4.35 \times 10^{-5}$ s^{-1} and a K_M of 1.9 ± 0.22 μM (Figure 4.7) while W279L showed a k_{cat} of $3.8 \times 10^{-3} \pm 8.8 \times 10^{-5}$ s^{-1} and a K_M of 9.45 ± 1.10 μM (Figure 4.8).
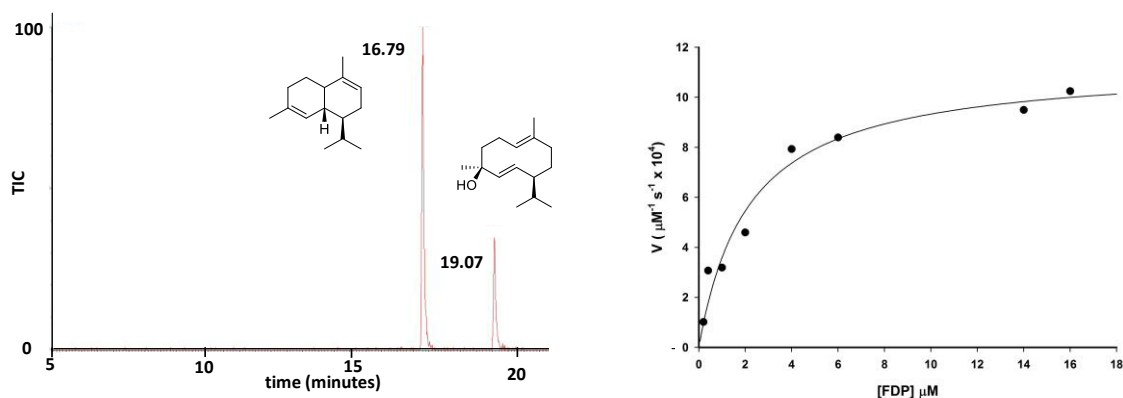
Figure 4.6 Left: Gas chromatogram of the pentane extractable products arising from the incubation of DCS_W279M with FDP; Right: representative Michaelis-Menten plot for the production of radiolabeled hexane extractable products from [1-³H]-FPP catalysed by DCS_W279M.
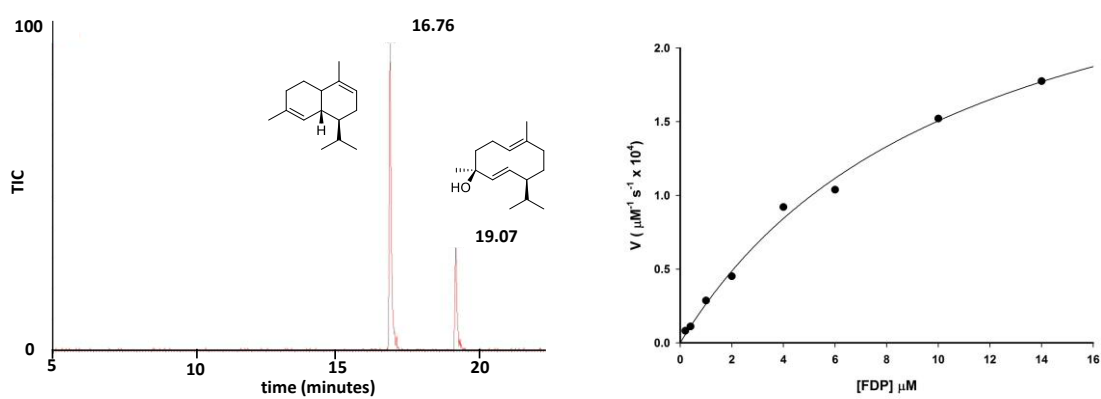
Figure 4.7 Left: Gas chromatogram of the pentane extractable products arising from the incubation of W279L with FDP; Right: representative Michaelis-Menten plot for the production of radiolabeled hexane extractable products from [1-³H]-FPP catalysed by DCS_W279L.

Although the k_{cat} values found for these two mutants were comparable with the DCS_His$_6$, both the K_M values resulted to be higher when compared to the wild type. In particular, as the K_M for W279L is 9.45 µM, it is clear that the substitution of trp in position 279 with leucine, strongly decreased the substrate binding affinity of FDP.

Based on these results, it was proposed that a hydrophilic residue in position 279 should form inadequate interactions with other residues in the active site pocket, and therefore compromise the catalytic activity and facilitate the formation of secondary products such as GD4ol. Consequently, tryptophan 279 was replaced with non-aromatic and hydrophilic amino acids like glutamine, glutamic acid and aspartic acid. These modifications in the active site led to a considerable amount of

137

GD4ol formed when compared to the DCS-His$_6$. More specifically, W279E, W279Q and W279D produced a ratio of DCN:GD4OL of 1:1, 3:2 and 2:3 respectively.

Kinetics analysis of W279Q (Figure 4.9, right) and W279D (Figure 4.10, right) showed a compromised enzyme-substrate binding affinity, as they gave K_M values of 8 and 9.24 µM respectively, values almost 10 times the K_M value of wild type for FDP. On the other hand, the K_M of W279E is comparable to the DCS-His$_6$ although the k_{cat} is reduced by 10 times (Figure 4.11).
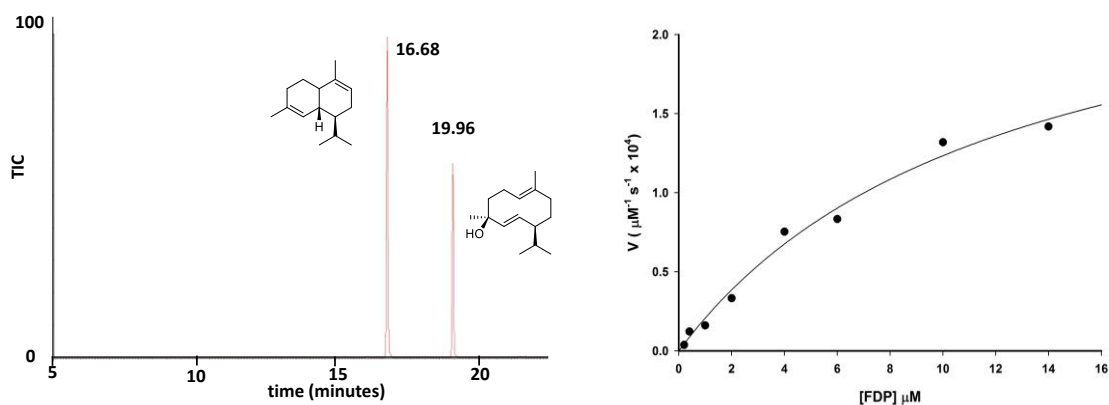
Figure 4.8 Left: Gas chromatogram of the pentane extractable products arising from the incubation of W279Q with FDP; Right: representative Michaelis-Menten plot for the production of radiolabeled hexane extractable products from [1-³H]-FPP catalysed by DCS_W279Q.
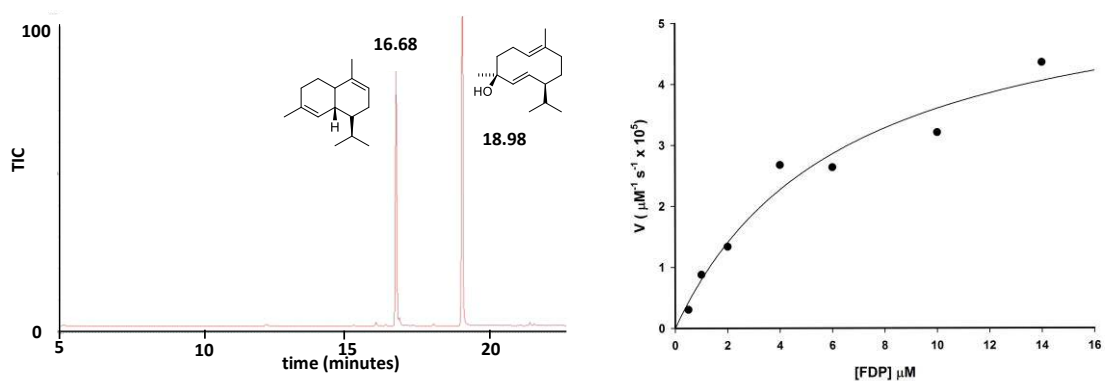
Figure 4.9 Left: Gas chromatogram of the pentane extractable products arising from the incubation of W279D with FDP; Right: representative Michaelis-Menten plot for the production of radiolabeled hexane extractable products from [1-³H]-FPP catalysed by DCS_W279D.
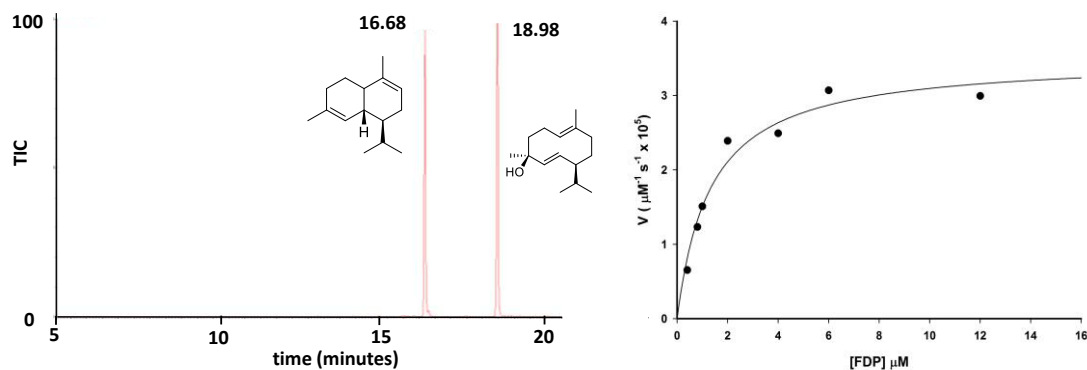
Figure 4.10 Left: Gas chromatogram of the pentane extractable products arising from the incubation of W279E with FDP; Right: representative Michaelis-Menten plot for the production of radiolabelled hexane extractable products from [1-³H]-FPP catalysed by DCS_W279E.

The product distributions showed an almost linear relationship (Figure 4.12) between the size of the amino acids and the alcohol production across the mutants generated, pointing out that the van der Waals volume of this residue is of primary importance for the DCN:GD4ol ratio formed.
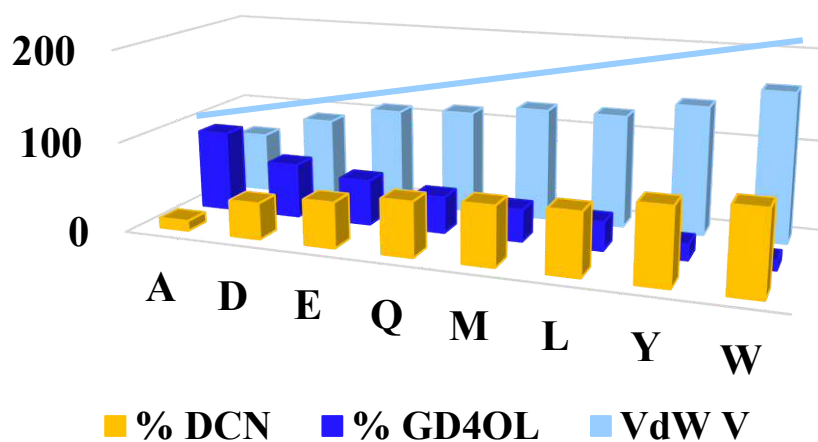
Figure 4.11 Histogram showing the product distribution produced by the mutants, related to the mutated amino acids van der Waalls volume. [98]

More specifically, these results suggest that the aromaticity of Trp 279 does not seem to determine product distribution. In fact, the replacement with negatively charged amino acids, such as aspartate or glutamate, or neutral alkyl residues, such as Leu or Ala, do not alter the reaction products; they only increase the proportion of water capture in direct proportion to the van der Waals volume of their side chain. In fact, when the hydrophobic residue W279 was substituted with less bulky

139

residues, a significant amount of the alcohol GD4ol was produced when compared to wild-type (Figure 4.8). This may be due to an extra space created in the active site, whereby water from the bulk solvent can enter and quench the ($3Z,7E$)-germacryl cation. The size of the channel appears to be depending on the size of residue 279 so that small residues, such as alanine, allow water ingress and the generation of large amount of GD4ol. It is therefore proposed that the W279 amino acid is involved in the stabilisation of the transition state following the formation of *cis*-germacradienyl cation, pushing the equilibrium trough the formation of cadinyl cation.

It is also possible that the substitution of the residue W279 with smaller amino acid residues might result in a misfolded protein, with an open conformation, leaving the active site, and therefore the substrate, exposed to the outer solvent.

Following this, the diphosphate group may act as a general base for the final deprotonation step (Figure 4.13). When W279 is replaced with a smaller, non-aromatic residue this process may be perturbed; C1 and C6 of FDP are too far apart to facilitate the final ring closure and extra space in the active site opens a pore, whereby water can enter the active site to quench the ($3Z,7E$)-germacryl cation (Figure 4.13).
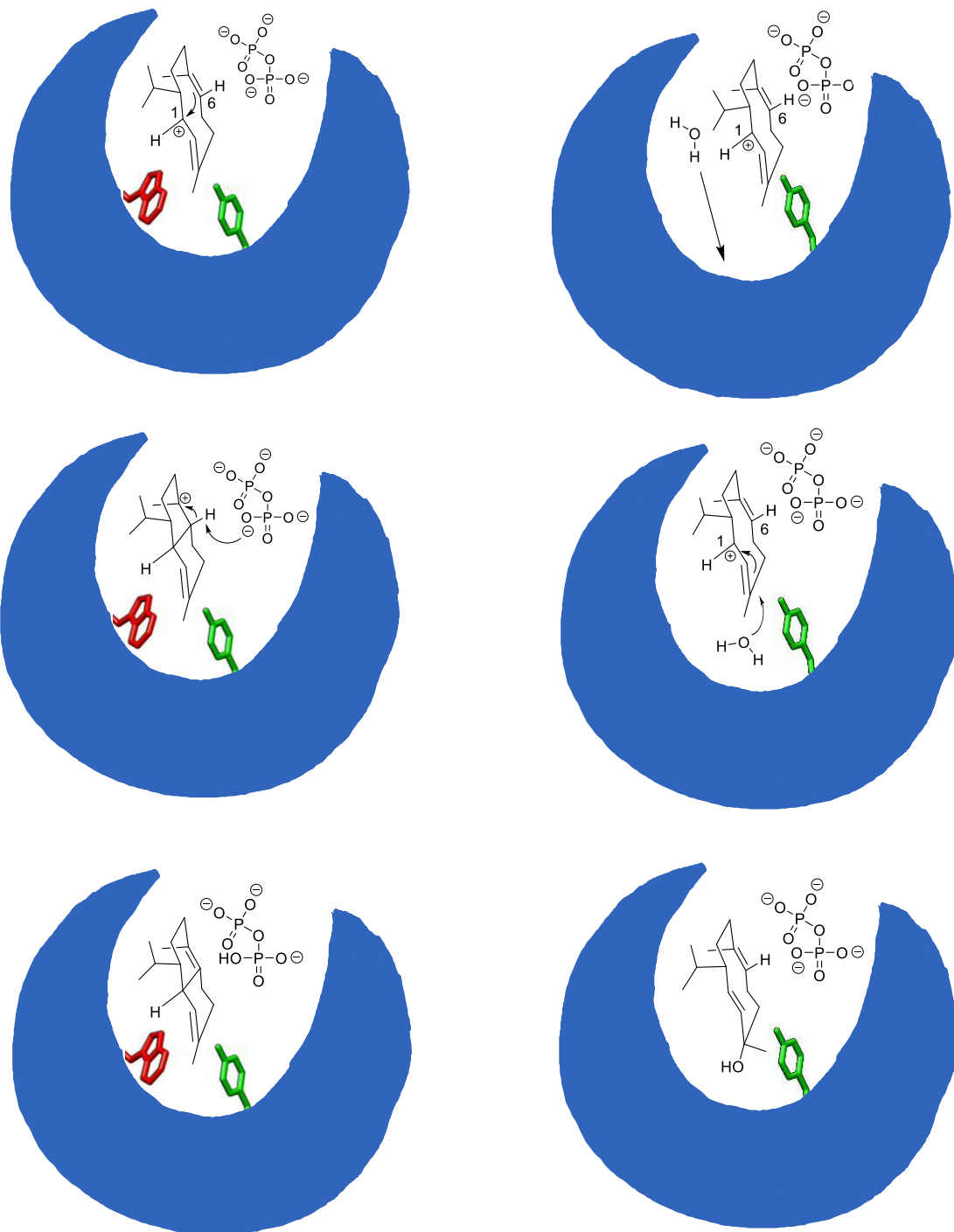
Figure 4.12 Graphic representations of the active site of wild-type (left) and mutated (right) DCS to show the water channel in the active site created by the disruption of the interaction between trp 279 (red) and tyr 410 (green). Water is proposed to ingress through this gap and attach at C3 of 2 GD4ol.

Summary and conclusion

Seven clones with mutation of the amino acid in position 279 were generated: hydrophobic and hydrophilic residues replacing W279 were investigated to demonstrate the effect of the lipophilicity in the desolvatation of the DCS active site. Kinetics data and product distribution are summarised in Table 4.1.

Table 4.1 Product distributions arising from incubations of DCS_His$_6$ and mutants with FDP and steady state kinetic data.

	k_{cat} (s^{-1})	K_M (μM)	DCN	GD4OL
DCS-His6	$1.260 \times 10^{-3} \pm 5 \times 10^{-6}$	0.58 ± 0.11	90 %	10 %
W279E	$5.94 \times 10^{-4} \pm 5 \times 10^{-6}$	1.45 ± 0.09	50 %	50 %
W279Q	$3.00 \times 10^{-3} \pm 1.51 \times 10^{-5}$	8.00 ± 4.00	60 %	40 %
W279D	$6.68 \times 10^{-4} \pm 9 \times 10^{-6}$	9.24 ± 3.00	40 %	60 %
W279L	$3.80 \times 10^{-3} \pm 9 \times 10^{-5}$	9.45 ± 1.10	68 %	32 %
W279M	$1.09 \times 10^{-3} \pm 4 \times 10^{-5}$	1.90 ± 0.20	65 %	35 %
W279A	$3.120 \times 10^{-3} \pm 9 \times 10^{-6}$	2.23 ± 0.51	11 %	89 %
W279Y	$7.32 \times 10^{-4} \pm 1.2 \times 10^{-5}$	4.28 ± 0.70	83 %	17 %

Site direct mutagenesis of the residue W279 indicates that the presence of this amino acid is essential in order to shield the substrate from the outer solvent during the conversion of the linear FDP in the cyclic sesquiterpene DCN, showing that the relative amounts of DCN and GD4ol formed are dependent on the volume of the side chain of residue 279. It is proposed that modification of the specific aminoacid 279 could form a water channel that allows outer solvent to enter the active site and quench the intermediate carbocations, leading to the formation of GD4ol.

It is important to note also that the addition of a hexahistidine tag on the C-terminus led to the formation of significant quantities of GD4ol. This is consistent with the hypothesis that an accurate series of loop movements must happen in order to effect closure the active site of DCS, otherwise water can ingress and quench the intermediate carbocations.

It is also demonstrated that DCS_His$_6$ can be engineered to a GD4ol synthase with a single amino acid mutation, where the aromatic residue W279 is replaced with an

alanine. This shows that the product profile of a sesquiterpene can be modified by the introduction of a single point mutations in its active site.

CHAPTER 5 Conclusions and Future Work

5.1 Overview

This project describes an investigation of the catalytic mechanism of δ-cadinene synthase. This was achieved through performing enzymatic inhibition of DCS with aza-compounds. These aza-compounds were designed to mimic the putative intermediate carbocations formed in one of the possible DCS cyclisation mechanisms: a 1,6- cyclisation reaction. A new purification protocol for DCS was developed, in order to obtain the protein in its active form.   Then, a new enantioselective synthetic route was developed to prepare the aza-analogues, which were tested with AS and ADS first and then with DCS, using a known assay employing radioactive FDP. In addition to the synthesis of the aza-analogues and testing these with the three sesquiterpenes, this project also describes the investigation of DCS the active site contour, in particular the study of the role of the aminoacid W279. Seven mutants were designed and produced to study the contribution of W279 in the desolvatation of the active site pocket. Furthermore, DCS was engineered to produced GD4ol as the major product with a single point mutation.

5.2 Synthesis of the aza-analogues

The formation of the sesquiterpene δ-cadinene is thought to be formed via one of two possible reaction pathways, as catalysed by DCS. These both begin with initial formation of a carbocation through PP_i cleavage but then involve an initial 1,6 or 1,10 ring closure, with the formation of the two key intermediates α-bisabolyl (**33**) and the germacradienyl cation (**52**) respectively (Figure 5.1). The aza-analogues chosen in this studies, the aza-bisabolyl cation (**60**) and the aza-germacradienyl cation (**85**) were designed to mimic the key carbocations **33** and **52**. Both enantiomers of **60** have been previously synthesised by Coates and colleagues[71]. Here is reported a new enantioselective synthesis, four steps shorter and safer than the Coates ones, with an overall yield of 2.2 % (Scheme 5.1).
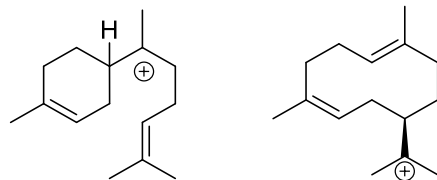
α-bisabolyl cation   cis-germacradienyl cation

33   **52**

Figure 5.1 Chemical structures of 33 and 52.
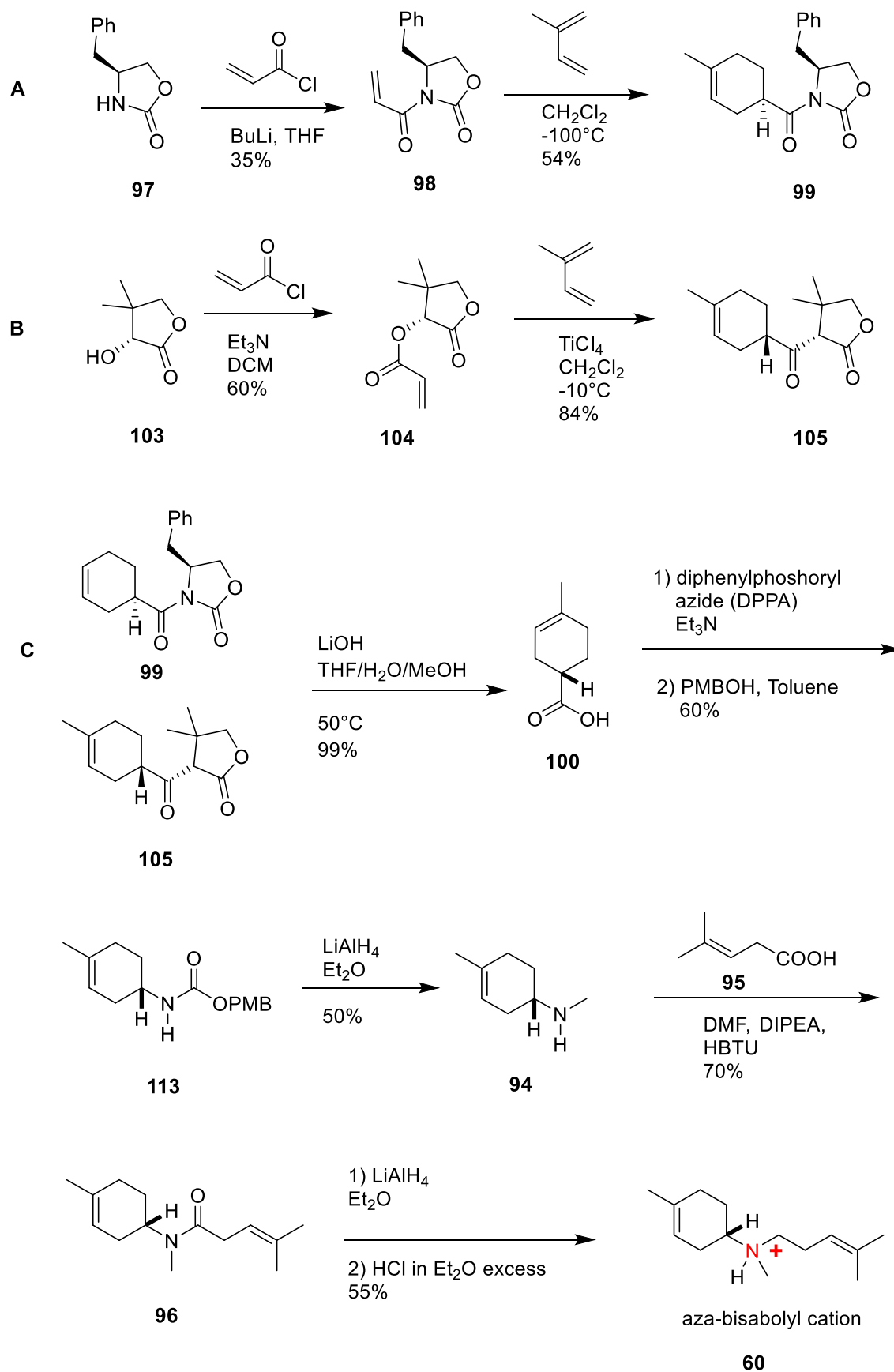
Scheme 5.1 Synthetic pathway for the formation of the aza-bisabolyl cations 60.

The synthesis of the aza-germacradienyl cation (**85**) has not been reported in literature. The synthetic approach used in this work aimed to prepare the aza-analogue in its racemic form. The proposed synthesis is shown in Scheme 5.2.
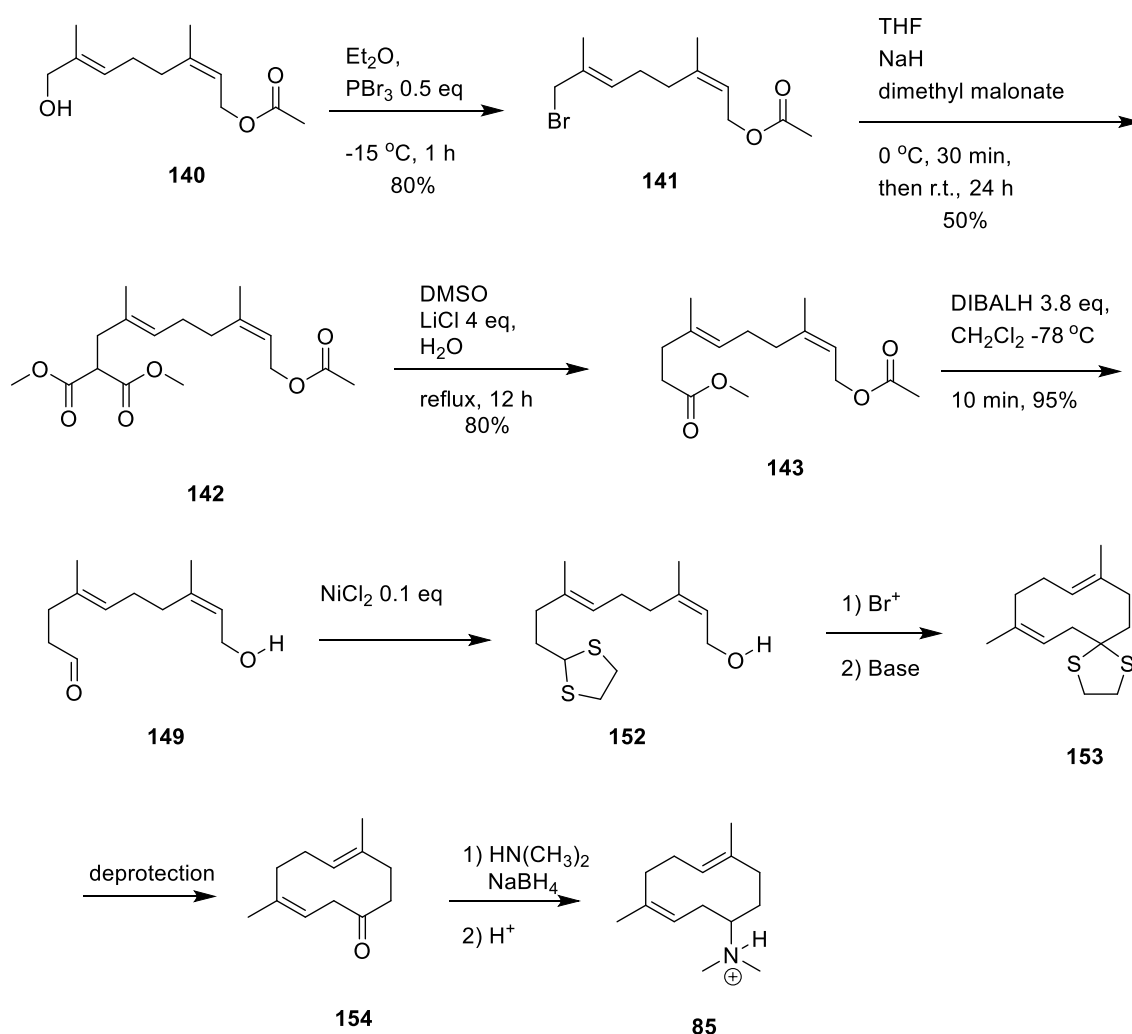
Scheme 5.2 Proposed synthetic pathway to form the germacradienyl cation aza-analogue 85.

It was not possible to explore the cyclisation reactions (**152** to **153**) and to conclude the synthesis of **85**. Florence Huynh, a PhD student in the Allemann group, is attempting to obtain the cyclic compound **153** with the intent to synthesise **85** and perform the remaining inhibition studies.

5.3 AS and ADS inhibition studies

A negative and a positive control, in order to evaluate whether the aza-bisabolyl cation was a good mimic of **33** were initially carried out, testing the synthesised analogues **60** with AS and ADS. These cyclases are two intensively studied sesquiterpene synthases for which the cyclisation mechanisms are known to go

through a 1,10- and a 1,6-closure respectively. Kinetic data obtained for AS and ADS are summarised in Table 5.1 and 5.2 respectively.

Table 5.1 AS Kinetics inhibition data for aza-analogues of α-bisabolyl cation (60) AS K_M= 2.42 ±11 μM k_{cat} = 1x10^{-2} ± 2x10^{-5} s^{-1}.

Inhibitor	+250 PP$_i$ (μM) K_i (μM)	K_i (μM)
(*S*)-60	255 ± 23	295 ± 23
(*R*)-60	489 ± 62	472 ± 48

Table 5.2 ADS Kinetics inhibition data for aza-analogues of α-bisabolyl cation (60) ADS K_M= 2 ± 0.15 μM k_{cat}= 1.19x10^{-2} ± 52x10^{-5} s^{-1}.

Inhibitor	+250 PP$_i$ (μM) K_i (μM)	K_i (μM)
(*S*)-60	1.5 ± 0.5	25 ± 5
(*R*)-60	3.7 ± 1.9	50 ± 17

(*R*)-60 and (*S*)-60 did not prove to be substrates of AS, and poor inhibition activity was found. On the other hand, both (*R*)-60 and (*S*)-60 acted as strong competitive inhibitors of amorphadiene synthase. The inhibition properties of the aza-analogues were enhanced by the presence of PP$_i$ in the reaction mixture. These results showed that both analogues were able to enter the ADS active site but they were unable to be turned-over by the enzyme, therefore providing strong evidence of their similarity to the putative bisabolyl carbocation intermediate (**33**). Also, it appears that the stereochemistry of the inhibitor does not to have a big impact on the outcome of the inhibition studies.

5.4 DCS purification protocol optimisation and inhibition studies

A new expression protocol was developed in order to obtain soluble DCS. Consequently, the base extraction step previously needed to bring the protein in

solution was avoided. In addition, a six-histidine tag was introduced into the C-terminus of the DCS to improve the efficiency of the purification protocol.

When **60** was tested with DCS, it clearly acted as a competitive inhibitor of the sesquiterpene synthase. As expected, inhibition properties of **60** were enhanced by the presence of PP_i in the reaction mixture. Kinetic data are summarised in Table 5.3 below. It is curious to note that **(R)-60** acted as a strong inhibitor of DCS only with PP_i in the reaction mixture (Scheme 5.3).

Table 5.3 DCS_His$_6$ Kinetics inhibition data for aza-analogues of α-bisabolyl cation (60). DCS_His$_6$, K_M= 0.58 ± 11 μM; k_{cat} = 1.260 x 10^{-3} ± 5 x 10^{-6} s^{-1}.

Inhibitor	+250 PP_i (μM) K_i (μM)	K_i (μM)
(S)-60	1.5 ± 0.5	25 ± 5
(R)-60	2.5 + 0.5	1700 + 300

These results are evidence for 1,6-cyclisation pathway previously proposed (Scheme 1.10, Red). It can be said that the DCS-catalysed biosynthesis of the sesquiterpenes DCN involves the formation of the α-bisabolyl cation as the key intermediate.

5.5 DCS mutagenesis studies

Seven DCS-His$_6$ clones were generated to investigate the role of the residue W279 in the desolvatation of the active site: W279E, W279Q, W279D, W279L, W279M, W279A and W279Y. Kinetic data of the mutants and their product distributions are summarised in Figure 5.2 below and Table 4.1.
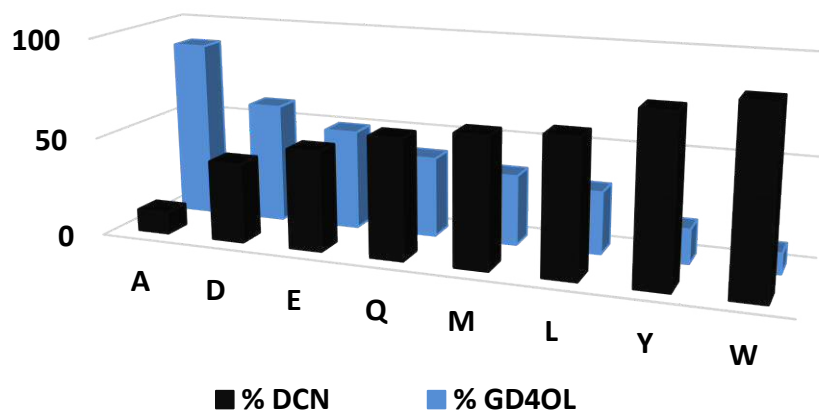
Figure 5.2 Histogram showing the product distributions arising from incubations of DCS-His$_6$ and mutants.

When W279 was mutated to smaller and less hydrophobic residues, the amount of GD4ol formed gradually increased (Table4.1), indicating that this amino acid is required in order to protect the cationic species from water during the conversion of the linear FDP in the cyclic sesquiterpene DCN. Finally, it is also shown that DCS_His$_6$ can be engineered to a GD4ol synthase with a single amino acid mutation, where the aromatic residue W279 is replaced with an alanine. This may be due to a water tunnel created by the absence of the steric hindrance of W279, or to a possible protein misfolding caused by the absence of the hydrophobic interaction of W279 with the contour active site.

5.6 Future work

Future investigation on DCS-catalysed reaction might be the completion of the synthesis of germacradienyl-aza analogue (**85**). Then, a positive and negative test, on AS and ADS respectively, will be necessary to confirm that **85** is a good mimic of the **52**. Finally, inhibition studies of DCS with **85** will give more insight on DCS reaction mechanism. More evidence towards a 1,6-cyclisation closure will be obtained if **85** proves not to be a competitive inhibitor of DCS, therefore, the 1,10-cyclisation closure could be excluded from the possible mechanisms used by DCS to turn over FDP. On the other hand, if **85** will act as a strong competitive inhibitor, it could be hypothesised that this sesquiterpene cyclase might be a promiscuous enzyme, able to catalyse the formation of DCN through different biosynthetic pathways. This last hypothesis is also supported by the ambiguous results obtained

by previous studies,[49,46,43] and by ability of DCS to produce GD4OL when the active site is altered in its amino acid composition.

Further site-direct mutagenesis investigation might target aminoacids in or in proximity to the active site, other than G276, I130, T407, C408, G409, L413, E455 and M523, which have already been proven to not be directly involved in the formation of DCN.[99,100] In addition, computational modelling of the loop movements that mediate the closure of the active site will elucidate how and if these movements influence the entrance of water in the active site and consequently quench carbocations intermediate.

This work is a step forward to the overarching goal of a deep understanding of how terpene synthases perform their catalytic process. Since these proteins can generate a great skeletal complexity in one synthetic step, they may in the future be powerful synthetic biocatalysts for the generation of many new compounds for the benefit for the society. For example, previous studies on ADS led to the hypothesis that sesquiterpene synthases that naturally produce only hydrocarbon products can be challenged with heteratom substituted substrates to produce sesquiterpenoid analogues for medical and agrochemical purposes. [86]

CHAPTER 6   **Materials and Methods**

6.1 Biological methods

6.1.1 Materials

Oligonucleotide primers for site-directed mutagenesis were purchased from Eurofins or Sigma-Aldrich, Pfu DNA polymerase and unstained protein marker were purchased from Thermofisher scientific, dNTP's were purchased from Promega, [1-^{3}H]-FDP was purchased from American Radiolabelled Chemicals, 'Ecoscint™ O' and 'Ecostint™ A' scintillation fluids were purchased from National Diagnostics.

The spin columns for DNA mini-preparations were purchased from Epoch and dialysis membranes was purchased from Medicell. All other chemicals were purchased from Sigma-Aldrich, Fisher Scientific or Melford. All mutated and ligated constructs were confirmed by DNA sequence analysis using the internal Eurofins facilities (School of Bioscience, Cardiff University, UK).

Nickel beads used for nickel affinity chromatography were purchased from Expedeon^{LTD}.

DNA concentration was measured using a Nanodrop 3300 Fluorospectrometer from Thermo Fisher Scientific.

UV spectroscopy was performed using a Jasco V-660 spectrophotometer.

Protein concentration was measured by the Bradford method[95] using commercial reagents and commercial bovine serum as the calibration standard.

GC-MS analysis of incubation products was performed on a Waters GCT Premier apparatus fitted with: column A = J&W Scientific DB-5MS column (30 m x 0.25 mm internal diameter), column B= Agilent J&W DB-35MS (30 m x 0.25 mm internal diameter), and a Micromass GCT Premiere detecting in the range m/z 50-800 in EI+ mode with a scan every 0.95 s with a scan time of 0.9 s. Method 1: injection temperature 100 °C; with a split ratio of 5:1; initial pressure 1 kPa, scans in function: 1525 ; initial oven temperature 80 °C, ramp of 4 °C/min to 180 °C (2 min hold) , flow 1 mL/min, retention window 0 to 28 min; Method 2: injection port at 100 °C; split ratio 5:1; initial pressure 1 kPa; scans in function: 1449; initial temperature 80 °C hold, ramp of 4 °C/min to 180 °C (15 min hold), then 20 °C/min to 250 °C, flow 1 mL/min, retention window 0 to 28 min.

Two strains of *E. coli* were used in this investigation:

XL1-BLUE for PCR amplification of all genes and in the production of mini-preparations of DNA for sequencing purposes.

BL21(DE3)-Codon Plus RP (BL21-RP) for expression and large scale production of all enzymes.

6.1.2 Competent cells

Preparation

Non-selective LB medium (10 mL) was inoculated with the desired cell line (55 µL, XL1-BLUE or BL21-RP) and incubated overnight at 37° C whilst shaking (200 rpm). 1 mL of the overnight culture was used to inoculate 100 mL of non-selective LB media until an optical density of 0.6 AU at 600 nm was reached. The cells were placed on ice for 15 min, harvested at 3400 *g,* and the supernatant solution was discarded. The cells were re-suspended in calcium chloride buffer 1 (40 mL), placed on ice for 15 min, and centrifuged again as previously described. The cells were re-suspended in 4 mL of calcium chloride buffer 2 and divided into 50 µL aliquots before being frozen in liquid nitrogen.

Calcium chloride buffer 1

Calcium chloride (1.11 g, 10 mM) was dissolved in deionised water (100 mL). The solution was then sterilised *via* autoclave at 121 °C for 20 minutes.

Calcium chloride buffer 2

Glycerol (15% v/v in water) and calcium chloride (1.11 g, 10 mM) were dissolved in deionised water (80) mL, the total volume was brought up to 100 mL. The solution was then sterilised *via* autoclave at 121 °C for 20 minutes.

6.1.3 Supercompetent cells

Preparation

Super-competent cells were prepared by the same method as described above for the competent cells, but using rubidium chloride buffer 1 and rubidium chloride buffer 2 instead of calcium chloride buffer 1 and calcium chloride buffer 2 respectively.

Rubidium chloride buffer 1

Calcium chloride (1.11 g, 10 mM), potassium acetate (295 mg, 3 mM) glycerol (15% v/v), manganese chloride (0.692 g, 5.5 mM) and rubidium chloride (0.120 g, 1 mM) were dissolved in deionised water (80 mL), the pH was adjusted to 5.8 using acetic

acid 1 M and the total volume was brought up to 100 mL. The solution was then sterilized using a 0.2 μM syringe filter and stored at 4 °C.

Rubidium chloride buffer 2

Calcium chloride (0.830 g, 7.5 mM), 3-(*N*-morpholino)propanesulfonic acid (0.200 g, 1 mM) glycerol (15% v/v) and rubidium chloride (0.120 g, 1 mM) were dissolved in deionized water (80 mL), the pH was adjusted to 6.5 with NaOH 1 M and the total volume was brought up to 100 mL. The solution was then sterilised using a 0.2 μM syringe filter and stored at 4 °C.

6.1.4 Growth media

Luria-Bertani (LB) medium

Tryptone (10 g), yeast extract (5 g), and NaCl (10 g) were dissolved in deionized water (0.5 L) and the final volume brought up to 1 L. The solution was sterilized in an autoclave at 121 °C and stored at 4 °C. The required antibiotic was added immediately before use under sterile conditions.

LB agar plates

Tryptone (10 g), yeast extract (5 g), and NaCl (10 g) were dissolved in deionised water (0.5 L) and the final volume brought up to 1 L. The solution was sterilised in an autoclave at 121 °C for 20 minutes. When the solution was cold enough to hold by hand, ampicillin (100 μg/mL) was added and poured into plates (ca. 40 mL for each) under sterile conditions. The solution was allowed to cool and the plates stored at 4 °C.

6.1.5 Sterile solutions

Ampicillin solution

Ampicillin (100 mg) was dissolved in deionised water (2 mL) to give a concentration of 50 mg/mL. The solution was aliquoted and stored at ⁻20 °C after filtration with a 0.2 μM syringe filter.

50% glycerol solution

Glycerol (50 mL) was added to 50 mL of deionized water to give the 50% v/v solution. The mixture was then sterilized in an autoclave at 121 °C for 20 minutes and stored at 4 °C.

6.1.6 Buffers

Cell lysis buffer 1 (ADS)

Tris-base (6.06 g, 50 mM), NaCl (29.29 g, 50 mM), β-mercaptoethanol (1.2 mL, 20 mM), imidazole (340 mg, 5 mM) and glycerol (15% v/v, 100 mL) were dissolved in deionized water (800 mL). The pH was adjusted to 8.0 and the total volume was brought up to 1 L. The buffer was then degassed under vacuum for 2 h and stored at room temperature.

Cell lysis buffer 2 (DCS and AS)

Tris-base (4.8 g, 20 mM), EDTA (3.7 g, 5 mM) and β-mercaptoethanol (700 μL, 5 mM) were added to deionised water (800 mL). The pH was adjusted to 8.0 and the total volume was brought up to 1 L. The buffer was then degassed under vacuum for 2 h and stored at room temperature.

Incubation buffer 1 (ADS)

HEPES (0.95 g, 20 mM), $MgCl_2$ (0.2 g, 5 mM) and DTT (0.154 g, 1 mM) were dissolved in deionised water (150 mL). The pH was then adjusted to 7.5 and the total volume was brought up to 200 mL.

Incubation buffer 2 (AS)

Tris base (0.4884 g, 20 mM), EDTA (3.7g, 5 mM), β-mercaptoethanol (70 μL, 5 mM), $MgCl_2$ (0.20 g, 5 mM) and glycerol (15% v/v, 30 mL) were added to 100 mL of deionised water. The pH was adjusted to 7.5 and the total volume was brought up to 200 mL.

Incubation buffer 3 (DCS)

HEPES (0.596 g, 25 mM), $MgCl_2$ (0.152 g, 15 mM) and DTT (0.038 g, 5 mM) were added to 70 mL of deionised water. The pH was then adjusted to 7.5 and the total volume brought up to 100 mL.

Ni^{2+} column/binding buffer

Tris-HCl (100 mM, 12.4 g), and NaCl (500 mM, 29.5 g) were added to 900 mL of deionised water, the pH adjusted to 8.0 and the total volume was brought up to 1 L.

Dialysis buffer 1 (ADS)

HEPES (26.0 g, 25 mM), NaCl (23.4 g, 100 mM), and DTT (618 mg, 1 mM) were dissolved in deionised water (4 L). The pH was then adjusted to pH 7.5.

Dialysis buffer 2 (AS and DCS)

Dialysis buffer was prepared dissolving Tris-base (3.6 g) and β-mercaptoethanol (1.1 mL) in 1 L of deionised water. The pH was then adjusted to 7.0 and the total volume was taken up to 3 L.

SDS running buffer

Glycine (150 g, 2 M), SDS (10% w/v, 10 g) and Tris-base (30.4 g, 250 mM) were dissolved in 1 L of deionised water. The running buffer solution was diluted 1:9 with deionised water prior to use.

SDS sample buffer

Tris-HCl solution (1.25 mL, 0.5 M, pH 6.8), glycerol (2.5 mL), bromophenol blue (200 µL of 0.6 % w/v solution), 10% SDS (2 mL of 10 % w/v solution) and β-mercaptoethanol (500 µL) were dissolved in deionised water (3.55 mL).

SDS-PAGE stain buffer

Comassie brilliant blue G-250 (0.50 g, 6 mM) was added to a mixture of ethanol and water (180 mL, 1:1). Glacial acetic acid (20 mL, 10% v/v) was added last.

SDS-PAGE de-stain buffer

Glacial acetic acid (100 mL) was added to a solution mixture of ethanol (400 mL) and deionised water (500 mL).

QIAprep® spin miniprep buffers:

- P1: Tris-HCl (3.94 g, 50 mM) and EDTA (1.86 g, 10 mM) were added to deionised water (450 mL), the pH was adjusted to 8 and RNase A (25.0 mg, 1.82 µM) was added before the total volume was taken up to 500 mL. The buffer was stored at 4 °C.

- P2: NaOH (0.8 g, 0.2 M) and SDS (1.00 g, 1% w/v, 34.7 mM) were dissolved in 100 mL of deionised water.

- N3: Guanidine hydrochloride (38.2 g, 4 M) and potassium acetate (4.90 g, 500 mM) were dissolved in deionised water (90 mL). The pH was then adjusted to 4.2 and the total volume was taken up to 100 mL

- EB: Tris-HCl (600 mg, 20 mM) was dissolved in deionised water (340 mL), the pH was adjusted to 8.5, and the total volume was taken up to 400 mL.

-PE: NaCl (117 mg, 20 mM) and Tris-HCl (32.0 mg, 2.00 mM) were added to deionised water (20 mL), and the pH was adjusted to 7.5 before the total volume was taken up to 100 mL with ethanol.

-PB: Guanidine hydrochloride (47.8 g, 5 M) and Tris-HCl (300 mg, 20 mM) were added to deionised water (62 mL) and the pH was adjusted to 7.5. The total volume was taken up to 100 mL with ethanol.

BSA: BSA (10 mg) was dissolved in deionised water (10 mL). 1 mL aliquots of the prepared solution were stored at -20 °C until required

Bradford reagent: Brilliant blue G250 (40 mg, 0.24 mM) was dissolved in ethanol (4 mL) and phosphoric acid (80%, 40 mL) was added. The final volume was brought up to 400 mL with deionised water and stored in a dark bottle at 4 °C.

6.1.7 Transformation of competent cells

An aliquot of frozen competent cells (BL21 (DE-3) or XL1-BLUE) prepared as described in sec. 6.1.2, was allowed to defrost on ice for 15 minutes, then 0.5 μL of ice-cold enzyme DNA (0.01 pmol) was added. The mixture was incubated on ice for 30 minutes, heat shocked at 42 °C in a water bath for 40 s, and then returned to ice for 5 min. 1 mL of non-selective sterile LB medium was added to the mixture and the resulting culture was incubated at 37 °C with shaking at 150 rpm for 1 h. Cells were harvested at 30.000 g for 1 min and the supernatant solution was discarded. The cell pellet was resuspended in 50 μL of LB medium, then spread onto a LB-agar plate containing ampicillin (180 mg/mL), and incubated at 37 °C overnight.

6.1.8 Large scale expression

A single colony was picked from a plate prepared as stated in 6.1.7 and used to inoculate 100 mL of LB medium containing 200 μL of ampicillin solution at 50 mg/mL. This culture was incubated at 37 °C overnight with shaking at 150 rpm. A portion (10 mL) of this stationary phase culture was then used to inoculate 500 mL LB medium containing ampicillin (50 μg/ml).

From here the large scale expression protocol differs from enzyme to enzyme:

Method A (ADS)

The inoculated 500 mL LB medium was incubated at 37 °C with shaking at 150 rpm until the optical density reached 0.5 AU at 600 nm. IPTG (final concentration 0.4 mM) was added and the culture was allowed to grow for 6 h at 20 °C before being harvested by centrifugation at 4000 g for 10 minutes. The supernatant solution was decanted and the cell pellet was stored at ⁻20 °C until required.

Method B (AS and WT_DCS)

The inoculated 500 mL LB medium was incubated at 37 °C with shaking at 150 rpm until the optical density reached 0.6 AU at 600 nm. IPTG (final concentration 0.5 mM) was added and the culture was allowed to grow for 4 h at 37 °C before being

harvested by centrifugation at 4000 g for 10 minutes. The supernatant solution was decanted and the cell pellet was stored at $^-$20 °C until required.

Test expression of DCS_His$_6$

In order to optimise the expression protocol for DCS_His$_6$, several test expressions were carried out varying the temperature, the length, and the amount of IPTG used. They were carried out on a 500 mL scale. 1 mL samples were taken prior to IPTG addition and every hour after induction. The cells in these samples were centrifugated (3300 g, 1 min), dissolved in SDS-sample buffer, and analyzed by SDS-PAGE (section 6.1.12).

Table 6.1 Test expression conditions for the optimisation of DCS_H$_6$ overexpression.

Entry	Temperature (°C)	Time (h)	IPTG (mM)
1	37	4	0.1
2	37	4	0.2
3	37	4	0.4
4	20	20	0.1
5	20	20	0.2
6	20	20	0.3

Method C (DCS_H$_6$ and mutants)

The inoculated 500 mL LB medium was incubated at 37 °C with shaking at 150 rpm until the optical density reached 0.6 AU at 600 nm. IPTG (final concentration 0.3 mM) was added and the culture was allowed to grow for 24 h at 20 °C before being harvested by centrifugation at 4000 g for 10 minutes. The supernatant solution was decanted and the cell pellet was stored at $^-$20 °C until required.

6.1.9 Protein purification

Method A (ADS)

A cell pellet was allowed to defrost on ice and then resuspended in 20 mL of cell lysis buffer 1. Lysozyme (0.5 mg/mL) was added and the solution was stirred at 0 °C for 1 h before being lysed by sonication on ice (5 s pulses followed by 10 s rest period, repeated for a total of 3 min). After sonication, the lysate was separated from the pellets by centrifugation at 30.000 g for 30 min, loaded onto a 2 cm Amintra NTA (Nitrilotriacetic acid) Ni^{2+} column (Expedeon^{LTD}), and eluted under gravity controlled flow. After 40 minutes the column was washed with 2 column volumes

(CV) of binding buffer. The column was then washed with a gradient of imidazole (from 5 to 300 mM) in binding buffer. ADS eluted with 60-100 mM imidazole in binding buffer, the fractions containing pure protein were analyzed by SDS-PAGE. Those fractions containing the protein were then dialyzed in dialysis buffer 1 and concentrated by Amicon™ ultrafiltration using a Millipore 30,000 MW cut off membrane.

Method B (AS and WT_DCS)

A cell pellet was allowed to defrost on ice, resuspended in 20 mL of cell lysis buffer 2, and lysed by sonication on ice (5 s pulses followed by 10 s rest period, repeated for a total of 3 min). The lysate was centrifuged (at 30.000 g, 30 min, 4 °C) and the supernatant solution discarded. The pellet was then resuspended in cell lysis buffer 2 (approximately 10 mL) and the pH of the stirred mixture was adjusted to 12 by addition of 1 M NaOH. After stirring at 0 °C for 30 min, β-mercaptoethanol (final conc. 5 mM) was added and the pH was adjusted to 8 by addition of 1 M HCl. After stirring for a further 30 min at 0 °C the solution was centrifuged at 30.000 g for 30 min. The pellet was discarded, the protein solution (approximately 25 mL) was loaded onto a diethylaminoethyl anion exchange column (DEAE, 75 mL), and washed (5mL/min) with cell lysis buffer 2 until baseline absorbance (at 280 nm) was observed. Following this the protein was eluted using cell lysis buffer 2 containing a 0.5-1 M NaCl gradient over 4 CV (flow rate 5 mL/min). The fractions absorbing at 280 nm were analysed by SDS-PAGE and those containing protein of the expected molecular weight were dialysed in dialysis buffer 2, pooled, and concentrated by Amicon™ ultrafiltration using a Millipore 30,000 MW cut off membrane.

Method C (DCS_His$_6$ and mutants)

The cell pellets were allowed to defrost on ice, resuspended in 20 mL of Ni^{2+} column buffer, and lysed by sonication on ice (5 s pulses followed by 10 s rest period, repeated for a total of 3 min). After sonication, the lysate was separated from the pellet, loaded onto a 2 cm Amintra NTA (Nitrilotriacetic acid) Ni^{2+} column (Expedeon^{LTD}), and eluted under gravity controlled flow. After 40 min the column was washed with 2 column volumes (CV) of binding buffer. The column was then washed with a gradient of imidazole (from 5 to 300 mM) in binding buffer. DCS_His$_6$ and related mutants eluted with 60-100 mM imidazole in binding buffer, the

fractions containing pure protein were analysed by SDS-PAGE. Those fractions containing the protein were then dialysed in buffer 2 and concentrated by Amicon™ ultrafiltration using a Millipore 30,000 MW cut off membrane.

6.1.10 Protein concentration

The protein concentrations were determined by Bradford assay.[95]

Bradford assay methodology:

A range of concentrations of bovine serum albumin protein (BSA) from 0.01 to 0.1 µg/mL were prepared. Bradford reagent (1 mL, Coomassie Brilliant Blue dye) was then added and the absorbance was measured from 400 to 600 nm with a Jasco V-660 spectrophotometer. The ratio of absorbances at 590 nm and 450 nm was calculated and used to plot a standard calibration curve. The procedure was repeated for the purified proteins and the ratio of absorbances compared to the BSA standard to calculate the concentration of each sample. Usually, two measurements per enzyme were carried out, and the final protein concentration resulted by the average of these two calculated values.

6.1.11 Protein activity

Enzyme activity was confirmed by incubation of 50 µL of purified enzyme with 1 µM of FDP in 250 µL of incubation buffer. The reaction was then overlaid with 500 µL of hexane and gently agitated at room temperature for 16 h. The products were extracted with hexane (2 × 600 µL) and then analyzed by GC-MS. The purity of the protein was determined by SDS-PAGE.

6.1.12 SDS-PAGE protocol

SDS stacking buffer preparation

Acrylamide/Bisacrylamide (1.7 mL, 30 % solution in water), Tris-base (0.5 M, 2.5 mL, pH = 6.8) and 10% SDS (0.1 mL) were dissolved in 5.7 mL of deionized water.

SDS resolving buffer preparation

Acrylamide/Bisacrylamide (4 mL, 30% solution) Tris-base (1.5 M, 2.5 mL, pH= 8.8) and 10% SDS (0.1 mL) were dissolved in 3.4 mL of deionized water.

To initiate polymerisation, 100 µL of freshly prepared ammonium persulfate (APS, 10% w/v) and 20 µL of *N,N,N',N'-* tetramethylenediamine (TEMED) were added immediately prior to pouring the gels between two glass plates. After pouring the

resolving solution, it was covered by a layer of isopropanol and allowed to polymerise. Excess isopropanol was then removed by blotting paper and the stacking gel was poured. A comb was inserted in order to create loading wells. After polimerisation, the comb was carefully removed, the fraction samples (10 µL) were incubated with protein marker for 5 minutes at 85 °C, and loaded into the loading wells. Running buffer was added and the gel was run at 200 V for 50 minutes. The gel was then stained in SDS gel stain buffer for 30 min. Then gel de-stain buffer was used until bands became visible. Fractions with bands that corresponded to the respective relative molecular mass of the purified enzyme were pooled together.

6.1.13 Size-exclusion chromatography

Size exclusion chromatography was carried out with a Superdex 200 10/300 GL prepacked gel filtration column (24 mL CV) on an AKTA FPLC system. Samples of 500 µL were loaded into the loop and then eluted through the column with 1.5 CV of Na_2PO_4 buffer (1 mL, pH 7.5) at a rate of 0.5 mL/min while monitoring UV absorbance at 280 nm.

6.1.14 Circular Dichroism spectroscopy

All the Circular Dichroism measurements were carried out on an Applied PhotoPhysics Ltd Chirascan™ spectrometer. Samples of the respective enzyme (10 µM) were prepared in potassium phosphate buffer (10 mM, pH = 7). A blank scan with potassium phosphate buffer alone was taken before take any scan of the protein samples. Typically, a 0.1 cm path length cuvette was used and the CD spectrum was recorded from 190 to 400 nm.

To convert the spectra obtained by CD spectroscopy to mean residue ellipticity (MRE) equation 7.1 was used:

Equation 6.1

$$[\Theta]_{MRE} = \frac{[\Theta]}{10 \cdot n \cdot c \cdot l}$$

Where, θ = molar ellipticity in millidegrees, n = number of backbone peptide bonds, c = protein molar concentration in the sample and l = length of the cuvette used.

6.1.15 Enzyme kinetics

Kinetic assay

Steady state kinetics parameters were obtained by radioactive assay using tritiated FDP ([1-^{3}H] FDP, specific activity 3.11 mCi/mmol) as the substrate. The reactions were prepared on ice using incubation buffer (final volume 250 µL) and an increasing concentration of the labelled FDP (from 2 to 25 µM). The reactions were initiated by adding a constant concentration of the respective enzyme (0.1 µM) to each reaction. The reactions were incubated at 30 °C for 10 min and then quenched by addition of EDTA (100 mM, 100 µL). Products were extracted with *n*-hexane (3 x 800 µL). The organic extracts were passed through silica (approximately 500 mg, poured into 15 mL of EcoScint™ (National Diagnostic) scintillation fluid, and analysed by scintillation counting for 10 min. The amount of tritiated product was determined by comparison with the counts determined from the unconverted tritiated FDP sample. The data was fitted to the Michaelis-Menten equation using Systat SigmaPlot 10:

Equation 6.2

$$V = \frac{V_{max}\,[S]}{K_M + [S]}$$

Equation 6.3

$$k_{cat} = \frac{V_{max}}{T.E.A.}$$

where T = reaction time in s, A = FDP activity, E = enzyme concentration.

6.1.16 Inhibition studies

Inhibition study assays followed the same protocol described for the kinetic assay with the difference that in each series of reactions with increased FDP concentration, an increased fixed concentration of the inhibitor was added before being initiated by the addition of the respective enzyme (i.e. in each series of reactions with increasing substrate concentration, the concentration of inhibitor remains constant). The Lineweaver-Burk (LB) plot was used for the identification of the inhibition type. LB plot derives from the reciprocal values of the Michaelis-Menten equation:

Equation 6.4

$$\frac{1}{V} = \frac{1}{V_{max}} + \frac{K_M}{V_{max}[S]}$$

6.1.17 Polymerase chain reaction (PCR)

The site-directed mutagenesis and gene amplification done in this work was carried out by PCR using *E. coli* XL1-BLUE as the template and designed oligonucleotide primers.

Introduction of C-terminal 6xHis tag into DCS

A single nucleotide deletion was required to bring the 6xHis coding sequence of pET21d in frame with the DCS coding sequence. A Quickchange site-directed mutagenesis kit (Stratagene) was used to introduce the desired deletion according to the manufacturer's instructions. The primers used for the deletion were as follows:

DCS_Histag_fw **5'-GAACCAATTG CACTTGAGGA TCCGAATTC-3'**

DCS_Histag_rv **5'-GAATTCGGAT CCTCAAGTGC AATTGGTTC-3'**

Site direct mutagenesis

The Quickchange site-directed mutagenesis kit (Stratagene) was used to introduce the desired mutation according to the manufacturer instructions. Plasmids were purified from overnight LB/ampicillin cultures (5 mL) using the QIAGEN miniprep kit as described by the manufacturer. Mutations were confirmed by DNA sequence

analysis using the internal WalesBioGrid facilities (School of Bioscience, Cardiff University, UK).

The mutagenic primers for DCS were designed using PrimerX as follow:

Table 6.2 Designer primers for site direct mutagenesis.

W279Q	Forward: 5' GAGTTGTTGAAGGTTACTTTCAGATCTCTGGAGTGTACTTTG 3'
	Reverse: 5' CAAAGTACACTCCAGAGATCTGAAAGTAACCTTCAACAACTC 3'
W279D	Forward: 5' GTTGTTGAAGGTTACTTTGACATCTCTGGAGTGTACTTTG 3'
	Reverse: 5' CAAAGTACACTCCAGAGATGTCAAAGTAACCTTCAACAAC 3'
W279M	Forward:5'AGTTGTTGAAGGTTACTTTATGATCTCTGGAGTGTACTTTG 3'
	Reverse:5' CAAAGTACACTCCAGAGATCATAAAGTAACCTTCAACAACTC 3'
W279L	Forward: 5' GAGTTGTTGAAGGTTACTTTCTGATCTCTGGAGTGTACTTTG 3'
	Reverse: 5' CAAAGTACACTCCAGAGATCAGAAAGTAACCTTCAACAACTC 3'
W279A	Forward: 5' GAGTTGTTGAAGGTTACTTTGCGATCTCTGGAGTGTACTTTG 3'
	Reverse: 5' CAAAGTACACTCCAGAGATCGCAAAGTAACCTTCAACAACTC 3'
W279Y	Forward: 5' GAGTTGTTGAAGGTTACTTTTACATCTCTGGAGTGTACTTTGAG 3'
	Reverse: 5' CTCAAAGTACACTCCAGAGATGTAAAAGTAACCTTCAACAACTC 3'

PCR procedure

Sterile H_2O (39 µL), Pfu-polymerase buffer (5 µL), dNTPs (1 µL, 10 mM), 2 µL of forward and reverse primers 0.1 mM, 1 µL template DNA 0.01 pmol and 1 µL Pfu-polymerase (2.5 U/µL) were added to a PCR tube and followed PCR protocol (Table 6.3). The parental DNA was digested with 1 µL *Dpn*I (10 U/µL) for 1 h at 37 °C. The reaction was cooled on ice before transformation into XL1-Blue *E. coli* cells. Mutations were confirmed by DNA sequence analysis using Eurofins MWG Operon's DNA sequencing service.

Table 6.3 PCR protocol used in this work.

Step	Temperature (°C)	Time (min)
Initial denaturation	95	3
Denaturation	95	1
Annealing	55	2
Elongation (x 15)	72	12
Final elongation	72	10

DNA purification

A single colony from the XL1-Blue *E. coli* cells transformed with the respective PCR product was used to inoculate 10 mL of ampicillin selective LB medium and the mixture was incubated over night at 37 °C whilst shaking at 150 rpm. The cells were then harvested at 15000 g for 10 min. The QIAprep spin miniprep kit (QIAGEN, Crawley, UK) was used to isolate the pure plasmid. The DNA sequencing was performed in the School of Biosciences at Cardiff University.

6.1.18 Calculation of Errors

Weighted mean standard error

The estimated true values for k_{cat}, K_i and K_M were calculated based on the weighted average, because each measurement for the same experiment was carried out independently and separately (Equation 6.5).

Equation 6.5

$$X_{WAV} = \frac{\Sigma\, w_i x_i}{\Sigma\, w_i}$$

Where x_i represents each value in the sample and w_i are the reciprocal squares of each measurements individual uncertainty, calculated using equation 6.6.

Equation 6.6

$$w_i = \frac{1}{\sigma_i^2}$$

Furthermore, the errors in this work are expressed as the standard error of the weighted mean (σ_{wav}) that is defined by equation 6.7.

Equation 6.7

$$\sigma_{wav} = \frac{1}{\sqrt{\Sigma w_i}}$$

Propagation of error

The propagation of errors for k_{cat}/K_M was calculated with equation 6.8.

Equation 6.8

$$\text{If } Z = X/Y, \text{ then}$$

$$\frac{\Delta Z}{Z} = \sqrt{\left(\frac{\Delta X}{X}\right)^2 + \left(\frac{\Delta Y}{Y}\right)^2}$$

Where X and Y are the independent values experimentally measured, ΔX and ΔY are their respective errors, Z is the calculated value and ΔZ is its propagation error.

Normalisation

When data was normalised, the following equation of unity-based normalisation was used:

Equation 6.9

$$X' = \frac{X - X_{min}}{X_{max} - X_{min}} \times 100$$

Where X' is the normal value, X is the original value and X_{max} and X_{min} are the maximum and the minimum values of the data set, respectively.

6.2 Synthetic methodology

6.2.1 General methods and materials

All chemicals were purchased from Sigma-Aldrich, Alfa-Aesar, or Fisher Scientific, and used without further purification unless otherwise stated. Anhydrous tetrahydrofuran (THF), diethyl ether (Et_2O), toluene, and acetonitrile were obtained from a MBraun SPS800 solvent purification system. Dichloromethane (CH_2Cl_2) and trimethylamine (Et_3N) were distilled under nitrogen over calcium hydride and potassium hydroxide, respectively. ^1H NMR, ^{13}C NMR, ^{31}P NMR, and ^{19}F NMR spectra were measured on Bruker Avance III 600, Bruker Avance 500, Bruker Avance III HD 400, and Bruker Fourier 300 NMR spectrometers. The spectra are reported in order

as chemical shifts in parts per million (ppm), downfield from tetramethylsilane (^{1}H and ^{13}C), trichlorofluoromethane (^{19}F), and phosphoric acid (^{31}P), integral, multiplicity, coupling and assignment, respectively. Assignments are made to the limitations of COSY, DEPT 90/135, gradient HSQC, and gradient HMBC spectra. Mass spectra were measured on a Waters GCT Premier time of flight mass spectrometer and a Waters LCT time of flight mass spectrometer. The methods used are the same as described in Section 7.1.1. Thin layer chromatography (TLC) was performed on pre-coated aluminium plates of silica G/UV254. TLC visualisations were performed with 4.2% ammonium molybdate and 0.2% ceric sulfate in 5% sulfuric acid (Hanessian's stain), or by UV light. The optical rotations were determinated using a UNiPol L-serie L1000/L2000 Schmidt+Haesch polarimeter. All measurements were performed at room temperature using a 5 cm long cell path and a wavelength of 269 nm.

Infrared (IR) spectra were obtained using a Jasco V-660 spectrophotometer.

Ion-exchange chromatography was performed using ion-exchange resin (Amberlyst 131 wet, H+ form) pre-equilibrated with ion-exchange buffer (25 mM NH_4HCO_3 containing 2% isopropanol, 2 CV). Reverse phase HPLC was performed on a system comprising of a Dionex P680 pump and a Dionex UVD170U detector unit. The column used was a 150 x 21.2 mm Phenomenex Luna C-18 column.

6.3 Synthesis of (*S*)- and (*R*)- enantiomers of aza-analogue 60 mimicking the α-bisabolyl cation.

(*R*)- and (*S*)-N,4-dimethyl-*N*-(4-methylpent-3-en-3yl)cyclohex -3-en-1 ammonium chloride (60)
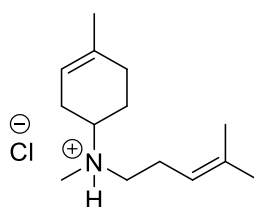
Product **116** was dissolved in Et$_2$O (1 mL) and HCl (1 M in anhydrous Et$_2$O) was added slowly. A light yellow precipitate was formed. The ether was evaporated and the salt stored in 1.2 mL of deionised water.

¹H NMR (300 MHz, MeOD) δ 5.38 (1 H, br, H$_3$CC=C*H*), 5.14 (1 H, t, *J* = 5.0 Hz, H$_3$CC=C*H*CH$_2$CH$_2$N), 3.58 – 3.42 (1 H, m, C*H*N), 3.32 (1 H, dd, *J* = 4.9, 1.6 Hz, C*H*HCH$_2$N), 3.25-2.97 (1 H, m, CH*H*CH$_2$N), 2.85 (3 H, s, C*H*$_3$N), 2.59 – 2.39 (2 H, m, =CC*H*$_2$CH$_2$CHN), 2.39 – 2.26 (2 H, m, =CCH$_2$C*H*$_2$CHN), 2.26 – 2.05 (2 H, m, =CHCH$_2$C*H*$_2$CHN), 1.84 (2 H, dd, *J* = 12.2, 10.4 Hz,), 1.76 (3 H, s, =CC*H*$_3$), 1.72 (6 H, s, C*H*$_3$CC*H*$_3$).

¹³C NMR (75 MHz, MeOD) δ 136.1 (HC=*C*CH$_3$), 134.3 (CH=*C* (CH$_3$)$_2$) 117.6 (*C*H=CCH$_3$) 116.5 (NCH$_2$CH$_2$*C*H=CCH$_3$), 61.8, 61.5 (*C*HN), 53.0, 52.5 (*C*H$_2$N), 35.9, 35.2 (CH$_3$N) 29.1, 29.0 (*C*H$_2$CH$_2$CHN), 25.7 (=CH*C*H$_2$N), 24.5 (*C*H$_2$CCH$_3$), 24.2, 24.0 (NCH$_2$*C*H$_2$), 23.25, 22.64 (*C*H$_3$C=), 21.64 (*C*H$_3$CCH$_3$), 16.65 (CH$_3$C*C*H$_3$).

IR (cm^{-1}) 2972 (broad, N-H stretch), 1379 (C-N stretch), 1161, 1051 and 1022 (C-N stretch), 950, 879, 815 (C=C bending)

HR-MS (AP$^+$) calculated for C$_{14}$H$_{26}$N: 208.2065, found 208.2057

m.p. 131-133 °C

(*S*)-**60:** α^{20}$_D$ −62.2 (MeOH, c=0.09)

(*R*)-**60:** α^{20}$_D$ +57.1 (MeOH, c=0.09)

(*R*)- and (*S*)-*N*-methyl-1-(4-methylcyclohex-3-en-1-yl)methanamine (94)
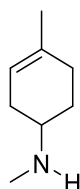
To a solution of carbamate **113** (100 mg, 0.4 mmol) in anhydrous diethyl ether (7 mL) at 0 °C, LiAlH$_4$ (50 mg, 1.28 mmol) was added. The mixture was then heated to reflux for 5 h. The reaction was cooled to 0 °C before it was quenched by the addition of water (6 mL) and an excess of 15% NaOH aqueous solution (6 mL). The resulting mixture was let stirring at 0 °C for 1 h, and the precipitate was removed by filtration on celite. The organic phase was extracted with water (2 × 10 mL) and the reunited layers were then washed with 10 % HCl (2 × 10 mL) and the organic fraction was discarded. The combined aqueous layers were basified with 10 % NaOH (15 mL) until pH = 12 was reached. The product was extracted with diethyl ether (4 × 15 mL), then dried over anhydrous MgSO$_4$, and filtered. The solvent was removed *in vacuo* to give the product **94** as a very volatile colorless oil (20 mg, 40%).

¹H NMR (300 MHz, CDCl₃) δ 5.24 (1 H, m br, C*H*=), 2.55 (1 H, dt, *J* = 16.6, 8.0 Hz, C*H*NH₂), 2.37 (3 H, s, HNC*H*₃), 2.25 – 2.10 (1 H, m, N*H*), 1.99 – 1.87 (2 H, m, C*H*₂CH=C), 1.87 – 1.66 (2 H, m, CH₂C*H*₂C=CH), 1.61 (1 H, broad m, C*H*₂CH₂C=CH)1.60 (3 H, s, H₂C=CC*H*₃), 1.45 – 1.26 (1 H, m, C*H*₂CH₂C=CH).

¹³C NMR (75 MHz, CDCl₃) δ 134.0 (C=*C*CH₃), 119.1 (*C*=CCH₃), 54.8 (*C*HNH), 32.7 (*C*H₂CHNH), 32.1 (C=CH*C*H₂CH), 29.7 (*C*H₃N), 29.0 (*C*H₂C=), 23.4 (*C*H₃C=)

(*S*)-94: α²⁰_D -79 (c 1.00, CHCl₃)

(*R*)-94: α²⁰_D +84 (c 1.00, CHCl₃)

Data in agreement with literature.[71]

4-methylpent-3-enoic acid (95)
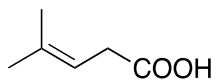
To a stirred aqueous solution of NaOH (2 M, 10 mL), **124** (630 mg, 6.62 mmol) in MeOH (10 mL) was added and the resulting mixture was refluxed for 5 h. The solution was allowed to reach room temperature and was diluted with water (30 mL). The aqueous layer was then washed with diethyl ether (3 × 30 mL) before being acidified to pH 2 by the addition of conc. HCl (9 mL). The acidic solution was extracted with diethyl ether (3 × 30 mL), the combined organic extracts were washed with brine (3 × 30 mL), dried over MgSO₄,

and the solvent removed in *vacuo* to give 4-methyl-3-pentenoic acid as a colorless oil (352 mg, 46 %).

¹H NMR (300 MHz, CDCl₃) δ 5.30 (tdt, *J* = 5.71, 5.71, 2.92, 1.40, 1.40 Hz, 1 H, −C*H*=),3.10 (d, *J* = 7.17 Hz, 2 H, C*H*₂), 1.66 (s, 3 H, C*H*₃), 1.77 (s, 3 H, C*H*₃)

¹³C NMR (300 MHz, CDCl₃) δ 201.6 (*C*=O), 170.2 (*C*=CH), 68.3 (C=*C*H), 26.1 (*C*H₂), 20.5 (*C*H₃)

LR-MS (EI+) m/z: 114.06(100% M +), 113.08 (40), 96.05 (55), 79.05 (50), 77.03 (40), 72.08 (90), 69.06 (100), 67.05 (62), 65.03 (30), 55.05 (38), 53.04 (35)

HR-MS (EI⁺) calculated for C₆H₁₀O₂ 114.0681: found 114.0678

Data in agreement with literature data.[71]

(R)- and (S)-N,4-dimethyl-N-(4-methylcyclohex-3-en-1-yl)pent-3-enamide (96)
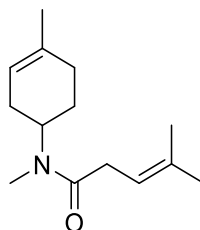
To a stirred solution of **95** (172 mg, 1.5 mmol) and DIPEA (775 mg, 6.0 mmol) in anhydrous DMF (6 mL), HBTU (1.15 g, 3.0 mmol) was added and the resulting mixture was stirred at room temperature for 20 min before **94** (358 mg, 1.5 mmol) was added. The reaction was then stirred for 24 h at room temperature. The solvent was removed *in vacuo* and the residue was dissolved in diethyl ether (20 mL). The solution was washed with water (2 × 25 mL), NaHCO$_3$ (2 × 25 mL), 10% HCl (2 × 10 mL), and brine (25 mL) before it was dried over MgSO$_4$ and the solvent removed *in vacuo*. The residue was purified by flash chromatography on silica (EtOAc:hexane 4:6) yielding **96** as a colorless oil (166 mg, 50%).

^{1}H NMR (400 MHz, CDCl$_3$) δ 5.24 (2 H, dd, *J* = 14.6, 8.0 Hz, NCHCH$_2$C*H*= and =C*H*CH$_2$C=O), 4.70-4.54 (0.5 H, m, C*H*N), 3.75 (0.5 H, dd, *J* = 12.6, 9.7 Hz, C*H*N), 3.01 (2 H, dd, *J* = 12.6, 6.8 Hz, C*H*$_2$C=O), 2.75 (1.5 H, s, C*H*$_3$N), 2.72 (1.5 H, s, C*H*$_3$N), 2.20-1.86 (5 H, m, C*H*$_2$CH$_2$CHC*H*$_2$), 1.71-1.88 (1 H, m, CH$_2$CH$_2$CHC*H*$_2$), 1.75 (s, 3 H, CNCH$_2$=CHC*H*$_3$), 1.68 (3 H, s, =CC*H*$_3$), 1.66 (3 H, s, =CC*H*$_3$).

(S)-96 : α^{20}$_D$ ⁻9.5, (CHCl$_3$, c=0.9)

(R)-96 : α^{20}$_D$ +10, (CHCl$_3$, c=0.9)

HR-MS (EI$^+$) calculated for C$_{14}$H$_{23}$NO : 221.1780, found 221.1779

Data are in agreement with literature.[71]

(S)-3-acryloyl-4-benzyloxazolidin-2-one (98)
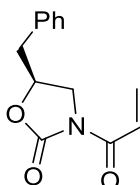
To a solution of (*S*)-4-benzyloxazolidin-2-one (1.00 g, 5.60 mmol) in anhydrous THF (12 mL) at ⁻78 °C, *n*-BuLi (2.1 M in THF, 3.14 mL, 6.59 mmol) was added dropwise over 30 minutes and the mixture stirred for a further 3 h at -78 °C. Freshly distilled acryloyl chloride (557 mg, 6.16 mmol) was added dropwise over 20 minutes and the reaction stirred for 2 h at ⁻78 °C. The reaction was then allowed to warm to room temperature overnight. The reaction was quenched with sat. NH₄Cl (20 mL) and extracted with diethyl ether (3 × 30 mL). The organic layer was washed with water (3×40 mL), saturated aqueous NaHCO₃ (3×40 mL), dried (MgSO₄), filtered, and concentrated under reduced pressure. Column chromatography (hexane:ethyl acetate 6:4) afforded **98** as a colorless solid (452 mg, 35%).

¹H NMR (CDCl₃, 300 MHz) δ ppm 7.45 (dd, 1H, *J* = 6.0, 18.0 Hz, C*H*=CH₂), 7.23 (m, 5H, aromatic Hs), 6.54 (dd, 1H, *J*$_{H,H}$ = 18.0, 18.0 Hz, CH*H*=CH₂), 5.87 (dd, 1H, *J* = 9.0, 9.0 Hz, C*H*H=C), 4.68 (m, 1H, CHN), 4.14 (m, 2H, CH₂O), 3.29 (dd, 1H, *J* = 9.0, 9.0 Hz, C.H*H*Ph), 2.74 (dd, 1H, *J* = 12.0, 12.0 Hz C*H*HPh)

α²⁰$_\mathbf{D}$ -86 (CH₂Cl₂, c = 0.65).

Data are in agreement with literature.[71]

(*R*)-4-benzyl-3-((*S*)-4-methylcyclohex-3-enecarbonyl)oxazolidin-2-one (99)
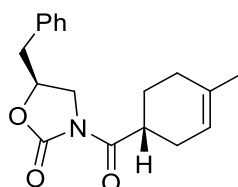
To a solution of chiral auxiliary **98** (200 mg, 0.86 mmol) at ⁻100 °C, isoprene (1.72mL, 17.2 mmol) in anhydrous CH₂Cl₂ (5.0 mL), and Et₂AlCl (1.2 mL, 1.5 eq) were added. The reaction was stirred at ⁻100 °C for 30 min. Then the mixture was poured into aqueous hydrochloric acid (1 M, 20 mL). The mixture was extracted with CH₂Cl₂ (2 × 10 mL). The combined organic layers were dried with anhydrous MgSO₄, filtered, and concentrated under reduced pressure. The product was purified by flash chromatography on silica (EtOAc:hexane:Et₃N 92:7:1) to yield the Diels-Alder adduct (**99**) as a colorless crystalline solid (139 mg, 54%).

¹H NMR (300 MHz, CDCl$_3$) δ 7.34 – 7.10 (5 H, m, aromatic H's), 5.36 (1 H, br., C*H*=C), 4.63 (1 H, dt, *J* = 16.6, 6.9 Hz, C*H*N), 4.23 – 3.95 (2 H, m, C*H*$_2$O), 3.60 (1 H, t, *J* = 8.8 Hz, C*H*C=O), 3.20 (1 H, dd, *J* = 13.2, 3.3 Hz, CH*H*Ph), 2.70 (1 H, dd, *J* = 13.3, 9.5 Hz, C*H*HPh), 2.20-1.6 (6 H, m, C*H*$_2$C*H*$_2$CHC*H*$_2$C=C), 1.64 (3H, s, C*H*$_3$)

α^{20}$_D$ +79 (CH$_2$Cl$_2$, c = 1.4).

LR-MS (EI+) m/z: 299.15 (100% M +), 300.16 (15), 269.06 (18), 267.07 (50), 232.10 (20), 178.08 (100), 146.07 (30), 140.03 (55), 122.07 (20), 91.00 (65), 63.00 (30).

Data are in agreement with literature.[71]

(*R*)- and (*S*)-- 4-Methylcyclohex-3-ene-1-carboxylic acid (100)
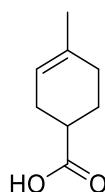
To a solution of **99** or **105** (0.32 mmol) in THF:MeOH:H$_2$O (1:1:1, 1.5 mL), LiOH • 10 H$_2$O (67 mg, 1.6 mmol) was added, and the resulting mixture was vigorously stirred for 1 h at 50 °C. The reaction was then cooled to room temperature and concentrated under reduced pressure. The resulting slurry was dissolved in H$_2$O and extracted with CH$_2$Cl$_2$ (3 × 5 mL). The resulting aqueous phase was acidified to pH = 2 at 0 °C with HCl 15%, extracted 3 times with a mixture of *n*-pentane:CH$_2$Cl$_2$ 98:2 v/v, dried over Na$_2$SO$_4$, and concentrated *in vacuo* to give **100** as a white powder (35 mg, 80%).

¹H NMR (CDCl$_3$, 300 MHz) δ 5.32 (1H, s, C*H*=), 2.54-2.39 (1 H, m, C*H*-COOH), 2.17 (2H, m, -C*H*$_2$CH=C), 1.93 (3 H, m, C*H*H-C*H*$_2$), 1.69 (1H, m, CH*H*-CH$_2$), 1.59 (3H, s, C*H*$_3$)

¹³C NMR (100 MHz, CDCl$_3$) δ 182.3 (HO*C*=O), 133.8 (HC=*C*CH$_3$), 119.0 (CH$_2$-H*C*=CCH$_3$), 39.0 (H*C*-COOH), 29.13 (*C*H$_2$C=CH$_3$), 27.3 (*C*H$_2$CH=CCH$_3$), 25.5 (*C*H$_2$CH$_2$C=CH), 23.5 (*C*H$_3$)

(*S*)-100 : **α^{20}$_D$** -80.6 (CHCl$_3$, c = 0.5); -106.4 (95% EtOH, c=4)

(*R*)-100: **α^{20}$_D$** +93 (CHCl$_3$, c = 0.5); + 105.5 (95% EtOH, c=4)

m.p. 82-92 °C

LR-MS (EI+) m/z: 140.06 (100% M +), 136.06 (15), 125.05 (40), 122.06 (100), 95.87 (100), 94.06 (100), 93.07 (80), 79.04 (100), 77.03 (100), 68.06 (90), 67.04 (100)

Data are in agreement with literature [82,103]

(R)-4,4-dimethyl-2-oxotetrahydrofuran-3-yl acrylate (104)
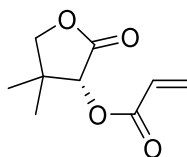
Freshly distilled propenoyl chloride (0.41 mL, 5 mmol) was added over 1 h to a stirred solution of (R)-pantolactone (500 mg, 3.84 mmol) and Et$_3$N (583 mg, 5.76 mmol) in anhydrous CH$_2$Cl$_2$ (10 mL) at $^-$24 °C. The resulting mixture was stirred for 5 h at $^-$24 °C, and subsequently washed with 10 mL of aqueous 1 M HCl. The aqueous phase was then extracted with CH$_2$Cl$_2$ (3 × 20 mL). The combined organic phases were washed with saturated NaHCO$_3$ solution (3 × 20 mL), water (3 × 20 mL) and brine (3 × 20 mL). The organic phase was dried over MgSO$_4$, concentrated under reduced pressure and the residue was purified by flash chromatography on silica (EtOAc:Hexane 4:6) to yield the pure compound as a yellow oil (375 mg, 53% yield).

¹H NMR (300 MHz, CDCl$_3$) δ 6.48 (1 H, d, *J* = 17.3 Hz, CH*H*=C), 6.18 (1H, dd, *J* = 17.3, 10.4 Hz, C*H*=CH$_2$), 5.93 (1H, d, *J* = 10.4 Hz, C*H*H=C), 5.40 (1H, s, C=OC*H*-O), 4.03 (2 H, s, C*H*$_2$-OC=O), 1.17 (3 H, s, CH$_3$), 1.08 (s, 3 H, CH$_3$)

¹³C NMR (63 MHz, CDCl$_3$) δ ppm 174.7 (O*C*=OCHO), 172.5 (O*C*=OC=H$_2$), 134.0 (H$_2$*C*=CHC=O), 118.7 (H$_2$C=*C*HC=O), 76.1 (OC=O*C*HO), 74.6 (O*C*H$_2$CH), 40.2 (*C*-(CH$_3$)$_2$), 23.4 (CH$_3$), 23.0 (CH$_3$).

α²⁰$_D$ 10 (CH$_2$Cl$_2$, c = 17)

Data are in agreement with literature [82,83]

(R)-4.4-dimethyl-2-oxotetrahydrofuran-3-yl-(S)-4-methylcyclohex-3-ene-1-carboxylate (105)
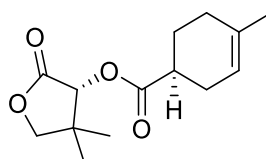
To a solution of **104** (302 mg, 1.67 mmol) in anhydrous CH_2Cl_2 (5 mL) at -10 °C, $TiCl_4$ (0.82 mL, 0.82 mmol, 1.0 M solution in CH_2Cl_2) was added, and the resulting solution was stirred under argon at ⁻10 °C for 1 h. Isoprene (0.23 mL, 2.3 mmol) was then added over 5 min and the mixture was left stirring for 3 h at -10 °C. The reaction was quenched by addition of finely pulverised $Na_2CO_3 \bullet 10\ H_2O$, water (5 mL). The aqueous phase was then extracted with CH_2Cl_2 (3 × 20 mL). The organic layers were combined, washed with H_2O (3×10 mL), brine (3×10 mL), dried over $MgSO_4$, and concentrated under reduced pressure. The residue was purified by flash chromatography on silica (EtOAc:hexane 2:8) to yield pure **105** as a clear oil (353 mg, 85% yield).

¹H NMR (300 MHz, CDCl₃) δ 5.32 (1 H, s, OC*H*C=O,) and (1 H, br C*H*=), 3.98 (2 H, s, CHC*H₂*O), 2.69 - 2.51 (1 H, m, C*H*-C=O), 2.19 (2 H, m broad, CHO-C*H₂*C=), 1.98 (3 H, m, C*H*H-CH₂), 1.73 (1H, m, -CH*H*-CH₂), 1.58 (s, 3H, C*H₃*C=), 1.13 (3H, s, C*H₃*), 1.04 (3 H, s, C*H₃*).

¹³C NMR (75 MHz, CDCl₃) δ ppm 174.7 (O*C*=OCHO), 172.5 (O*C*=OC=H₂), 134.0 (HC=*C*CH₃), 118.7 (H*C*=CCH₃), 76.1 (OC=O*C*HO), 74.6 (O*C*H₂C), 40.2 (*C*-(CH₃)₂), 38.9 (CH₂*C*H-C=O), 28.9 (HC=C*C*H₂), 27.7 (C=CH*C*H₂), 25.2 (HC=CCH₂*C*H₂), 23.4 (C*C*H₃), 23.0 (C*C*H₃), 19.8 (*C*H₃C=CH).

LR-MS (EI+) m/z: 252.13 (50%), 122.07 (20), 94.08 (100), 79.05 (30), 67.05 (10)

α²⁰_D -51.3 (CHCl₃, c = 1).

Data are in agreement with literature.[83,103]

(*R*)- and (*S*)-4-Methoxybenzyl [(4-methylcyclohex-3-en-1-yl) methyl)-carbamate (113)
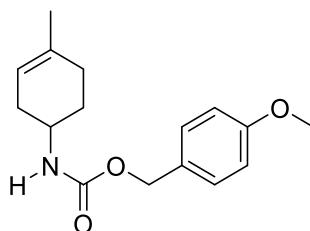
To a solution of **100** (1.3 g, 9.3 mmol) in anhydrous toluene (20 mL) at 0 °C, diphenylphosphoryl azide (2.2 mL, 10.2 mmol) and Et₃N (3.9 mL, 27.8 mmol) were added. The resulting mixture was left stirring for 3 h at 100 °C before 4-methoxybenzyl alcohol (1.27 mL, 10.2 mmol) was added, and the reaction was left

stirring over night at 100 °C. The reaction was then allowed to reach room temperature and the solvent was evaporated *in vacuo.* The residue was the purified by flash chromatography on silica (EtOAc:*n*-hexane 1:9) to yield the pure compound as yellow crystalline solid (1.28 g, 80% yield).

^{1}H NMR (300 MHz, CDCl$_3$) δ 7.23 (2 H, dt, *J*= 2.9 Hz, *J* = 5.3 C*H* aromatic Hs), 6.81 (2 H, dt, *J* = 2.9 Hz, *J* = 5.32, C*H* aromatic Hs), 5.21 (1 H, bro, *H*C=C), 4.95 (3 H, s, -OC*H$_2$*-Ph), 4.67-460 (1 H, m, C*H*N), 3.74 (3 H, s, -OC*H$_3$*), 2.29-2.20 (2 H, m, CH$_2$-C*H$_2$*CHN), 1.93 (2 H, m, C*H$_2$*-CH$_2$CHN), 2.01-1.86 (2 H, m, CH-C*H$_2$*CHN), 1.55 (3 H, s, CH$_3$C=CH).
^{13}C NMR (75 MHz, CDCl$_3$) δ 159.5 (=*C*O-CH$_3$), 155.8 (NH*C*=O), 134.1 (C=*C*CH$_3$), 130.0 (*C*=C aromatic), 128.7 (*C*CH$_2$O), 118.3 (*C*=CCH$_3$), 113.9 (*C*=C aromatic), 66.3 (C*C*H$_2$O), 62.8 (*C*HN), 55.3 (O*C*H$_3$), 31.9 (*C*H$_2$CHN), 28.4 (*C*H$_2$C=C), 28.0 (*C*H$_2$C=C), 23.4 (=C*C*H$_3$).
IR thin layer (cm^{-1}) 3300 (N-H stretch), 2900-2700 (C-H stretch) 1700-1500 (m,m, aromatic), 1650 (C=O ester stretch), 1250 (C-N stretch), 830 (aromatic CH bending);
(*S*)-113: α^{20}$_D$ -9.3, (c = 0.6, CHCl$_3$)
(*R*)-113: α^{20}$_D$ +12 (c = 0.6, CHCl$_3$)
m.p. 69-71 °C
LR-MS (EI+) m/z: 275.15 (100% M +), 276.15 (20), 259.12 (18), 258.12 (60), 231.12 (25), 228.1128(12), 214.16 (100).
HR-MS (EI$^+$) calculated for C$_{16}$H$_{21}$NO$_3$: 275.1522, requires 275.1521.

(*R*)- and (*S*)-*N*,4-dimethyl-*N*-(4-methylpent-3-en-3-yl)cyclohex-3-en-1-amine (116)
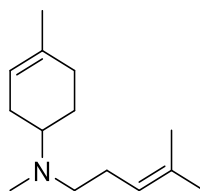
To a stirred solution of **96** (41 mg, 0.19 mmol) in anhydrous diethyl ether at 0 °C, LiAlH$_4$ (33 mg, 0.87 mmol) was added. The mixture was heated to reflux for 6 h and allowed to reach room temperature for 12 h. The reaction was quenched by the addition of water (6 mL) and 15% NaOH aqueous solution (6 mL) at 0 °C stirred for

1 h at 0 °C. The white precipitate was removed by filtration on celite and the filtrate was extracted with diethyl ether (2 × 25 mL). The combined organic layers were dried with Na_2SO_4, concentrated under reduced pressure, and the residue was purified by flash chromatography on silica (Et$_2$O:MeOH 1:9) to yield the compound **116** as a yellow oil (32 mg, 65% yield).

^{1}H NMR (300 MHz, CDCl$_3$) δ 5.27 (1 H, d, J = 2.4 Hz, H$_3$CC=CH), 5.03 (1H, t, J = 5.6 Hz, H$_3$CC=CHCH$_2$CH$_2$N), 2.64 – 2.44 (1 H, m, CHN), 2.38 (2 H, ddd, J = 7.6, 5.8, 2.6 Hz, CH_2N), 2.23 (3 H, s, CH_3N), 2.08 (2 H, dd, J = 15.5, 7.2 Hz, CH$_2$CH_2C=), 2.04 – 1.85 (4 H, m, CH_2CH_2CHN), 1.85 – 1.67 (2 H, m, =CHCH_2CHN), 1.62 (3 H, s, CNCH$_2$CH=CCH_3), 1.57 (3 H, s, =CCH_3), 1.55 (3 H, s, =CCH_3).

^{13}C NMR (75 MHz, CDCl$_3$) δ 133.9 (HC=CCH$_3$), 132.6 (CH=CCH$_3$), 122.1 (CH=CCH$_3$), 120.0 (NCH$_2$CH$_2$$C$H=CCH$_3$), 58.9 ($C$HN), 53.5 ($CH_2$N), 37.9 ($CH_2CH_2$CHN), 30.8 (=CH$CH_2$N), 27.2 ($CH_2CCH_3$), 26.5 (CH$_3$N), 25.7($CH_2CH_2$N), 25.6 ($CH_3CCH_3$), 23.2 (CH$_3CCH_3$), 17.8 ($CH_3$C=).

HR-MS (EI$^+$) calculated for C$_{14}$H$_{25}$N : 207.1987, found 207.1990

(S)-116 : α^{20}$_D$ $^-$61 (CHCl$_3$, c=1)

(R)-116 α^{20}$_D$ +63 (CHCl$_3$, c=1)

Data are in agreement with literature.[71]

6.3.1 Synthesis of the cis-germacradienyl aza-analogue

(Z)-2-((3,7-dimethylocta-2,6-dien-1-yl)oxy)tetrahydro-2H-pyran (124)

To a stirred solution of nerol (8 g, 52 mmol) in CH$_2$Cl$_2$ (100 mL) 3,4-dihydropyran (5.6 mL, 62 mM) and pyridinium p-toluensulfonate (260 mg, 1.04 mM) were added and the resulting mixture was left to stir at room temperature for 24 h. The solvent was removed under reduced pressure, the crude residue was re-dissolved in diethyl ether (30 mL), and washed with aqueous sodium bicarbonate solution (3 × 30 mL), brine (3 × 30 mL) and water (3 × 30 mL). The reunited organic layers were dried over Na$_2$SO$_4$ and concentrated under reduced pressure to give compound **124** (11.9

g, 98%). The obtained compound was judged by NMR to be sufficiently pure to be used for the next step without any further purification.

¹H NMR δ (300 MHz, CDCl$_3$) δ 5.30 (1 H, t, J = 6.9 Hz, C=CH), 5.08 – 4.98 (1 H, C=CHCH$_2$), 4.56 (1 H, t, J = 3.3 Hz, OCHO), 4.14 (1 H, dd, J = 11.8, 6.6 Hz, C=CHCHHO), 3.90 (1 H, dd, J = 11.8, 7.5 Hz, OCHH), 3.81 (1 H, ddd, J = 11.1, 7.7, 3.3 Hz, C=CHCHHO), 3.44 (1 H, dd, J = 10.5, 5.3 Hz, OCHH), 2.11 – 1.94 (4 H, m, CH_2CH_2C=), 1.87 – 1.72 (1 H, m, CH$_2$CHHCH$_2$CHO), 1.68 (3 H, s, CH_3), 1.64 (3 H, s, CH_3), 1.60 (3 H, s, CH_3), 1.55 (2 H, d, J = 9.9 Hz, CH_2CHO), 1.53 – 1.38 (3 H, m, CH_2CHHCH$_2$CHO).

¹³C NMR δ (75 MHz, CDCl$_3$) δ 140.4 (C=CHCH$_2$O), 131.8 (CH$_3$$C$=CH), 123.8 (C=$CHCH_2$O), 121.5 (CH$_3$C=$C$H), 97.8 (O$C$HO), 63.4 (C=CH$CH_2$O), 62.1 (OCHO$CH_2$), 32.1 ($CH_2$C=CH), 30.6 (OCH$CH_2$), 26.7 ($CH_2CH_2$C=CH), 25.6 (OCH$_2$$CH_2$), 25.5, 23.5 ($CH_3$C=CHCH$_2$O), 19.5 ($CH_3CCH_3$), 17.6 (CH$_3CCH_3$).

LR-MS (EI+) m/z: 238.19

Data are in agreement with the literature [101]

(2E,6Z)-2,6-dimethyl-8-((tetrahydro-2H-pyran-2-yl)oxy)octa-2,6-dien-1-ol (125)

To a stirring suspension of SeO$_2$ (244 mg, 2.2 mmol) and salicylic acid (303 mg, 2.2 mM) in CH$_2$Cl, t-butyl hydroperoxide (6.36 mL, 66 mM) was added and the resulting mixture was left to stir at room temperature for 30 min. The mixture was then cooled to 0 °C and **124** was added (5 g, 22 mM). The reaction was left to stir at 0 °C for 12 h before the solvent was removed under reduce pressure. The crude residue was dissolved in diethyl ether (30 mL) and washed with aqueous sodium bicarbonate solution (3 × 30 mL), copper sulfate (3 × 30 mL), sodium sulfite (3 × 30 mL), brine (3 × 30 mL), and water (3 × 30 mL). The organic layer was then dried over Na$_2$SO$_4$, concentrated under reduced pressure, and the residue was purified by flash chromatography on silica (EtOAc:hexane 4:6) to yield the pure compound **125** as a dark yellow oil (1.14 g, 20% yield).

¹H NMR δ (300 MHz, CDCl$_3$) δ 5.38 – 5.23 (2 H, m, C=C*H* and C=C*H*CH$_2$), 4.57 (1 H, dt, *J* = 7.0, 3.6 Hz, C=CHC*H*HO), 4.15 (1 H, ddd, *J* = 11.8, 6.7, 1.1 Hz, OC*H*HCH$_2$), 4.07 – 3.92 (1 H, m, OC*H*HCH$_2$), 3.90 (2 H, s, C*H$_2$*OH), 3.82 (1 H, ddd, *J* = 11.3, 7.4, 3.8 Hz, C=CHCH*H*O), 3.52 – 3.38 (1 H, m, OCH*H*CH$_2$), 2.22 – 1.97 (4 H, m, C*H$_2$*C*H$_2$*C=), 1.76 (1 H, dd, *J* = 8.6, 4.1 Hz, CH$_2$CH*H*CH$_2$CHO), 1.69 (3 H, s, C*H$_3$*), 1.58 (3 H, s, C*H$_3$*), 1.48 (5 H, ddd, *J* = 13.5, 8.8, 3.0 Hz, C*H$_2$*C*H*HC*H$_2$*CHO).

¹³C NMR δ (75 MHz, CDCl$_3$) δ 140.4 (*C*=CHCH$_2$O), 131.8 (CH$_3$*C*=CH), 123.8 (C=*C*HCH$_2$O), 121.5 (CH$_3$C=*C*H), 97.7 (O*C*HO), 63.3 (C=CH*C*H$_2$O), 62.0 (OCHO*C*H$_2$), 32.1 (*C*H$_2$C=CH), 30.6 (OCH*C*H$_2$), 26.7 (*C*H$_2$CH$_2$C=CH), 25.6 (O*C*H$_2$*C*H$_2$), 25.5, 23.5 (*C*H$_3$C=CHCH$_2$O), 19.5 (*C*H$_3$CCH$_3$), 17.6(CH$_3$C*C*H$_3$).

LR-MS (AP+) m/z: 277.18 (100% M+Na$^+$), 278.18 (20)

Data are in agreement with the literature. [104]

2-(((2*Z*,6*E*)-8-chloro-3,7-dimethylocta-2,6-dien-1-yl)oxy)-tetrahydro-2H-pyran (132)

To a cold (0 °C) solution of alcohol **125** (1.65 g, 6.4 mM) in anhydrous DMF (50 mL), LiCl (543 mg, 12.8 mM), *s*-collidine (2.08 mL, 16 mM) and methanesulfonyl chloride (1 mL, 12.8 mM) were added, and the resulting mixture was left stir at room temperature for 3 h. The reaction was then quenched by the addition of cold water (10 mL) and the mixture was washed with Et$_2$O (3 × 20 mL), aqueous sodium bicarbonate solution (3 × 20 mL), copper nitrate saturated solution (3 × 20 mL), brine (3 × 20 mL), and water (3 × 20 mL). The organic layer was then dried over Na$_2$SO$_4$ and concentrated under reduced pressure to yield the crude compound **132** (1.4 g, 80%)

¹H NMR (400 MHz, CDCl$_3$) δ 5.5-5.45 (1 H, br., C=C*H*), 5.39 – 5.26 (1 H, m, C=C*H*CH$_2$), 4.61 – 4.50 (1 H, m, OC*H*O), 4.15 (1 H, dd, *J* = 11.8, 6.6 Hz, C=CHC*H*HO), 4.00 (1 H, t, *J* = 6.8 Hz, OC*H*HCH$_2$), 3.94 (2 H, s, C*H$_2$*Cl), 3.89 (1 H, d, *J* = 11.1 Hz, C=CHCH*H*O), 3.44

(1 H, ddd, J = 10.8, 5.0, 4.5 Hz, OCHHCH$_2$) 2.07 (4 H, m, CH_2CH$_2$C=), 1.69 (3 H, s, CH_3), 1.67 (3 H, s, CH_3), 1.64-1.40 (6 H, m, CH_2CH$_2$CH$_2$CHO).

^{13}C NMR (63 MHz, CDCl$_3$) δ 139.7 (C=CHCH$_2$O), 132.1 (ClCH$_2$$C$=CH), 130.0 (C=$CHCH_2$O), 122.1 (C=$CHCH_2CH_2$), 97.8 (O$C$HO), 63.2 (C=CH$CH_2$O), 62.2 (OCHO$CH_2$), 52.3 (Cl$CH_2$), 31.4 ($CH_2$C=CH), 30.7 (OCH$CH_2$), 26.6 ($CH_2CH_2$C=CH), 25.5 (OCH$_2$$CH_2$), 23.4 ($CH_3$C=CHCH$_2$O), 19.5 ($CH_3CCH_2$Cl), 14.1 (OCH$CH_2CH_2$).

Synthesis of (2Z,6E)-8-hydroxy-3,7-dimethylocta-2,6-dien-1-yl acetate (140)
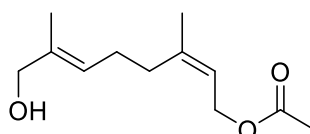
To a stirred solution of salicylic acid (352 mg, 2.55 mM) in CH$_2$Cl$_2$ (80 mL) selenium oxide (282 mg, 2.55 mM) and *tert*-butyl hydroperoxide (7.36 mL, 76.41 mM) were added. The resulting mixture was left to stir at room temperature for 1 h. The solution was then cooled to 0 °C and neryl acetate (5.5 mL, 25.47 mM) was added. The reaction was stirred for 24 h at 0 °C before the solvent was removed under reduced pressure. The crude residue was dissolved in diethyl ether (30 mL) and washed with aqueous sodium bicarbonate solution (3 × 30 mL), copper sulfate (3 × 30 mL), sodium sulfite (3 × 30 mL), brine (3 × 30 mL), and water (3 × 30 mL). The organic layer was then dried over Na$_2$SO$_4$ concentrated under reduced pressure and the residue was purified by flash chromatography on silica (EtOAc:hexane 4:6) to yield the pure compound **140** as a brown oil (0.174 g, 30% yield).
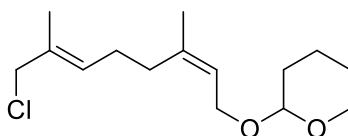
^{1}H NMR (400 MHz, CDCl$_3$) δ 5.49 – 5.19 (2 H, m, CH=C), 4.52 (2 H, d, J = 7.2 Hz, CH_2CH=), 3.93 (2 H, s, CH_2OH), 2.20 – 1.99 (4 H, m, =CCH_2CH$_2$C=), 1.95 (3 H, s, CH_3C=OOCH$_2$), 1.73 (3 H, s, CH_3), 1.62 (3 H, s, CH_3).

^{13}C NMR (101 MHz, CDCl$_3$) δ 171.2 (C=O), 141.9 (C=CHCH$_2$O), 135.5 (C=CH), 124.5 (C=CHCH$_2$O), 119.4 (C=CHCH$_2$CH$_2$), 68.4 (CH$_2$OH), 61.1 (CH$_2$OC=O), 31.7 (CH$_3$C=O), 25.9 (CH$_2$C=CH), 23.3 (CH$_2$CH$_2$C=CH), 20.9 (CH$_3$), 13.6 (CH$_3$).

IR thin layer (cm^{-1}) 3065 (O-H stretch), 1256 (C-O stretch), 912 (C=C bending), 740 (C-H bend).

Data are in agreement with literature.[104]

Synthesis of (2Z,6E)-8-chloro-3,7-dimethylocta-2,6-dien-1-yl acetate (141)
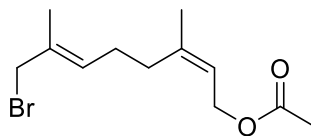
To a stirred solution of **140** (1 g, 4.7 mM) in anhydrous diethyl ether (20 mL) at ⁻15 °C was slowly added phosphorus tribromide (0.22 mL, 2.3 mM). The resulting mixture was left to stir at -15 °C until TLC analysis (hexane:EtOAc 8:2) showed the complete consumption of the starting material. The reaction was then allowed to reach room temperature and water (30 mL) was added. The organic layer was washed with aqueous sodium bicarbonate solution (3 × 30 mL), water (30 mL), brine (3 × 30 mL), dried over Na_2SO_4, and finally concentrated under reduced pressure. Due to the instability of the bromide, **141** was promptly used in the next reaction without any further purification.

¹H NMR (400 MHz, $CDCl_3$) δ 5.49 – 5.19 (2 H, m, C*H*=C), 4.52 (2 H, d, *J* = 7.2 Hz, C*H₂*CH=), 3.93 (2 H, s, C*H₂*Br), 2.20 – 1.99 (4 H, m, =CC*H₂*C*H₂*C=), 1.95 (3 H, s, C*H₃*C=OOCH₂), 1.73 (3 H, s, C*H₃*), 1.62 (3 H, s, C*H₃*).

Synthesis of dimethyl 2-((2E,6Z)-8-acetoxy-2,6-dimethylocta-2,6-dien-1-yl)malonate (142)
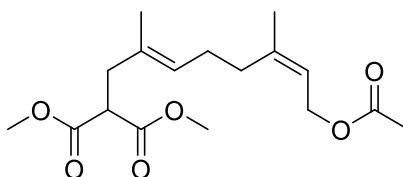
To a stirred solution of sodium hydride (142 mg, 4.7 mM) in anhydrous THF (30 mL) at 0 °C, dimethyl malonate (620 mg, 4.7 mM) was slowly added and left to stir at 0 °C for 30 min. Crude compound **141** was added and the resulting mixture was left to stir at room temperature for 24 h. Saturated aqueous ammonium chloride solution (20 mL) was then added. The organic layer was washed with brine (3 × 30 mL) and water (3 × 30 mL), dried over Na_2SO_4, concentrated under reduced pressure, and

the residue was purified by flash chromatography on silica (EtOAc:Hex 1:9) to yield the pure compound **142** as a yellow oil (766 mg, 50% yield).

¹H NMR (400 MHz, CDCl₃) δ 5.28 (1 H, t, *J* = 7.1 Hz, C*H*=), 5.12 (1 H, br., C*H*=), 4.47 (2H, d, *J* = 7.3 Hz, C*H₂*OCOCH₃), 3.65 (6H, s, C*H₃*OOCCHCOOC*H₃*), 3.50 (1 H, t, *J* = 7.8 Hz, CH₃OOCC*H*COOCH₃), 2.51 (2 H, d, *J* = 7.8 Hz, C*H₂*CHCOOCH₃), 2.07-1.98 (4 H, br, C*H₂*C*H₂*C=CH), 1.98 (3 H, s, CH₂OCOC*H₃*), 1.68 (3 H, s, C*H₃*C=CH), 1.55 (3 H, s, C*H₃*C=CH).

¹³C NMR (101 MHz, CDCl₃) δ 170.9 (CH₂O*C*OCH₃), 169.4 (CH₃OO*C*CH*C*OOCH₃), 142.1 (CH₃*C*=CHCH₂O), 131.5 (CH₃*C*=CHCH₂), 126.5 (CH₃C=*C*HCH₂O), 119.3 (CH₃C=*C*HCH₂), 60.9 (*C*H₂OCOCH₃), 52.3 (*C*H₃OOCCHCOO*C*H₃), 50.4 (CH₃OO*CC*HCOOCH₃), 38.5 (*C*H₂CHCOOCH₃), 31.7 (HC=C*C*H₂CH₂), 26.5 (HC=CCH₂*C*H₂), 23.3 (*C*H₃COOCH₂), 20.9 (*C*H₃C=CH), 15.6 (*C*H₃C=CH).

IR thin layer (cm⁻¹) 2953 (C-H stretch), 1732 (C=O ester stretch) 1436-1238, (C-O stretch), 1153, 1022, 914-744 (C=C bending)

LR-MS (ES+) m/z: 349.16 (100%, M+Na⁺), 366.14 (3) 365.14 (22), 289.10 (5), 235.13 (1), 203.10 (1), 185.09 (2).

HR-MS (ES+) calculated for C₁₇H₂₆O₆Na [M+Na⁺]: 349.1627, found 349.1637

Synthesis of methyl (4E,8Z)-10-acetoxy-4,8-dimethyldeca-4,8-dienoate (143)
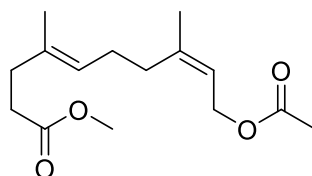
To a stirred solution of dimethyl malonate **142** (250 mg, 0.8 mM) in DMSO (20 mL) LiCl (136 mg, 3.2 mM) and 20 μL of water were added, and the resulting mixture was heated to reflux for 12 h. The solution turned from light yellow to dark brown. The mixture was then allowed to reach room temperature before being extracted with Et₂O (3 × 30 mL). The organic phase was washed with cold water (5 × 30 mL) to remove residual DMSO, dried over Na₂SO₄, and concentrated under reduced pressure. The residue was purified by flash chromatography on silica (EtOAc:hexane 1:9) to yield pure compound **143** as a yellow oil (172 mg, 80% yield).

¹H NMR (400 MHz, CDCl$_3$) δ 5.29 (1 H, t, J = 7.2 Hz, C*H*=CH$_2$O), 5.07 (1 H, br., C*H*=CH$_2$CH$_2$), 4.48 (2 H, d, J = 7.3 Hz, C*H*$_2$OCOCH$_3$), 3.59 (3 H, s, C*H*$_3$OC=OCH$_2$CH$_2$), 2.34 (2 H, t, J = 8.0 Hz, CH$_2$C*H*$_2$C=OOCH$_3$), 2.22 (2 H, t, J = 8.0 Hz, C*H*$_2$CH$_2$C=OOCH$_3$), 2.10- 2.00 (4 H, br, C*H*$_2$C*H*$_2$C=CH), 1.98 (3 H, s, CH$_2$OCOC*H*$_3$), 1.69 (3 H, s, C*H*$_3$C=CH), 1.54 (3 H, s, C*H*$_3$C=CH).

¹³C NMR (101 MHz, CDCl$_3$) δ 173.8 (CH$_2$O*C*OCH$_3$), 171.0 (=CHCH$_2$*C*OOCH$_3$), 142.3 (CH$_3$*C*=CHCH$_2$O), 134.1 (CH$_3$*C*=CHCH$_2$CH$_2$), 124.2 (CH$_3$C=*C*HCH$_2$), 119.2 (CH$_3$C=*C*HCH$_2$O), 61.0 (*C*H$_2$OCOCH$_3$), 51.5 (*C*H$_2$OCOC*H*$_3$), 34.5 (*C*H$_2$CH$_2$C=O), 32.8 (CH$_2$*C*H$_2$C=O), 31.9 (HC=C*C*H$_2$CH$_2$), 26.4 (HC=CCH$_2$*C*H$_2$), 23.4 (CH$_2$OCOC*H*$_3$), 21.0 (*C*H$_3$C=CH), 15.9 (*C*H$_3$C=CH).

IR thin layer (cm^{-1}) 1730 (C=O ester stretch), 904.62 (alkene bending), 727-648 (CH bending)

LR-MS (ES+) m/z: 291.15 (100% M+Na$^+$), 307.12 (90), 308.14 (30), 309.12 (20), 365.14 (10)

HR-MS (ES$^+$) calculated for C$_{15}$H$_{24}$O$_4$Na [M+Na$^+$]: 291.16, found 291.1573.

Synthesis of (4E,8Z)-10-hydroxy-4,8-dimethyldeca-4,8-dienal (149)
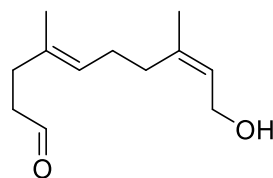
To a stirred solution of ester **143** (0.280 g, 0.7 mM) in anhydrous CH$_2$Cl$_2$ (50 mL) at -78 °C, DIBALH (1 M solution in hexane, 2.7 mL) was slowly added over 5 min. The resulting mixture was left to stir at -78 °C until TLC analysis (hexane:ethylacetate 9:1) showed complete consumption of the starting material. Methanol (1 mL) and Rochelle's salt solution (5 mL) were added, and the mixture was energetically stirred for 1 h. The slurry was filtered on Celite, and the organic phase was washed with brine (3 × 30 mL). The reunited aqueous layers were back extracted with Et$_2$O (3 × 30 mL). The combined organic phases were dried over Na$_2$SO$_4$ and concentrated under reduced pressure to yield the crude aldehyde **149** (0.194 g, 95%). As **149** resulted to be an unstable compound, it was used for the next step promptly without any further purification.

¹H NMR (400 MHz, CDCl₃) δ 9.67 (1 H, s, O=C*H*), 5.36 (1 H, t, *J* = 6.7 Hz, C*H*=CH₂O), 5.06 (1 H, br., C*H*=CH₂CH₂), 4.03 (2 H, d, *J* = 6.9 Hz, C*H*₂OH) 2.45 (2 H, t, *J* = 6.7 Hz, CH₂C*H*₂C=O), 2.25 (2 H, t, *J* = 7.2 Hz, C*H*₂CH₂C=O), 2.11-1.90 (4 H, br., s, C*H*₂C*H*₂C=CH), 1.67 (3 H, s, C*H*₃C=CH), 1.55 (3 H, s, C*H*₃C=CH).

LR-MS (ES+) m/z: 219.15 (100%, M+Na⁺)

Synthesis of (2*Z*,6*E*)-9-(1,3-dithian-2-yl)-3,7-dimethylnona-2,6-dien-1-ol (152)
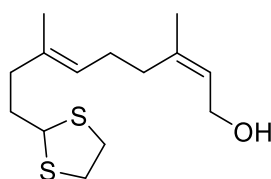
To a stirred solution of aldehyde **149** (0.100 g, 0.51 mM) in CH₂Cl₂ (20 mL) were added 1,3-propanedithiol (53 mg, 0.56 mM) and catalytic amount of oven-dried NiCl₂. The resulting mixture was left to stir at room temperature for 12 h. The reaction mixture turned yellow and then dark brown over time. The organic solution was washed with brine (3 × 30 mL) and water (3 × 30 mL), dried over Na₂SO₄, and concentrated under reduced pressure. The residue was purified by flash chromatography on silica (EtOAc:hexane 2:8) to yield pure compound **152** as a yellow oil (79 mg, 55% yield).

¹H NMR (400 MHz, CDCl₃) δ 5.37 (1 H, t, *J* = 6.8 Hz, C*H*=CH₂OH), 5.08 (1 H, br., C*H*=CH₂CH₂), 4.35 (1 H, t, *J* = 7.1 Hz, SC*H*S), 4.04 (2 H, d, *J* = 7.1 Hz, C*H*₂-OH), 3.23 – 3.03 (4 H, m, SC*H*₂C*H*₂S), 2.17 – 1.92 (8 H, m, C*H*₂C*H*₂CHS and C*H*₂C*H*₂C=CH), 1.65 (3 H, s, C*H*₃C=CH), 1.57 (3 H, s, C*H*₃C=CH).

¹³C NMR (101 MHz, CDCl₃) δ 138.6 (CH₃*C*=CHCH₂OH), 133.3 (CH₃*C*=CHCH₂CH₂), 123.7 (CH₃C=*C*HCH₂OH), 123.5 (CH₃C=*C*HCH₂CH₂), 58.0 (*C*H₂OH), 51.9 (S*C*HS), 38.0 (*C*H₂CHS), 37.3 (S*C*H₂*C*H₂S), 36.6 (*C*H₂CH₂CHS), 30.7 (HC=C*C*H₂CH₂), 25.4 (HC=C*C*H₂*C*H₂), 22.3 (*C*H₃C=CH), 14.9 (*C*H₃C=CH).

IR thin layer (cm⁻¹) 3311 (broad O-H stretch), 906 (C=C bending), 727 (C=C bending), 648 (C-H bending).

LR-MS (EI+) m/z: 272.13 (10), 254.12 (30), 252.20 (50), 250.08 (30), 248.07 (20), 246.05 (32), 244.09 (55), 228.08 (8), 227.099 (6), 226.08 (100), 220.00 (8), 218.02 (8).

HR-MS (EI$^+$) calculated for $C_{14}H_{24}OS_2$: 272.1269, found 272.1263.

CHAPTER 7   Bibliography

(1)   Opitz, S.; Kunert, G.; Gershenzon, J. *J. Chem. Ecol.* **2008**, *34* (4), 508–522.

(2)   Sacchettini, J. C. *Science (80-85).* **2013**, *53* (9), 1689–1699.

(3)   Humphrey, A. J.; Beale, M. H. *Plant Second. Metab. Occur. Struct. Role Hum. Diet* **2006**, 47-50.

(4)   Incardona, J. P.; Eaton, S. *Curr. Opin. Cell Biol.* **2000**, *12* (2), 193–203.

(5)   Maxfield, F. R.; Tabas, I. *Nature* **2005**, *438* (7068), 612–621.

(6)   Dufourc, E. J. *J. Chem. Biol.* **2008**, *1* (1–4), 63–77.

(7)   Ikonen, E. *Nat. Rev. Mol. Cell Biol.* **2008**, *9* (2), 125–138.

(8)   Ikonen, E. *Physiol. Rev.* **2006**, *86*, 1237–1261.

(9)   Rao, A. V.; Rao, L. G. *Pharmacol. Res.* **2007**, *55* (3), 207–216.

(10)   Britfon, G. *FASEB J.* **1995**, *9* (15), 1551–1558.

(11)   Rodrigues, D. B.; Mariutti, L. R. B.; Mercadante, A. Z. *J. Chromatogr. A* **2016**, *1457*, 116–124.

(12)   Son, E. J.; Kim, J. H.; Kim, K.; Park, C. B. *J. Mater. Chem. A* **2016**, *0*, 1–24.

(13)   Uchimiya, M.; Stone, A. T. *Chemosphere* **2009**, *77* (4), 451–458.

(14)   Moqrich, A. *Science (80-.).* **2005**, *307* (5714), 1468–1472.

(15)   Christianson, D. W. *Science (80-.).* **2007**, *316* (5821), 60–61.

(16)   Clifford, K.; Cornforth, J. W.; Mallaby, R.; Phillips, G. T. *J. Chem. Soc. D Chem. Commun.* **1971**, No. 24, 1599.

(17)   Instrumentation, A. *Tetrahedron* **1991**, *41* (32), 6231–6242.

(18)   D. Gordon. *Tetrahedron Lett.* **1999**, *40* (17), 653–656.

(19)   Gräwert, T.; Groll, M.; Rohdich, F.; Bacher, A.; Eisenreich, W. *Cell. Mol. Life Sci.* **2011**, *68* (23), 3797–3814.

(20)   Kim, S.; Heo, K.; Chang, Y.; Park, S.; Rhee, S.; Kim, S. *J. Nat. Prod.* **2006**, *69*, 758–762.

(21)   Picaud, S.; Mercke, P.; He, X.; Sterner, O.; Brodelius, M.; Cane, D. E.; Brodelius, P. E. *Arch. Biochem. Biophys.* **2006**, *448* (1–2), 150–155.

(22)   Cane, D. E.; Prabhakaran, P. C.; Oliver, J. S.; McIlwaine, D. B. *J. Am. Chem. Soc.* **1990**, *112* (8), 3209–3210.

(23)   Cane, D. E.; Prabhakaran, P. C.; Salaski, E. J.; Harrison, P. H. M.; Noguchi, H.; Rawlings, B. J. *J. Am. Chem. Soc.* **1989**, *111* (24), 8914–8916.

(24) Wendt, K. U.; Schulz, G. E. *Structure* **1998**, *6* (2), 127–133.

(25) Chen, F.; Tholl, D.; Bohlmann, J.; Pichersky, E. *Plant J.* **2011**, *66* (1), 212–229.

(26) Degenhardt, J.; Köllner, T. G.; Gershenzon, J. *Phytochemistry* **2009**, *70* (15–16), 1621–1637.

(27) L. Sangeetha Vedulaa; Jiaoyang Jiangb, Tatiana Zakhariana, David E. Caneb,*, and D. W. C. *Arch Biochem Biophys* **2008**, *15* (Suppl 2), 184–194.

(28) Christianson, D. W. *Chem. Rev.* **2006**, *106*, 3412–3442.

(29) González, V.; Grundy, D. J.; Faraldos, J. A.; Allemann, R. K. *Org. Biomol. Chem.* **2016**, *14* (31), 7451–7454.

(30) Shishova, E. Y.; Di Costanzo, L.; Cane, D. E.; Christianson, D. W. *Biochemistry* **2007**, *46* (7), 1941–1951.

(31) Gennadios, H. A.; Gonzalez, V.; Di Costanzo, L.; Li, A.; Yu, F.; Miller, D. J.; Allemann, R. K.; Christianson, D. W. *Biochemistry* **2009**, *48* (26), 6175–6183.

(32) Yoshikuni, Y.; Martin, V. J. J.; Ferrin, T. E.; Keasling, J. D. *Chem. Biol.* **2006**, *13* (1), 91–98.

(33) Cane, D. E.; Tandon, M.; Prabhakaran, P. C. *J. Am. Chem. SOC* **1993**, *115* (8), 103–108.

(34) Cane, D. E. *Chem. Rev.* **1990**, *90* (7), 1089–1103.

(35) Brock, N. L.; Dickschat, J. S. *ChemBioChem* **2013**, *14* (10), 1189–1193.

(36) Caruthers, J. M.; Kang, I.; Rynkiewicz, M. J.; Cane, D. E.; Christianson, D. W. *J. Biol. Chem.* **2000**, *275* (33), 25533–25539.

(37) Forcat, S.; Allemann, R. K. *Chem. Commun.* **2004**, *15*, 2094–2095.

(38) Forcat, S.; Allemann, R. K. *Org. Biomol. Chem.* **2006**, *4* (13), 2563–2567.

(39) Deligeorgopoulou, A.; Allemann, R. K. *Biochemistry* **2003**, *42* (25), 7741–7747.

(40) Deligeorgopoulou, A.; Taylor, S. E.; Forcat, S.; Allemann, R. K. *Chem. Commun..* **2003**, No. 17, 2162–2163.

(41) Calvert, M. J.; Taylor, S. E.; Allemann, R. K. *Chem. Commun. (Camb).* **2002**, No. 20, 2384–2385.

(42) Miller, D. J.; Yu, F.; Knight, D. W.; Allemann, R. K. *Org. Biomol. Chem.* **2009**, *7* (5), 962–975.

(43) Cane, D. E.; Tsantrizos, Y. S. *J. Am. Chem. Soc.* **1996**, *118* (42), 10037–10040.

(44) Faraldos, J. A.; Kariuki, B.; Allemann, R. K. *J. Org. Chem.* **2010**, *75* (4), 1119–1125.

(45) Faraldos, J. A.; Allemann, R. K. *Org. Lett.* **2011**, *13* (5), 1202–1205.

(46) Shishova, E. Y.; Yu, F.; Miller, D. J.; Faraldos, J. A.; Zhao, Y.; Coates, R. M.;

Allemann, R. K.; Cane, D. E.; Christianson, D. W. *J. Biol. Chem.* **2008**, *283* (22), 15431–15439.

(47) Rynkiewicz, M. J.; Cane, D. E.; Christianson, D. W. *Biochemistry* **2002**, *41* (6), 1732–1741.

(48) Aaron, J. A.; Lin, X.; Cane, D. E.; Christianson, D. W. *Biochemistry* **2010**, *49* (8), 1787–1797.

(49) Faraldos, J. A.; Miller, D. J.; González, V.; Yoosuf-Aly, Z.; Cascón, O.; Li, A.; Allemann, R. K. *J. Am. Chem. Soc.* **2012**, *134* (13), 5900–5908.

(50) M.V.D. Kamp, J. S.; Żurek, J.; Allemann, R. K.; Mulholland, A. J. *Biochemistry* **2013**, *52*, 8094–8105.

(51) Calvert, M. J.; Ashton, P. R.; Allemann, R. K. *J. Am. Chem. Soc.* **2002**, *124* (39), 11636–11641.

(52) Miller, D. J.; Gao, J.; Truhlar, D. G.; Young, N. J.; Gonzalez, V.; Allemann, R. K. *Org. Biomol. Chem.* **2008**, *6* (13), 2346–2354.

(53) Wallaart, T. E.; Bouwmeester, H. J.; Hille, J.; Poppinga, L.; Maijers, N. C. A. *Planta* **2001**, *212*, 460–465.

(54) Paddon, C. J.; Westfall, P. J.; Pitera, D. J.; Benjamin, K.; Fisher, K.; McPhee, D.; Leavell, M. D.; Tai, a; Main, a; Eng, D.; Polichuk, D. R.; Teoh, K. H.; Reed, D. W.; Treynor, T.; Lenihan, J.; Fleck, M.; Bajad, S.; Dang, G.; Dengrove, D.; Diola, D.; Dorin, G.; Ellens, K. W.; Fickes, S.; Galazzo, J.; Gaucher, S. P.; Geistlinger, T.; Henry, R.; Hepp, M.; Horning, T.; Iqbal, T.; Jiang, H.; Kizer, L.; Lieu, B.; Melis, D.; Moss, N.; Regentin, R.; Secrest, S.; Tsuruta, H.; Vazquez, R.; Westblade, L. F.; Xu, L.; Yu, M.; Zhang, Y.; Zhao, L.; Lievense, J.; Covello, P. S.; Keasling, J. D.; Reiling, K. K.; Renninger, N. S.; Newman, J. D. *Nature* **2013**, *496* (7446), 528–532.

(55) Artemisinin production review. **2009**, *4* (4), 261–267.

(56) Westfall, P. J.; Pitera, D. J.; Lenihan, J. R.; Eng, D.; Woolard, F. X.; Regentin, R. **2012**, *109* (3), 111–118.

(57) Ro, D.; Paradise, E. M.; Ouellet, M.; Fisher, K. J.; Newman, K. L.; Ndungu, J. M.; Ho, K. A.; Eachus, R. A.; Ham, T. S.; Kirby, J.; Chang, M. C. Y.; Withers, S. T.; Shiba, Y.; Sarpong, R.; Keasling, J. D. **2006**, *440* (April), 3–6.

(58) Bertea, C. M.; Freije, J. R.; van der Woude, H.; Verstappen, F. W.; Perk, L.; Marquez, V.; de Kraker, J. W.; Posthumus, M. a.; Jansen, B. J.; De Groot, A.; Franssen, M. C.; Bouwmeester, H. J. *Planta Med.* **2005**, *71*, 40–47.

(59) Picaud, S.; Olofsson, L.; Brodelius, M.; Brodelius, P. E. *Arch. Biochem. Biophys.* **2005**, *436* (2), 215–226.

(60) Benedict, C. R.; Alchanati, I.; Harvey, P. J.; Liu, J.; Stipanovic, R. D.; Bell, A. A. *Phytochemistry* **1995**, *39* (2), 327–331.

(61) Davis, G. D.; Essenberg, M. *Phytochemistry* **1995**, *39* (3), 553–567.

(62) Bianchini, G. M.; Stipanovic, R. D.; Bell, A. A. *J. Agric. Food Chem.* **1999**, *47* (10), 4403–4406.

(63) Alchanati, I.; Patel, J. A. A.; Liu, J.; Benedict, C. R.; Stipanovic, R. D.; Bell, A. A.; Cui, Y.; Magill, C. W. *Phytochemistry* **1998**, *47* (6), 961–967.

(64) Arigoni, D. *Pure Appl. Chem.* **1975**, *41* (1–2), 219–245.

(65) Davis, E. M.; Tsuji, J.; Davis, G. D.; Pierce, M. L.; Essenberg, M. *Phytochemistry* **1996**, *41* (4), 1047–1055.

(66) Benedict, C. R.; Lu, J. L.; Pettigrew, D. W.; Liu, J.; Stipanovic, R. D.; Williams, H. J. *Plant Physiol.* **2001**, *125* (4), 1754–1765.

(67) Faraldos, J. A.; Zhao, Y.; O'Maille, P. E.; Noel, J. P.; Coates, R. M. *ChemBioChem* **2007**, *8* (15), 1826–1833.

(68) Faraldos, J.; Gonzalez, V.; Li, A., R. K. Allemann *J. Am. Chem. Soc.* **2012**,*7,* 8–12.

(69) Poulter, C. D.; King, C. R. *J. Am. Chem. Soc.* **1982**, *104* (24), 1422–1424.

(70) Poulter, D. **1978**, 307–313.

(71) Cane, D. E.; Yang, G.; Coates, R. M. *J. Org. Chem.* **1992**, *57* (9), 3454–3462.

(72) Faraldos, J. A.; Kariuki, B. M.; Coates, R. M. *Org. Lett.* **2011**, *13* (5), 836–839.

(73) Karcher, S. C.; Laufer *J. Med. Chem.* **2009**, *52* (6), 1778–1782.

(74) Van Nhien, A. N.; Tomassi, C.; Len, C.; Marco-Contelles, J. L.; Balzarini, J.; Pannecouque, C.; De Clercq, E.; Postel, D. *J. Med. Chem.* **2005**, *48* (13), 4276–4284.

(75) Taton, M.; Ceruti, M.; Catrel, L.; Rahiert, A.; Biologie, D.; Cnrs, M. P.--upr; Botanique, I. De; Cellulaire, D. E. **1996**, *43* (1), 75–81.

(76) Steiger, A.; Pyun, H.-J.; Coates, R. M. *J. Org. Chem.* **1992**, *57* (12), 3444–3449.

(77) Nakano, C.; Kudo, F.; Eguchi, T.; Ohnishi, Y. *ChemBioChem* **2011**, *12* (15), 2271–2275.

(78) Evans, D. A.; Chapman, K. T.; Bisaha, J. *J. Am. Chem. Soc.* **1984**, *106*, 4261–4263.

(79) Evans, D. A.; Chapman, K. T.; Bisaha, J. *J. Am. Chem. Soc.* **1988**, *110* , 1238–1256.

(80) Chen, Z.; Lin, L.; Chen, D.; Li, J.; Liu, X.; Feng, X. *Tetrahedron Lett.* **2010**, *51* , 3088–3091.

(81) Jones, G. B.; Chapman, B. J.; Mathews, J. E. *J. Org. Chem.* **1998**, *63*, 2928–2938.

(82) Poll, T.; Sobczak, A.; Hartmann, H.; Helmchen, G. *Tetrahedron Lett.* **1985**, *26* (26), 3095–3098.

(83) Laura, A.; Fabio, B.; Adriano, C.; Renzo, R. *Synth. Commun.* **1995**, *25* (19), 1909–2921.

(84) Muto, S.; Nishimura, Y.; Mori, K. *Eur. J. Org. Chem.* **1999**, 2159–2165.

(85) S. Matsubara, K. Horiuchi, K. Takai, K. U. *Chem. Lett.* **1995**, *24*, 259–260.

(86) Demiray, M.; Tang, X.; Wirth, T.; Faraldos, J. A.; Allemann, R. K. *Angew. Chemie - Int. Ed.* **2017**, *56* (15), 4347–4350.

(87) Stritzke, K.; Schulz, S.; Laatsch, H.; Helmke, E.; Beil, W. *J. Nat. Prod.* **2004**, *67* (3), 395–401.

(88) Fairlamb, I. J. S.; Dickinson, J. M.; O'Connor, R.; Cohen, L. H.; Van Thiel, C. F. *Bioorg. Chem.* **2003**, *31* (1), 80–97.

(89) Chong, H. S.; Sun, X.; Chen, Y.; Sin, I.; Kang, C. S.; Lewis, M. R.; Liu, D.; Ruthengael, V. C.; Zhong, Y.; Wu, N.; Song, H. A. *Bioorg. Med. Chem.* **2015**, *23* (5), 1169–1178.

(90) Kaelz, B. no corporate data available, Synthesis and Structure Determination of Chiral Galanthamine Derivates. **1999**

(91) Mascall, K. C.; Jacobi, P. A. *Tetrahedron Lett.* **2012**, *53*, 1620–1623.

(92) Khan, A. T.; Mondal, E.; Sahu, P. R.; Islam, S. *Tetrahedron Lett.* **2003**, *44* (5), 919–922.

(93) Sandifer, R. *J. Am. Chem. Soc.* **1982**, *4*, 7376–7378.

(94) McGeady, P.; Pyun, H. J.; Coates, R. M.; R, C. *Arch. Biochem. Biophys.* **1992**, *299* (1), 63–72.

(95) Bradford, M. M. *Anal. Biochem.* **1976**, *72* (1–2), 248–254.

(96) Gonzalez, V.; Touchet, S.; Grundy, D. J.; Faraldos, J. A.; Allemann, R. K. *J. Am. Chem. Soc.* **2014**, *136* (41), 14505–14512.

(97) Chen, C. R.; Makhatadze, G. I. *BMC Bioinformatics* **2015**, *16* (1), 101.

(98) Cantor; C. R. and Schimmel; P. R. Biophysical Chemistry, 1980, W. H. Freeman and Co., S. F. *Biophysical chemistry*; 1980.

(99) Li, A. *PhD Thesis, Cardiff University*; 2011.

(100) Beyer, H. *PhD Thesis, Cardiff University*; 2008.

(101) Khan, A. T.; Ghosh, S.; Choudhury, L. H. *European J. Org. Chem.* **2005**, No. 22, 4891–4896.

(102) Davisson, V.; Woodside, A.; Timothy, R. N.; Stremler, K. E.; Muehlbacjer, M.; Poulter, C. D.*J.. Am. Chem. Soc* **1986**, No. 51, 4768–4779.

(103) Watkins, W. J. Preparation of thiophencarboxylic acid derivatives for use as flaviviridae viruses inhibitors, 2013.

(104) Isao, K.; Shinji, T.; Nishikawa, F.; Shibuya, H. *Chem. Pharm. Bull.* **1983**, *31*, 2639–2651.